Cyclic Plasticity with an Emphasis on Ratchetting

by

Yanyao Jiang

CYCLIC PLASTICITY WITH AN EMPHASIS ON RATCHETTING

BY

YANYAO JIANG

B.S., Northeastern University of Technology, 1983
M.S., Zhejiang University, 1986

THESIS

Submitted in partial fulfillment of the requirements
for the degree of Doctor of Philosophy in Mechanical Engineering
in the Graduate College of the
University of Illinois at Urbana-Champaign, 1993

Urbana, Illinois

UNIVERSITY OF ILLINOIS AT URBANA-CHAMPAIGN

THE GRADUATE COLLEGE

SEPTEMBER 1993
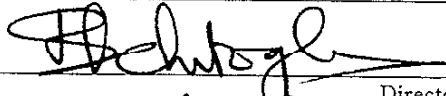
WE HEREBY RECOMMEND THAT THE THESIS BY

YANYAO JIANG

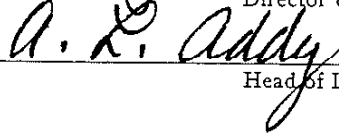ENTITLED **CYCLIC PLASTICITY WITH AN**

EMPHASIS ON RATCHETTING

BE ACCEPTED IN PARTIAL FULFILLMENT OF THE REQUIREMENTS FOR

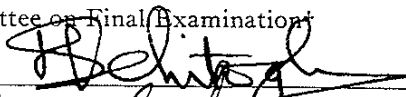THE DEGREE OF **DOCTOR OF PHILOSOPHY**
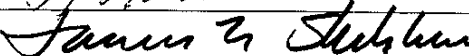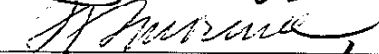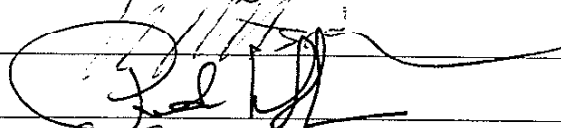
Director of Thesis Research

Head of Department

Committee on Final Examination†

Chairperson

† Required for doctor's degree but not for master's.

O-517

CYCLIC PLASTICITY WITH AN EMPHASIS ON RATCHETTING

ABSTRACT

Two types of plasticity formulations, Armstrong-Frederick and Mroz multiple surface, were evaluated to determine their applicability to model ratchetting and other complex cyclic loading. A limited experimental base exists for loadings such as multiple step proportional and nonproportional loading. Ratchetting experiments have been conducted using a 1070 steel to broaden the experimental base with which the existing plasticity models were evaluated. All the Armstrong-Frederick type models are able to predict reasonable stress response for the balanced nonproportional loading. The Mroz multiple surface type models are inferior to Armstrong-Frederick type models for nonproportional loading.

Under single step loading, the experimental ratchetting rate decreases with increasing number of loading cycles for both proportional and nonproportional loadings, and can be fit using a power law relation. For multiple step loading, the material exhibits a memory of the previous loading history, and could ratchet in the direction opposite to the mean stress. The memory effect dissipates with increasing number of loading cycles. The Ohno-Wang model is the only existing model which can correlate with some of the experimental ratchetting observed for 1070 steel. A shortcoming of the Ohno-Wang model is its inability to predict a constant ratchetting rate for nonproportional loading, and adequately reflect the memory effect for multiple step loading.

Using a concept of the limiting surface for a backstress part, a new plasticity model is proposed to refine the Ohno-Wang model. The capability of the new model to improve predictions for long term and multiple step ratchetting is demonstrated. A convenient procedure to determine the material constants for the model, which is also applicable to other Armstrong-Frederick type models, is described. The new plasticity model is applicable to a broad range of cyclic material behaviors including cyclic hardening/softening, non-Masing behavior, stress level effect, and a variety of ratchetting responses.

ACKNOWLEDGMENTS

TABLE OF CONTENTS

LIST OF TABLES

LIST OF FIGURES

NOMENCLATURE

$a^{(i)}, a_1^{(i)}, a_2^{(i)}$	Material constants (i=1, 2, ..., M)
a_a	Material constant in the Armstrong-Frederick hardening rule
a_b	Scalar function in the Bower hardening rule
a_p	Scalar function in the Prager-Ziegler hardening rule
a_χ	Constant
b_k	Constant
$b_1^{(i)}, b_2^{(i)}$	Material constants (i=1, 2, ..., M)
b_χ	Constant
c_a	Scalar function in the Armstrong-Frederick hardening rule
c_{b1}, c_{b2}	Constants in the Bower hardening rule
$c^{(i)}$	Scalar functions (i=1, 2, ..., M)
$c_0^{(i)}$	Material constants (i=1, 2, ..., M)
c_{r1}, c_{r2}	Constants
d	Prefix denoting increment or differentiation
E	Young's modulus
f	Yield surface function
$f_1^{(i)}, f_2^{(i)}$	Scalar functions (i=1, 2, ..., M)
g	Memory surface function
G	Linear modulus of elasticity in shear
h	Plastic modulus function
$H(g)$	Heaviside step function
$\underline{I}$	Unit tensor
k	Yield stress in simple shear
k_0	Initial yield strength for a cyclic hardening/softening material
$\underline{L}$	Unit vector of the total backstress, $\underline{\alpha}$
$\underline{L}^{(i)}$	Unit vector of the backstress, $\underline{\alpha}^{(i)}$ (i=1, 2, ..., M)
m	Constant
M	Positive integer
$\underline{n}$	Unit exterior normal to the yield surface at the stress state
N	Number of loading cycles
p	Equivalent plastic strain
Q	Constant

$r^{(i)}$	Material constant representing the radius of a limiting surface (i=1, 2, ..., M)
$R^{(i)}$	Radius of the *i*th surface in the Mroz multiple surface type hardening rules (i=1, 2, ..., M)
R_M	Size of the memory surface
$\underset{\sim}{S}$	Deviatoric stress tensor (i=1, 2, ..., M)
$W^{(i)}$	Scalar functions (i=1, 2, ..., M)
$\underset{\sim}{\alpha}$	Total backstress tensor
$\underset{\sim}{\beta}$	Internal state variable in the Bower hardening rule (tensor)
$\underset{\sim}{\alpha}^{(i)}$	*i*th backstress tensor (i=1, 2, ..., M)
δ_{ij}	Kronecker delta
Δ	Prefix denoting range
$\underset{\sim}{\varepsilon}^e$	Elastic strain tensor
$\underset{\sim}{\varepsilon}^p$	Plastic strain tensor
$\underset{\sim}{\varepsilon}$	Total strain tensor
ε^p	Axial plastic strain
ε_r	Ratchetting strain in a specified direction
ε_{r0}	Constant
μ	Poisson's Ratio
$\underset{\sim}{\sigma}$	Stress (tensor)
σ	Axial stress
Γ, Φ, Ω	Symbols representing functions
Φ_∞	Constant
ω	Constant
$\xi^{(i)}$	Material constants (i=1, 2, ..., M)
$\underset{\sim}{\nu}$	Mroz translation vector
$\underset{\sim}{\dot{\nu}}$	Garud translation vector
$\chi^{(i)}$	Hardening rule exponent (i=1, 2, ..., M)
$\chi_0^{(i)}$	Hardening rule coefficient (i=1, 2, ..., M)

1. INTRODUCTION AND OBJECTIVES

Cyclic plasticity deals with the nonlinear stress-strain response of a material subjected to repeated external loading. The theory of plasticity is a part of the broad and fascinating subject of mechanics of materials or continuum mechanics, which spans the spectrum from the fundamental aspects of elastic and inelastic behavior to the practical solution of engineering problems (Drucker, 1988). The phenomenon of cyclic plasticity, its impact on the design and analysis of mechanical systems, and its role in assessing integrity of structures, are well recognized (Chaboche, 1989a; Drucker, 1988; Ohno, 1990). Plastic deformation is difficult to avoid in many design situations. The elastic-plastic stress-strain response plays a pivotal role in the design and failure analyses of many components in practical applications.

Early studies of elastic-plastic deformation concentrated mainly on the monotonic and uniaxial loading conditions (Bairstow, 1911; Besseling, 1958; Budiansky, 1959; Coffin, 1960; Iwan, 1967; Kennedy; 1956; Krempl, 1969, Landgraf, 1970; Landgraf et al., 1969; Lazan, 1949; Manjoine, 1949; Masing, 1926; Morrow, 1964; Morrow and Sinclair, 1958; Prager, 1945). Recently, efforts have been directed toward cyclic multiaxial plasticity, both proportional and nonproportional (Benallal and Marquis, 1987a, 1987b; Benallal et al., 1989a, 1989b; Bower, 1987; Chaboche, 1986, 1987, 1989b, 1989c; Garud, 1981a, 1982, 1991; Hassan et al., 1992; Inoue et al., 1985, 1989, 1991; Lamba, 1976; Lamba and Siderbottom, 1978a, 1978b; Lebey and Roche, 1979; Lu and Mohamed, 1987; McDowell, 1981, 1983a, 1983b, 1985a, 1985b, 1985c, 1987, 1991, 1992; McDowell and Lamar, 1989; McMeeking, 1982; Mroz, 1967, 1969; Ohno, 1982; Ohno and Wang, 1991a, 1991c, 1993a, 1993b; Yamanouchi et al., 1976). Most researchers have concentrated on the strain-controlled tests where stress relaxation occurs with asymmetric cycling. In the past, experimental control capabilities have limited many researches to strain-controlled testing. The more complicated, yet, more general case of loading which involves ratchetting remains a challenge to the researchers in the field. Cyclic ratchetting refers to progressive and directional accumulation of strain in asymmetric load/stress controlled testing. Depending on the load magnitude and the initial material condition, the ratchetting deformation could result in tensile, compressive or shear failures.

The current interest in cyclic plasticity stems from the author's earlier work on rolling contact. The stress/strain state under rolling contact is multi-axial and nonproportional, representing one of the most complex analyses for a plasticity model. The consecutive deformation resulting from rolling contact will be accumulated, which could result in ratchetting failure of a component.

In this work, the cyclic plasticity of metals will be studied and the emphasis will be placed on the observation and modeling of the cyclic ratchetting phenomenon. The investigation is focused mainly on a critique and comparison of existing theories dealing with cyclic plasticity for loadings which involve ratchetting. The subsequent development of a new approach suitable for the stress/strain predictions under general multiaxial elastic-plastic loading conditions is compared to previous work and experimental results.

1.1. Objectives, Scope and Out-Line

A number of plasticity models have been developed. The first objective of this work is to determine how well the existing models of assessing cyclic plasticity compare with observations from laboratory tests. A literature survey is therefore undertaken with the purpose of critical examination and comparison of the cyclic plasticity theories. Details of this survey are given in Chapter 2 of this thesis. All the plasticity theories discussed are within the framework of unchanged yield surface shape and yield surface translation. Emphasis is placed on the recent plasticity models which are able to predict ratchetting. This review will be limited to room temperature applications in which effects of creep, temperature, and rate-dependence are negligible for the materials considered.

Any theoretical cyclic plasticity model should reflect experimental observations. Therefore, the second objective of this work is to explore ratchetting under various loading conditions. Some ratchetting phenomena not previously reported are observed and will be presented in Chapter 3. These experimental observations involve both uniaxial tension-compression and nonproportional multiaxial loading.

In order to describe the stress-strain response of a material under complicated cyclic loading, it seems logical to attempt to use the existing mathematical framework of incremental plasticity. An evaluation of some existing theories are undertaken and the results are presented in Chapter 4. Predictions obtained using the existing theories are compared with the experimental results. From the comparisons, it becomes clear that most of these

existing theories are unable to quantitatively model the long term ratchetting. Of all the theories evaluated, the model developed by Ohno and Wang (1991a, 1991c, 1993a, 1993b) is found to be the best model for predicting ratchetting. Some deficiencies with the Ohno-Wang model are pointed out.

The results of Chapter 4 lead to the pursuit of the third major objective: the development of a new plasticity model with the capability of quantitatively predicting cyclic ratchetting under general multiaxial nonproportional loading. The Ohno-Wang model is refined to accomplish this goal, and detailed derivation of the new model is presented in Chapter 5. A procedure to determine the material constants in the new model is forwarded in Chapter 6. Verification of the new model is discussed in Chapter 7. Improvements in the ratchetting predictions of the experimental results are achieved utilizing the new model. Finally, in the last chapter, the main conclusions of this investigation are listed along with recommendations for future work.

2. CONSTITUTIVE EQUATIONS FOR CYCLIC PLASTICITY: REVIEW OF LITERATURE

Plasticity models or constitutive equations are mathematical relations describing the stress-strain response of a material subjected to external loading. When developing the constitutive equations, some basic assumptions are always made. In general, the stress-strain response of a material is time dependent, strain rate dependent, path or history dependent, and temperature dependent. For most metals at or near room temperature subjected to repeated loading under isothermal conditions, it is sufficient as a first approximation to consider that path-dependent factors dominate the stress-strain response. These assumptions are carried forward throughout this research. In addition, it is assumed that the material is uniform, homogeneous, and initially isotropic.

Two classes of constitutive equations have been developed, based on one of the following thermodynamic concepts (Chaboche, 1989a).

1) The present state of the material depends only on the present and past values of observable variables, giving rise to hereditary theories.

2) The present state of the material depends only on the present values of observable variables and a set of internal state variables.

The first concept was used by Valanis (1971a, 1971b, 1980) in the development of the endrochronic theory, and by Krempl (1975) in his viscoplasticity formulation. The second approach has been developed in various ways, using the concept of yield surface in the case of rate-independent plasticity. Constitutive equations can be formalized in stress space, plastic strain space, or mixed stress/strain space (Klisinski *et al.*, 1992). This thesis will make use of the concept of yield surface and internal state variables to model the plastic deformation in stress space.

Because a number of existing plasticity models will be discussed throughout this work, name(s) after the major investigator(s) are given in order to facilitate discussion. To list all persons involved with a given theory would be impossible in many cases. Therefore, the case of a name given for a model is not intended to slight other investigators, but rather a convenience when referring repeatedly to a given theory.

2.1. Notations

A second order Cartesian tensor is denoted by a bold letter with a tilde below. The components of a tensor are denoted using the plain form of the same letter with subscript indices. A colon between two tensors denotes their inner (dot or scalar) product. For example, A_{ij} and B_{ij} are the components of the two tensors $\underset{\sim}{A}$ and $\underset{\sim}{B}$ respectively, then,

$$\underset{\sim}{A}:\underset{\sim}{B} = \sum_{i=1}^{3} \sum_{j=1}^{3} A_{ij} B_{ij} = A_{ij} B_{ij} \ . \tag{2.1}$$

Define one of the invariants of the tensor $\underset{\sim}{A}$ as,

$$|\underset{\sim}{A}| = \sqrt{\underset{\sim}{A}:\underset{\sim}{A}} \ . \tag{2.2}$$

The unit tensor is $\underset{\sim}{I}$, i.e.,

$$I_{ij} = \delta_{ij} \ , \tag{2.3}$$

where δ_{ij} is the Kronecker delta. A symbol with a bracketed subscript or superscript represents a number series instead of components of a tensor. For example, $c^{(i)}$ (i=1, 2, ..., M) represents a number series ranging from 1 to M, and $c^{(i)}$ along generally denotes the ith component of the number series. The prefix "d" is used to denote increment or differentiation. The prefix "Δ" denotes range. It is a common practice to refer to some of the tensors as "vectors", particularly in describing a hardening rule, although a tensor and a vector are not physically equivalent. This practice will be followed where convenient.

Conventional nomenclature is used from time to time. Because the loading cases of uniaxial loading and biaxial axial-torsion are the major topics of experimental cyclic plasticity, stresses and strains are often cited relative to a reference frame for a given specimen and testing machine. Customary symbols instead of tensorial expressions are used to describe the stress and strain quantities. The axial stress is denoted by σ and the corresponding plastic strain by ε^p. For biaxial axial-torsion, the shear stress, denoted by τ, refers the orthogonal shear stress on the plane perpendicular to the specimen axis. The shear strain is the engineering orthogonal shear strain, γ, which has a factor of two difference from the tensorial shear strain component. In the next section, the

basic framework of infinitesimal elastic theory and incremental plasticity theories will be reviewed to formalize the reader with the associated notation.

2.2. Basic Framework

2.2.1 Elastic Stress-Strain Relations and Plastic Strain Assumption

It is assumed in the theory of small deformations that the total strain can be decomposed additively into the elastic and plastic parts,

$$d\underline{\varepsilon} = d\underline{\varepsilon}^e + d\underline{\varepsilon}^p \ , \tag{2.4}$$

where $\underline{\varepsilon}$ denotes total strain, and $\underline{\varepsilon}^e$ and $\underline{\varepsilon}^p$ are the elastic and plastic strains respectively.

For the elastic part, it is assumed that Hook's Law is applicable,

$$d\underline{\varepsilon}^e = \frac{d\underline{\sigma}}{2G} - \frac{\mu}{E} (d\underline{\sigma}{:}\underline{I})\underline{I} \ , \tag{2.5a}$$

or,

$$d\varepsilon_{ij}^e = \frac{d\sigma_{ij}}{2G} - \frac{\mu}{E} d\sigma_{kk}\delta_{ij} \ . \tag{2.5b}$$

where $\underline{\sigma}$ is the stress tensor, E is Young's modulus of elasticity, G is the linear modulus of elasticity in shear, and μ is Poisson's ratio. For a homogeneous isotropic material the three constants are not independent and are related as follows: The elastic shear modulus, G, is given in terms of Young's modulus, E, and Poisson's ratio, μ, by,

$$G = \frac{E}{2(1+\mu)} \ . \tag{2.6}$$

It should be noted that a material which has been subjected to plastic deformation is no longer isotropic. Young's modulus, E, and Poisson's ratio, μ, are not constants. However, the anisotropy introduced by small plastic deformation has minimal influence on the elastic properties. Therefore, in the practical applications, E and μ are generally assumed to be constant.

The plastic incompressibility is assumed, i.e.,

$$d\underline{\varepsilon}^p : \underline{I} = 0 \ . \tag{2.7}$$

2.2.2. Yield Function

The material is assumed to follow the elastic stress-strain relations with zero plastic strains until the stresses satisfy the yield condition. The two most commonly used yield conditions are due to Tresca (maximum shear stress criterion) and von Mises (distortion energy criterion). The von Mises yield function is used throughout this work,

$$f = (\underline{S} - \underline{\alpha}):(\underline{S} - \underline{\alpha}) - 2k^2 = 0 \ , \tag{2.8}$$

where $\underline{S}$ is the deviatoric stress tensor,

$$\underline{S} = \underline{\sigma} - \frac{1}{3}(\underline{\sigma}:\underline{I})\,\underline{I} \ , \tag{2.9a}$$

or,

$$S_{ij} = \sigma_{ij} - \frac{1}{3}\sigma_{kk}\delta_{ij} \ . \tag{2.9b}$$

The quantity $\underline{\alpha}$ is the deviatoric backstress (center of the yield surface) and k is the yield stress in simple shear. The shape of the yield surface is generally assumed unchanged; however the size of the yield surface can be adapted to account for the transient behavior by allowing k to vary. It is also assumed that the yield surface can translate but cannot rotate. A schematic representation of the yield surface and the yield surface translation is shown in Figure 2.1.

2.2.3. Flow Rule

A flow rule is used to relate the increment of plastic strain and the increment of stress. The most commonly used rule for metals is known as the associated flow rule or the normality condition (Drucker, 1951, 1960). According to this postulate the plastic strain increment is collinear with the exterior normal to the yield surface at the present stress state. The normality condition mathematically can be expressed as,

$$d\underline{\varepsilon}^p = \frac{1}{h}\,\langle d\underline{S}:\underline{n}\rangle\,\underline{n} \ , \tag{2.10}$$

where $\langle\rangle$ denotes the MacCauley bracket (i.e., $\langle x\rangle = \frac{1}{2}(x + |x|)$). The unit exterior normal, $\underline{n}$, on the yield surface at the loading point is defined as,

$$\underline{n} = \frac{\underline{S} - \underline{\alpha}}{|\underline{S} - \underline{\alpha}|} , \tag{2.11}$$

and h is a scalar function often called the plastic modulus function. Under uniaxial loading, $h = \frac{2}{3} \frac{d\sigma}{d\varepsilon^p}$, where σ and ε^p are the axial stress and axial plastic strain respectively.

2.2.4. Consistency Condition

During elastic-plastic deformation a consistency condition should be satisfied. The consistency condition requires that the stress state should lie on the yield surface during elastic-plastic deformation, which can be expressed mathematically as,

$$df = 0 , \tag{2.12a}$$

or modifying Equation (2.12a),

$$d\underline{S} : \underline{n} - d\underline{\alpha} : \underline{n} - \sqrt{2}\, dk = 0 . \tag{2.12b}$$

When there is no change in the size of the yield surface (i.e., dk = 0), the previous equation can be expressed as,

$$d\underline{S} : \underline{n} = d\underline{\alpha} : \underline{n} . \tag{2.13}$$

Equation (2.13) implies that the projection of the backstress increment onto the normal direction is identical to the projection of the stress increment onto the same direction during elastic-plastic loading. From the flow rule, Equation (2.10), and the consistency condition, Equation (2.12), the plastic modulus function can be derived,

$$h = \frac{\underline{n} : d\underline{\alpha}}{dp} + \sqrt{2} \frac{dk}{dp} , \tag{2.14}$$

where the equivalent plastic strain increment, dp, is defined as follows,

$$dp = \sqrt{d\underline{\varepsilon}^p : d\underline{\varepsilon}^p} . \tag{2.15}$$

Equation (2.14) is used to determine the plastic modulus function, h, when the evolution of the backstress and the yield stress have been specified.

2.2.5. Hardening Rules

While the framework for most cyclic incremental plasticity models is the same for the previous sections, it is generally the hardening rule that distinguishes one plasticity model from another. A hardening rule specifies changes in the yield condition as a result of loading the material. Under the framework of kinematic yield function, a hardening rule specifies the translation of the yield surface, or, the evolution of the backstress.

The backstress in deviatoric space can be treated as a vector. Therefore, in this reference frame the backstress increment has both magnitude and direction. The plastic modulus function, h, is related to the backstress increment by Equation (2.14). That is to say that for the three variables, the direction of the backstress increment, the magnitude of the backstress increment, and the plastic modulus function, there are two independent variables. A hardening rule can either specify the direction of the backstress increment and the plastic modulus function, or both the direction and magnitude of the backstress increment. A more through review of hardening rules will occur in subsequent section.

2.3. Terminology

In order to avoid ambiguity, some frequently quoted terminology are defined below.

1. <u>Proportional and nonproportional loading</u>: Since the plasticity theories will be discussed in a stress based space, proportional loading is defined as the loading corresponding to a fixed radial line in the deviatoric stress space throughout the entire loading history. Any loading paths other than the proportional loading are nonproportional loading. This definition is different from that used by Kanazawa *et al.*(1979), Lamba (1976), Lamba and Sidebottom (1978a, 1978b), and McDowell (1983a, 1983b) who defined the proportional loading as the loading for which the total strain rate is radial and fixed in direction in the strain space.

2. <u>Active Loading and Elastic Unloading</u>: Elastic unloading refers to the loading region where the deformation is entirely elastic. From the viewpoint of yield surface, elastic unloading corresponds to the loading where the stress state is within the yield surface. When plastic deformation is involved, the loading is

called active loading for simplicity. Active loading corresponds to the loading where the stress state is on the yield surface. It should be noted that, in general, elastic deformation will occur simultaneously during active loading.

3. <u>Balanced and Unbalanced Loading</u>: Balanced loading refers to the loading under which a virgin material initially isotropic will undergo no ratchetting and/or mean stress relaxation. Unbalanced loading is that the loading under which a virgin material initially isotropic will produce strain ratchetting and/or stress relaxation.

4. <u>Cyclic Hardening/Softening</u>: Material properties that stabilize with cyclic loading history. These properties are often identified with the changes of stress response for constant amplitude strain-controlled tests. Cyclic hardening/softening behavior is asymptotic for most wrought metals with increased cycling.

2.4. Review of Literature
2.4.1. Linear Hardening Rule

Using only the isotropic hardening rule, which allows for uniform expansion of the yield surface, is considered unsuitable for applications involving cyclic loading because it does not mimic the Bauschinger effect commonly observed under reversed loading. With the primary aim of modeling the Bauschinger effect, Prager (1955) proposed the kinematic hardening rule which allows the yield surface to translate without changing its shape and size. The condition that the yield surface remains the same size implies that k is a constant in Equations (2.8) and (2.12b). This rule was subsequently modified by Ziegler (1959) and Shield and Ziegler (1958) to eliminate inconsistencies when applying the rule in a stress subspace. According to Ziegler (1959) the direction of translation of the yield surface is given by the vector joining its center and the stress point on the yield surface (Figure 2.1). Once the translation direction has been assumed, the consistency condition (Equation (2.12)) determines the magnitude of the translation. Mathematically the translation of the center of the yield surface can be expressed as,

$$d\underline{\alpha} = a_p \, d\underline{\varepsilon}^p \, ,$$
(2.16)

where a_p is in general a scalar function of the stress and plastic strain state. This relationship is often called the linear hardening rule, because of the linear

dependence of the translation increment of the yield surface on the plastic strain increment. Combining Equation (2.14) with Equation (2.16) leads to the following relationship for the plastic modulus function,

$$h = a_p + \sqrt{2}\frac{dk}{dp} \ .$$

(2.17)

According to the aforementioned derivation, a_p should be defined such that the plastic deformation can be fully determined. If a_p is assumed to be a constant, Equation (2.16) is corresponding to a bilinear stress-strain relation for uniaxial tension-compression when the yield stress is a constant. Alternatively, Drucker and Palgen (1981) related a_p to the second deviatoric stress invariant in an attempt to model ratchetting.

When both k and a_p are constants, the linear hardening rule predicts no ratchetting for the proportional loading, which leads to the common misconception that it is also true for nonproportional loading. The linear hardening rule will produce transient ratchetting for the nonproportional loading during the first few cycles, which depends on the loading path and magnitude. When the loading magnitude is equal to the shakedown limit, the predicted transient ratchetting can last dozens loading cycles before arresting (Jiang and Sehitoglu, 1993d). If the plastic modulus function is expressed as a function of the second deviatoric stress invariant (Drucker and Palgen, 1981), a constant ratchetting rate is predicted for both proportional and nonproportional stress-controlled unbalanced loading. The ratchetting rate predicted is generally much larger than the experimental results (Hassan et al., 1991, 1992; Jiang and Sehitoglu, 1993d). It has been demonstrated that the Prager-Ziegler rule does not correlate with experimental data for nonproportional cyclic loading (Lamba and Sidebottom, 1978a, 1978b; McDowell, 1981, 1983a). Further studies by McDowell (1985c) and Jiang and Sehitoglu (1993a) indicate that the experimental translation direction of the yield surface is different from the normal to the yield surface at the stress point for nonproportional loading.

2.4.2. Armstrong-Frederick Type Hardening Rules

Armstrong and Frederick (1966) developed a nonlinear kinematic hardening relation, introducing a recovery term associated to a strain memory effect. This term modifies the translation of the yield surface,

$$d\underset{\sim}{\alpha} = a_a \, d\underset{\sim}{\epsilon}^p - c_a \, \underset{\sim}{\alpha} \, dp \;,$$

(2.18)

where a_a is a constant, c_a is some scalar function of the plastic strain path, and dp remains as defined in Equation (2.15). Combining Equation (2.14) with Equation (2.18) results in the following expression for the plastic modulus function,

$$h = a_a - c_a \, \underset{\sim}{n}{:}\underset{\sim}{\alpha} + \sqrt{2} \, \frac{dk}{dp} \;.$$

(2.19)

With the introduction of a nonlinear term (recovery term), this model renders constant strain rate ratchetting under constant amplitude stress-controlled loading. Generally this model leads to large overestimations of ratchetting (Dafalias, 1981; Inoue *et al.*, 1985, 1989, 1991; Ohno and Wang, 1993b). For most metals a constant ratchetting rate is not observed (Bower, 1987; Kurath, 1992; McDowell, 1991; Moyar and Sinclair, 1962, 1963). From Equation (2.19) it is clear that under uniaxial tension-compression the relationship between the plastic modulus and the axial stress is linear, which, in general, differs from the experimental stress-strain response. With only two material constants (a_a and c_a) this model is unable to describe the stress-strain hysteresis loop accurately. Burlet and Cailletaud (1987) added one more term to equation (2.18) to consider the multiaxial ratchetting, and improved predictions were reported. However, this added term is effective only under nonproportional loading (Ohno, 1990).

Bower (1987, 1989) and Bower and Johnson (1989) modified the Armstrong-Frederick rule by adding one more internal state variable,

$$d\underset{\sim}{\alpha} = a_b \, d\underset{\sim}{\epsilon}^p - c_{b1} \left(\underset{\sim}{\alpha} - \underset{\sim}{\beta} \right) dp \;,$$

(2.20a)

and,

$$d\underset{\sim}{\beta} = c_{b2} \left(\underset{\sim}{\alpha} - \underset{\sim}{\beta} \right) dp \;.$$

(2.20b)

An additional internal state variable, $\underset{\sim}{\beta}$, has been introduced, which has an initial value of zero. The quantities a_b, c_{b1}, and c_{b2} are material constants. Similar to the nonlinear term, $c_a \, \underset{\sim}{\alpha}$, in the Amstrong-Frederick rule (Equation (2.18)), the term $c_{b1} \left(\underset{\sim}{\alpha} - \underset{\sim}{\beta} \right)$ in Equation (2.20a) serves as the driving force for ratchetting in the Bower model. Noting that $d\underset{\sim}{\beta}$ is proportional to $\left(\underset{\sim}{\alpha} - \underset{\sim}{\beta} \right)$, under the stress-controlled uniaxial tension-compression with non-zero mean stress, $c_{b1} \left(\underset{\sim}{\alpha} - \underset{\sim}{\beta} \right)$

decreases with the number of loading cycles. Therefore, this model is able to predict ratchetting rate decay (Bower, 1987, 1989; Bower and Johnson, 1989). When $c_{b2}=0$ the model reverts to the Armstrong-Frederick relation. However, the Bower model cannot describe the basic cyclic stress-strain curve accurately. Also it can predict the ratchetting rate decay only for a limited number of cycles, after which it predicts ratchetting arrest (Jiang and Sehitoglu, 1993a).

Nonlinear hardening rules based on the Amstrong-Frederick relation have been expressed in the form of a series expansion of the backstress. It was postulated (Chaboche *et al.*, 1979; Chaboche, 1987) that the total backstress is composed of additive parts,

$$\underset{\sim}{\alpha} = \sum_{i=1}^{M} \underset{\sim}{\alpha}^{(i)} \ , \tag{2.21}$$

where $\underset{\sim}{\alpha}$ is the total backstress, $\underset{\sim}{\alpha}^{(i)}$ is a part of the total backstress, i=1, 2, ..., M, and M is the number of backstress parts considered. Each backstress part follows an Amstrong-Frederick type relation,

$$d\underset{\sim}{\alpha}^{(i)} = c^{(i)} \left(r^{(i)} \, d\underset{\sim}{\varepsilon}^p - W^{(i)} \, \underset{\sim}{\alpha}^{(i)} \, dp \right) \qquad (i=1, 2, ..., M) \ , \tag{2.22}$$

where $c^{(i)}$ and $r^{(i)}$ are material constants associated with the ith part of backstress $\underset{\sim}{\alpha}^{(i)}$, and $W^{(i)}$ is a function of stress state (Moosbrugger and McDowell, 1989; McDowell, 1992). From Equation (2.14), the plastic modulus function is,

$$h = \sum_{i=1}^{M} c^{(i)} \left(r^{(i)} - W^{(i)} \underset{\sim}{\alpha}^{(i)} \! : \! \underset{\sim}{n} \right) + \sqrt{2} \frac{dk}{dp} \ . \tag{2.23}$$

Chaboche *et al.*'s (1979) initial model can be represented by $W^{(i)} = 1$, and Equation (2.22) takes the following form,

$$d\underset{\sim}{\alpha}^{(i)} = c^{(i)} \left(r^{(i)} \, d\underset{\sim}{\varepsilon}^p - \underset{\sim}{\alpha}^{(i)} \, dp \right) \qquad (i=1, 2, ..., M) \ . \tag{2.24}$$

Under asymmetric uniaxial loading this model predicts a ratchetting rate decay response consistent with experiments, but the duration of the transient response is short-lived. Subsequently, the model predicts a constant ratchetting rate (Jiang and Sehitoglu, 1993a).

Mroz (1981, 1983) discussed the Armstrong-Frederick rule and pointed out that the scalar function c_a in Equation (2.18) would depend on the magnitude of the backstress and might vanish for values less than some critical value. A recent model by Chaboche *et al.* (1991) introduced a threshold term,

$$W^{(i)} = \left\langle 1 - \frac{\xi^{(i)}}{\alpha^{(i)} : \alpha^{(i)}} \right\rangle \qquad (i=1, 2, ..., M) , \qquad (2.25)$$

where $\xi^{(i)}$ is the threshold level for dynamic recovery of the *i*th backstress $\alpha^{(i)}$. When $\alpha^{(i)}$ is below a certain level, $W^{(i)}$ will be zero and the kinematic hardening is linear. A backstress exceeding the critical value will result in $0 \leq W^{(i)} \leq 1$, and the kinematic hardening is then nonlinear. The initial Chaboche model, Equation (2.24), is characterized by $W^{(i)}=1$, and because the nonlinear term in Equation (2.22) is the driving force for ratchetting, it can be concluded that the introduction of the threshold, Equation (2.25), will make the model predict less ratchetting than the model without the threshold.

Ohno and Wang (1991a, 1991c, 1993a, 1993b) proposed two different threshold concepts,

Ohno-Wang I

$$W^{(i)} = H(g^{(i)}) \left\langle \underline{n} : \underline{L}^{(i)} \right\rangle \qquad (i=1, 2, ..., M) , \qquad (2.26)$$

Ohno-Wang II

$$W^{(i)} = \left(\frac{| \underline{\alpha}^{(i)} |}{r^{(i)}} \right)^{\chi^{(i)}} \left\langle \underline{n} : \underline{L}^{(i)} \right\rangle \qquad (i=1, 2, ..., M) . \qquad (2.27)$$

H is the Heaviside step function (i.e., $H(x)=1$ if $x \geq 0$ and $H(x)=0$ if $x<0$) and $\chi^{(i)}$ (i=1, 2, ..., M) are material constants. Other terms in Equations (2.26) and (2.27) are defined as follows,

$$\underline{L}^{(i)} = \frac{\underline{\alpha}^{(i)}}{| \underline{\alpha}^{(i)} |} \qquad (i=1, 2, ..., M) , \qquad (2.28)$$

$$| \underline{\alpha}^{(i)} | = \sqrt{\underline{\alpha}^{(i)} : \underline{\alpha}^{(i)}} \qquad (i=1, 2, ..., M) , \qquad (2.29)$$

and,

$$g^{(i)} = | \underline{\alpha}^{(i)} | - r^{(i)} \leq 0 \qquad (i=1, 2, ..., M) . \qquad (2.30)$$

$\underline{L}^{(i)}$ is the unit vector and $\left|\underline{\alpha}^{(i)}\right|$ is the magnitude of a backstress. $g^{(i)} = 0$ represents a surface in the deviatoric stress space, which is centered at the origin with a radius of $r^{(i)}$. According to Equation (2.30), $\left|\underline{\alpha}^{(i)}\right| \leq r^{(i)}$, therefore the Ohno-Wang Model I, Equation (2.26), can be treated as the special case of Ohno-Wang Model II, Equation (2.27), for $\chi^{(i)} = +\infty$ (Ohno and Wang, 1993a).

A graphic illustration of this hardening rule is shown in Figure 2.2. In the Ohno-Wang models each backstress $\underline{\alpha}^{(i)}$ is either within or on a limiting surface $g^{(i)} = 0$. For the Model I, Equation (2.26), when a backstress is within its limiting surface, $g^{(i)} < 0$ and $H(g^{(i)}) = 0$, then $W^{(i)} = 0$, which results in linear hardening according to Equation (2.22). For the Ohno-Wang model II, if $\chi^{(i)}$ becomes a large number, then $W^{(i)}$ is approximately zero when $\underline{\alpha}^{(i)}$ is within the limiting surface. As a result, the hardening corresponding to $\underline{\alpha}^{(i)}$ is approximately in the direction of $\underline{n}$ in Figure 2.1. When $\underline{\alpha}^{(i)}$ is on the limiting surface (i.e., $g^{(i)} = 0$), the model predicts $d\underline{\alpha}^{(i)} \cdot \underline{n} = 0$, irrespective of the selection of $\chi^{(i)}$. This implies that when $\underline{\alpha}^{(i)}$ is on the limiting surface the translation direction of this backstress will be in the tangential direction to the limiting surface and the backstress will not go out of its limiting surface.

The Ohno-Wang Model I, Equation (2.26), predicts a perfect hysteresis loop closure for proportional loading and therefore is generally not appropriate for ratchetting prediction. The constants $\chi^{(i)}$ (i=1, 2, ..., M) control both the rate and direction of the ratchetting predicted using the Ohno-Wang model II. With appropriate selection of the material constants, the Ohno-Wang model II can provide ratchetting predictions in close agreement with the experimental results, better than the previously discussed methodologies. Demonstration and discussion on the $\chi^{(i)}$ influence will be presented in the following chapter. In subsequent discussions the terminology Ohno-Wang model refers to the Ohno-Wang model II.

2.4.3. Mroz Multiple Surface Type Models

For the purpose of modeling the observed stress-strain response of a material under cyclic loading, Mroz (1967, 1969) introduced the concept of a field of plasticity moduli. It is a generalization of the uniaxial stress-strain curve in the sense that instead of using only one point such as the elastic limit, several points are selected on the uniaxial stress-strain curve (refer to Figure 2.3). Corresponding to each point, a surface in the stress space is defined to be geometrically similar to the initial yield surface. Mroz postulated that these

surfaces define regions in the stress space, each having a constant plastic modulus function. Incidentally, Iwan (1967) proposed a similar multiple surface model to consider the Bauschinger effect for Masing type materials.

Using his concept of the field of plastic moduli, Mroz (1967, 1969) proposed that the translation direction of a surface is given by the vector joining the present state of stress P on the ith surface with the state of stress P' on the $(i+1)$th surface such that the two surfaces have a common exterior normal $\underline{n}$ (see Figure 2.4). Without considering the surface size changes, the Mroz hardening rule can be expressed in the following form,

$$d\underline{\alpha}^{(i)} = \frac{d\underline{S}:\underline{n}}{\underline{v}:\underline{n}} \; \underline{v} \; ,$$

(2.31)

with the vector quantity, $\underline{v}$, defined as,

$$\underline{v} = \sqrt{\frac{2}{3}} \left(R^{(i+1)} - R^{(i)} \right) \underline{n} + \underline{\alpha}^{(i+1)} - \underline{\alpha}^{(i)} \; ,$$

(2.32)

where $\underline{\alpha}^{(i)}$ and $R^{(i)}$ represent the center and radius of the ith surface respectively. The term $\underline{\alpha}^{(i)}$ is the backstress of the ith surface at the current stress state. The interpretation of $\underline{\alpha}^{(i)}$ for a Mroz type model differs from the Armstrong-Frederick concept.

Garud (1981a, 1981b, 1982), in examining hardening rules, found that the translation direction of the yield surface according to both the Mroz and Prager-Ziegler rules was independent of the stress increment, and this independence would create an inconsistency problem in the finite stress increment calculation. In order to avoid this possible inconsistency, Garud proposed a new hardening rule that related the surface translation direction to the stress increment direction. Referring to Figure 2.5, if the stress increment were so large that it joined point P on the ith surface and P' on the $(i+1)$th surface, so that the two surfaces were tangential on point P' where the ith surface had its center on O'_i, the translation direction of the ith surface is in the direction of the vector joining O_i and O'_i, and the magnitude of translation is determined by a consistency condition. After the point P' is determined, the unit normal at P' can be calculated. The vector joining point P and point P' can be expressed as,

$$\underline{v}' = \sqrt{\frac{2}{3}} \left(R_{(i+1)} - R_{(i)} \right) \underline{n}' + \underline{\alpha}_{(i+1)} - \underline{\alpha}_{(i)} \; ,$$

(2.33)

where $\underline{n}'$ is the unit normal at point P' which is called the incremented stress state. Similar to Equation (2.31), the translation of the ith surface is,

$$d\underline{\alpha}^{(i)} = \frac{d\underline{S}:\underline{n}'}{\underline{\dot{v}}:\underline{n}'} \underline{\dot{v}} \ . \tag{2.34}$$

Because the surface does not rotate, the vector joining $O'_{(i)}$ and $O_{(i)}$ is geometrically identical to the vector joining P' and P'' (refer to Figure 2.5). Other than the prime notation, both sets of equations for the Mroz and Garud hardening rules seem similar. Clearly the only difference between the Garud rule and the Mroz rule is that the translation direction in the Mroz rule is determined by the normal $\underline{n}$ of the current stress state while in the Garud rule the translation direction is determined by the normal $\underline{n}'$ of the incremented stress state.

The Mroz/Garud model can accurately duplicate the Bauschinger effect for proportional loading, and was found to be superior to the Prager-Ziegler rule when predicting the stress response under the multiaxial strain-controlled loading conditions (Hunsaker et al., 1976; Lamba, 1976; Lamba and Sidebottom, 1978a, 1978b; McDowell, 1983a). The Mroz/Garud model does not predict ratchetting for any proportional loading. However, this multiple surface model predicts ratchetting for general nonproportional loading (Garud, 1991). The constant ratchetting rate predicted by Mroz/Garud type models for the nonproportional loading never decays, and hence the predicted ratchetting strains are often larger than the experimental results.

In discussing Mroz/Garud multiple surface relations, it has been always taken for granted that (i) the surfaces be tangential on the point of stress state, and (ii) in the course of translation the surfaces will never intersect. McDowell (1989) discussed the possible surface intersection for the two-surface plasticity theory. Actually, this can be theoretically proven to be true (Jiang and Sehitoglu, 1993d) for an infinitesimal loading increment. Referring to Figure 2.4 and Figure 2.5, when the stress state reaches point P', both the Mroz and Garud rules predict that the ith surface and $(i+1)$th surface will be tangential at point P'. Clearly, when the number of surfaces is large enough, these two models will result in identical stress-strain predictions. Because the translation direction of a surface is dependent on the relative positions of the consecutive surfaces, it becomes evident that the number of surfaces employed has an influence on the surface

translations, hence on the predicted results. The implication of the Mroz/Garud multiple surface rules will be discussed further later in the text.

Mroz (1981, 1983) discussed the similarity between the multiple surface rules and the Armstrong-Frederick type rules. Ohno and Wang (1991b) and Wang and Ohno (1991) further formalized the relationship between the Mroz multiple surface type hardening rules and Armstrong-Frederick type hardening rules. The Armstrong-Frederick type hardening rules were explained using a multiple surface concept. However, the translations of the surfaces do not follow the Mroz or Garud hardening rules. The differences between the two types of hardening rules are reflected in the predictions for nonproportional loading.

To reduce the computational time involved with the Mroz type model, two surface plasticity models, a yield surface and a bounding surface, were developed. The translation of the yield surface follows either the Mroz hardening rule (Dafalias, 1981; Dafalias and Popov, 1975, 1976; Krieg, 1975, Voyiadjis and Sivakumar, 1991), Equations (2.31) and (2.32), or Garud hardening rule (Tsing and Lee, 1983), Equations (2.33) and (2.34). Generally there is a nonlinear hardening relationship that occurs between these two surfaces. The plastic modulus function was taken as a function of a "distance" between the yield surface and bounding surface. This "distance" can be represented by Mroz distance, $|\underline{v}|$ (Dafalias and Popov, 1975, 1976; Krieg, 1975), Garud distance, $|\underline{v}'|$ (Tsing and Lee, 1983), Prager-Ziegler distance (the distance between the two surfaces in the normal direction to the yield surface at the stress state), or the second invariant of the deviatoric stress (Jiang and Sehitoglu, 1993c). Successful modeling has been achieved using the two-surface models (Bruhns and Pape, 1989; Bruhns et al., 1992; Chaboche, 1989b; Chang and Lee, 1986b; Iwata, 1991; Lu and Mohamed, 1987; McDowell, 1985a, 1985b, 1985c; Moosbrugger and McDowell, 1990; Takahashi and Ogata, 1991; Tanaka et al., 1987; Tsuji, 1989) for the proportional and nonproportional strain-controlled loading. On the other hand, Hashiguchi (1988, 1993a, 1993b) discussed the basic characteristics of the multiple surface and two surface models and pointed out the mechanical requirements that those models should satisfy.

Two surface models exhibit constant ratchetting rate, and the direction is always consistent with the mean stress direction for proportional loading. These results contrast to the decay of ratchetting rate and possible non-coincidence of ratchetting direction with the mean stress observed in multiple step loading experiments. Generally, the two surface plasticity theory cannot fundamentally

correlate cyclic strain accumulation under proportional and nonproportional loading over a variety of amplitudes and mean stresses (McDowell, 1992).

2.5. Transient Behavior

2.5.1. Cyclic Hardening

Traditional hardening rules are basically useful for the description of a stabilized stress-strain state. The transient cyclic behavior of a material often needs separate consideration. Transient behavior is often identified by the experimental stress-strain response under balanced loading, particularly under fully reversed and strain-controlled uniaxial tension-compression. For example, under the strain-controlled balanced loading, the stress amplitude changes with time, and saturates with loading history. This phenomenon is often referred to as cyclic hardening/softening.

Two methods can be used to describe the cyclic hardening/softening. The first method considers the cyclic hardening/softening through change in the yield strength as a function of the equivalent plastic strain or the accumulative plastic strain energy density. A relation between the size of the yield surface and the equivalent plastic strain can be (Chaboche et al., 1979),

$$dk = b_k (Q - k) dp , \qquad (2.35a)$$

where b_k and Q are constants. With an initial value $k = k_0$, integrating Equation (2.35a) results in,

$$k = Q - (Q - k_0) \exp(-b_k p) , \qquad (2.35b)$$

where Q is the stabilized yield strength.

The other method considers the hardening by changing the hardening modulus in the kinematic evolution. For instance, one can consider $c^{(i)}$ and $r^{(i)}$ in Equation (2.24) as functions of the equivalent plastic strain instead of constants. Marquis (1979) expressed Equation (2.24) as,

$$d\underline{\alpha}^{(i)} = a^{(i)} d\underline{\varepsilon}^p - \Phi(p) c^{(i)} \underline{\alpha}^{(i)} dp \qquad (i=1, 2, ..., M) , \qquad (2.36)$$

with the following expression for $\Phi(p)$,

$$\Phi(p) = \Phi_\infty + \left(1 - \Phi_\infty\right) e^{-\omega p} , \qquad (2.37)$$

where $a^{(i)}$ (i=1, 2, ..., M), $c^{(i)}$ (i=1, 2, ..., M), Φ_∞, and ω are constants.

As schematically shown in Figure 2.6 for the uniaxial tension-compression case, a material may display cyclic hardening, softening, or a combined hardening and softening. For convenience during the aforementioned discussion, H, the plastic modulus of the stress-plastic strain loop, is plotted as a linear function of the stress range, $\Delta\sigma$, although this is not necessary for the validity of the arguments forwarded. The first method is simple and can be conveniently incorporated into a hardening rule. When a Mroz or Armstrong-Frederick type model is employed, H-$\Delta\sigma$ curves parallel to the initial cycle (Figure 2.6) will result. However, for the two-surface models, since hardening is determined by the distance between the two surfaces, the change in yield surface size will also alter the hardening modulus. For the case of two-surface models, parallel lines will not occur. In general, change of the yield surface size alone cannot properly describe the cyclic hardening of many different materials. This is especially true for the single crystal copper (Mughrabi, 1978; Winter, 1974). The second method, Equations (2.36) and (2.37), is appropriate for the consideration of the monotonic hardening or softening, but unable to consider the combined hardening/softening. For any of the plasticity models previously discussed, the assumption of Equations (2.36) and (2.37) results in non-parallel lines in Figure 2.6. Mixed behavior modeling can be achieved by adding one more term in Equation (2.37).

In considering the cyclic hardening, McDowell (1992) and Moosbrugger and McDowell (1989, 1990) combined the concepts of Equations (2.35) and (2.36). They assumed that the yield stress was a functional of the equivalent plastic strain increment and $r^{(i)}$ (i=1, 2, ..., M) within the framework of Equation (2.22) were functions of the equivalent plastic strain. This combination provides a better description of the cyclic hardening behavior for steels.

2.5.2. Plastic Strain Range Effect: Memory Surface

Several investigations show that the asymptotic stress value of cyclic hardening can be dependent on the prior history, especially in stainless steel (Chaboche et al., 1979). This influence of plastic strain range on the stabilized cyclic response is evident from the comparison between the different methods used to obtain the cyclic curve (Chaboche, 1989). Experimental observation of non-Masing behavior is an indicator of such memory effects. Another example

of the memory effects of prior loading history is the stress level influence on ratchetting, which Chaboche and Nouailhas (1989a, 1989b) referred to as "quasireversed" (small mean stress) versus "quasirepeated" (large mean stress).

Basic kinematic and isotropic variables are not able to describe the plastic strain memory effects: kinematic hardening is stable in nature and isotropic hardening saturates towards a unique value (Chaboche, 1989). In order to formulate a model with plastic strain memory, Chaboche et al. (1979) introduced a new internal variable to track prior deformation. The concept uses a memory surface in the plastic strain space, which Ohno (1982) and Ohno and Kachi (1986) called the cyclic non-hardening range. This memory surface (Chaboche et al., 1979) can translate and expand in the plastic strain space, and the radius of this memory surface represents the maximum plastic strain range of the entire loading history. The yield stress and hardening behavior are related to this memory surface. When the plastic strain state is within the memory surface, the yield strength will not change (non-hardening). McDowell (1985a) incorporated a recovery term in the evolution equation of the surface, allowing contraction of the memory surface when the plastic strain is within the memory surface.

A memory surface was also introduced in the stress space to memorize the maximum backstress of the prior history (Chaboche, 1989; Mroz, 1981, 1983; Mroz and Trampczynski, 1984). Bruhns and Pape (1989) and Bruhns et al. (1992) used a similar memory surface in stress space to consider the transient behavior in the framework of a two-surface model. The transient cyclic behavior was modeled by altering the yield stress, which was assumed to be directly dependent on the size of the memory surface. The memory surface introduced by Bruhns et al. differs from those of Chaboche et al. (1979) and Ohno (1982) in that the former allows the memory surface to contract when a higher loading level is followed by a lower one. The experimental observations under multiple step loading (Tanaka et al., 1985a) and non-Masing behavior (Abdel-Raouf et al., 1977; Bayerlein et al., 1987; Li and Laird, 1993; Mughrabi, 1978; Winter, 1974) reveal that the memory of a previous higher loading amplitude fades with the subsequent number of loading cycles, suggesting that the ability for a memory surface to contract is necessary for the description of the transient behavior in many materials. The non-Masing behavior is more likely controlled by a maximum stress instead of stress/strain range. Furthermore, from the ratchetting experiments under multiple step loading, it becomes clear that a

strain parameter may not be appropriate (Jiang and Sehitoglu, 1993d) for the consideration of stress level effect on ratchetting.

2.5.3. Nonproportionality Effect

It has been well recognized since the experimental work of Lamba (1976) and Lamba and Sidebottom (1978a, 1978b) that nonproportional loading results in a higher resistance to plastic flow than does the proportional loading (Benallal and Marquis, 1978a, 1978b; Benallal et al., 1988, 1989a, 1989b; Benallal et al., 1989; Cailletaud et al., 1984; Kanazawa et al., 1979; Krempl and Lu, 1983, 1984; McDowell, 1983a, 1985a, 1985b; McDowell and Socie, 1985; Ning and Xu, 1991; Nouailhas et al., 1983; Ohashi et al., 1985a, 1985b; Tanaka et al., 1985a, 1985b). Experimentally the nonproportionality effect is observed via two related aspects: that under nonproportional loading the stabilized equivalent stress is higher, and hence the transient cyclic hardening is more significant than under proportional loading. Some stainless steels display more remarkable nonproportional hardening than other materials. This hardening was explained by increased dislocation interaction due to nonproportional loading (McDowell, 1983a; Doong, 1989; Doong and Socie, 1991). Different approaches have been proposed to describe such effects (Benallal et al., 1985; Krempl and Yao, 1987; Lindholm et al., 1984; McDowell, 1985a, 1987; Nouailhas et al., 1984; Tanaka et al., 1987). They are generally based on some proportional/nonproportional loading indices. A simple and powerful approach was proposed by Benallal and Marquis (1987a, 1987b) and Benallal et al. (1988, 1989a), who used sin θ (refer to Figure 2.1 for θ) as a measure of nonproportionality. The effect interacts with the flow rule by increasing the yield stress. Benallal et al. (1988, 1989a) observed from experiments that mean strain does not affect cyclic hardening even under nonproportional loading with a material that displays a memory effect. The strain based parameters for considering the nonproportionality, such as those by Krempl and Yao (1987), and McDowell (1985a, 1987) would predict a mean strain effect even though their experiments were conducted with balanced loading.

2.5.4. Cross-Hardening Effect

The cross-hardening effect usually refers to the phenomenon of a sudden increase in the stress response observed when the strain-controlled loading is changed from one "proportional" (note the different definitions for proportional loading) path to another (Benallal and Marquis, 1987b; Cailletaud et al., 1984;

Chang and Lee, 1986a; Krempl and Lu, 1984, 1989; McDowell, 1983a; Ohashi *et al.*, 1985; Tanaka *et al.*, 1985b). This effect is very significant for some stainless steels like Type 316. Experimentally, the first proportional loading is allowed to stabilize. If a second "proportional" path with identical equivalent strain amplitude is then chosen, the initial equivalent stress will be higher than the previous stabilized state, but will soften to the level typical for that equivalent strain range without prior loading (Benallal and Marquis, 1987b; Benallal *et al.*, 1987b). Further experimental efforts to model this cross-hardening effect have been performed by McDowell (1983a) and Doong (1989).

Within the basic framework of plasticity (refer to Figure 2.1), it can be found that a combination of two "proportional" loading paths results in nonproportional loading to the material. At the end of the first proportional loading, the yield surface is not centered at the origin due to prior plastic deformation. As a result, the second "proportional" path will not have $\sin \theta = 0$ initially (Figure 2.1). Hence, the cross-hardening may be a reflection of the nonproportionality of loading rather than a separate effect. On the other hand, the cross-hardening effect is not significant for 1045 steel (Kurath, 1993).

2.5.5. Discussion

For most materials without metallurgical transformation or other microstructural changes during the cyclic loading, it is a general phenomenon that the stress-plastic strain curve is either convex (tensile loading) or concave (compressive loading). In general, strain hardening decreases with increasing plastic deformation. A mathematical generalization of this phenomenon is,

$$d\underline{\alpha}:\underline{n} > 0 \ . \tag{2.38}$$

This condition has been explicitly incorporated in all the hardening rules discussed in the previous section. Enforcing the consistency condition, Equation (2.12), with the Inequality (2.38), one obtains,

$$dk < \frac{d\underline{S}:\underline{n}}{\sqrt{2}} \ . \tag{2.39}$$

The resulting inequality is a condition that must be satisfied at any time for the evolution of the size of the yield surface during active loading. Many researchers have ignored this condition. For the hardening Equation (2.35a) for the evolution

of the size of the yield surface, the Inequality (2.39) results in the following relation,

$$b_k (Q - k) < \frac{h}{\sqrt{2}} , \qquad\qquad (2.40)$$

where h is the plastic modulus function. When modeling transient behavior the aforementioned condition may not always be satisfied. It is suggested that in considering refinements in hardening relations that the condition expressed by Equation (2.38) should be enforced.

Examining experimental investigations on nonproportional cyclic plasticity, it seems evident that nonproportionality has a remarkable effect on the deformation behavior of some materials subjected to cyclic loading. However, the method of comparison for the nonproportionality effect has not been adequately defined. Most of the reports for the nonproportionality effect have come from the comparisons of the stress responses under proportional and non-proportional loading with the "same" strain range. Since both stress and strain are tensorial qualities, the scalar quantities, equivalent stress and equivalent total/plastic strain, were generally employed in the comparison. Equivalent stress is either based on the Tresca or von Mises criteria. The total equivalent strain is defined in a way similar to that used for the equivalent plastic strain increment (refer to Equation (2.15)). It has often been stipulated that plastic deformation is path dependent, which implies that the equivalent stresses are usually not the same for the same equivalent strains if the loading paths are different. The applicability of equivalent stress-strain for nonproportional loading is questionable. In fact, utilizing equivalent stress or strain concepts when comparing the proportional/nonproportional loading may more realistically reflect path dependence.

When discussing nonproportionality, one always implicitly assumes that a hardening rule alone does not account for this effect. However, this is not true. As a matter of fact, all the discussed incremental hardening rules, including the linear hardening rule of Prager-Ziegler, consider nonproportionality, irrespective of the ability to correlate with experiments. A simple affirmation of this assertion can be done by using these hardening rules to predict both proportional and nonproportional loading and compare the results, as will be done later in the text.

3. EXPERIMENTAL OBSERVATIONS

3.1. Introduction

Experimental observations are the basis for most theoretical cyclic plasticity formulations. Interest in ratchetting can be traced back to Bairstow (1911) who made some careful observations of strain accumulation in a steel under cyclic uniaxial loading with tensile mean stress. Axial strain extension due to unbalanced uniaxial loading was the subject of a number of early investigations at elevated temperature (Kennedy, 1956; Lazan, 1949; Manjoine, 1949; Meleka and Evershed, 1960), as well as room temperature (Benham, 1961; Benham and Ford, 1961; Coffin, 1960). Other observations of remarkable strain accumulation at low temperatures have been cited in multiaxial nonproportional loadings (Moyar, 1960; Moyar and Sinclair, 1962, 1963; Wood and Bendler, 1962). Renewed interest in cyclic ratchetting is reflected by the recent experimental works of Bower (1987, 1989), Chaboche et al. (1991), Hassan and Kyriakides (1992), Hassan et al. (1991, 1992), Inoue et al., (1985, 1989, 1991), Ishikawa and Sasaki (1991), Kapoor and Johnson (1992), Lebey and Roche (1979), McDowell (1991), Pellissier-Tanon et al. (1982), and Ruggles and Krempl (1989). Some of the ratchetting experiments reported recently in the literature are summarized in Table 1. Theoretical efforts have been made toward to modeling the experimentally observed ratchetting (Chaboche, 1989c, 1991; Chaboche and Nouailhas, 1989a, 1989b; Chaboche et al., 1989, 1991; Drucker and Palden, 1981; Garud, 1991; Guionnet, 1992; McDowell, 1992; Ohno and Wang, 1991a, 1991c, 1993a, 1993b; Voyiadjis and Sivakumar, 1991).

In view of the investigations on cyclic ratchetting, few comprehensive experimental studies have been conducted under multiaxial stress states, complex loading paths, and for large numbers of cycles. Yamanouchi et al., (1976) conducted ratchetting tests on thin tubes of 316 stainless steel under cyclic axial strain and constants internal pressure at both room temperature and high temperature. They found that the progressive diametral increase of the tube specimen followed a power law relation with respect to the number of loading cycles. Lebey and Roche (1979) used thin tube specimens of 304 L steel and applied cyclic shearing strain with constant axial stress. Consecutive axial elongation was observed with loading cycles. Pellissier-Tanon et al. (1982)

conducted some uniaxial ratchetting experiments on a stainless steel to evaluate the material's ability to resist ratchetting deformation. Bower (1987, 1989) tested two different materials for the ratchetting properties. A hard-drawn copper was found to ratchet at approximately constant rates under load-controlled proportional and nonproportional loading. A rail steel was found to display ratchetting rate decay. Solid specimens were used in the nonproportional axial-torsion testing and some computational difficulties were noted in the stress and strain analysis since the measurements of the extension and twist angle were made between the two loading grips (Bower, 1987, 1989). Hassan and Kyriakides (1992), and Hassan et al. (1991, 1992) conducted ratchetting tests under both uniaxial tension-compression and biaxial axial-tension on two low carbon steels. A 1020 steel displayed ratchetting at a nearly constant rate and the other steel, 1026, with slightly higher carbon content displayed ratchetting rate decay. One deficiency in these experiments is that the ratchetting tests were conducted for only a few dozen loading cycles. McDowell (1991) conducted ratchetting tests on a rail steel and found that the material displayed long term ratchetting rate decay under both proportional tension-compression and nonproportional axial-torsion. The experimental ratchetting responses investigated in the literature were under the condition that the stress magnitudes were maintained unchanged during the entire loading history. The cyclic ratchetting behavior under multiple step loading, in which the stress magnitudes change between loading steps, needs further exploration. With this background, an experimental program was initiated to explore the cyclic ratchetting behavior of 1070 steel. This study focuses on the ratchetting phenomena for (i) a large number of loading cycles, (ii) proportional and nonproportional loading, and, (iii) multiple step loading.

3.2. Experimental Procedure

The material used in this investigation is 1070 steel. Specimens were machined from hot rolled bars which had been normalized at 870°C for 4 hours followed by air-cooling. Chemical composition and mechanical properties of this material are shown in Tables 2 and 3 respectively. The microstructure of 1070 steel is shown in Figure 3.1. Both uniaxial solid specimens and multiaxial tubular specimens were used for the ratchetting tests. The geometry and dimensions of the specimens are shown in Figure 3.2. The specimens were polished to about a 30 micron surface finish before testing. A 100kN digital control closed loop servohydraulic test frame was used for the uniaxial tests. A 12.7mm gauge

length extensometer calibrated to 10% full scale was used to measure the axial deformation and an extensometer with 12% to 15% capacity was used to measure the diametral strain. The biaxial axial-torsion tests using tubular specimens were conducted employing a digital control closed loop servohydraulic biaxial testing machine which has axial and torsional load capacities of 222kN and 2260N-m respectively. A 25mm gauge length extensometer was used to measure the axial and torsional deformations(10% full scale axial and 5 degrees full scale torsional). All data acquisition and control were performed with microcomputers. Testing was conducted at room temperature using a sinusoidal waveform. All the tests were conducted at a frequency of 0.5 Hz. Two kinds of tests were conducted on both uniaxial solid specimens and biaxial tubular specimens. One is a single step test in which the stress magnitudes are constant during the test. The other is a multiple step test, which is composed of several single step tests.

For the selected loading cycle, the computer acquires 200 data points per channel which are stored for subsequent analysis. During the ratchetting experiments, caution has been taken to ensure that the deformation is not excessively large so that the microstructural parameters, hence the basic material properties, are not altered. Secondly, the load instead of the stress is the controlled parameter in the test. When the total deformation is small, the stress change during the test will be small, and the test can be defined as stress-controlled. For the uniaxial tests, the cross-sectional area is corrected by the measured diametral strain during data reduction and the true stress is calculated with the instantaneous cross-sectional area. The true strain is obtained accordingly and used in reporting the results. Uniaxial experiments verified the plastic incompressibility condition during elastic-plastic deformation, and this assumption was employed for calculating true stresses for the biaxial experiments. The corresponding fatigue lives for the load level chosen are large enough that no fatigue failure, nor any measurable crack growth, is expected. Tests were conducted to failure to ensure that this assumption was valid.

3.3. Experimental Results

3.3.1. Basic Material Properties

Fully reversed uniaxial strain-controlled tests were performed to obtain the fundamental properties of the material. A stair-step strain-controlled sequence test with a combination of increasing-decreasing blocks in strain was conducted using one specimen. For each loading block, the test was run until the

stress response stabilized. The stable stress-strain loops were identical to those observed for the single strain level tests. Shown in Figure 3.3(a) are the stable hysteresis loops for 1070 steel at different strain ranges. The non-Masing character of the loops should be noted. Figure 3.3(b) shows the hysteresis loops with matched upper branches, indicating that the non-Masing behavior of this material can be characterized by an increase in the yield stress for the larger stress/strain level. This indicates that a memory surface will probably be useful in any subsequent deformation analysis.

3.3.2. Single Step Loading

Figure 3.4 illustrates the basic ratchetting phenomenon. The ratchetting behavior is depicted for stress-controlled uniaxial loading with a compressive mean stress. The stress-strain response is presented in Figure 3.4(a). In Figure 3.4(b) the ratchetting strains are plotted against the logarithm of the number of cycles. The ratchetting strain is the average of maximum and minimum strains in a cycle. Non-closure of hysteresis loops during ratchetting caused the use of this terminology instead of mean strain. Noting the logarithmic intervals and the logarithm scale selection in the figure, the ratchetting rate in both axial and diametral directions decreases with the number of cycles. The volumetric strain, which is the sum of the axial ratchetting strain and twice the diametral ratchetting strain, remains unchanged during the ratchetting test. This result indicates that the material satisfies incompressibility during ratchetting deformation and the results are not masked by microstructural changes. Figure 3.4(c) shows the relationship between the axial ratchetting strain and the diametral ratchetting strain. The relationship is linear and the rate of the diametral ratchetting strain over the axial ratchetting strain is 0.5. This result also confirms the plastic incompressibility condition.

Figure 3.5 illustrates typical ratchetting behavior for proportional axial-torsion loading. In this case a tubular specimen is subjected to simultaneous axial stress and shear stress so that the principal stress directions are unchanged. The stress-strain responses in axial and shear directions are shown in Figure 3.5(a) and 3.5(b) respectively. In this experiment ratchetting is produced in both axial and shear directions. The decay of strain accumulation with increasing loading cycles is observed in both axial and shear directions. In Figure 3.5(c) the shear ratchetting strain is plotted against the axial ratchetting strain. Notably, the ratchetting deformation in the shear direction is linearly related to the

ratchetting deformation in the axial direction for the proportional axial-torsion condition.

Nonproportional axial-torsion tests have been conducted, and some detailed results are presented in Figures 2.6 and 2.7. The loading paths, namely the "ellipse" and "apple" shaped, represent typical nonproportional loadings where the directions of the principal stresses vary with time. The axial and torsional loading ranges for both loading paths are similar. As shown in Figure 3.6 for the "ellipse" shaped path, there is strain accumulation in the axial direction, but practically no shear strain ratchetting. Under the "apple" shaped loading path (Figure 3.7) however, ratchetting is observed in both axial and shear directions. The ratchetting rate decay under nonproportional loadings is similar to that observed for uniaxial and proportional loadings. From Figure 3.7(b) it can be inferred that under nonproportional loading, the ratchetting in the shear direction is not linear with respect to the ratchetting in the axial direction.

3.3.3. Multiple Step Loading

Shown in Figure 3.8 are representative stress-strain responses for a three-step loading with an identical mean stress in each step. The stress ranges are 750MPa and 850MPa in the first and second loading steps respectively. Step 3 is the repeat of step 1. The mean stress is 280MPa for all the three loading steps and each step consists of 520 loading cycles. Note that the abscissa is broken for the three steps, since they would have overlapped if placed on the same plot. The ratchetting in step 1 is similar to that observed for a single step test (Figure 3.4). However, the ratchetting rate in step 2 is smaller when compared to the single step test. When the stress range is reduced in step 3, the ratchetting rate is considerably smaller than step 1 which has identical stress levels. A closer look at the detailed data in step 3 shows that the axial strain ratchetting is about 0.03% in the first 10 cycles and 0.01% for the rest of the cycles. The results from this test indicate that for the step loading where mean stress is maintained constant and stress range varies, the ratchetting rate decreases with the number of cycles but the ratchetting direction does not change.

It has been generally accepted that the ratchetting direction follows the mean stress direction. However, this assertion does not always hold true. Referring back to Figure 3.7, one can find that ratchetting in the shear direction occurred without a shear mean stress. Clearly the ratchetting direction under nonproportional loading is determined by the details of the loading path and

history, as will be discussed later. In fact ratchetting direction can be opposite to the mean stress even under uniaxial tension-compression.

Figure 3.9 shows the stress-strain response for a two-step loading test. The stress range and mean stress are 830MPa and 415MPa respectively in step 1. The stress range in step 2 is the same as that in step 1 but the mean stress is zero. Again each loading step consists of 520 cycles. As expected for the loading in step 1, plotted in dashed lines in Figure 3.9, the strain ratchets in the positive direction. However, in step 2, plotted in solid lines in the figure, the strain ratchets in the opposite direction. It has been experimentally verified that with a compressive mean stress in step 1, and identical conditions for step 2, a mirror image of this phenomenon will occur. This indicates that with zero mean stress under uniaxial tension-compression there may be ratchetting in one direction or the other, dependent on the previous history. Furthermore it is possible that for a positive mean stress loading, there may be negative ratchetting or vice versa.

The stress-strain response under a three-step uniaxial test is presented in Figure 3.10. In this experiment, the mean stresses change with the loading steps but the stress amplitude is maintained approximately constant for each step. The number of cycles per step was not 520, as was the case in the previous experiments. The mean stress is increased in step 2 and reduced in step 3 to approximately the same level as in step 1. In all three steps, the mean stresses are positive. The ratchetting follows the mean stress direction in steps 1 and 2. However, when the mean stress is reduced in step 3, the ratchetting is in the opposite direction observed for the two previous steps.

Figure 3.11 shows ratchetting for uniaxial four-step loading. The stress range is about 400MPa in each loading step while the mean stress in each loading step is different. The ratchetting for step 1 loading (mean stress is 208MPa) is similar to that shown in Figure 3.4. When the mean stress is reduced to 77MPa in step 2, the strain ratchets in the direction opposite to the mean stress direction. When the mean stress is changed to -125MPa in step 3, the ratchetting is in the negative direction. After step 3, the mean stress is reduced to -20MPa in step 4. From the right plot of Figure 3.11(b) it can be ascertained that even with a negative mean stress, the strain ratchets in the positive direction.

Similar results to those shown in Figure 3.9 have been reported by Dolan (1965) on 4340 steel. Dolan noted that, "the plastic stretch of the specimen from the previous cycling was gradually being partially recovered by a cyclic-dependent shortening". The back ratchetting after a tensile mean stress loading

history might be explained by strain recovery. This implies that there might be a tendency for the material to recover from a non-zero strain state to zero deformation. However, the results shown in Figure 3.11(b) contradicts Dolan's deformation-recovery explanation. Referring to Figure 3.11, the axial strains in the four loading steps are all positive. According to the deformation-recovery explanation the strain should have ratcheted in the negative direction in Step 4, when in fact, the results show the opposite trend. The deformation may recover to some degree, but clearly such recovery is not significant.

To further define ratchetting phenomena for this material, more uniaxial multiple step tests have been conducted, and the results are displayed in Figures 2.12 through 2.14. The stress ranges are 800MPa for both steps in the test shown in Figure 3.12. The mean stresses are 200MPa and 77MPa in step 1 and step 2, respectively. Step 1 experiences 64 cycles. The stress-strain response for step 1 is produced on the left side, and the response for step 2 is shown on the right side of Figure 3.12. In step 2, referring to the cycle labels in Figure 3.12, the strain ratchets in the opposite direction to mean stress for about the first 250 cycles and then shifts to the same direction for the remainder of the cycles of the block. Comparing the two-step loading history of Figure 3.13 with Figure 3.11(a), it can be found that the only difference between the two cases is that in the Figure 3.11(a) case, step 1 experiences 4100 cycles while in Figure 3.12 step 1 experiences only 64 cycles. In other words, if step 1 in Figure 3.12 had experienced a higher number of loading cycles, the strain in step 2 would ratchet in the opposite direction for all the loading cycles. The ratchetting phenomenon displayed in Figure 3.12 indicates that the duration of the previous loading step has a profound influence on the ratchetting of the current loading step.

To illustrate the change in ratchetting direction further, consider the results from a two-step test (Figure 3.13) where for step 1 the stress range is 800MPa and the mean stress is -200MPa, and for step 2 the stress range is 875MPa and the mean stress is -77MPa. It can be found in the left plot of Figure 3.13 for that step 2 the strain ratchets in the positive direction for about 1000 cycles, followed by a shift in ratchetting in the negative direction. Referring to the ratchetting behavior in Figure 3.11(a), it is noted that if the stress ranges were the same in both steps the ratchetting in step 2 would be all in the positive direction opposite to the mean stress. This suggests that the relative ratio of the stress ranges between the loading steps also plays a dominant role in the ratchetting of the following step.

In order to gain further insight into the previous history effect, the influence of a single overload on the ratchetting behavior is shown in Figure 3.14. Firstly the uniaxial specimen undergoes a monotonic tensile loading up to a maximum stress of 830MPa, which corresponds to an axial strain of about 2.5%. The subsequent loading has a stress range of 840MPa and a mean stress of 100MPa (maximum stress is 520MPa). Referring to the cycle labels in Figure 14, it is found that the strain ratchets in the negative direction for the first 2000 cycles and then switches to the positive direction. Obviously, the ratchetting direction would agree with the mean stress direction if there had been no overload involved.

Multiple step ratchetting tests under axial-torsion loading have been conducted and some of the results are displayed in Figures 3.15 through 3.18. The loading paths of a two-step proportional loading are shown in Figure 3.15(a). Both axial and shear stress ranges in the two steps are the same. In step 1 loading, the axial mean stress is 310MPa and the shear mean stress is 118MPa. In step 2, the axial mean stress is reduced to 78MPa and the shear mean stress is reduced proportionally to 30MPa. The axial stress-strain responses for the two-step loading are displayed in Figure 3.15(b) and analogous results are shown in Figure 3.15(c) for the shear stress-strain response. It can be found that when the mean stresses are reduced in step 2, the strains in both axial and shear directions ratchet in negative directions opposite to the mean stresses. This phenomenon is consistent with the uniaxial cases discussed previously (Figure 3.11).

A two-step axial-torsion loading path is shown in Figure 3.16(a) and the axial stress-strain and shear stress-strain responses for steps 1 and 2 are shown Figure 3.16(b) and Figure 3.16(c) respectively. Step 1 represents proportional compression-torsion, where the axial mean stress is -300MPa and the shear mean stress is -110MPa. In step 2, the axial mean stress is reduced to zero, while the other loading parameters remain the same. In the right-hand side plots in these figures, it can be seen that as a result of the change of axial mean stress, the axial strain ratchets in the positive direction and the ratchetting in the shear direction displays a complicated behavior. The shear strain ratchets in the positive direction opposite to its mean stress during the first 60 cycles, then in the negative direction for the remainder of the cycles. A similar phenomenon was observed when, instead of changing axial mean stress from step 1 to step 2, the shear stress is reduced to zero. In this case the shear strain ratchets in the opposite direction to its previous direction in step 1, while the axial ratchetting

direction changes during step 2. It should be noted that due to step 1 loading, step 2 causes this path to be nonproportional.

In Figure 3.17 the results of a two-step axial-torsion nonproportional test are presented. In each step the axial stress is constant while the shear stress is cycled symmetrically. The axial mean stress in the first step is 300MPa and the shear stress amplitude is 230MPa. In the second loading step, the shear stress amplitude is 230MPa but the axial stress is reduced to 60MPa. The result of the axial stress change, as shown in Figure 3.17(c), is that the ratchetting direction changes in step 2. Clearly the mean axial stresses in both steps are positive and the ratchetting in the negative direction during step 2 develops as a result of the previous history.

In Figure 3.18 an "ellipse" shaped path with tensile mean stress in the axial direction is followed by a pure shear loading. Due to the "ellipse" shaped loading path in step 1, the pure shear loading in step 2 results in ratchetting in the negative axial direction.

3.4. Discussion of the Experimental Results

The 1070 steel used in this investigation displays ratchetting rate decay under single step loading. Although decay of strain accumulation is observed, it does not result in ratchetting arrest (no ratchetting), even for tens of thousands of loading cycles. However, strain ratchetting may accelerate under certain circumstances in multiple step loading. Referring to Figure 3.12, due to the change of ratchetting direction in step 2, the absolute value of the ratchetting rate reaches its minimum (zero) at the moment of direction change. For example, the ratchetting rate at cycle 512 is larger than the ratchetting rate at cycle 256 where the ratchetting changes from negative to positive axial direction. Nevertheless, the ratchetting rate acceleration is short-lived for 1070 steel. For long term loading histories, a decrease in the ratchetting rate is always observed for this material.

From the experimental results of multiple step proportional loading, it is noted that when the mean stress does not vary between the loading steps, the ratchetting direction is unaltered. When the mean stress is reduced in magnitude yet maintains the same sign after a loading step, the material memory of the previous loading history will alter the driving force for the current loading step. The material will display a tendency to ratchet in the opposite direction of the mean stress and a minimum rate phenomenon will occur as discussed in the

previous paragraph. The magnitude of this material memory is dependent on the details of the previous loading history, including the loading amplitudes and number of cycles. Again, the memory of prior loading history dissolves with increasing loading cycles. It seems that carbon content of the steel plays a significant role in the ratchetting rate decay observed. AISI 1020 carbon steel displayed a near constant ratchetting rate (Hassan and Kyriakides, 1992). Slow ratchetting rate decay was found in 1026 carbon steel (Hassan and Kyriakides, 1992; Hassan *et al.*, 1992). Due to the limited number of cycles in these tests, it is unclear whether there is no decay, or that lowered carbon content merely delays this decay. The 1045 steel (Kurath, 1993) and 1070 steel which contain a higher percentage of carbon display greater ratchetting rate decay (or at least earlier) in comparison to a 1026 steel. Higher carbon content steels may be expected to exhibit even faster ratchetting rate decay. It should be noted that heat treatment may also play a determinant role in the qualitative ratchetting behavior of a carbon steel.

3.5. Description of Strain Ratchetting under Constant Amplitude Loading

All the experimental ratchetting data has been carefully analyzed. The following expression is found to be appropriate for describing the ratchetting rate for both single step and multiple step stress-controlled loading,

$$\frac{d\varepsilon_r}{dN} = c_{r1} N^m + \frac{c_{r2}}{N} \ , \tag{3.1}$$

where ε_r represents ratchetting strain in a specified direction, N is the number of cycles counting from the beginning of each loading step, and c_{r1}, c_{r2}, m are constants. From Equation (3.1) it follows that the ratchetting strain is,

$$\varepsilon_r = \frac{c_{r1}}{m+1} N^{m+1} + c_{r2} \ln N + \varepsilon_{r0} \ , \tag{3.2}$$

where ε_{r0} is a constant. To maintain consistency with regard to the integration, only cases where $m \neq -1$ will be considered. The case of $m = -1$ is considered with the second term of Equation (3.1). Equations (3.1) and (3.2) can describe the ratchetting for a wide range of materials. When $m = 0$, the first term in Equations (3.1) and (3.2) represent constant ratchetting which was observed in copper

(Bower, 1989) and low carbon steel (Hassan and Kyriakides, 1992; Benham and Ford, 1961).

For the single step loading cases, the ratchetting rate can be adequately described by Equation (3.1) with $c_{r2}=0$. Figure 3.19 contrasts the prediction of Equation (3.2) along with the experimental data. The description of ratchetting under multiple-step loading using Equation (3.2) is shown in Figure 3.120. It should be noted that $c_{r2} \neq 0$ was necessary to describe multiple step loading. From all those calculations on 1070 steel the exponent m ranges from -0.5 to -1.0, depending on the stress magnitudes and stress state.

In general the relationship between the constants in Equations (3.1) and (3.2) with the loading parameters is more complicated. For example, these equations cannot describe the ratchetting behavior under random stress cycling. The presentation of these equations serves two main purposes. The first is that these equations represent a simple mathematical form to characterize ratchetting for constant amplitude loading. With this simple relationship, the ratchetting results can be extended to a large number of loading cycles where experiment or theoretical simulation is very time consuming. The second purpose is that this description could serve as a "benchmark" for evaluating the constitutive models for predicting ratchetting behavior. A plasticity model unable to mimic these equations is certainly deficient in more complex ratchetting predictions.

3.6. Conclusions

The experimental results on 1070 steel under various loading conditions lead to the following conclusions:

(1) The 1070 steel displays non-Masing behavior which can be characterized by an increase in yield stress for the larger stress ranges. During ratchetting deformation, the plastic incompressibility condition is valid.

(2) The ratchetting direction is coincident with the mean stress direction under single step proportional loading. There is no inevitable relation between the mean stresses and ratchetting directions when the loading is nonproportional.

(3) Under single step loading conditions, the ratchetting rate decreases with increasing number of loading cycles under both proportional and nonproportional loadings, and can be described by a power law relation.

(4) Under multiple step loadings, the material exhibits a strong memory of the previous loading history. The material could ratchet in a direction opposite

to the mean stress or could reverse ratchetting direction with time. Due to this memory effect the strain ratchetting of 1070 steel may accelerate under certain circumstances. Such memory has a great influence on the subsequent ratchetting, and tends to dissipate with an increased number of loading cycles.

(5) The multiple step test provides a means to refine ratchetting models utilizing the basic framework of cyclic plasticity.

4. EVALUATION OF EXISTING PLASTICITY MODELS

In this chapter, six existing plasticity models will be evaluated and comparisons will be made with the experimental results under both strain and stress controlled conditions. Emphasis will be placed on the capabilities of the models to predict ratchetting behavior. The models under consideration are, Armstrong-Frederick (1966), Bower (1987), Chaboche (1979, 1983), Garud (1981a, 1981b), Mroz (1966), and Ohno-Wang (1991a, 1991c, 1993a, 1993b). The Chaboche model refers to the initial form proposed by Chaboche et al. (1979) represented by Equation (2.23). The Ohno-Wang model refers to Ohno-Wang Model II, Equations (2.22) and (2.27). Due to the insignificance of the transient behavior of the materials investigated, the transient behavior will be neglected in the theoretical simulations. All of these models were presented in Chapter 2.

In the simulations 800-4000 incremental steps are used for a cycle. Numerical analyses were conducted employing double precision. Precautions have been incorporated into the programming to avoid possible numerical overflow and accumulation of numerical errors. During active loading the program checks to insure that the stress state is always on the yield surface. It should be pointed out that the large number of incremental steps selected for a loading cycle in the simulations is not suggesting that these plasticity models always need so many increments. Instead, it is a practical way to insure that the simulations mimic the character of the model rather than any step size sensitivity displayed by different models.

4.1. Strain-Controlled Balanced Loading

Experimental results of SAE 1045 steel are taken from Fatemi (1985) and Kurath (1993). Stress-strain hysteresis loops from fully reversed uniaxial strain-controlled tests (Kurath, 1993) are used to determine the material constants in all the plasticity models. The constants used in the models are presented in Tables 4-7. Five terms are used in the backstress series expansion (M=5) for the Chaboche and Ohno-Wang models. The 90 degree out-of-phase nonproportional axial-torsion results (Fatemi, 1985) under a strain-controlled condition are taken to compare with the simulations from different plasticity models. The two loading paths, namely Path I and Path II, with different strain amplitudes are

shown in Figure 4.1. The comparisons between experimental and predicted results are present in Figures 4.2 through 4.5.

In Figure 4.2 the stress responses obtained using the Armstrong-Frederick, Bower, and Chaboche models are compared with the experimental results. The Bower and Armstrong-Frederick models produce very similar predictions for the two loading paths. The stress levels predicted by the Chaboche model are very close to the experimental data. Figure 4.3 demonstrates the Ohno-Wang model's capability with the selection of $\chi^{(i)} = 0$ and $+\infty$ (i=1, 2, 3, 4, 5). With either selection of $\chi^{(i)}$, the Ohno-Wang model predicts approximately identical results and very close agreement is observed between predictions and experiments. Clearly the selection of $\chi^{(i)}$ in the Ohno-Wang has an insignificant influence on the prediction of the stress response for this loading condition. Furthermore, by comparing Figure 4.2 with Figure 4.3 it is evident that all the Armstrong-Frederick type models produce practically identical predictions. It is understandable that the Chaboche and Ohno-Wang models correlate with experiments better than the Armstrong-Frederick and Bower models, because the former models contain more material constants.

The constant N_s in Figure 4.4 and Figure 4.5 represents the number of surfaces employed when evaluating the Mroz and Garud models. The predicted stress responses by the Mroz and Garud models are practically identical when the number of surfaces are the same. For a path with small plastic strains (Path I), the number of surfaces in the Mroz and Garud models does not have any significant influence on the predicted results. However, the number of surfaces influences the predicted results when the loading magnitude is increased (Path II). This effect on the prediction for the Mroz type models is mainly attributed to the change in the translation directions of the surfaces. Recall that the translation direction is dependent on the positions of the active and next surfaces. The number of surfaces was found to have an insignificant influence on the plastic modulus function, h. The correlation with the experiment by the Mroz and Garud models is inferior to the Armstrong-Frederick type models when predicting stress response for strain-controlled nonproportional loading.

Similar to many materials, the nonproportionality effect was reported for 1045 steel (Fatemi, 1985; Fatemi and Kurath, 1988; Fatemi and Socie, 1988; Fatemi and Stephens, 1989). The predicted results in Figures 4.2 and 4.3 suggest that these six models are able to consider the nonproportionality effect, since the calculated stresses are greater than or equal to the experimental observations.

The Mroz and Garud models display a higher nonproportionality effect than the Armstrong-Frederick type models. This is consistent with the previous discussion on nonproportionality (see Section 2.6.3).

4.2. Stress-Controlled Unbalanced Loading

The experimental results for 1070 steel are used to evaluate the ability of a plasticity model to predict ratchetting. The material constants for each model are listed in Tables 4-7. The basic material constants in the models are obtained by fitting the uniaxial stress-strain hysteresis loop of a 1% strain amplitude test. The stress-strain ratchetting data of the selected cycles is recorded from the experiment. The ratchetting strain, which is the average of two extreme strains in a cycle, is obtained for each of these cycles. Cubic spline fitting is employed to compute the experimental ratchetting rate (the amount of ratchetting strain per loading cycle). For an impartial and strict evaluation of a plasticity model's ability to predict ratchetting, the ratchetting rate is used when comparing predicted and experimental results whenever it is possible. It has been noted that for 1070 steel under constant amplitude loading, the ratchetting rate decreases with increasing number of cycles. The relationship between the ratchetting strain and the number of cycles can be best described by a power law, which is often presented on log-log scales. However, due to the possible sign change of the ratchetting direction under the multiple step loading conditions, ratchetting rate cannot be shown in logarithmic coordinates for all tests. Therefore, in the following discussion, both the accumulated ratchetting strain and the ratchetting rate are used in the comparison of the predicted and the experimental results.

4.2.1. Armstrong-Frederick, Bower, Chaboche, Mroz, and Garud Models

An "ellipse" shaped nonproportional loading path under stress-controlled axial-torsion is shown in Figure 4.6(a). The strain responses for the first 16 cycles are shown in Figure 4.6(b). Predicted strain responses for the first 16 cycles by the Armstrong-Frederick, Bower, Chaboche, Garud, and Mroz models are shown in Figure 4.7. Experimental ratchetting strains in both axial and shear directions for the first 100 cycles are summarized in Figure 4.8, along with the predictions of the five plasticity models. From Figure 4.7 and Figure 4.8, it can be found that there are two major aspects of the experimental ratchetting that the models fail to capture. One is the ratchetting rate decay. Except the Bower model, the other

four models predict constant ratchetting. Experimentally, the ratchetting rate decreases continuously with more loading cycles. The Bower model produces ratchetting rate decay for a limited period of loading cycles, followed by ratchetting arrest (zero ratchetting). The other aspect is that all five models predict ratchetting in the shear direction while the experimental results show minimal ratchetting in this direction. The Bower model predicts a ratchetting direction change in the shear direction. It has been forwarded by Chaboche (1989b) as a general comment, that the Mroz and Garud multiple surface models always produce fully closed stress-strain loops. However, the Mroz and Garud models predict constant ratchetting (hysteresis loops not closed) and the predicted results do not coincide with the experiments (Figure 4.7(d), Figure 4.8). As was observed for strain-controlled loading cases, the Garud and Mroz models are practically identical in predicting ratchetting. These models not only overestimate the ratchetting strain but also often predict incorrect ratchetting direction. Improvements in the capabilities of the five models discussed would be desirable, especially for long history ratchetting predictions.

4.2.2. Ohno-Wang Model

Figures 4.9 and 4.10 provide an overview of ratchetting experiments and predictions by the Ohno-Wang model for typical proportional and non-proportional loading paths. The solid lines in Figures 4.9 and 4.10 are obtained from a uniaxial test and a nonproportional axial-torsion test respectively. The nonproportional axial-torsion experiment consists of fully reversed shear with superimposed static axial stress. The stress-strain response for this loading has been presented in Figure 2.17(b). In Figure 4.10 the ratchetting in the shear direction is not shown because in this case both the experiment and the predictions by the model demonstrate no shear ratchetting. In both cases, the experimental axial ratchetting rate varies from around 10^{-3} per cycle at the beginning of the loading to on the order of 10^{-6} per cycle after a few thousand cycles. Since the experimental results are approximately a straight line on log-log coordinates, the ratchetting rates follow a power law. Predictions presented in the two figures with dotted lines are obtained by using the Ohno-Wang model with a different set of exponents $\chi^{(i)}$ (i=1, 2, ..., 10); $\chi^{(i)}$ ranges for 0 to $+\infty$.

From the predictions of the Ohno-Wang model, it is obvious that the exponents $\chi^{(i)}$ (i=1, 2, ..., M) in the model control the predicted ratchetting rate. This contrasts with the insensitivity observed for $\chi^{(i)}$ previously for fully

reversed strain-controlled loading. The larger the exponents $\chi^{(i)}$ (i=1, 2, ..., M), the faster the model predicts the ratchetting rate decay. For the uniaxial test, the model with $\chi^{(i)} = 0$ (i=1, 2, ..., 10) produces slow ratchetting rate decay for the first 100 cycles before constant rate. When $\chi^{(i)} = +\infty$ (i=1, 2, ..., M), no ratchetting is predicted for the uniaxial loading. This is because the model with $\chi^{(i)} = +\infty$ (i=1, 2, ..., M) produces a perfect hysteresis loop closure. For the nonproportional loading consisting of fully reversed shear with constant axial stress (Figure 4.10), the Ohno-Wang model predicts ratchetting rate decay for any selection of $\chi^{(i)}$. When $\chi^{(i)} = +\infty$ (i=1, 2, ..., M), the model predicts ratchetting decay for about 50 cycles before ratchetting arrest. The inability of the model to predict constant ratchetting may prevent the model from being applied to materials exhibiting constant ratchetting under nonproportional loading. This will be further discussed later.

Naturally, the exponents $\chi^{(i)}$ (i=1, 2, ..., 10) are not necessary all the same. With the help of diagrams similar to Figures 4.9 and 4.10, an approximate conjecture can be made for the exponents $\chi^{(i)}$ (i=1, 2, ..., 10). With an estimation of the ranges for the exponents $\chi^{(i)}$ (i=1, 2, ..., 10), a trial-and-error procedure can be employed and a judicious selection of the exponents $\chi^{(i)} = 0$ (i=1, 2, ..., 10) can be made based on the fitting of the prediction with the experiment. For the material investigated, 1070 steel, it is found that the Ohno-Wang model with $\chi^{(1)} = 0.5$, $\chi^{(2)} = 2$, $\chi^{(3)} = \chi^{(4)} = 5$, and $\chi^{(5)} = \chi^{(6)} = \chi^{(7)} = \chi^{(8)} = \chi^{(9)} = \chi^{(10)} = 6$ offers a best fit with the experimental results for tension-compression ($\frac{\Delta\sigma}{2} = 405$ MPa, $\sigma_m = 205$ MPa). The final fit using these constants is shown in Figure 4.11. Next, the results predicted for other loading cases when using the model with this selection of the exponents $\chi^{(i)}$ (i=1, 2, ..., 10) are examined (Figures 4.12-4.20).

Illustrations of the nonproportional loading paths and multiple step loading paths accompany each of the figures with ratchetting results. The solid lines represent the experimental results and the dotted lines are always the predictions of the Ohno-Wang model. All the comparisons are based on either the accumulated ratchetting strain or ratchetting rate when possible. The abscissa in each of these figures represents the number of cycles and is in logarithmic scale. When the ordinate denotes ratchetting rate, a logarithmic scale is used. The absolute value is used when the ratchetting rate is negative, as would be the case for ratchetting in the compressive direction. A linear scale is used when the ordinate is the accumulated ratchetting strain.

The comparisons made in Figures 4.11-4.20 are self evident, and do not require elaborate explanation. Generally speaking, the Ohno-Wang model can correlate with the experimental results very well for various loading conditions as well as for a large number of loading cycles. The model captures the experimentally observed power law ratchetting rate decay. Equally important, the model is able to consider the previous history effect and predict ratchetting opposite to the mean stress direction (see Figure 4.15 and Figures 4.17-4.19) for multiple step loading. In the cases where the accumulated ratchetting strains are used in the comparison, the error of the prediction from the experiment is accumulated with the loading cycles. For example, the difference between the theory and experiment in step 2 of the loading shown in Figure 4.19 is mainly attributed to the error accumulated in the first step.

Inspection of the results from Figure 4.11 to Figure 4.20 resolves the first discrepancy between the prediction and experimental data. In Figure 4.14(b), where the results of the shear ratchetting strain are presented for the "apple" shaped loading path, the Ohno-Wang model predicts minimal ratchetting in the shear direction, while the experiment shows a significant strain accumulation in the positive shear direction. Figures 4.16 and 4.17 indicate that the model does not adequately predict the change of the ratchetting direction for the second loading step. This disagreement is more obvious in the case of Figure 4.16 where the experiment shows a clear change in ratchetting direction for the second step, while the model predicts near zero ratchetting for this loading step. Compared with the other cases, the agreement for the three-step case shown in Figure 4.18 is even less desirable.

The results presented in Figure 4.20 reveal the major deficiency in the model. The uniaxial case shown in the upper plot is for a small mean stress or low stress level, which was referred to by Chaboche and Nouailhas (1989a, 1989b) as quasireversed. The case in the lower plot represents the high mean stress (high stress level) case, or quasirepeated (Chaboche and Nouailhas, 1989a, 1989b). From Figure 4.20, the Ohno-Wang model overestimates the ratchetting rate for a higher stress level loading and underestimates ratchetting rate for a lower stress level loading. Therefore, some consideration should be put into incorporating the stress level effect in the Ohno-Wang model. This stress level effect may be partially responsible for the diminished agreement between predictions and experiments found in the cases of multiple-step loadings (Figure 4.16, Figure 4.18).

4.3. Discussion

The Mroz multiple surface models can appropriately duplicate the experimentally observed Bauschinger effect for proportional loading. However, these multiple surface models have difficulty characterizing transient cyclic plasticity behavior. From the comparisons of the theoretical predictions with the experiments, it has been noted that the Mroz/Garud multiple surface models provide results inferior to the Armstrong-Frederick type models in stress response prediction for the strain-controlled balanced loading. Clearly, the Mroz/Garud models are not able to predict ratchetting for the proportional loading, yet these multiple surface models are able to predict strain ratchetting for the nonproportional loading. The predicted ratchetting results are not in agreement with the experiments. As was pointed out earlier, the models' inability to correlate with the experiments is caused mainly by the inappropriate specification of the backstress translation direction of the yield surface. In other words, the hardening rules, Equations (2.31)-(2.34), do not give the correct translation direction under the basic framework of cyclic plasticity. Without going into further discussion, it can be concluded that the multiple surface models of Mroz and Garud do not capture the characteristics of cyclic plasticity for the nonproportional loading and therefore, their applications may be limited to balanced proportional loading. Because of this, the two-surface models, which are the simplifications of the Mroz/Garud multiple surface models, possess similar disadvantages, hence, are not suitable for general cyclic plasticity prediction. From the practical application point of view, the Mroz/Garud models are more complicated mathematically and computer simulations are much more time consuming than the Armstrong-Frederick type models.

All the Armstrong-Frederick type models can adequately predict the stress responses for the strain-controlled balanced loading. The basic Armstrong-Frederick model, Equation (2.18), serves as a fundamental basis for the Armstrong-Frederick type models. Due to its simple mathematical form, the basic Armstrong-Frederick model can provide adequate stress responses for the strain-controlled balanced loading; but is not sufficient for the general cyclic plasticity predictions. In the Armstrong-Frederick type models, a series expansion of backstresses improves the predicted stress responses for the strain-controlled balanced loading. For example, the Chaboche model can predict satisfactory stress response for the strain-controlled balanced loading when M,

the number of backstresses, is 5. For balanced proportional loading, increasing the number of backstresses should increase the accuracy of the stress-strain loop description. For nonproportional loading cases, an increase in the number of backstresses also changes the evolution of the total backstress which determines the subsequent plastic deformation. The influence of the number of the backstresses for an Armstrong-Frederick type model is asymptotic in nature. This effect is more profound for unbalanced loading than for balanced loading.

The Bower model and the basic Armstrong-Frederick model produce very similar stress response for the strain-controlled balanced loading. Due to the introduction of the additional internal variable β the Bower model, Equation (2.20), can predict ratchetting with a sign opposite to the mean stress for proportional loading, and can predict ratchetting rate decay for any loading case. However, this plasticity model always predicts a ratchetting arrest after a certain number of loading cycles and it cannot predict the ratchetting direction change when the variable β neutralizes as the loading cycles increase. By adjusting the material constants in the model the predictions can be improved to some degree, but such adjustment of the material constants cannot change the overall tendency of the model. For example, when the constant c_{b1} in Equation (2.20) is a smaller number the period of the ratchetting rate decay predicted will be longer. However, in this case, the overall ratchetting prediction will be very different from the experiment. Despite the inaccuracy of the predictions, the Bower model displays some advantages. The additional internal variable β enables the model to predict decreasing, increasing, and constant ratchetting. The variable β on the other hand serves as a means to memorize the previous loading history. From the experimental observation on the ratchetting behavior under both single and multiple step loadings, it seems that such an internal variable may be necessary and promising. An improvement can be made on the Bower model by employing the same decomposition of the backstress similar to that used in the Chaboche model and the Ohno-Wang model (Equation (2.21)). A possible advantage of such generalization of the Bower model over the Ohno-Wang model would be that the former is able to predict constant ratchetting for any loading cases, knowing that $\beta_{ij}=0$ recovers the Chaboche model which predicts constant ratchetting. As will be discussed in a forthcoming chapter, an Armstrong-Frederick model can be interpreted with a limiting surface concept and the variable β represents the center of the limiting surface.

The Ohno-Wang and the Chaboche models predict similar stress response for strain-controlled balanced loading. For the balanced loading the exponents $\chi^{(i)}$ (i=1, 2, ..., M) in the Ohno-Wang model have minimal influence on the predicted results. The characteristics of the Ohno-Wang model are reflected in the ratchetting predictions. Of all the plasticity models evaluated, the Ohno-Wang model is the only one that can appropriately correlate with the ratchetting experiments for a material which displays ratchetting rate decay. It should be pointed out that the ratchetting strain is a second order effect; therefore, it is extremely difficult for a model to predict the ratchetting accurately for large number of loading cycles. The simulation of transient behavior with this model, though insignificant for 1070 steel, has not been included. Considering all these factors and the performance of the Ohno-Wang model when predicting the ratchetting for the 1070 steel, the Ohno-Wang model is promising for general cyclic plasticity.

One shortcoming of the Ohno-Wang model is its inability to predict constant ratchetting for nonproportional loading. This is because when $\chi^{(i)}=0$ (i=1, 2, ..., M) the Ohno-Wang model does not recover to the Chaboche model which predicts constant ratchetting for any loading path. For the proportional loading case, the Ohno-Wang model at $\chi^{(i)}=0$ (i=1, 2, ..., M) and the Chaboche model predict similar ratchetting results. However, for nonproportional loading the difference between the predictions by the two models is significant (Jiang and Sehitoglu, 1993a, 1993b). In fact, the Chaboche model is represented by $W^{(i)}=1$ while the Ohno-Wang model at $\chi^{(i)}=0$ results in $W^{(i)} = \langle \underline{n}:\underline{L}^{(i)} \rangle$ which is not equal to unity for the nonproportional loading (refer to Equations (2.22), (2.24), (2.27)). A plasticity model that possesses the essential characteristics of the Ohno-Wang model and at the same time is able to predict constant ratchetting for any loading path would be an improvement on the Ohno-Wang model, which is in fact the subject of the next chapter. Furthermore, the stress level effect may be considered to improve the Ohno-Wang model in predicting ratchetting for different stress levels. For the general cases, the Ohno-Wang model should consider all the transient material properties, such as cyclic hardening, the stress level effect, the non-Masing behavior, and the additional nonproportionality effect.

Ratchetting and stress relaxation are two reflections of one material property. The mechanism of strain ratchetting under the stress-controlled condition and stress relaxation under the strain-controlled condition is the same.

A model that can adequately predict strain ratchetting should also predict stress relaxation as well.

4.4. Conclusions

The evaluation of the existing plasticity models with experiments leads to the following conclusions:

1. The unbalanced loading is critical for the evaluation of a plasticity model.

2. All the Armstrong-Frederick type models discussed are able to predict reasonable stress response for the nonproportional strain-controlled loading. For strain-controlled balanced loading, the Bower model and the initial Armstrong-Frederick model produce very similar results, and the Chaboche and Ohno-Wang models with the same number of backstresses predict practically identical stress response. The exponents $\chi^{(i)}$ (i=1, 2, ..., M) in the Ohno-Wang model do not have any significant influence on the predicted results for the balanced loading.

3. Mroz and Garud multiple surface models are approximately identical for the prediction of stress-strain response. The predicted stress response by the Mroz/Garud models are inferior to Armstrong-Frederick type models for nonproportional strain-controlled loading. The Mroz/Garud models are able to produce strain ratchetting under stress-controlled nonproportional loading. However, the models are not suitable for ratchetting prediction.

4. The Ohno-Wang model is the best of all the models evaluated. The predicted stress response by using the Ohno-Wang model for strain-controlled loading is in very close agreement with the experiments. More importantly, the model can appropriately correlate with the experimental ratchetting of the 1070 steel for various loading conditions. A shortcoming of the Ohno-Wang model lies in its inability to predict constant ratchetting for nonproportional loading. In addition, the transient cyclic material behavior should be incorporated in the model.

5. DEVELOPMENT OF A NEW PLASTICITY MODEL

Based on the evaluation and discussion of the available plasticity models, it has been concluded that the predictions obtained using the Mroz/Garud multiple surface models do not quantitatively agree with the experimental results for either strain-controlled nonproportional balanced loading or the stress-controlled unbalanced loading. Hence, multiple surface concepts will not be incorporated into the new model. The Armstrong-Frederick type models predict reasonable stress values for both proportional and nonproportional strain-controlled loading. The Ohno-Wang model, with the introduction of a threshold, correlates with single-step experimental ratchetting observations even for long term loading histories.

Due to its demonstrated capability of predicting some of the ratchetting phenomena discussed in Chapter 4, the Ohno-Wang model will be used as a basis for the new model. One shortcoming of the Ohno-Wang model is its inability to predict constant ratchetting for nonproportional loading, a characteristic which will be overcome in the new formulation. In addition, the transient cyclic material behaviors such as cyclic hardening, non-Masing character, and the stress level effect on the strain ratchetting will also be incorporated. The new model will use limiting surfaces with a series expansion of the backstresses. The concept of a limiting surface will provide a new avenue by which the class of Armstrong-Frederick models can be interpreted.

5.1. A General Class of Hardening Rules

A series expansion of backstresses, as was expressed in Equation (2.21) is used in the current formulation and, it is assumed that each backstress part $\underline{\alpha}^{(i)}$ takes the following tensorial form,

$$d\underline{\alpha}^{(i)} = f_1^{(i)} \left(\underline{n} - f_2^{(i)} \underline{L}^{(i)} \right) dp \qquad (i=1, 2, ..., M) \ . \tag{5.1}$$

The quantity $\underline{n}$ is the unit normal (Equation (2.11)), dp is the equivalent plastic strain increment (Equation (2.15)), and $\underline{L}^{(i)}$ is the unit vector of the ith backstress (Equation (2.28)). The quantities $f_1^{(i)}$ and $f_2^{(i)}$ in Equation (5.1) are scalar functions of the backstresses, which satisfy the following conditions,

__CONDITION 1__ $f_1^{(i)}$ is single-valued and non-negative, and

__CONDITION 2__ $f_2^{(i)} \geq \underline{n} : \underline{L}^{(i)}$ when $|\underline{\alpha}^{(i)}| = r^{(i)}$ ($r^{(i)} > 0$).

Equation (5.1) and the two aforementioned conditions will be used to construct a limiting surface concept. From Equation (5.1), it can be derived that,

$$d\underline{\alpha}^{(i)} : \underline{L}^{(i)} = f_1^{(i)} \left(\underline{n} : \underline{L}^{(i)} - f_2^{(i)} \underline{L}^{(i)} : \underline{L}^{(i)} \right) dp = f_1^{(i)} \left(\underline{n} : \underline{L}^{(i)} - f_2^{(i)} \right) dp \quad . \quad (5.2)$$

According to CONDITION 1, $f_1^{(i)}$ is greater than or equal to zero. The equivalent plastic strain increment, dp, is also non-negative. Therefore from Equation (5.2), the sign of the quantity $d\underline{\alpha}^{(i)} : \underline{L}^{(i)}$ is the same as the sign of the quantity $\left(\underline{n} : \underline{L}^{(i)} - f_2^{(i)} \right)$. Knowing that $f_2^{(i)} \geq \underline{n} : \underline{L}^{(i)}$ when $|\underline{\alpha}^{(i)}| = r^{(i)}$ (CONDITION 2), examination of Equation (5.2) leads to the following inequality,

$$d\underline{\alpha}^{(i)} : \underline{L}^{(i)} \leq 0 \qquad \text{when } |\underline{\alpha}^{(i)}| = r^{(i)} \quad . \tag{5.3}$$

Since the backstresses are initially zero, the previous inequality implies that whenever $\underline{\alpha}^{(i)}$ reaches a surface with a radius $r^{(i)}$, the increment of $\underline{\alpha}^{(i)}$, $d\underline{\alpha}^{(i)}$, makes an obtuse or right angle to $\underline{\alpha}^{(i)}$. As a result of this characteristic of the translation of a backstress part, the backstress part will never go beyond a surface which has a radius of $r^{(i)}$ and is centered at the origin. This surface will be referred to as a limiting surface for a backstress part in subsequent discussions.

The framework characterized by Equation (5.1) with CONDITION 1 and CONDITION 2 represents a class of nonlinear hardening rules where the total backstress is divided into several parts and each part of the total backstress has a limiting surface. It can be found that all of the Armstrong-Frederick type hardening rules, including those of Chaboche _et al._ (1979, 1987, 1991) and Ohno-Wang (1991a, 1991c, 1993a, 1993b), are specific cases within this framework. For example, the Chaboche hardening rule without a threshold is represented by $f_1^{(i)} = c^{(i)} r^{(i)}$ and $f_2^{(i)} = \dfrac{|\underline{\alpha}^{(i)}|}{r^{(i)}}$ (refer to Equation(2.24)), which also satisfy the two conditions. The basic Armstrong-Frederick rule, Equation (2.18), is the case for which M=1, $f_1^{(1)} = a_a$, $f_2^{(1)} = \dfrac{c_a}{a_a} |\underline{\alpha}|$. For this model, there is a limiting surface for the total backstress $\underline{\alpha}$ with a radius of $r^{(1)} = \dfrac{a_a}{c_a}$. With this generalization, the existing Armstrong-Frederick type hardening rules can be explored with a limiting surface concept. In other words, a prevalent characteristic of all the Armstrong-

Frederick type hardening rules is the current interpretation of the limiting surface for a backstress part. The difference between the Armstrong-Frederick type hardening rules lies in the distinctive specification of the magnitude and direction of a backstress part within a limiting surface. Such an interpretation allows the material constants for these models to be determined via a standard procedure, which will be the focus point of the next chapter. More importantly, the limiting surface concept provides a convenient framework to construct refined hardening algorithms.

5.2. A New Hardening Rule

Assume that the total backstress $\underline{\alpha}$ is divided into M parts (Equation (2.21)). It is now proposed that each backstress part $\underline{\alpha}^{(i)}$ takes on the following specific form,

$$d\underline{\alpha}^{(i)} = c^{(i)} r^{(i)} \left(\underline{n} - \left(\frac{\|\underline{\alpha}^{(i)}\|}{r^{(i)}} \right)^{\chi^{(i)}+1} \underline{L}^{(i)} \right) dp \qquad (i=1, 2, ..., M) . \qquad (5.4)$$

In general, $c^{(i)}$, $r^{(i)}$, and $\chi^{(i)}$ are three sets of non-negative and single-valued scalar functions. A geometric interpretation of the new hardening rule is presented in Figure 5.1. The limiting surface for the ith backstress part $\underline{\alpha}^{(i)}$ has a radius of $r^{(i)}$. If the exponent $\chi^{(i)} >> 0$, the nonlinear term in Equation (5.4) is approximately zero when the backstress $\underline{\alpha}^{(i)}$ is within the limiting surface ($\left| \underline{\alpha}^{(i)} \right| < r^{(i)}$). As a result of this inequality, the increment of this backstress part, $d\underline{\alpha}^{(i)}$, follows the normal direction, $\underline{n}$, to the yield surface (Figure 5.1a) for both proportional and nonproportional loading. The nonlinear term in Equation (5.4) is fully recovered when the backstress is on the limiting surface ($\left| \underline{\alpha}^{(i)} \right| = r^{(i)}$) (Figure 5.1b), and $d\underline{\alpha}^{(i)}$ is no longer in the normal direction to the yield surface. This condition is often referred to as dynamic recovery in the literature. For proportional loading, $\underline{L}^{(i)}$ is either consistent with $\underline{n}$ or opposite to it (i.e., $\underline{L}^{(i)} = \pm\underline{n}$). Therefore, for proportional loading when $\underline{\alpha}^{(i)}$ is on the limiting surface, $d\underline{\alpha}^{(i)}$ is either zero ($\underline{L}^{(i)} = \underline{n}$) or opposite to $\underline{\alpha}^{(i)}$ ($\underline{L}^{(i)} = -\underline{n}$).

The resulting plastic modulus function corresponding to the new hardening rule (Equation (5.4)) is,

$$h = \sum_{i=1}^{M} c^{(i)} r^{(i)} \left(1 - \left(\frac{\|\underline{\alpha}^{(i)}\|}{r^{(i)}} \right)^{\chi^{(i)}+1} \underline{L}^{(i)}{:}\underline{n} \right) + \sqrt{2} \frac{dk}{dp} , \qquad (5.5)$$

or,

$$h = \sum_{i=1}^{M} h^{(i)} + \sqrt{2}\,\frac{dk}{dp} \ , \tag{5.6}$$

where,

$$h^{(i)} = c^{(i)} r^{(i)} \left(1 - \left(\frac{\left| \alpha^{(i)} \right|}{r^{(i)}} \right)^{\chi^{(i)}+1} \underset{\sim}{L}^{(i)} {:} \underset{\sim}{n} \right) \qquad (i=1, 2, ..., M) \ . \tag{5.7}$$

The quantity $h^{(i)}$ represents the contribution of the ith backstress to the plastic modulus function.

Comparing Equation (5.4) with the Ohno-Wang II hardening rule (Equations (2.22) and (2.27)), one can find that the difference between the two hardening rules is that the Ohno-Wang rule includes the MacCauley bracket term $\langle \underset{\sim}{L}^{(i)} {:} \underset{\sim}{n} \rangle$. The implication of the format is that when a backstress part $\underset{\sim}{\alpha}^{(i)}$ is on the limiting surface, the increment of this backstress part, $d\underset{\sim}{\alpha}^{(i)}$, is in the direction tangential to the limiting surface ($\underset{\sim}{L}^{(i)} {:} \underset{\sim}{n} \geq 1$) or follows the normal direction to the yield surface ($\underset{\sim}{L}^{(i)} {:} \underset{\sim}{n} < 1$, refer to Figure 2.2). When $\underset{\sim}{\alpha}^{(i)}$ is within the limiting surface, translation of the backstress part is again in a direction normal to the yield surface. In contrast to the Ohno-Wang model, in the current hardening rule, $d\underset{\sim}{\alpha}^{(i)}$ always makes an obtuse angle with $\underset{\sim}{\alpha}^{(i)}$ for nonproportional loading when $\underset{\sim}{\alpha}^{(i)}$ is on the limiting surface (refer to Figure 2.2 and Figure 5.1). The new hardening rule differs little from the Ohno-Wang model for the deformation modeling of proportional loading, especially when $\chi^{(i)}$ ($i=1, 2, ..., M$) are large numbers. Nonproportional loading is where the effects of this term become important. It should be noted that when $\chi^{(i)} = 0$ ($i=1, 2,...$ M) the new hardening rule duplicates the initial Chaboche model (Chaboche et al., 1979; Chaboche, 1987) represented by Equation (2.24). Since the Chaboche model has the ability to predict constant ratchetting for any cyclic loading, the new hardening rule will be able to overcome the Ohno-Wang model's inability to predict constant ratchetting for nonproportional loading. The presence of non-zero $\chi^{(i)}$ terms enables the new hardening rule to model materials that display ratchetting rate decay.

5.3. A Memory Surface

The purpose of a memory surface is to consider the cyclic material behavior which is neither a monotonic function of the loading history nor a direct function of an internal variable such as the backstress. A memory surface is introduced in the deviatoric stress space to improve the prediction of transient behavior. A scalar function g is used to represent this surface,

$$g = |\underset{\sim}{\alpha}| - R_M \leq 0 \ , \tag{5.8}$$

where $|\underset{\sim}{\alpha}|$ is the magnitude of the total backstress $\underset{\sim}{\alpha}$ as defined by Equation (2.2). The evolution for the variable R_M, the radius of the memory surface, is,

$$dR_M = H(g) \langle L : d\underset{\sim}{\alpha} \rangle - c_M \left\langle 1 - \frac{|\underset{\sim}{\alpha}|}{R_M} \right\rangle dp \ . \tag{5.9}$$

The tensorial quantity $\underset{\sim}{L}$ is defined in terms of the total backstress as follows,

$$\underset{\sim}{L} = \frac{\underset{\sim}{\alpha}}{|\underset{\sim}{\alpha}|}. \tag{5.10}$$

Again, H in Equation (5.9) is the Heaviside step function (H(x)=1 if x≥0 and H(x)=0 if x<0). The initial value for R_M is zero. In numerical analysis, it is often practical to assume R_M to be a small number. A schematic illustration of the proposed memory surface is presented in Figure 5.2. When the total backstress $\underset{\sim}{\alpha}$ is on the memory surface and is moving outward (Figure 5.2(a)), the memory surface expands so that the condition of Equation (5.8), g =0, is satisfied. When the backstress is moving within the memory surface, the memory surface may contract (if c_M>0) with subsequent plastic deformation (Figure 5.2(b)). This ability of the surface to contact mirrors experimental results where the memory of prior events decays with additional cycling. The cyclically stabilized memory surface will have a radius which is the maximum $|\underset{\sim}{\alpha}|$ of the $\underset{\sim}{\alpha}$ locus for the loading history under which the material stabilized. This geometrically implies that the memory surface and the $\underset{\sim}{\alpha}$ locus inscribe at one point (Figure 5.2(c)). The current value of R_M more strongly reflects the recent prior loading history rather than the entire history.

Several memory surface concepts have been developed. The difference between the existing memory surface concepts lies in the choice of plastic strain

space and stress space, the "stress/strain range" or "maximum stress/strain" to measure the memory effect, and whether there is a recovery term. Chaboche *et al.* (1979), Ohno (1982), and Ohno and Kachi (1986) developed memory surfaces based on plastic strain space and used the "strain range" as a measure for the prior history effect without a recovery term. McDowell (1985a) incorporated a recovery term in the evolution equation of the surface in strain space employing "strain range" as a measuring parameter. Within the framework of a two-surface model, Bruhns *et al.* (1992) introduced a memory surface in stress space, also including a recovery term that allowed the surface to contract. They used "maximum stress" to quantify the memory effect.

A stress based memory surface was chosen for the current model. The interpretation of "stress range" or "maximum stress" as a measure for stress level effect was based on the results of two different tests. Recall the stress level effect displayed in the comparisons of the experiments with the Ohno-Wang model predictions shown in Figures 4.11 and 4.20. The uniaxial ratchetting tests have approximately the same stress range. The difference between these uniaxial tests is the maximum stress. The other test was for the non-Masing behavior. Shown in Figure 5.4 are two hysteresis loops at cycle 4100 for two uniaxial tests with different maximum stresses but similar stress ranges. It can be concluded from this figure that a "maximum stress" is a more appropriate measure for the memory surface than the "stress range", because the larger maximum stress test has a smaller plastic strain range. This is reflected by the choice of maximum $|\alpha|$ as the radius of the memory surface.

5.4. Cyclic Hardening

Transient behavior can be considered by allowing the constants, $c^{(i)}$, $r^{(i)}$, or $\chi^{(i)}$, utilized in the limiting surface concept (Section 5.2) to become functions of loading variables. Cyclic hardening can be considered with $c^{(i)}$ being functions of the accumulated plastic strain,

$$c^{(i)} = c_0^{(i)}\left(1 + a_1^{(i)}e^{-b_1^{(i)}p} + a_2^{(i)}e^{-b_2^{(i)}p}\right) \qquad (i=1, 2, ..., M) \ , \qquad (5.11)$$

where $c_0^{(i)}$, $a_1^{(i)}$, $a_2^{(i)}$, $b_1^{(i)}$, and $b_2^{(i)}$ are material constants. This expression is similar to that proposed by Marquis (1979), but Equation (5.11) contains one more term. When the material displays monotonic hardening or monotonic softening, only

two terms in Equation (5.11) are needed. When the material behavior is mixed hardening/softening, all three terms are necessary.

In a modification of the Ohno-Wang hardening rule, Equations (2.22) and (2.27), McDowell (1992) suggested that the cyclic hardening be considered through coefficients $r^{(i)}$ (i=1, 2, ..., M) as functions of the accumulated plastic strain. In this case, there is a possibility for a backstress $\underline{\alpha}^{(i)}$ to be outside of the limiting surface, which violates CONDITION 2 and may lead to qualitative changes in the translation of the backstress part. To illustrate this possibility, consider a uniaxial tension-compression test. Assume that a material is undergoing elastic-plastic deformation and a backstress $\underline{\alpha}^{(i)}$ has been saturated (on a limiting surface with radius $r^{(i)}$). According to either the Ohno-Wang or the new hardening rule, $\underline{\alpha}^{(i)}$ should stay on the limiting surface as long as the uniaxial loading is maintained in the same direction. Furthermore, consider that the limiting surface is allowed to contract with plastic deformation when simulating cyclic softening. Contraction of a limiting surface when the backstress $\underline{\alpha}^{(i)}$ has been saturated could result in $\underline{\alpha}^{(i)}$ being outside of the limiting surface, if additional conditions are not enforced. In order to avoid unnecessary complexity, the use of $c^{(i)}$ when modeling this behavior eliminates a possible inconsistency.

The 1070 steel used for a majority of the comparisons does not display appreciable cyclic hardening, hence an alternate material is chosen to examine the performance of Equation (5.11) in conjunction with the new hardening rule for cyclic hardening. Uniaxial test results of 6061-T6 aluminum alloy (Kurath, 1992), which displays significant cyclic hardening, are compared with the simulations in Figure 5.4. Because the material displays monotonic cyclic hardening, only the first two terms in Equation (5.11) are considered. In the simulation, the constant M in Equation (5.11) is 5 and other material constants are listed in Table 8 for the aluminum alloy. Clearly, the new hardening rule incorporating Equation (5.11) duplicates the experimentally observed cyclic hardening.

5.5. Nonproportionality and Stress Level Effects on Ratchetting

It was demonstrated earlier in the text that the primary influence of the exponents $\chi^{(i)}$ (i=1, 2, ..., M) is on the ratchetting predictions. If stress level and nonproportionality have effects on ratchetting, modification of $\chi^{(i)}$ seems appropriate. The quantity $(\underline{n} : \underline{L}^{(i)})$ is incorporated into the formulation of $\chi^{(i)}$ to

consider the nonproportionality effect on ratchetting in the following mathematical relation,

$$\chi^{(i)} = \chi_0^{(i)} \left(2 - \underline{n}{:}\underline{L}^{(i)}\right) \qquad (i=1, 2, ..., M) \; , \qquad (5.12)$$

where $\chi_0^{(i)}$ is a constant for a given stress level. The exponent $\chi_0^{(i)}$ can be further related to the size of the memory surface, R_M, to consider the stress level effect on ratchetting. The following relationship is found to be suitable to model the stress level effect,

$$\chi_0^{(i)} = Q^{(i)} \left(1 + a_\chi e^{b_\chi R_M}\right) \qquad (i=1, 2, ..., M) \; , \qquad (5.13)$$

where $Q^{(i)}$ (i=1, 2, ..., M), a_χ, and b_χ are constants. Combining Equation (5.12) with Equation (5.13) results in,

$$\chi^{(i)} = Q^{(i)} \left(2 - \underline{n}{:}\underline{L}^{(i)}\right)\left(1 + a_\chi e^{b_\chi R_M}\right) \; . \qquad (5.14)$$

Because $\left(\underline{n} : \underline{L}^{(i)}\right)$ can be interpreted as a measure of nonproportionality, the term $\left(2 - \underline{n}{:}\underline{L}^{(i)}\right)$ takes into account the nonproportionality effect on ratchetting. Roughly speaking, Equation (5.12) implies that the exponents $\chi^{(i)}$ (i=1, 2, .., M) are larger under nonproportional loading than under proportional loading. The term $\left(1 + a_\chi e^{b_\chi R_M}\right)$ in Equation (5.13) accounts for the stress level effect. For higher stress levels, the memory surface is larger. As a result, $\chi^{(i)}$ is larger. Therefore, the predicted ratchetting rate will be smaller than when $\chi^{(i)}$ is a constant. This is consistent with the experimental observations on 1070 steel and those reported by Chaboche and Nouailhas (1989a, 1989b).

5.6. Non-Masing Behavior

Jhansale (1975) suggested that the non-Masing behavior be modeled by considering changes in the yield stress. Ellyin et al. (Lefebvre and Ellyin, 1984; Ellyin, 1985; Golos and Ellyin, 1988) also used a similar concept to incorporate non-Masing behavior when refining a fatigue damage parameter. The non-Masing results on various materials (Abdel-Raouf et al., 1977; Golos and Ellyin, 1988; Jhansale, 1975; Jiang and Sehitoglu, 1993d; Li and Laird, 1993; Winter, 1974) indicate that the change in yield stress is a reasonable choice to model this phenomenon. Because the non-Masing behavior is related to the recent loading

history, the size of the memory surface can be used to model the non-Masing behavior. For the 1070 steel, the following relationship is sufficient,

$$k = k_1 \left(1 + a_k e^{c_k R_M} \right) ,$$

(5.15)

where k_1, a_k, and c_k are constants. It can be derived that the consideration of the non-Masing behavior through k will automatically satisfy the condition set forth for the increment of k (Equation (2.38)) in Section 2.5.5. The simulation of non-Masing behavior using Equation (5.15) in conjunction with the new hardening rule and experimental results are shown in Figure 5.5. The material constants used for 1070 steel are listed in Table 8. Equation (5.15) is able to capture the phenomenon both qualitatively and quantitatively.

5.7. Generalization and Discussion

It should be noted that within the framework of hardening rules previously introduced, the limiting surfaces for the backstresses (Equation (5.1)) do not translate at any time. A more general hardening rule with the limiting surface having the ability to translate can be constructed. In this case, an additional internal variable, $\underset{\sim}{\beta}$, to describe the center of the limiting surface should be included. Mathematically, this general framework of hardening rules can be expressed as,

$$\underset{\sim}{\alpha} = \sum_{i=1}^{M} \underset{\sim}{\alpha}^{(i)} ,$$

(5.16)

$$\underset{\sim}{\beta} = \sum_{i=1}^{M} \underset{\sim}{\beta}^{(i)} ,$$

(5.17)

$$d\underset{\sim}{\alpha}^{(i)} = f_1^{(i)} \left(\underset{\sim}{n} - f_2^{(i)} \underset{\sim}{L}^{(i)} \right) dp \qquad (i=1, 2, ..., M) ,$$

(5.18)

where,

$$\underset{\sim}{L}^{(i)} = \frac{\underset{\sim}{\alpha}^{(i)} - \underset{\sim}{\beta}^{(i)}}{\left| \underset{\sim}{\alpha}^{(i)} - \underset{\sim}{\beta}^{(i)} \right|} \qquad (i=1, 2, ..., M) ,$$

(5.19)

$$\left| \underset{\sim}{\alpha}^{(i)} - \underset{\sim}{\beta}^{(i)} \right| = \sqrt{\left(\underset{\sim}{\alpha}^{(i)} - \underset{\sim}{\beta}^{(i)} \right) : \left(\underset{\sim}{\alpha}^{(i)} - \underset{\sim}{\beta}^{(i)} \right)} \qquad (i=1, 2, ..., M) .$$

(5.20)

The quantities $f_1^{(i)}$ and $f_2^{(i)}$ are functions of the backstresses, which satisfy the following general conditions,

CONDITION 1a $f_1^{(i)}$ is a single-valued non-negative, and,

CONDITION 2a $f_2^{(i)} \geq \underset{\sim}{n} : \underset{\sim}{L}^{(i)}$ when $\left| \underset{\sim}{\alpha}^{(i)} - \underset{\sim}{\beta}^{(i)} \right| = r^{(i)}$ $(r^{(i)} > 0)$

There is a limiting surface for the quantity $\left(\underset{\sim}{\alpha}^{(i)} - \underset{\sim}{\beta}^{(i)} \right)$. The limiting surface has a radius of $r^{(i)}$ and is centered at $\underset{\sim}{\beta}^{(i)}$ (Figure 5.6). The characteristics of this limiting surface is similar to that discussed in section 5.2. The difference between Equation (5.1) and Equations (5.15)-(5.19) is that in Equation (5.1) the center of the limiting surface is fixed at the origin while according to Equations (5.16)-(5.19), the center of the limiting surface can translate. With the additional capability of translation for the limiting surfaces, Equations (5.16)-(5.19) represent a class of hardening rules which theoretically could handle more complex material behavior. These possibilities include additional anisotropy due to preloading a material and nonproportional hardening beyond that inherently predicted by the models. It is noted that the Bower model, Equation (2.20), is a special case where M=1, $f_1^{(1)} = a_b$, and $f_2^{(1)} = \frac{c_{b1}}{a_b} \left| \underset{\sim}{\alpha} - \underset{\sim}{\beta} \right|$. There is a limiting surface for $\left(\underset{\sim}{\alpha} - \underset{\sim}{\beta} \right)$ which has a radius of $r^{(1)} = \frac{a_b}{c_{b1}}$. Bower (1987) used this term to improve the modeling of ratchetting rate decay.

Analogous to the new hardening rule presented in Section 5.2, a possible choice for $f_1^{(i)}$ and $f_2^{(i)}$ could be,

$$ f_1^{(i)} = c^{(i)} r^{(i)} \qquad (i=1, 2, ..., M) , \qquad (5.21) $$

$$ f_2^{(i)} = \left(\frac{\left| \underset{\sim}{\alpha}^{(i)} - \underset{\sim}{\beta}^{(i)} \right|}{r^{(i)}} \right)^{\chi^{(i)}+1} \qquad (i=1, 2, ..., M) . \qquad (5.22) $$

A schematic illustration for the model described by Equations (5.21) and (5.22) is presented in Figure 5.6

It should be noted that the evolution for the internal variable $\underset{\sim}{\beta}^{(i)}$ has yet to be formalized. From the ratchetting analyses performed (discussed in the subsequent chapter), such an additional variable is found unnecessary for 1070 steel. Therefore, the presentation of the more general framework of hardening rules may be useful for future studies of different materials.

In the previous sections, the cyclic hardening was related to the accumulated equivalent plastic strain with a power law relation. The parameter $(\underline{n} : \underline{L}^{(i)})$ was used to characterize the nonproportionality effect on ratchetting, and the size of the memory surface was used to consider the stress level effect on both ratchetting and non-Masing behavior. It should be noted that for other materials the detailed relationships for nonproportionality effects, stress level effect, and consideration of non-Masing behavior could differ in form from those forwarded in Equations (5.11)-(5.15). Based on the previous arguments forwarded with regard to the limiting surface size, it may be convenient to set $r^{(i)}$ (i=1, 2, ..., M) as constants, while the other two sets of coefficients, $c^{(i)}$ and $\chi^{(i)}$ (i=1, 2, ..., M), can be further functions of the stress state to consider the transient cyclic behavior. General expressions for $c^{(i)}$ and $\chi^{(i)}$ could take the following forms,

$$c^{(i)} = \Omega^{(i)}(p, R_M, \underline{n} : \underline{L}^{(i)}) \qquad (i=1, 2, ..., M) \ , \tag{5.23}$$

$$\chi^{(i)} = \Gamma^{(i)}(R_M, \underline{n} : \underline{L}^{(i)}) \qquad (i=1, 2, ..., M) \ , \tag{5.24}$$

where $\Omega^{(i)}$ and $\Gamma^{(i)}$ denote functions. Because $\chi^{(i)}$ (i=1, 2, ..., M) have influence only for the unbalanced loading, $c^{(i)}$ (i=1, 2, ..., M) should consider all the cyclic transient material properties observed in balanced loading. Obviously, $c^{(i)}$ (i=1, 2, ..., M) are strong functions of the accumulated equivalent strain, p, for cyclic hardening/softening materials. The nonproportionality effect can be significant for materials such as stainless steel, where translation of the limiting surface (i.e., $\underline{\beta}^{(i)}$) may be an effective technique. The stress level effect on transient behavior may also be considered for some materials within the constants for $c^{(i)}$ (i=1, 2, ..., M). Further systematic experiments under both balanced and unbalanced loading are needed for different materials before a detailed relationship equivalent to Equations (5.11)-(5.15) can be formalized.

The model does not consider the cross-hardening effect observed in stainless steel (Tanaka et al, 1985a, 1985b; McDowell, 1983a). As has been discussed previously, cross-hardening is material dependent. Because the material investigated in this work, 1070 steel, displays insignificant cross hardening, no attempt has been made to model this material behavior. However, within the framework introduced in this chapter, it seems possible to consider

the cross-hardening with the introduction of another memory parameter. Cross-hardening is in fact a reflection of the nonproportionality effect when the loading path changes. This effect fades with increasing number of loading cycles in a subsequent loading step. With this in mind, a reasonable variable which can be related to a memory parameter for describing the cross-hardening effect could be $\underline{L}:\underline{n}$, where $\underline{L}$ is the unit vector of the total backstress (Equation (5.10)) and $\underline{n}$ is the unit normal on the yield surface at the stress state (refer to Figure 2.1). The value of $\underline{L}:\underline{n}$ characterizes the overall nonproportionality. For proportional loading, $|\underline{L}:\underline{n}| \equiv 1$. For nonproportional loading, $|\underline{L}:\underline{n}| \leq 1$. When a proportional path ($|\underline{L}:\underline{n}| \equiv 1$) is changed to another "proportional" path, the value of $|\underline{L}:\underline{n}|$ experiences a sudden change from 1 to a value less than 1. As the loading cycles increase in the subsequent loading history, the value of $|\underline{L}:\underline{n}|$ approaches 1. This change of the $|\underline{L}:\underline{n}|$ value is consistent with the sudden change in the stress response of the subsequent loading step. A parameter memorizing $|\underline{L}:\underline{n}|$, which fades with loading history, may be constructed in an analogous fashion to that forwarded for the memory surface described by Equations (5.8)-(5.10). Additional coefficients in the $c^{(i)}$ (i=1, 2, ..., M) format could be added for this memory parameter, which could then consider the cross-hardening effect. The details of the formulation for cross-hardening are left for future studies.

The stress-strain response of the first reversal (monotonic stress-strain response) under uniaxial tension-compression can be very different from those of the subsequent cycles. This is especially significant for medium and low carbon steels which display a distinct upper yield strength which depends strongly on the stress/strain rate of the loading. This first reversal behavior is difficult to consider within the current framework of incremental plasticity. For balanced loading, the first reversal behavior has no effect on the stabilized stress-strain predictions. However, it has significant effect on the total ratchetting predicted for stress-controlled unbalanced loading. For more accurate ratchetting predictions, the first reversal behavior may need to be considered separately.

6. DETERMINATION OF MATERIAL CONSTANTS

When a plasticity model involves a number of material constants, it is always desirable that the material constants can be easily determined from the results of simple experiments. In this chapter, a computational procedure is introduced to determine the material constants for the mathematical model developed in the previous chapter. While particular forms may differ, the following procedure is applicable to the class of hardening rules introduced in Section 5.2. The concept of a limiting surface for a backstress facilitates the determination of the constants. The final format of the new model under consideration is listed in Table 9.

6.1. Analysis of Uniaxial Tension-Compression

For the uniaxial tension-compression test, let $\sigma = \sigma_{11}$ and $\varepsilon^p = \varepsilon^p_{11}$ represent the axial stress and axial plastic strain respectively. Consideration of the one dimensional problem results in the following simplifications,

$$\left| \underset{\sim}{\alpha}^{(i)} \right| = \sqrt{\frac{3}{2}} \ \left| \alpha^{(i)}_{11} \right| , \tag{6.1a}$$

$$L^{(i)}_{11} = \frac{\alpha^{(i)}_{11}}{\left| \underset{\sim}{\alpha}^{(i)} \right|} = \pm \sqrt{\frac{2}{3}} , \tag{6.1b}$$

$$n_{11} = \pm \sqrt{\frac{2}{3}} . \tag{6.1c}$$

In order to determine the material constants, assume that the uniaxial loading begins from the most compressive stress state where all the backstresses are saturated. With this initial condition, Equation (2.15) takes the following form,

$$dp = \sqrt{\frac{3}{2}} \ d(\Delta \varepsilon^p) , \tag{6.2}$$

where $\Delta\varepsilon^p$ is the axial plastic strain range measured from the strain state corresponding to the most compressive stress state. When the hardening rule, Equation (5.4), is simplified for the one dimensional problem, it results in,

$$d\left(\frac{\sqrt{\frac{3}{2}}\alpha_{11}^{(i)}}{r^{(i)}}\right) = \left[1 - \left(\frac{\sqrt{\frac{3}{2}}\left|\alpha_{11}^{(i)}\right|}{r^{(i)}}\right)^{\chi^{(i)}} \frac{\sqrt{\frac{3}{2}}\alpha_{11}^{(i)}}{r^{(i)}}\right] d\left(c^{(i)}\Delta\varepsilon^p\right)$$

$$(i=1, 2, ..., M) . \qquad (6.3)$$

Equation (6.3) represents a differential equation where $\Delta\varepsilon^p$, the plastic strain range, is the only independent variable and $\alpha_{11}^{(i)}$ (i=1, 2, ..., M) are the functions of $\Delta\varepsilon^p$, as was stipulated for Equation (5.4).

Without loss of generality, let,

$$x = c^{(i)}\Delta\varepsilon^p; \qquad y = \frac{\sqrt{\frac{3}{2}}\alpha_{11}^{(i)}}{r^{(i)}} ; \qquad \text{and} \quad m = \chi^{(i)} . \qquad (6.4)$$

The differential equation, Equation (6.3), simplifies to,

$$\frac{dy}{dx} = 1 - |y|^m \, y . \qquad (6.5)$$

Because the loading begins from the most compressive stress state where all the backstresses were assumed to be saturated in that direction, the initial condition is,

$$\alpha_{11}^{(i)} = -\sqrt{\frac{2}{3}}r^{(i)} \qquad \text{when } \Delta\varepsilon^p = 0 , \qquad (6.6a)$$

or corresponding to the simplification in Equation (6.5),

$$y\big|_{x=0} = -1 . \qquad (6.6b)$$

The differential equation, Equation (6.5), with the initial condition stipulated in Equation (6.6b), can be solved numerically using a Gaussian integration method (Gerald and Wheatley, 1984). Three solutions, corresponding

to m=0, 2, and +∞, result from the implementation of the aforementioned technique, and are shown in Figure 6.1. It can be found that all solutions to the differential equation are curves which are asymptotic at y=1. Subsequent numerical analysis has verified that this asymptotic curve is valid for initial conditions $1 \geq y|_{x=0} \geq -1$. Since $|\underline{\alpha}^{(i)}| = \sqrt{\frac{3}{2}}|\alpha_{11}^{(i)}|$ (Equation 6.1) for uniaxial tension-compression, the asymptotic curve represents a limiting surface for the one dimensional problem. Figure 6.1 reveals that the solution to the differential equation does not have a strong dependence on the exponent m. When the exponent m is larger than a certain value, the relationship between x and y is approximately bilinear, leading to

$$y = 1 \qquad \text{when } x = 2 \ . \tag{6.7}$$

When the bilinear solution is incorporated into Equation (6.4), the aforementioned solution (Equation (6.7)) is equivalent to,

$$\alpha_{11}^{(i)} = \sqrt{\frac{2}{3}}r^{(i)} \qquad \text{when } c^{(i)}\Delta\varepsilon^p = 2 \qquad (i=1, 2, \dots M) \ . \tag{6.8}$$

Again, applying the stipulations inferred by Equation (6.1), Equation (6.8) can be summarized as follows,

$$\frac{|\underline{\alpha}^{(i)}|}{r^{(i)}} = 1 \qquad \text{when } c^{(i)}\Delta\varepsilon^p = 2 \qquad (i=1, 2, \dots M) \ , \tag{6.9}$$

where $\Delta\varepsilon^p$ is the plastic strain range at which the ith backstress part $\underline{\alpha}^{(i)}$ is saturated. Invoking the concept of a limiting surface has allowed a special relation between $c^{(i)}$ and $\Delta\varepsilon^p$ to be formulated. This relationship will be vital when attempting to determine $c^{(i)}$ and $r^{(i)}$ in subsequent sections. Two methods will be discussed in Sections 6.2.1 and 6.2.2 to determine these constants.

6.2. Determination of $c^{(i)}$ and $r^{(i)}$

While $c^{(i)}$ (i=1, 2, … M) and k, the yield stress, may be used as functions to model transient behavior, it is assumed that they remain constant for a given reversal. If no transient behavior is considered, the stabilized deformation should be used. Also assume that $\chi^{(i)}$ (i=1, 2, … M) are infinitely large. Since $\chi^{(i)}$

has its most pronounced influence on ratchetting, which is not under consideration here, this assumption has minimal effect on the quantitative values for the constants, $c^{(i)}$ and $r^{(i)}$ (i=1, 2, ... M). The major implication of this assumption is that the uniaxial stress-strain curve predicted is piece wise linear. One of the solutions to the differential equation, utilizing these assumptions, becomes,

$$\left(\frac{\left|\underline{\alpha}^{(i)}\right|}{r^{(i)}}\right)^{\chi^{(i)}+1} = 0 \qquad \text{when } \left|\underline{\alpha}^{(i)}\right| < r^{(i)} \ , \tag{6.10a}$$

$$\left(\frac{\left|\underline{\alpha}^{(i)}\right|}{r^{(i)}}\right)^{\chi^{(i)}+1} = 1 \qquad \text{when } \left|\underline{\alpha}^{(i)}\right| = r^{(i)} \ , \tag{6.10b}$$

where $\left|\underline{\alpha}^{(i)}\right| = r^{(i)}$ infers saturation of the ith backstress $\underline{\alpha}^{(i)}$. Manipulating Equation (6.10) and Equation (5.5), the plastic modulus function can be expressed in the following form when only the backstresses, j=1 to (i-1), are saturated,

$$h_{(i)} = \sum_{j=i}^{M} c^{(j)} r^{(j)} \ . \tag{6.11}$$

The scalar $h_{(i)}$ is the value of the plastic modulus function between the intervals corresponding to point i and point i+1 (Figure 6.2). If $\Delta\varepsilon^p_{(i)}$ denotes the plastic strain range at which the ith backstress $\underline{\alpha}^{(i)}$ is saturated, then,

$$c^{(i)} \Delta\varepsilon^p_{(i)} = 2 \qquad (i=1, 2, ... M) \ . \tag{6.12}$$

Equations (6.11) and (6.12) govern the two sets of material constants $c^{(i)}$ and $r^{(i)}$. However, these two equations alone are not sufficient for the determination of the constants $c^{(i)}$ and $r^{(i)}$.

6.2.1. Determination of $r^{(i)}$ with Presumed $c^{(i)}$

When transient behavior such as cyclic hardening is ignored and $c^{(i)}$ (i=1, 2, ... M) remain constant, a simple procedure can be proposed to calculate the constants $r^{(i)}$ (i=1, 2, ... M). Select M points in the $\Delta\sigma$ - $\Delta\varepsilon^p$ curve from the uniaxial test (refer to Figure 6.2) so that the stress range, $\Delta\sigma_{(i)}$, and plastic strain range, $\Delta\varepsilon^p_{(i)}$, are known for any point i. Note that again $\Delta\varepsilon^p_{(i)}$ denotes the plastic strain

range at which the ith backstress $\alpha^{(i)}$ is saturated, and $\Delta\sigma_{(i)}$ is the stress range corresponding to $\Delta\varepsilon^p_{(i)}$. From Equation (6.12) it follows that,

$$c^{(i)} = \frac{2}{\Delta\varepsilon^p_{(i)}} \qquad (i=1, 2, ..., M) \ . \qquad (6.13)$$

For the uniaxial test the plastic modulus function at point i is computed according to Equation (6.11). Utilizing the results of Equation (6.13), the radius of the ith limiting surface can be computed as follows,

$$r^{(i)} = \frac{2}{3} \frac{H_{(i)} - H_{(i+1)}}{c^{(i)}} \qquad (i=1, 2, ..., M) \ , \qquad (6.14)$$

where

$$H_{(i)} = \frac{\Delta\sigma_{(i)} - \Delta\sigma_{(i-1)}}{\Delta\varepsilon^p_{(i)} - \Delta\varepsilon^p_{(i-1)}} \qquad (i=1, 2, ..., M) \ , \qquad (6.15)$$

$$\Delta\sigma_{(0)} = 2\sigma_y = 2\sqrt{3}\, k \ , \qquad (6.16a)$$

$$\Delta\varepsilon^p_{(0)} = 0; \qquad H_{(M+1)} = 0 \ . \qquad (6.16b)$$

The yield stress σ_y in Equation (6.16a) is half the linear elastic portion in Figure 6.2. The constant k is the yield stress in pure shear and is related to uniaxial loading via the von Mises criterion. The maximum stress range, $\Delta\sigma_{(M)}$, satisfies the following condition,

$$\Delta\sigma_{(M)} = \Delta\sigma_{max} = 2\sqrt{\frac{3}{2}} \sum_{i=1}^{M} r^{(i)} + 2\,\sigma_y \ , \qquad (6.17)$$

where $\Delta\sigma_{max}$ is the maximum stress range that the model is intended to simulate, often the saturation strength in the positive direction. The procedure (Equations (6.13)-(6.15)) is repeated until all $c^{(i)}$ and $r^{(i)}$ ($i=1, 2, ..., M$) have been determined.

6.2.2. Determination of $c^{(i)}$ with Presumed $r^{(i)}$

Within the context used to derive the current model (Section 5.4), the radii of the limiting surfaces, $r^{(i)}$ ($i=1, 2, ..., M$), are assumed to be constants. This method of determining $c^{(i)}$ and $r^{(i)}$ ($i=1, 2, ..., M$) is somewhat more complex.

However, when considering cyclic hardening through $c^{(i)}$ (i=1, 2, ..., M), this format will be useful to determine the constants in Equation (5.11). If a maximum stress range is given and the yield stress has been determined, from Equation (6.17) it follows that,

$$\sum_{i=1}^{M} r^{(i)} = \sqrt{\frac{2}{3}} \left(\frac{\Delta\sigma_{max}}{2} - \sigma_y \right) .$$
(6.18)

Once $\sum_{i=1}^{M} r^{(i)}$ is calculated from Equation (6.18), individual $r^{(i)}$ can be selected. Again, in Figure 6.3, $\Delta\varepsilon^p_{(i)}$ denotes the plastic strain range at which the ith backstress $\underline{\alpha}^{(i)}$ is saturated. The strategy is to find the stress and plastic strain ranges of each point in the stress-strain curve where the corresponding backstress part is saturated. This procedure begins from point M and follows the order M-1, M-2, ..., 1, 0. The plastic strain range at point M, $\Delta\varepsilon^p_{(M)}$, is obtained from the experimental stress-plastic strain curve, $\Delta\sigma = f(\Delta\varepsilon^p)$, for a selected maximum stress range $\Delta\sigma_{(M)}$. When $\Delta\sigma_{(M)}$ and $\Delta\varepsilon^p_{(M)}$ are known, $c^{(M)}$ is calculated from Equation (6.13). Now assume that the stress and strain ranges corresponding to points i+1, i+2,..., M have been found so that $c^{(j)}$ (j=i+1, i+2, ..., M) are all known. The next step is to determine the (i-1)th point. The slope of the line linking the point (i-1) and point i in the stress-strain reversal can be calculated using the following formula,

$$H_{(i)} = \frac{3}{2} \sum_{j=i}^{M} c^{(j)} r^{(j)} .$$
(6.19)

This segment of the stress-strain curve is modeled as piece wise linear and can be described by,

$$\Delta\sigma = \Delta\sigma_{(i)} + H_{(i)} \left(\Delta\varepsilon^p - \Delta\varepsilon^p_{(i)} \right) \qquad (i=1, 2, .., M) .$$
(6.20)

Point (i-1) is one of the piece wise linear segment points that intersects the experimental stress-plastic strain curve, $\Delta\sigma = f(\Delta\varepsilon^p)$ (Figure 6.3). Once the coordinates at point (i-1) are obtained, $c^{(i-1)}$ is calculated employing Equation

(6.13) for a known $\Delta\varepsilon^p_{(i-1)}$. The procedure is repeated until all M segments have been calculated.

There is one additional consideration that should govern the choice of $r^{(M)}$. In order that the other intersection points of the curve $\Delta\sigma = f(\Delta\varepsilon^p)$ and line $\Delta\sigma = \Delta\sigma_{(M)} + H_{(M)}\left(\Delta\varepsilon^p - \Delta\varepsilon^p_{(M)}\right)$ correspond to a lower stress/plastic strain, the slope of the straight line $H_{(M)}$ should be larger than the tangent of the curve $\Delta\sigma = f(\Delta\varepsilon^p)$ at point M. Mathematically, this implies,

$$H_{(M)} = \frac{3}{2} c^{(M)} r^{(M)} > \frac{df(\Delta\varepsilon^p_{(M)})}{d(\Delta\sigma)} \ .$$

(6.21)

Using Equation (6.21) with the condition forwarded in Equation (6.13) results in the following form for this inequality,

$$r^{(M)} > \frac{\varepsilon^p_{(M)}}{3} \frac{df(\Delta\varepsilon^p_{(M)})}{d(\Delta\sigma)} \ ,$$

(6.22)

where $\dfrac{df(\Delta\varepsilon^p_{(M)})}{d(\Delta\sigma)}$ represents the derivative of the stress-plastic strain curve, $\Delta\sigma = f(\Delta\varepsilon^p)$, at point M.

6.2.3. Discussion

The determination of the material constants $c^{(i)}$ and $r^{(i)}$ ($i=1, 2,..., M$) was based on the assumption that the exponents $\chi^{(i)}$ ($i=1, 2,..., M$) were large enough so that the plastic modulus function can be treated as a step function in terms of the plastic strain. In fact, the exponents $\chi^{(i)}$ ($i=1, 2,..., M$) have little influence on the stress-strain prediction for fully reversed tension-compression. Figure 6.4 shows the simulations using the new model for $\chi^{(i)}=0$ and $\chi^{(i)} = +\infty$ ($i=1, 2,..., M$) along with the experimental result. When $\chi^{(i)} = +\infty$ ($i=1, 2,..., M$), the predicted stress-strain hysteresis loop is piece wise linear. When $\chi^{(i)}=0$ ($i=1, 2,..., M$), the predicted stress-strain loop is smooth. In either case, the predicted stress-strain results are in close agreement with the experimental data. This indicates that the material constants $c^{(i)}$ and $r^{(i)}$ ($i=1, 2,..., M$) can be determined following the procedures introduced previously without considering the values of $\chi^{(i)}$ ($i=1, 2,..., M$). Referring to Figure 6.2 and Figure 6.3, it should be noted that points are

arranged beginning with the lowest stress/strain range. Because $c^{(i)}$ is inversely proportional to $\Delta\varepsilon^p_{(i)}$ (Equation (6.13)), it follows that $c^{(1)} \geq c^{(2)} \geq ... \geq c^{(M)} \geq 0$. The constant $r^{(i)}$ represents the radius of a limiting surface, therefore, $r^{(i)} > 0$ (i=1, 2, ..., M).

The first method (see Section 6.2.1) is very easy to implement. The values of $c^{(i)}$ (i=1, 2, ..., M) are obtained directly from a stress-strain curve and $r^{(i)}$ (i=1, 2, ..., M) are calculated. This method can be used in the cases where cyclic hardening is neglected, so there is no further relation of the constants $c^{(i)}$ with the loading history. For 1070 steel which displays minimal cyclic hardening, either procedure results in very similar predicted stress-strain curves. Cyclic hardening for some materials is considered through the constants $c^{(i)}$ (i=1, 2,..., M) in the hardening rule, Equation (5.4), the radii of the limiting surfaces $r^{(i)}$ (i=1, 2,..., M) are presumed to be constants irrespective of loading condition and history. The procedure introduced in Section 6.2.1 should be utilized to determine the $r^{(i)}$ (i=1, 2,..., M) from the stabilized cyclic stress-strain curve. Therefore, the procedure introduced in Section 6.2.2 should be used to determine $c^{(i)}$ (i=1, 2,..., M) for some selected stress-strain hysteresis curves which are representative of the transient behavior. Equation (5.11) is asymptotic at large number of cycles. When considering cyclic hardening, it is noted $c^{(i)}_0$ (i=1, 2, ..., M) are the values of $c^{(i)}$ (i=1, 2,..., M) for the stabilized stress-strain relation in Equation (5.11). The first procedure introduced in Section 6.2.1 can also be used to determine $c^{(i)}_0$ (i=1, 2, ..., M) by analyzing the stabilized stress-strain curve. Following the procedure in Section 6.2.2 and using the $r^{(i)}$ and $c^{(i)}_0$ (i=1, 2, ..., M) previously obtained, the $c^{(i)}$ (i=1, 2,..., M) corresponding to given cycles displaying cyclic hardening can be determined. These $c^{(i)}$ (i=1, 2,..., M) are plotted against p, the accumulated plastic strain, and then the relationship between $c^{(i)}$ (i=1, 2,..., M) and p can be established. From the $c^{(i)}$-p (i=1, 2, ..., M) relations, the constants $a^{(i)}_1$, $a^{(i)}_2$, $b^{(i)}_1$, and $b^{(i)}_2$ in Equation (5.11) can be determined through a best fit technique. When only cyclic hardening or softening is considered, the constants $a^{(i)}_2$ and $b^{(i)}_2$ (i=1, 2, ..., M) can be set to zero and the fitting technique can be simplified.

6.3. Non-Masing Behavior

Non-Masing behavior is considered through k which is proportional to the size of yield surface. By testing fully reversed strain-controlled tension-compression at different strain amplitudes, the k-R_M relationship can be established. This can be achieved by conducting an increasing/decreasing step

test with one specimen. In each step, the number of the loading cycles should be large enough so that the stress-strain responses stabilize. A certain percentage of offset can be employed to determine the yield stress from one of the stabilized loops. While the stabilized value of k may change slightly with the offset chosen, the model is not very sensitive to this choice. In general, the offset should be much less than the 0.2% offset typically reported for tensile testing (ASTM, 1993). Examination of Figure 3.3 and Tables 4 -8 reveal the lower values chosen for k. Then a shift of the loops as in Figure 3.2b allows determination of the change in yield stress, hence the change in k, for different stress levels. Since it was chosen to model the non-Masing behavior, a function of the memory surface, the following equation applies,

$$R_M = \sqrt{\frac{3}{2}} \, (\sigma_{max} - \sigma_y) = \sqrt{\frac{3}{2}} \, (\sigma_{max} - \sqrt{3} \, k) \, , \tag{6.23}$$

where σ_{max} is the maximum stress in the stabilized stress-strain hysteresis loop, σ_y is the yield stress for the stress level under consideration. From several selected stress/strain levels and their associated values of k, the k-R_M relationship using the format suggested in Equation (5.15) can be established. The constants, k_0, a_k, and b_k in Equation (5.15), can be obtained using a best fit technique.

6.4. Memory Surface

There is only one constant c_M associated with the concept of a memory surface (Equations (5.8) and (5.9)). For the purpose of discussion, consider two steps from the decreasing portion of the increasing/decreasing step test discussed in the previous sections. For this constant, c_M, the transient, not stabilized behavior will be considered. Since the stress amplitude in the second step is smaller than that of the first step, during the second step loading, H(g) = 0, and $|\alpha| \leq R_M$. Therefore,

$$dR_M = -c_M \left(1 - \frac{|\alpha|}{R_M} \right) dp \, , \tag{6.24a}$$

or,

$$R_M = R_{M0} - c_M \int_0^{\Delta p} \left(1 - \frac{|\alpha|}{R_M} \right) dp \, , \tag{6.24b}$$

where Δp is the accumulated plastic strain with reference to the beginning of the second loading step. R_{M0} is the stabilized memory surface size from the first step. It is assumed that during the second loading step, there is no more cyclic hardening/softening behavior. Therefore, any change in the stress response is attributed to changes in the yield strength which are related to changes in the size of the memory surface, R_M. The changes in yield stress can be determined from the experimental stress-strain response in a manner analogous to the previous section. Then the instantaneous memory surface size, R_M, is calculated using Equation (5.15). The constant c_M is then determined by the trial and error fitting of R_M-Δp relation. It should be noted that Equation (5.15) is valid for any loading state. Also, if a small-large cycle sequence were employed, the assumption of no further strain hardening could be more difficult to justify. Furthermore, the term containing the constant c_M in Equation (5.9) would be inactive for this sequence. These are the primary reasons why a large-small sequence was chosen to determine this constant.

6.5. Determination of Exponents $\chi^{(i)}$

At this point all constants for the new model except $\chi^{(i)}$ have been established. The exponents $\chi^{(i)}$ (i=1, 2, ..., M) have an insignificant influence on the balanced loading, therefore they are determined from unbalanced loading tests, specifically ratchetting tests. For a given stress level, the memory surface size, R_M, is a constant, and hence $\chi_0^{(i)}$ is a constant. The coefficients $\chi_0^{(i)}$ (i=1, 2, ..., M) can be determined from a uniaxial ratchetting test for a given stress range and mean stress. A change in the range and/or mean stress will alter the coefficients $\chi_0^{(i)}$ (i=1, 2, ..., M). Using the coefficients $\chi_0^{(i)}$ (i=1, 2, ..., M) obtained for several different one-step tests at different stress levels, the constants $\chi_0^{(i)}$, a_χ, and b_χ in Equation (6.13) can be determined using trial and error fitting.

7. VERIFICATION AND DISCUSSION OF THE NEW MODEL

The same experimental results forwarded in Chapter 4 which were employed to evaluate the existing plasticity models are again used to verify the new model. A detailed description of the experimental results will not be repeated here. Once again, due to the insignificant cyclic hardening experimentally observed for 1045 and 1070 steels, no cyclic hardening is considered in the simulations (i.e., in Equation (5.11), $a_1^{(i)} = a_2^{(i)} = 0$ (i=1, 2, ..., M)). A limited number of tests employing a 6061-T6 aluminum, which displays strain hardening were discussed in Section 5.4 to verify the format proposed for strain hardening (Equation (5.11)). The same methodology as was discussed in Section 4.1 is incorporated into the current numerical analysis.

7.1. Strain-Controlled Balanced Loading

For 1045 steel under strain control, the number of terms, M, for the backstress expansion in the new hardening rule, Equation (5.4), is set to be 5. The material constants $c^{(i)}$ and $r^{(i)}$ (i=1, 2, 3, 4, 5) in the new hardening rule are obtained employing the procedure outlined in section 6.2.2 and are listed in Table 8. The non-Masing effect and stress level effect on ratchetting are not considered for the balanced strain-controlled cases (i.e., $a_\chi=0$ in Equation (5.13) and $a_k=0$ in Equation (5.14)). Additional experimental data for 1045 steel would be needed to determine these constants, but they have little influence for the loading paths discussed for this material.

Figure 7.1 presents a comparison between experimental results and the new model simulation for the strain-controlled nonproportional loading paths, Path I and Path II, shown in Figure 4.1. Close agreement between experimental and predicted results is observed. As was previously inferred, numerical values of the exponents $\chi^{(i)}$ do not influence the predicted results significantly for balanced loading. The two extreme values for $\chi^{(i)}$, 0 and $+\infty$, are examined to verify this stipulation. For Path I where the plastic strains are small, the values of the exponents $\chi^{(i)}$ (i=1, 2, ..., M) have some influence on the predicted stresses. However, for Path II where the strain amplitudes are larger, the predicted stress response is almost independent of the selection of the exponents.

It may be worthwhile at this time to compare the results of the Chaboche, the Ohno-Wang, and the new model when predicting the stress response for the nonproportional strain-controlled balanced loading. From Figure 4.2, Figure 4.3, and Figure 7.1, it is clear that all the three models produce nearly identical results for those two loading paths. It is noted that all three hardening rules represented by these three models are in the general structure expressed by Equation (5.1). Also the conditions (CONDITION 1 and CONDITION 2, Section 5.1) set forth for $f_1^{(i)}$ and $f_2^{(i)}$ in Equation (5.1) are satisfied by all three models. All three models utilize the relationship $f_1^{(i)} = c^{(i)}r^{(i)}$, but the choice of $f_2^{(i)}$ differs for the models. The Chaboche hardening algorithm uses $f_2^{(i)} = \dfrac{|\underline{\alpha}^{(i)}|}{r^{(i)}}$; the Ohno-Wang model employs $f_2^{(i)} = \left(\dfrac{|\underline{\alpha}^{(i)}|}{r^{(i)}}\right)^{\chi^{(i)}} \langle \underline{n}{:}\underline{L}^{(i)} \rangle$, and the new hardening rule assumes $f_2^{(i)} = \left(\dfrac{|\underline{\alpha}^{(i)}|}{r^{(i)}}\right)^{\chi^{(i)}}$. The similarity of the predictions obtained using these three models indicates that the difference in the mathematical forms characterized by $f_2^{(i)}$ in Equation (5.1) for these three models does not have any significant impact on the numerical simulation of balanced loading. One characteristic of balanced loading is that the locus of $\underline{\alpha}^{(i)}$ form a closed path. While differences in $f_2^{(i)}$ may affect the instantaneous position of $\underline{\alpha}^{(i)}$, the similar stress predictions indicate that the loci of $\underline{\alpha}^{(i)}$ (i=1, 2, ..., M) display a similar correspondence. Therefore, balanced loading does not provide an avenue to differentiate these models for different specifications of backstress translation within the limiting surface.

It should be noted that the comparisons of the predictions by the three models were based on the same numerical conditions: an identical number of terms (M) for the backstress expansion, no consideration of the transient cyclic behavior, and the same number of incremental steps for a cycle in the simulations. All the material constants with the same symbols have identical values regardless of model (refer to Table 6, 7, and 8 for 1045 steel). This reflects that the procedures presented in Sections 6.2.2 and 6.2.3 for the determination of the material constants $c^{(i)}$ and $r^{(i)}$ can also be applied to the Chaboche and Ohno-Wang models. Minimal improvement can be made for the Chaboche, the Ohno-Wang, and the new model predictions for balanced loading if (i) M being a larger number, (ii) consideration of the transient cyclic behavior, and, (iii) an appropriate selection of $\chi^{(i)}$ for the Ohno-Wang and new models.

7.2. Stress-Controlled Unbalanced Loading

Experimental data for 1070 steel previously discussed in Figures 4.6 to 4.20 are again utilized to examine the new model's capability to predict unbalanced loading. The number of terms for the backstress expansion, M, is now 10 because a larger number of terms is needed to model ratchetting. Again, cyclic hardening is neglected and the material constants $c^{(i)}$ and $r^{(i)}$ (i=1, 2, ..., 10) are the same as those for the Ohno-Wang model (refer to Tables 7 and 8). In Figures 7.2 and 7.3 the experimental ratchetting rates are presented on logarithmic coordinates along with simulations obtained using the new model with different values for $\chi^{(i)}$ (i=1, 2,..., 10). These two figures demonstrate the pronounced influence of the exponents $\chi^{(i)}$ on the ratchetting rate predicted for both proportional and nonproportional loading. They are similar to Figures 4.9 and 4.10 where predictions using the Ohno-Wang model were presented. Clearly, the larger the numerical values of the exponents $\chi^{(i)}$ (i=1, 2,..., 10), the faster the models predict ratchetting rate decay. Comparing Figure 7.2 and 4.9 reveals that both models predict similar quantitative ratchetting rate behavior for the uniaxial simulation. In fact it can be inferred that the two models are practically identical when predicting ratchetting for proportional loading. Comparison of the results in Figure 7.3 with those in Figure 4.10 indicates that the difference between the two models lies in their predictions for the nonproportional loading case. When $\chi^{(i)}$ =0 (i=1, 2, ..., 10) the new model predicts a slight ratchetting rate decay for the first 100 cycles and then constant ratchetting. That is to say, when neglecting cyclic hardening, the new plasticity model can predict ratchetting from near constant rate to zero rate (ratchetting arrest) for both proportional and nonproportional loading. This is an improvement over the Ohno-Wang model which is unable to predict constant ratchetting rate for nonproportional loading.

For a specific material, the exponents $\chi^{(i)}$ (i=1, 2,..., M) in the new model do not necessarily have the same values as indicated in the discussions of Figure 7.3. From the analysis of the one step uniaxial experimental ratchetting results for 1070 steel, the constants in the expression for $\chi^{(i)}$ (i=1, 2, ..., M) (Equation (5.14)) are determined via the procedures forwarded in Section 6.5 and are listed in Table 8. The new model ratchetting predictions using these constants are compared with the experimental results in Figure 7.4 through 7.11. An overview of this data will lead to the conclusion that the new model correlates the ratchetting experiments very well. Improvements over the Ohno-Wang model can be found in the following aspects. Comparing Figure 7.6 with Figure 4.14,

the two models predict nearly the same axial ratchetting for the "apple" shaped loading path, but the new model correlates shear ratchetting better than the Ohno-Wang model. In the multiple step cases (Figures 7.8 and 7.9), the new model predicts the changes of ratchetting direction in very close agreement with the experimental observation, while relatively the Ohno-Wang model does not predict the ratchetting of the second loading step as well (refer to Figures 4.16 and 4.17). Figure 7.4 reveals that the current consideration of the stress level effect on ratchetting is an improvement over the Ohno-Wang model (Figure 4.20).

For 1070 steel which exhibits ratchetting rate decay, the new plasticity model differs little from the Ohno-Wang model for one step tests. It was noted that in using the Ohno-Wang model, no memory surface was included. The improved ratchetting prediction obtained for multiple step tests using the new model is mainly ascribed to the consideration of the stress level effect. In other words, if a memory surface is incorporated into the Ohno-Wang model, a better correlation with experiments for a material which displays a stress level effect would be expected. One fundamental difference between the Ohno-Wang model and the new one lies in its capability to predict constant or near constant ratchetting rates. This difference is reflected in the representation of $f_{(i)}^2$ in Equation (5.1).

The number of terms for the backstress expansion, M, has a weak influence on the predicted stress-strain responses for balanced loading, but a strong influence on the ratchetting prediction for unbalanced loading. From the aforementioned discussion, for ratchetting rate decay prediction, M should be larger than 1. For the prediction of long term ratchetting rate decay, M=5~10 seems sufficient. Ratchetting predictions for a large number of loading cycles is time consuming when both M and the number of incremental steps for a loading cycle are large numbers. Compromises may have to be made between the accuracy of the prediction and the number of loading cycles simulated. It is suggested that detailed ratchetting predictions be made for a limited number of loading cycles, and the results can then be extrapolated for longer loading histories using Equation (3.1) or Equation (3.2).

7.3. Generalization of the Characteristics of $\chi^{(i)}$

It has been pointed out that the exponents $\chi^{(i)}$ (i=1, 2,..., M) have an insignificant influence when using the new model or the Ohno-Wang model to

predict balanced loading. As was indicated in Figures 7.2 and 7.3, the exponents $\chi^{(i)}$ (i=1, 2,..., M) control the ratchetting rate predicted. In fact, by adjusting $\chi^{(i)}$ (i=1, 2,..., M), the new model can predict ratchetting that mimics a variety of experimental observations. Figure 7.12 displays the sensitivity of the selection of $\chi^{(i)}$ (i=1, 2,..., M) and the type of ratchetting predicted. Except $\chi^{(i)}$ (i=1, 2,..., M), the other material constants used in the simulations are those previously used for 1070 steel (Table 8). When $\chi^{(i)}$ =1 (i=1, 2,..., 10), the model predicts ratchetting rate decay for about 300 cycles, for both proportional and nonproportional loading, after which a constant rate is predicted. When $\chi^{(10)}$ is changed from 1 to $+\infty$ while maintaining all the other conditions, the predicted ratchetting rate is identical to that when $\chi^{(i)}$ =1 (i=1, 2,..., 10) for about 200 cycles. No constant ratchetting rate will be predicted when $\chi^{(10)}= +\infty$. Instead, ratchetting arrest is expected after about 10^4 cycles. These observations indicate that the exponent $\chi^{(M)}$ has minimal influence on the prediction of the ratchetting rate for the initial loading cycles. However, the long term ratchetting is mainly controlled by this exponent, $\chi^{(M)}$. It should be noted that the material constants $r^{(i)}>0$ (i=1, 2, ..., M) have been arranged in the order $c^{(1)} \geq c^{(2)} \geq .... \geq c^{(M)} \geq 0$ consistent with the procedure to derive these constants. For single step loading, each $\chi^{(i)}$ has a significant influence on the predicted ratchetting rate for a limited range of loading cycles. The exponents $\chi^{(i)}$ with small i's have strong control over the initial ratchetting rate, and a weak influence on the long term ratchetting. The exponents $\chi^{(i)}$ with large i's on the other hand control the ratchetting predicted for a large number of loading cycles at a given stress level.

There are four possible ratchetting rate tendencies (refer to Figure 7.13), namely, Region I: decayed ratchetting, Region II: constant ratchetting, Region III: ratchetting arrest, and Region IV: increasing ratchetting. A material subjected to a certain loading condition may display combinations of these four regions. From the previous discussion on the relationship between $\chi^{(i)}$ (i=1, 2, ..., M) and the ratchetting rate tendency predicted, the new model can handle the first three types of ratchetting. According to Hassan and Kyriakides (1992) and Hassan et al. (1992), ratchetting rate acceleration is related to the continuous cyclic softening of a material. Therefore, increased ratchetting rates can be predicted using the new model with $\chi^{(i)}=0$ (i=1, 2, ..., M) and considering cyclic softening. The relationship between $\chi^{(i)}$ (i=1, 2, ..., M) and the ratchetting rate tendency predicted shows the flexibility and the ability of the new model to predict various ratchetting rate tendencies.

It should be pointed out that in the aforementioned discussion on the influence of $\chi^{(i)}$ (i=1, 2, ..., M), all loadings considered were for one step tests at a given stress level. This choice serves well for the purpose of the discussion, but conclusions made excluding the stress level effects are valid from a general point of view. This property of the new model further illustrates how the exponents $\chi^{(i)}$ (i=1, 2, ..., M) would be selected in Section 6.5. It is noted from Figure 7.14 that the new model with the same material constants predicts the same ratchetting rate tendency for both proportional and nonproportional loading. This is one of the improvements in the new model in comparison to the Ohno-Wang model. These differences are attributed to the specification of $f_2^{(j)}$ in Equation (5.1) rather than the general tendencies for $\chi^{(i)}$.

7.4. Mechanics of Ratchetting

In this section, discussion of the $\alpha^{(i)}$ loci for balanced and unbalanced loading will be presented. To theoretically explain the mechanics of the new model for the ratchettting rate decay under general nonproportional loading is difficult. However, it may be helpful to discuss a cyclically stable unbalanced uniaxial simulation (Figure 7.14). For a cyclically stable material, the stress-strain response is totally determined by the variation of the plastic modulus function, h, or plastic modulus, H. Simplifying Equation (2.10) for uniaxial tension-compression, it follows,

$$d\sigma = \frac{2}{3} h \, d\varepsilon^p \ , \tag{7.1}$$

where σ and ε^p denote axial stress and axial plastic strain, respectively. For the stress-controlled condition, the following integrals apply,

$$\int_1^3 d\sigma = \int_1^3 \frac{2}{3} h \, d\varepsilon^p = 0 \ , \tag{7.2a}$$

or,

$$\int_1^2 h \, d\varepsilon^p + \int_2^3 h \, d\varepsilon^p = 0 \ . \tag{7.2b}$$

The lower and upper limits for the integral refer to the stress/strain states corresponding to minimum and maximum stress/strain in a reversal, as

illustrated in Figure 7.14. According to Equation (5.5), the plastic modulus function is,

$$h = \sum_{i=1}^{M} h^{(i)} = \sum_{i=1}^{M} c^{(i)} r^{(i)} \left[1 - \left(\frac{|\underset{\sim}{\alpha}^{(i)}|}{r^{(i)}} \right)^{\chi^{(i)}+1} \underset{\sim}{L}^{(i)} : \underset{\sim}{n} \right] , \tag{7.3}$$

where $\underset{\sim}{L}^{(i)} : \underset{\sim}{n} = \pm 1$ and $|\underset{\sim}{\alpha}^{(i)}| = \sqrt{\frac{3}{2}} \left| \alpha_{11}^{(i)} \right|$ for uniaxial tension-compression.

A ratchetting rate (ratchetting strain per cycle) can be expressed as,

$$\frac{d\varepsilon_r}{dN} = \int_{1}^{3} d\varepsilon^p . \tag{7.4}$$

Manipulating Equations (7.2)-(7.4), one can obtain the following forms for the ratchetting rate,

$$\frac{d\varepsilon_r}{dN} = \sum_{i=1}^{M} \frac{d\varepsilon_r^{(i)}}{dN} , \tag{7.5}$$

where

$$\frac{d\varepsilon_r^{(i)}}{dN} = \frac{c^{(i)} r^{(i)} \left[\int_{1}^{2} \left(\frac{|\underset{\sim}{\alpha}^{(i)}|}{r^{(i)}} \right)^{\chi^{(i)}+1} \underset{\sim}{L}^{(i)} : \underset{\sim}{n} \, d\varepsilon^p + \int_{2}^{3} \left(\frac{|\underset{\sim}{\alpha}^{(i)}|}{r^{(i)}} \right)^{\chi^{(i)}+1} \underset{\sim}{L}^{(i)} : \underset{\sim}{n} \, d\varepsilon^p \right]}{\sum_{j=1}^{M} c^{(j)} r^{(j)}}$$

$$(i=1, 2, ..., M) . \tag{7.6}$$

The term, $\frac{d\varepsilon_r^{(i)}}{dN}$, in the previous equations represents the contribution to ratchetting rate by the variation of an individual backstress. It is difficult to express the ratchetting rate in a concise and closed form. However, a few characteristics can be extracted from the examination of Equation (7.6). The denominator on the right side of Equation (7.6) is a constant since a cyclically stable material was assumed. If $\underset{\sim}{\alpha}^{(i)}$ varies symmetrically (i.e., no mean value), it

can be derived that the integral on the right-hand side of Equation (7.6) is zero, which results in $\frac{d\varepsilon_r^{(i)}}{dN} = 0$. Knowing that $r^{(i)}$ is the size of a limiting surface for the backstress $\underline{\alpha}^{(i)}$ infers that $\frac{|\alpha^{(i)}|}{r^{(i)}} \leq 1$. Since $\chi^{(i)}$ is assumed to be greater than or equal to zero, the quantity $\left(\frac{|\alpha^{(i)}|}{r^{(i)}}\right)^{\chi^{(i)}+1}$ is equal to or less than 1.0. Therefore, if $\chi^{(i)} = +\infty$, then $\frac{d\varepsilon_r^{(i)}}{dN} = 0$ because of the aforementioned inequality. When $\underline{\alpha}^{(i)}$ does not vary, then the quantity $\frac{|\alpha^{(i)}|}{r^{(i)}}$ is a constant that may be removed from the integral. The fixed vector, $\underline{L}^{(i)}$, whose scalar product with $\underline{n}$ will change sign for loading 1 to 2 and 2 to 3 (refer to Figure 7.14) should cause the sum of the integrals to be approximately zero, and hence $\frac{d\varepsilon_r^{(i)}}{dN} \approx 0$. Qualitatively, the larger the mean value of a backstress, the larger the contribution of this backstress to the ratchetting rate. However, there must be a mean value and amplitude if that backstress part contributes to ratchetting.

Figure 7.15 shows the variations of the backstresses using the new model with the loading cycles for a fully reversed uniaxial test. It should be noted that for the one dimensional problem of tension-compression, $\underline{\alpha}^{(i)}$ can be represented by the value of the component $\alpha_{11}^{(i)}$. The term, $\sqrt{\frac{3}{2}} \frac{\alpha_{11}^{(i)}}{r^{(i)}}$, is a normalized quality representing the backstress $\underline{\alpha}^{(i)}$ for the uniaxial case. In Figure 7.15, the number of terms for the backstress, M, is 5 since the desire is to qualitatively display the behavior of $\underline{\alpha}^{(i)}$. The material constants employed are listed in Table 10 and were chosen to illustrate the phenomenon. It should be noted that the selection of the material constants does not qualitatively alter the ensuing points of discussion. In Figure 7.15(b), all the backstresses vary symmetrically, and are independent of the loading history. When the backstress parts have an amplitude but no mean value, no ratchetting is predicted.

Identical material constants are used for a two step unbalanced uniaxial loading. The predicted ratchetting rates for both steps are shown in Figure 7.16(b), and the variations of the backstresses with the loading history are presented in Figure 7.16(c). During the first step loading, ratchetting rate decay is predicted. The corresponding variations of the backstresses shown on the left side of Figure 7.16(c) are responsible for the ratchetting rate decay. The magnitudes of backstress variations are in an order consistent with the size of $c^{(i)}$

(i=1, 2, 3, 4, 5). Subsequently, the mean values of $\alpha_{11}^{(1)}$ and $\alpha_{11}^{(2)}$ saturate to zero with increasing cycles and the mean values of $\alpha_{11}^{(4)}$ and $\alpha_{11}^{(5)}$ increase at the same time. The amplitudes of the backstresses do not change with loading cycles. According to Equation (7.6), for the same variation of the backstress and $\chi^{(i)}$, a larger value of $c^{(i)}r^{(i)}$ will result in a larger ratchetting rate. Because it was ● assumed that $r^{(1)} = r^{(2)} = r^{(3)} = r^{(4)} = r^{(5)}$, a larger $c^{(i)}$ results in a larger $c^{(i)}r^{(i)}$. The decrease of the mean values of $\alpha_{11}^{(1)}$ and $\alpha_{11}^{(2)}$ (corresponding to larger $c^{(i)}r^{(i)}$ values) mainly contributes to the initial ratchetting rate decay predicted. It should be noted that the mean value of the total backstress is proportional to the mean stress of the stress-controlled uniaxial loading cycle. Therefore, the sum of all the backstress has a fixed mean value for a given step in the loading. The decrease in the mean values of $\alpha_{11}^{(1)}$ and $\alpha_{11}^{(2)}$ is consistent with the increase of the mean values of $\alpha_{11}^{(4)}$ and $\alpha_{11}^{(5)}$. It is this shifting of the mean values of the backstresses in combination with the smaller amplitude of $\alpha_{11}^{(4)}$ and $\alpha_{11}^{(5)}$ that contributes to the continued ratchetting rate decay.

When the mean stress is zero in the second loading step, the new model predicts ratchetting in the direction opposite to that in the first step. From the right side of Figure 7.16(b), the ratchetting rate (absolute value) also decreases with increasing number of loading cycles, which again can be explained by the variations of the backstresses (refer to the right side of Figure 7.16(c)). When the loading for the second step with a different mean stress begins, there are sudden changes in the backstresses, which corresponds to a change in the ratchetting rate. The backstresses $\alpha_{11}^{(1)}$ and $\alpha_{11}^{(2)}$ with their mean values initially being negative contribute to the ratchetting rate in the negative direction, while the other three backstress parts with positive mean values produce ratchetting in the positive direction. As was previously stipulated, a larger amplitude of a backstress contributes more to the ratchetting rate, hence the overall ratchetting rate is negative. Because the mean stress in the second loading step is zero, all the mean values of the backstresses will approach to zero with increasing number of loading cycles. As a result, the ratchetting rate decreases with increasing number of cycles. For ratchetting under nonproportional loading, the ratchetting predicted using the new model may be explained in a similar way. However, for nonproportional loading, the ratchetting rate is not only dependent on the variations of the backstresses but also the variations of $\underline{L}^{(i)}:\underline{n}$ (i=1, 2, ..., M). A straightforward discussion is more difficult for unbalanced nonproportional

loading. It may be worthwhile to point out that for a material which does not exhibit ratchetting rate decay the new plasticity model will not predict ratchetting in the direction opposite to the mean stress for uniaxial loading, nor will the ratchetting direction change as was observed in 1070 steel. Further experimental study of multiple step tests are needed for a material displaying constant ratchetting rate for a one step test.

7.5. Physical Interpretation

Plastic deformation is attributed to the motion of dislocations, which are defects in the crystalline lattice of a solid metal's microstructure (Kuhlmann-Wilsdorf, 1989; Kuhlmann-Wilsdorf and Laird, 1979). Continued plastic deformation is often responsible for the generation of more dislocations (strain hardening), which interact and hinder each others subsequent motion (Bruhns et al., 1992). A macro-scale uniform polycrystalline material is composed of many crystalline regions, each exhibiting different properties. From the microstructure point of view, even a single crystal displays an inhomogeneous distribution of dislocations (Hesagawa et al, 1986), and the local and internal stress distributions are extremely inhomogeneous. Peak stress values occur in the tangled cell walls and low values are observed in the cell interior (Hesagawa et al, 1986). The macro-mechanical behavior reflects the response of the various material elements ability to resist external loads. It was empirically implied for the new hardening rule that a material is a combination of many material elements possessing different properties under cyclic loading. A material element does not necessarily represent a crystal, but a polycrystalline continuum which displays distinctive responses when subjected to the external loads. Each component, although having different values for the constants, is expected to display the same qualitative behavior. On the other hand, since a single term is used for a memory surface, it represents a single property of a polycrystalline material component.

Drucker (1987) stated that "The behavior of metals and alloys in the plastic range is enormously, essentially infinitely, complex. No mathematical expressions, no matter how elaborate, can portray the response in completely full and accurate detail. No finite number of experiments, no matter how carefully done, can provide all the physical information." A complementary difficulty is that, as a practical matter, the loading paths that can be explored experimentally are extremely limited. Microstructural interpretation of mechanical material

behavior has been limited to single crystal and simple loading conditions such as uniaxial or torsional loading (Asaro, 1983; Cuddy and Bassim, 1989; Dollar *et al.*, 1988; Hill, 1965; Kuhlmann-Wilsdorf, 1982; Mughrabi, 1983; Pedersen, 1987; Peirce *et al.*, 1982; Umakoshi *et al.*, 1984; Weng, 1979). The microstructural changes in a polycrystalline material subjected to nonproportional cyclic loading are still awaiting further experimental investigations. There may be a long way to go before there is a quantitative relation between microstructural details and phenomenal cyclic plasticity models for polycrystalline materials. Attempts to model the cyclic plasticity always have limitations. Accuracy referred to when evaluating a plasticity model is from the macro or engineering point of view, instead of microstructural perspective. Despite the fact that the current experimental facilities are not able to conduct all the possible triaxial stress states and nonproportional loadings, one rule always applies; that if a plasticity model cannot capture some basic character of cyclic plastic deformation for a simpler stress state, it is generally not applicable for the more general analysis.

8. CONCLUSIONS AND RECOMMENDATION FOR FUTURE WORK

This dissertation deals with deformation that involves cyclic plasticity, both theoretical and experimental. The research focused on three major topics: (i) an experimental investigation of the ratchetting behavior of 1070 steel, (ii) a survey of the existing plasticity theories and a comparison with experimental ratchetting observations, and (iii) development and verification of a new plasticity model. The incremental plasticity theories under consideration utilize the yield surface concept and describe kinematic hardening by specifying different translations for the yield surface. The study has been limited to considerations of path-dependent plasticity in which effects of rate and temperature dependence are neglected. The ensuing section will summarize the major conclusions from the three major topics.

8.1 Conclusions

The ratchetting experiments on 1070 steel under various loading conditions lead to the following conclusions:

1. The balanced loading experiments indicate that the material displays minimal cyclic hardening, however, non-Masing behavior is observed. For both balanced cyclic plasticity and ratchetting deformation, the plastic incompressibility condition is confirmed.

2. The ratchetting direction is coincident with the mean stress direction under single step proportional loading. There is no simple relation between the sign of the mean stress and ratchetting direction when the loading is nonproportional.

3. Under single step loading, the ratchetting rate decreases with increasing number of loading cycles for both proportional and nonproportional loadings, and can be fit using a power law relation.

4. For multiple step loading, the material exhibits a memory of the previous loading history. The material could ratchet in a direction opposite to the mean stress or could reverse ratchetting direction with time. Due to this memory effect the strain ratchetting may accelerate under certain circumstances, although such an acceleration in ratchetting rate is short-lived. The material's

memory of prior loading history has a great influence on the subsequent ratchetting, and dissipates with increasing number of loading cycles.

The literature survey has focused on a critique and comparison of existing cyclic plasticity models with an emphasis on the ability of the models to predict ratchetting. Plasticity models under consideration can be classified as either the Mroz multiple surface type or the Armstrong-Frederick type. The following conclusions can be drawn from the survey and comparison with experimental results:

5. The Mroz and Garud multiple surface models are approximately identical for the prediction of stress-strain response. The predicted stress response by the Mroz and Garud models is inferior to the Armstrong-Frederick type models for nonproportional strain-controlled loading. The Mroz and Garud models produce fully closed stress-strain loops and do not predict ratchetting for proportional loading, but predict strain ratchetting for stress-controlled nonproportional loading. These models are not suitable for general cyclic plasticity predictions. All the Armstrong-Frederick type models discussed are able to predict reasonable stresses for nonproportional strain-controlled loading. For strain-controlled balanced loading, the Bower model and the initial Armstrong-Frederick model produce very similar results, and the Chaboche and Ohno-Wang models with the same number of backstress parts predict practically identical stresses. Balanced loading does not provide an avenue to differentiate plasticity models, and hence ratchetting experiments are critical when evaluating plasticity models.

6. A prevalent characteristic of all the Armstrong-Frederick type hardening models is the interpretation that a limiting surface for a backstress part exists. The difference between the Armstrong-Frederick type hardening rules lies in the distinctive specification of the magnitude and direction for the translation of a backstress part within a limiting surface. Such an interpretation also allows the material constants for these models to be determined via a standard procedure, and the limiting concept provides a convenient framework to construct refined hardening algorithms.

7. The Ohno-Wang model is the best of all the existing models evaluated. The predicted stress response by using the Ohno-Wang model for strain-controlled loading is in very close agreement with the experiments. More importantly, the model can appropriately correlate with some of the

experimental ratchetting observed for 1070 steel. A shortcoming of the Ohno-Wang model is its inability to predict a constant ratchetting rate for nonproportional loading. In addition, the transient cyclic material behavior should be incorporated.

When analyzing the new experimental data, certain difficulties were encountered with existing plasticity models that resulted in a new set of constitutive relations being developed. An attempt has been made to develop a model that better describes a wider range of cyclic ratchetting. A limiting surface concept is generalized and used in the development of a new hardening rule. The total backstress is divided into many parts. A memory surface is introduced to consider the stress level effect on plastic deformation. Transient cyclic behaviors are then incorporated into the hardening rule. Cyclic hardening is considered through the coefficients $c^{(i)}$ ($i=1, 2, ..., M$) in the hardening rule as power functions of the accumulated plastic strain. The non-Masing behavior is considered through the yield stress as a function of the memory surface size. The exponents $\chi^{(i)}$ ($i=1, 2, ..., M$) in the hardening rule, which control the type of ratchetting predicted, are related to the size of the memory surface to consider the stress level effect. The following conclusions are related to this new plasticity model:

8. The new plasticity model was applied to the ratchetting predictions of 1070 steel. Its capability to improve long term ratchetting and multiple step ratchetting predictions was demonstrated.

9. The material constants in the new plasticity model can be divided into two independent groups; one group, $c^{(i)}$ and $r^{(i)}$ ($i=1, 2, ..., M$), which describes balanced loading and the other group, $\chi^{(i)}$ ($i=1, 2, ..., M$), which characterizes unbalanced loading. The independence of the two groups of material constants and the interpretation of the model with a limiting surface concept facilitate the determination of material constants. A procedure to determine the material constants in the models from simple uniaxial experiments was described in detail.

10. A large number of established models are used and new ones are being proposed. In addition to evaluating them via experimental evidence, it is particularly important to verify their mathematical properties such as uniqueness, reliability, and consistency so that desired results are obtained once they are implemented in numerical solutions. The relationship between

plasticity model terminology and the micro-mechanical behavior such as dislocation movement needs future study. The limiting surface and memory surface concepts may eventually be related to microstructural changes at least qualitatively.

8.2. Future Work

Future work on cyclic plasticity should include more experiments and theoretical refinements. The experimental ratchetting program presented in this thesis provided a broader understanding of cyclic plasticity. The proposed plasticity model provides a basis for future applications. Capabilities and limitations encountered lead to following suggestions:

a) Even with the experiments conducted in this investigation, a very limited number of experiments exist to evaluate current and future theoretical formulations. Therefore, more complex loading paths such as multiple ratchetting experiments consisting of proportional/nonproportional and nonproportional/nonproportional loading need to be conducted.

b) Rate and temperature dependence needs to be incorporated into the model to facilitate analysis of high temperature applications. This could be done by modifying the detailed relationships for the coefficients $c^{(i)}$, $r^{(i)}$, and $\chi^{(i)}$.

c) The cross-hardening behavior, which has not been included in the proposed model, could also be incorporated following the outlines in Section 5.7.

TABLES

Table 1 Summary of Ratchetting Experiments Reported Recently in the Literature

Investigator	Material and Specimen	Loading Condition	Cyclic Hardening or Softening	Ratchetting Behavior
Bower (1987)	Copper Rail Steel Solid Specimen	Proportional and Nonproportional Axial-Torsion	Stable N/A	Constant ratchetting rate Long term ratchetting rate decay
Hassan and Kyriakides (1992)	1020 Steel	Uniaxial Loading	Cyclic Softening	Near constant ratchetting rate
Hassan et al. (1992)	1026 Steel Tubular Specimen	Proportional and Nonproportional Axial-Internal Pressure	Stable	Slow Ratchetting rate decay
McDowell (1991)	Rail Steel Solid Specimen and Tubular Specimen	Proportional and Nonproportional Axial-Torsion	Insignificant Cyclic Softening	Long term ratchetting rate decay
Yamanouchi et al. (1976)	316 Stainless Steel Tubular Specimen Room Temperature and 550 °C	Cyclic Axial Strain with Constant Internal Pressure	N/A	Ratchetting Rate Decay

Table 2 Chemical Composition of Normalized 1070 Steel

C	Si	Mn	P	S	Cu	Ni	Cr	Mo	Fe
0.70	0.29	0.72	<0.05	0.041	0.09	0.04	0.07	<0.02	balance

Note: weight percent is reported

Table 3 Baseline Material Properties of 1070 Steel

1. Monotonic Properties

Young's Modulus, E	210000 MPa
Poisson's Ratio, μ	0.3
0.2% Offset	449 MPa
True Fracture Stress, σ_f	1250 MPa
True Fracture Strain, ε_f	0.53
Reduction in Area	30%

2. Cyclic Stress-Strain Relation

$$\frac{\Delta \varepsilon^p}{2} = \left(\frac{\Delta \sigma/2}{K}\right)^{\frac{1}{n}} \qquad K=1485 \text{ MPa} \qquad n=0.170$$

(at a strain amplitude of $\frac{\Delta \varepsilon}{2} = 1.0\%$)

Table 4 Material Constants Used in the Armstrong-Frederick Model

1045 Steel	k=100 MPa a_a= 87674 MPa c_a= 412
1070 Steel	k=115 MPa a_a= 96188 MPa c_a=285

Table 5 Material Constants Used in the Bower Model

1045 Steel	k=100 MPa a_b= 123690 MPa c_{b1}= 665 c_{b2}= 40
1070 Steel	k=115 MPa a_b= 127680 MPa c_{b1}= 420 c_{b2}= 40

Table 6 Material Constants Used in the Chaboche Model

1045 Steel k= 100 MPa M=5	$c^{(1)}= 691$ $c^{(2)}= 161$ $c^{(3)}= 28$ $c^{(4)}= 21$ $c^{(5)}= 0.91$
	$r^{(1)}= r^{(2)}= r^{(3)}= r^{(4)}= 71.4$ MPa $r^{(5)} = 314.4$ MPa
1070 Steel k= 115 MPa M=10	$c^{(1)}= 1510$ $c^{(2)}= 461$ $c^{(3)}= 177$ $c^{(4)}= 77$ $c^{(5)}= 39$ $c^{(6)}= 20$ $c^{(7)}= 12$ $c^{(8)}=6.7$ $c^{(9)}= 4.8$ $c^{(10)}= 2.7$
	$r^{(1)}= r^{(2)} = r^{(3)}= r^{(4)}= r^{(5)}= r^{(6)} =r^{(7)} = r^{(8)} = r^{(9)} = 63.5$ MPa $r^{(10)}= 245$MPa

Table 7 Material Constants Used in the Ohno-Wang Model

1045 Steel k=100 MPa M=5	$c^{(1)} = 691$ $c^{(2)} = 161$ $c^{(3)} = 28$ $c^{(4)} = 21$ $c^{(5)} = 0.91$
	$r^{(1)}= r^{(2)}= r^{(3)}= r^{(4)}= 71.4$ MPa $r^{(5)} = 314.4$ MPa
	$\chi^{(1)} =\chi^{(2)}=\chi^{(3)}= \chi^{(4)}=\chi^{(5)}= 0$ or $\chi^{(1)} =\chi^{(2)}=\chi^{(3)}= \chi^{(4)}=\chi^{(5)}= +\infty$
1070 Steel k=115 MPa M=10	$c^{(1)}= 1510$ $c^{(2)}= 461$ $c^{(3)}= 177$ $c^{(4)}= 77$ $c^{(5)}= 39$ $c^{(6)}= 20$ $c^{(7)}= 12$ $c^{(8)}=6.7$ $c^{(9)}= 4.8$ $c^{(10)}= 2.7$
	$r^{(1)}=r^{(2)} =r^{(3)}=r^{(4)}=r^{(5)}=r^{(6)} =r^{(7)} =r^{(8)} =r^{(9)} =63.5$ MPa $r^{(10)}=245$MPa
	$\chi^{(1)}= 0.5$ $\chi^{(2)}= 2$ $\chi^{(3)}= \chi^{(4)}=5$ $\chi^{(5)}= \chi^{(6)}=\chi^{(7)}= \chi^{(8)}=\chi^{(9)}= \chi^{(10)}= 6$

Table 8 Material Constants Used in the New Plasticity Model

1045 Steel M=5	$c_0^{(1)} = 691 \quad c_0^{(2)} = 161 \quad c_0^{(3)} = 28 \quad c_0^{(4)} = 21 \quad c_0^{(5)} = 0.91$ $a_1^{(i)} = a_2^{(i)} = 0 \ (i=1, 2, 3, 4, 5)$
	$r^{(1)} = 71.4\,\text{MPa} \quad r^{(2)} = 71.4\,\text{MPa} \quad r^{(3)} = 71.4\,\text{MPa} \quad r^{(4)} = 71.4\,\text{MPa}$ $r^{(5)} = 314.4\,\text{MPa}$
	$\chi_0^{(1)} = \chi_0^{(2)} = \chi_0^{(3)} = \chi_0^{(4)} = \chi_0^{(5)} = 0 \quad \text{or} \quad \chi_0^{(1)} = \chi_0^{(2)} = \chi_0^{(3)} = \chi_0^{(4)} = \chi_0^{(5)} = +\infty$ $c_M = 0 \quad k_1 = 115\,\text{MPa} \quad a_k = 0$
1070 Steel M=10	$c_0^{(1)} = 1510 \quad c_0^{(2)} = 461 \quad c_0^{(3)} = 177 \quad c_0^{(4)} = 77 \quad c_0^{(5)} = 39$ $c_0^{(6)} = 20 \quad c_0^{(7)} = 12 \quad c_0^{(8)} = 6.7 \quad c_0^{(9)} = 4.8 \quad c_0^{(10)} = 2.7$ $a_1^{(i)} = a_2^{(i)} = 0 \ (i=1, 2, ..., 10)$
	$r^{(1)} = r^{(2)} = r^{(3)} = r^{(4)} = r^{(5)} = r^{(6)} = r^{(7)} = r^{(8)} = r^{(9)} = 63.5\,\text{MPa}$ $r^{(10)} = 245\,\text{MPa}$
	$a_\chi = 0.0293 \quad b_\chi = 0.0128\,\text{MPa}^{-1}$ $Q_0^{(1)} = 0.25 \quad Q_0^{(2)} = 1.0 \quad Q_0^{(3)} = Q_0^{(4)} = 2.3$ $Q_0^{(5)} = Q_0^{(6)} = Q_0^{(7)} = Q_0^{(8)} = Q_0^{(9)} = 2.75 \quad Q_0^{(10)} = 4.5$
	$c_M = 10 \quad k_1 = 92.7\,\text{MPa} \quad a_k = 0.0361 \quad c_k = 0.0094 \ 1/\text{MPa}$
Al6061-T6 M=5	$c^{(1)} = 4576\,(1 - 0.74\,e^{-1.63p}) \qquad c^{(2)} = 2267\,(1 - 0.86\,e^{-0.92p})$ $c^{(3)} = 386\,(1 - 0.94\,e^{-1.74p}) \qquad c^{(4)} = 33\,(1 - 0.97\,e^{-2.73p})$ $c^{(5)} = 2\,(1 - 0.99\,e^{-4.20p})$
	$r^{(1)} = r^{(2)} = r^{(3)} = r^{(4)} = r^{(5)} = 57.2\,\text{MPa}$
	$\chi_0^{(1)} = \chi_0^{(2)} = \chi_0^{(3)} = \chi_0^{(4)} = \chi_0^{(5)} = 2$
	$c_M = 0 \quad k_1 = 115\,\text{MPa} \quad a_k = 0$

Table 9 Summary of Mathematical Expressions for the New Plasticity Model

		Expression	Description
Yield Surface	Eq.(2.8)	$f = (\underline{S} - \underline{\alpha}):(\underline{S} - \underline{\alpha}) - 2k^2 = 0$	k is the yield stress in pure shear.
Flow Rule	Eq.(2.10)	$d\underline{\varepsilon}^p = \dfrac{1}{h}\langle d\underline{S}:\underline{n}\rangle\,\underline{n}$	$\underline{n} = \dfrac{\underline{S} - \underline{\alpha}}{\sqrt{(\underline{S} - \underline{\alpha}):(\underline{S} - \underline{\alpha})}}$ h is the plastic modulus function.
Hardening Rule	Eq.(2.21)	$\underline{\alpha} = \sum\limits_{i=1}^{M} \underline{\alpha}^{(i)}$	$dp = \sqrt{d\underline{\varepsilon}^p:d\underline{\varepsilon}^p}$; $\ \left|\underline{\alpha}^{(i)}\right| = \sqrt{\underline{\alpha}^{(i)}:\underline{\alpha}^{(i)}}$
	Eq.(5.4)	$d\underline{\alpha}^{(i)} = c^{(i)} r^{(i)}\left[\underline{n} - \left(\dfrac{\left|\underline{\alpha}^{(i)}\right|}{r^{(i)}}\right)^{\chi^{(i)}+1}\underline{L}^{(i)}\right] dp$ (i=1, 2, ..., M)	$\underline{L}^{(i)} = \dfrac{\underline{\alpha}^{(i)}}{\left|\underline{\alpha}^{(i)}\right|}$
Memory Surface	Eq.(5.8)	$g = |\underline{\alpha}| - R_M \leq 0$	$|\underline{\alpha}| = \sqrt{\underline{\alpha}:\underline{\alpha}}$; $\ \underline{L} = \dfrac{\underline{\alpha}}{|\underline{\alpha}|}$ $H(g) = 0$ when $g < 0$ $H(g) = 1$ when $g \geq 0$ c_M is a constant.
	Eq.(5.9)	$dR_M = H(g)\langle \underline{L}:d\underline{\alpha}\rangle - c_M\left\langle 1 - \dfrac{|\underline{\alpha}|}{R_M}\right\rangle dp$	
Cyclic Hardening	Eq.(5.11)	$c^{(i)} = c_0^{(i)}\left(1 + a_1^{(i)}\, e^{-b_1^{(i)}p} + a_2^{(i)}\, e^{-b_2^{(i)}p}\right)$ (i=1, 2, ..., M)	$a_1^{(i)}$, $b_1^{(i)}$, $a_2^{(i)}$, $b_2^{(i)}$ are constants describing cyclic hardening.
Nonproportionality and Stress Level Effects	Eq.(5.14)	$\chi^{(i)} = \chi_0^{(i)}\left(2 - \underline{n}:\underline{L}^{(i)}\right) = Q^{(i)}\left(1 + a_\chi\, e^{b_\chi R_M}\right)\left(2 - \underline{n}:\underline{L}^{(i)}\right)$ (i=1, 2, ..., M)	a_χ and b_χ are constants considering the stress level effect on ratchetting.
Non-Masing Behavior	Eq.(5.15)	$k = k_1\left(1 + a_k\, e^{b_k R_M}\right)$	k_1 is the initial yield stress. a_k and b_k are constants.

Table 10 Material Constants Used in the Simulations Shown in
Figures 7.15 and 7.16

M=5
$c_0^{(1)} = 574$ $c_0^{(2)} = 88$ $c_0^{(3)} = 25$ $c_0^{(4)} = 8$ $c_0^{(5)} = 2$ $a_1^{(i)} = a_2^{(i)} = 0$ (i=1, 2, 3, 4, 5)
$r^{(1)} = r^{(2)} = r^{(3)} = r^{(4)} = r^{(5)} = 131$ MPa
$\chi_0^{(1)} = 1$ $\chi_0^{(2)} = 10$ $\chi_0^{(3)} = 50$ $\chi_0^{(4)} = 100$ $\chi_0^{(5)} = 1000$ $a_\chi = 0$ $k_1 = 110$ MPa $a_k = 0$ $c_M = 0$

FIGURES
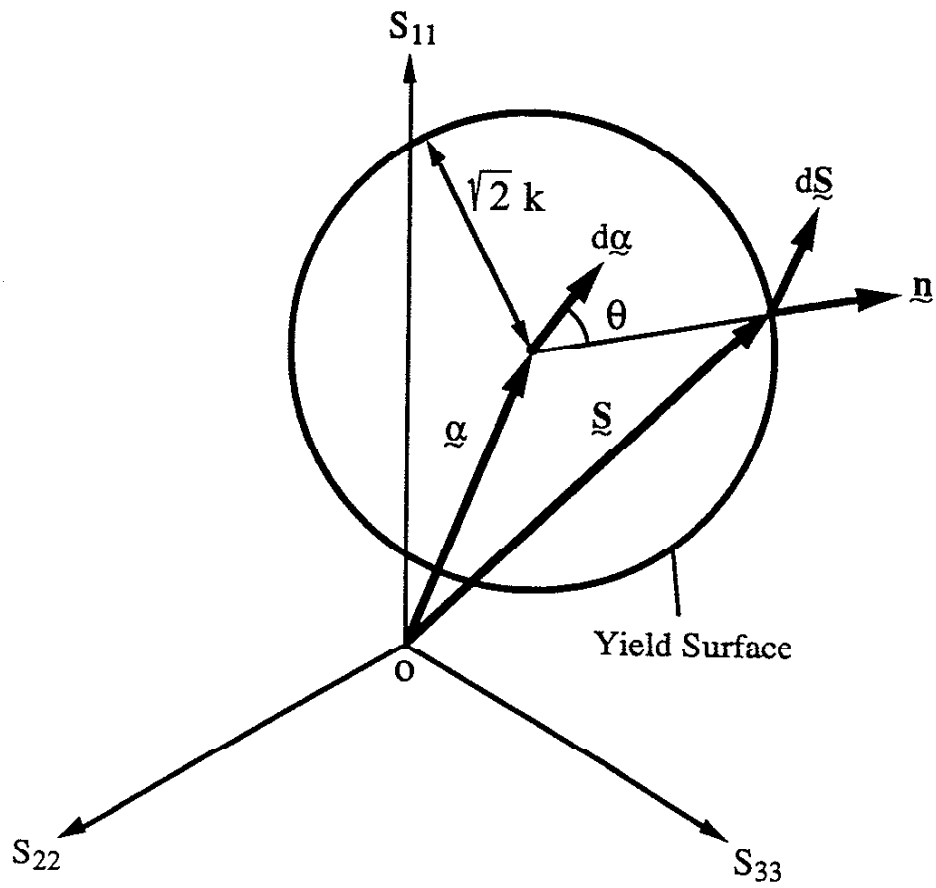
Figure 2.1 Generalized von Mises Yield Surface with Kinematic
Translation in Deviatoric Stress Space

(a) Within Limiting Surface

(b) On Limiting Surface
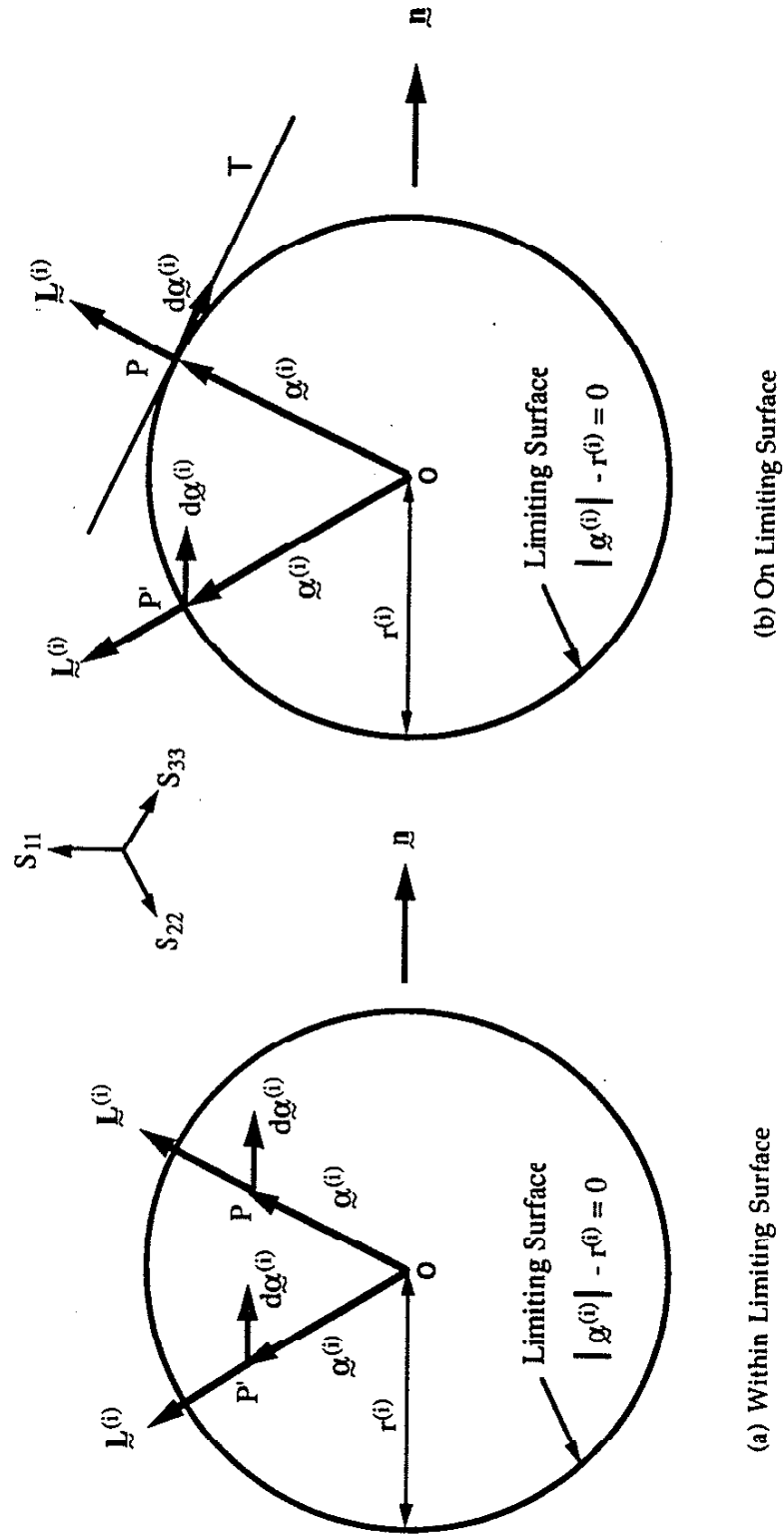
Figure 2.2 Geometric Interpretation of the Ohno-Wang Hardening Rule
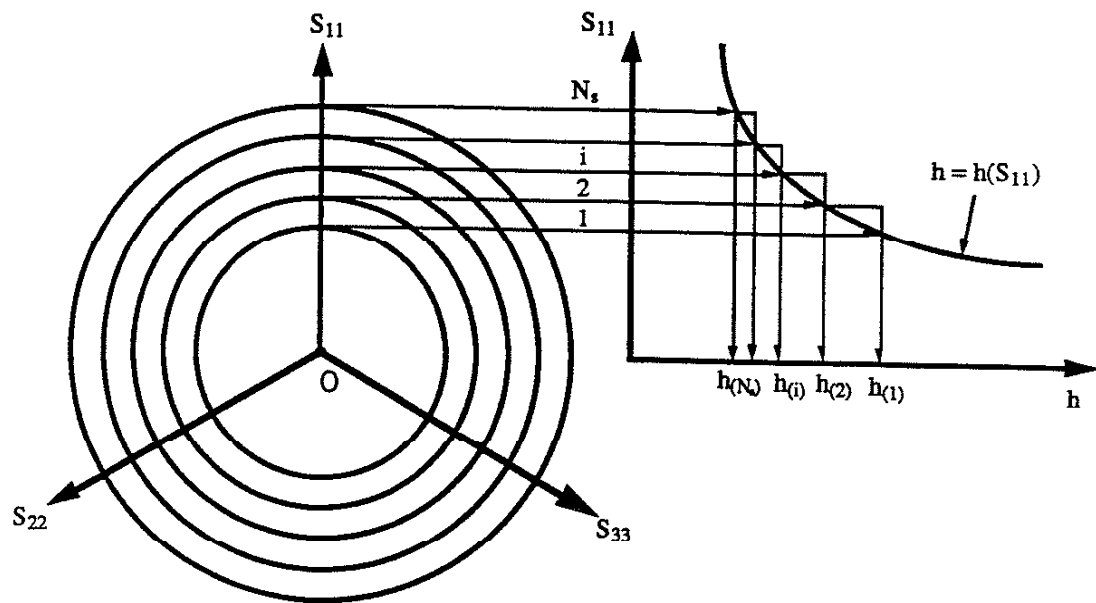
Figure 2.3 Typical Field of Mroz Constant Plastic Modulus Functions
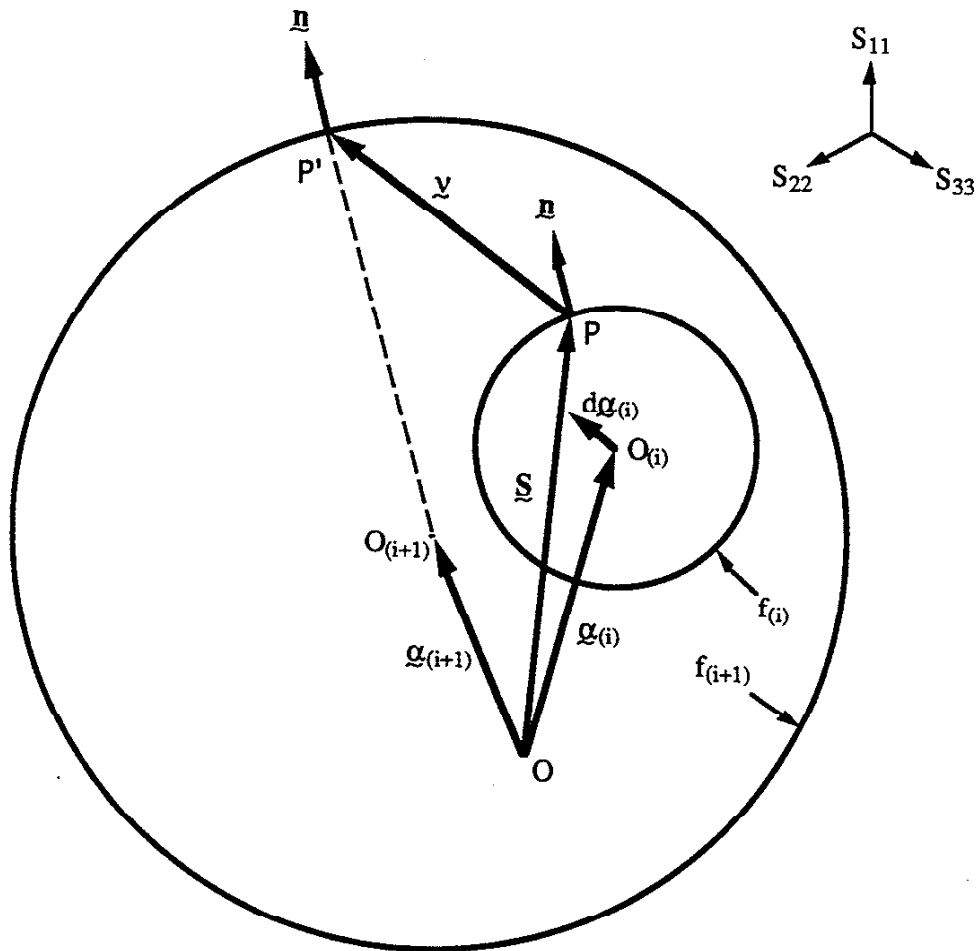
Figure 2.4 Schematic of the Mroz Hardening Rule Illustrating Translation
Direction
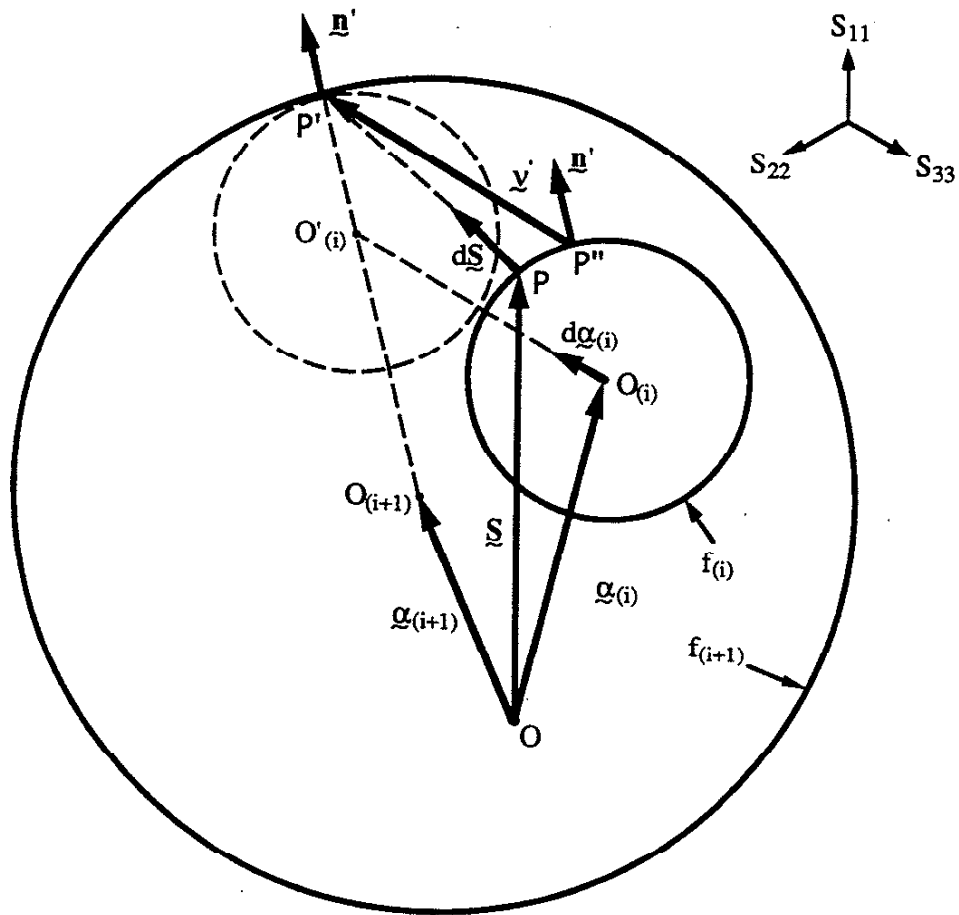
Figure 2.5 Schematic of the Garud Hardening Rule Illustrating Translation
Direction

$$H \approx \frac{d(\Delta\sigma)}{d(\Delta\varepsilon^p)}$$

1 Cyclic Hardening
2 Cyclic Softening
3,4 Mixed Cyclic Hardening/Softening

- - - - - First Cycle
——— Stabilized Cycle
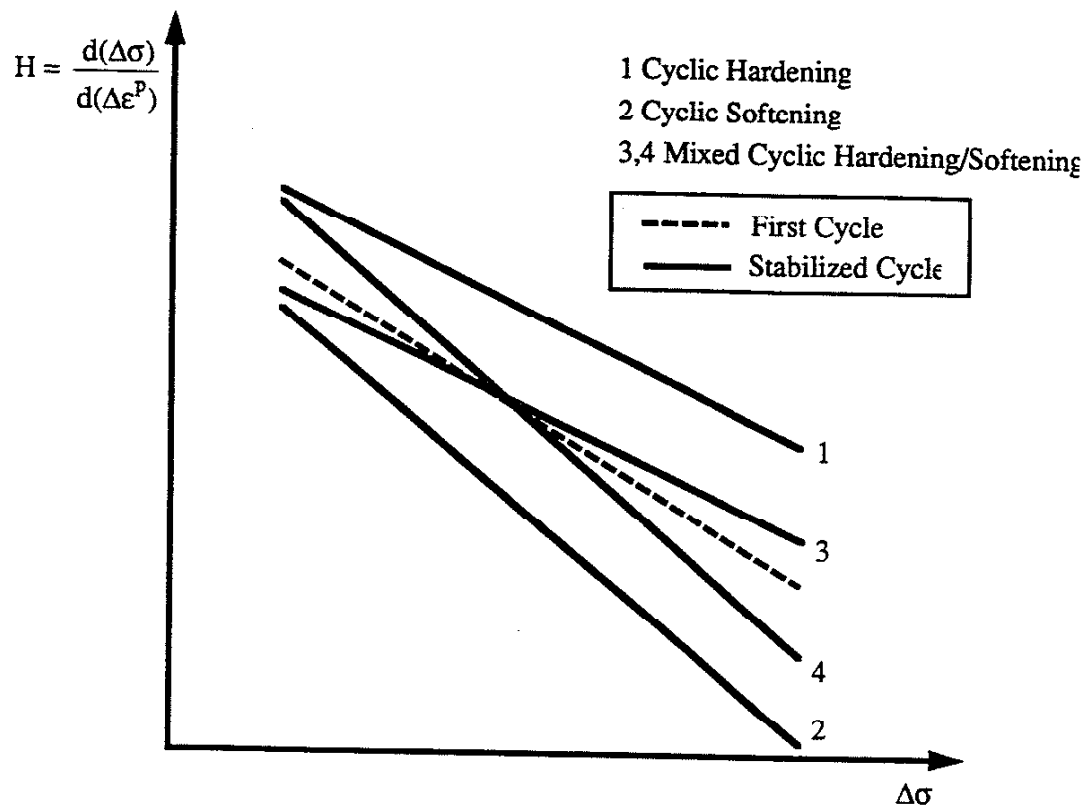
Figure 2.6 Possible Changes in the Hardening Modulus when Transient
Behavior Occurs
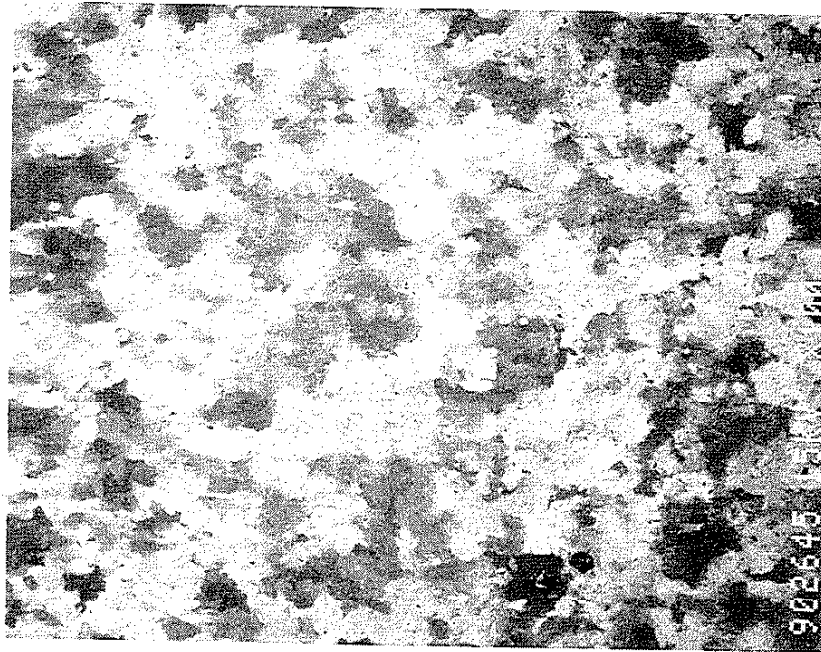
X100
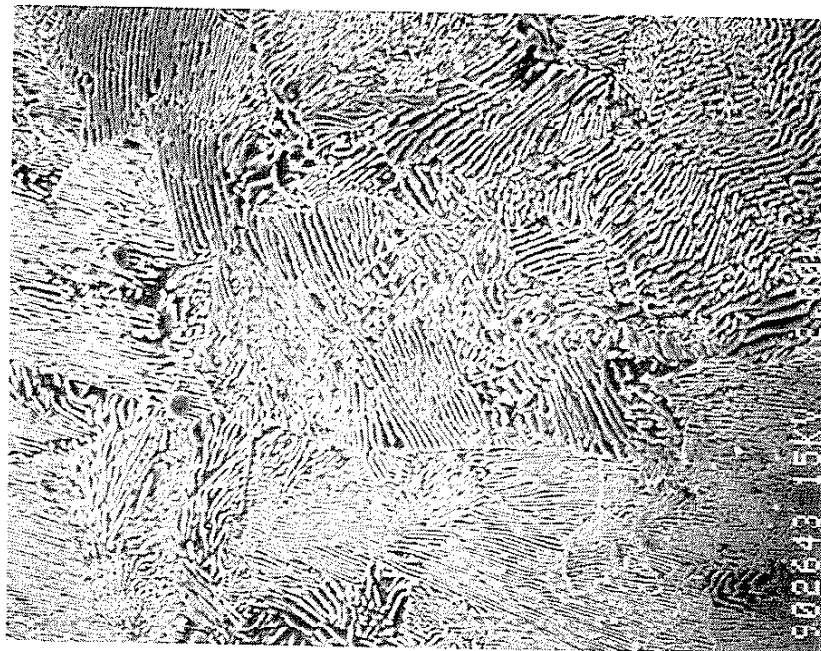
X2000

Figure 3.1 Microstructure of 1070 Steel
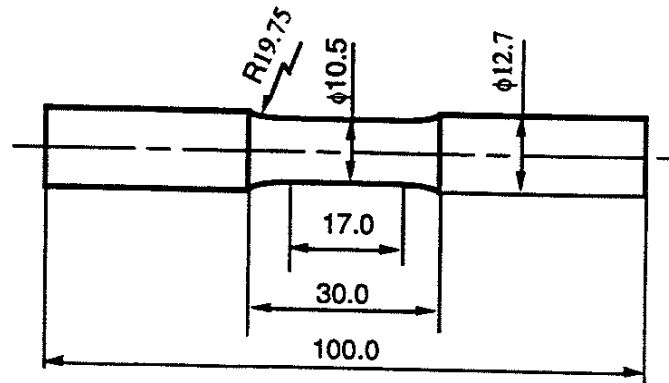
(a) Uniaxial Solid Test Specimen
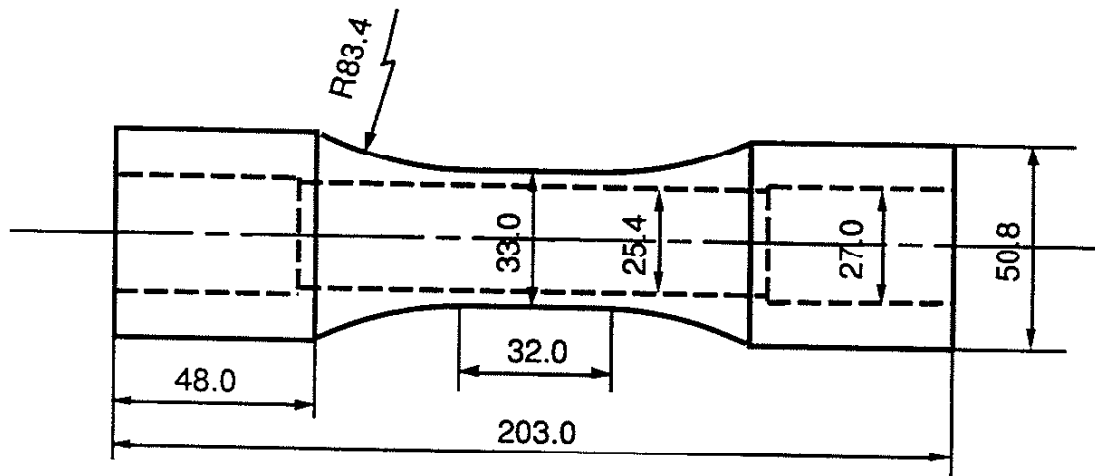
(b) Axial-Torsion Tubular Test Specimen

Figure 3.2 Test Specimen Dimensions (all values given in mm)
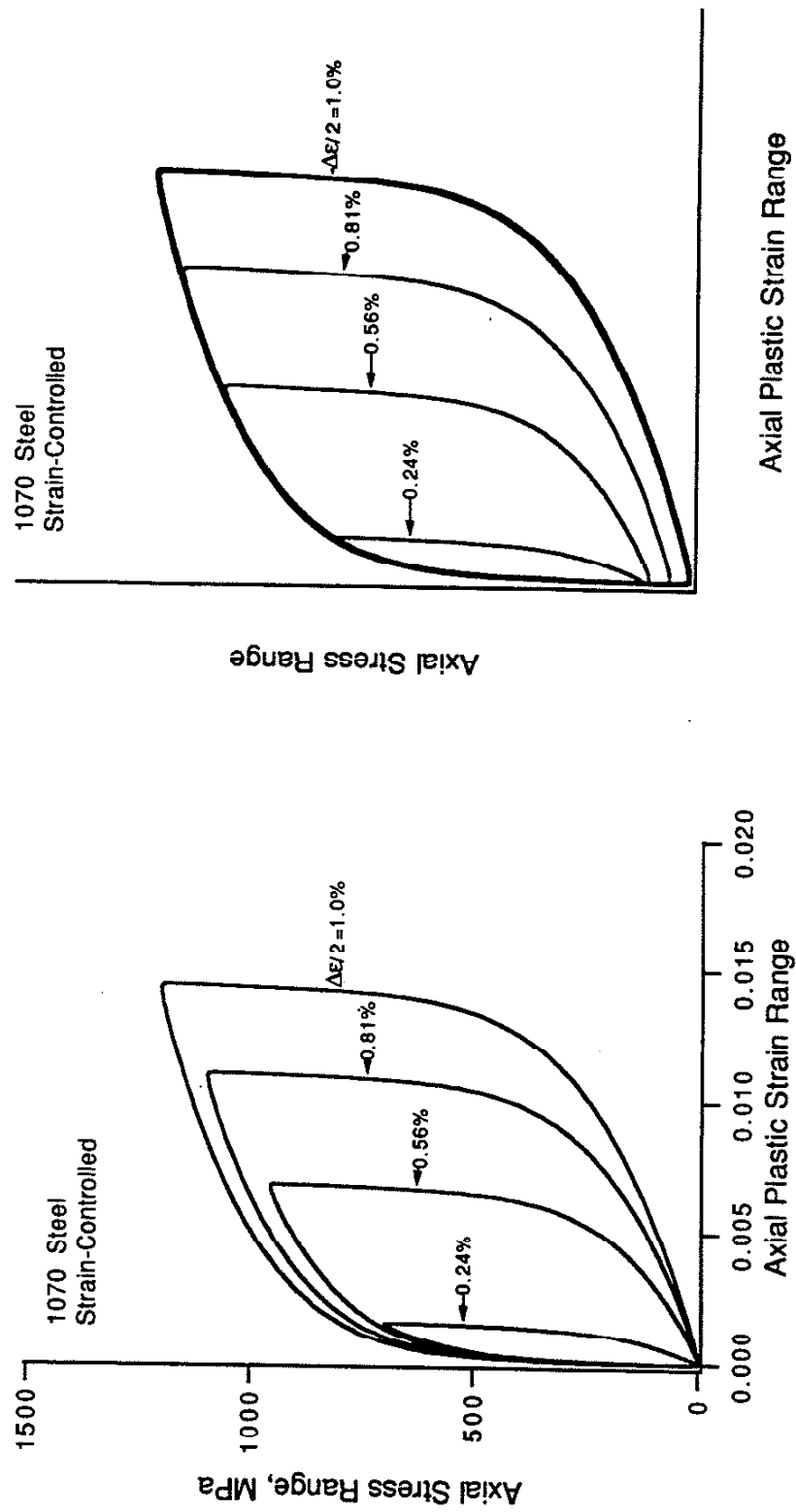
(a) Hysteresis Loops with Matched Lower Tips

(b) Hysteresis Loops with Matched Upper Branches

Figure 3.3 Stable Hysteresis Loops of 1070 Steel for Fully Reversed Strain-Controlled Uniaxial Loading

(a) Stress-Strain Response

(b) Ratchetting Strain vs. Number of Cycles

(c) Diametral Ratchetting Strain vs. Axial Ratchetting Strain
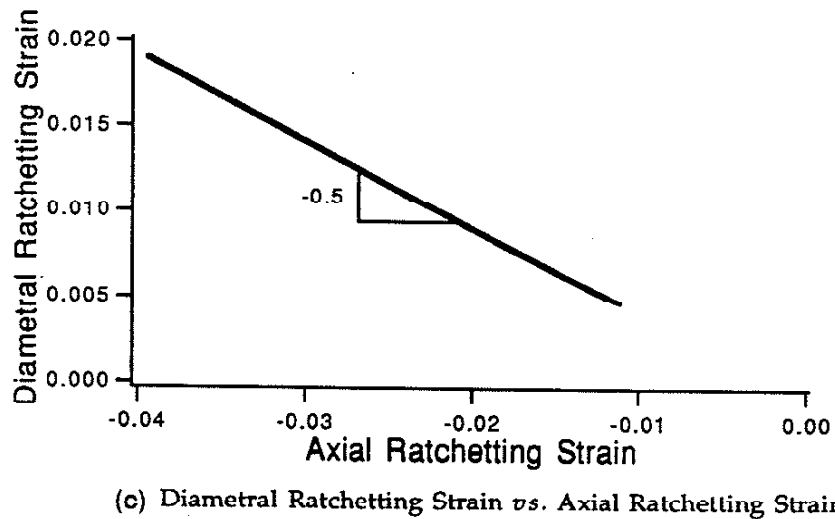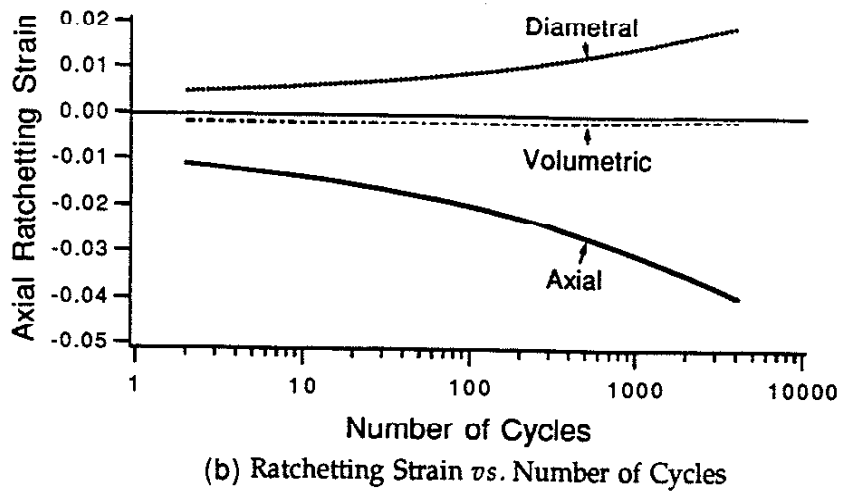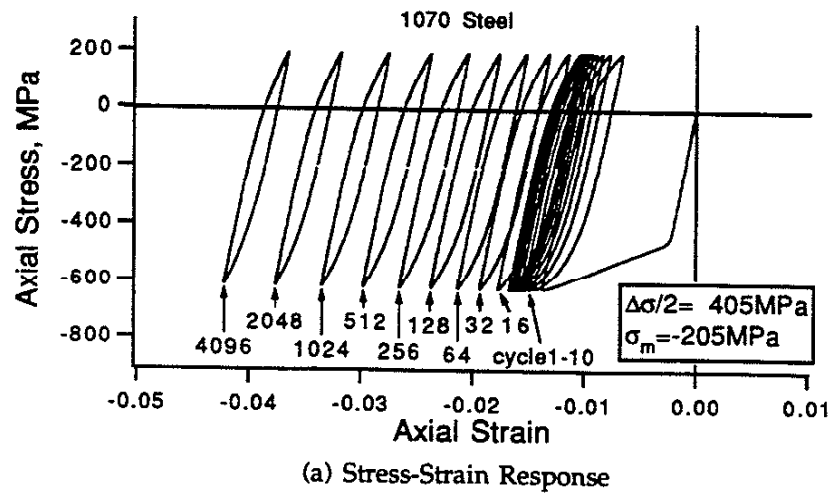
Figure 3.4 Experimental Ratchetting for Uniaxial Loading
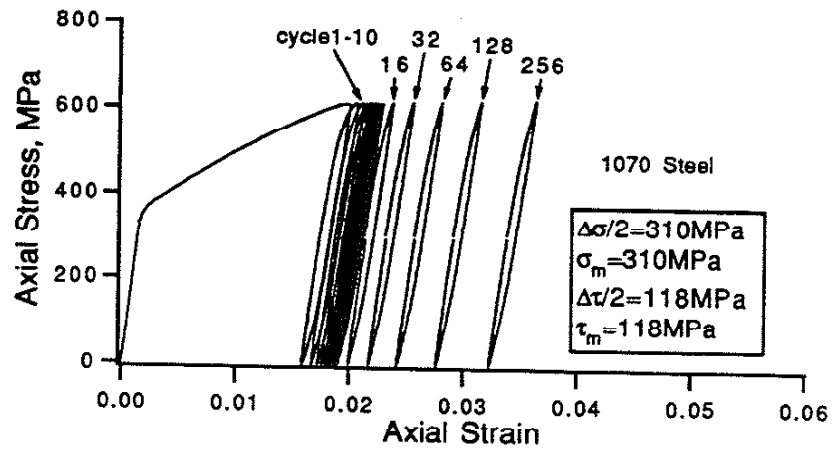
(a) Axial Stress-Strain Response
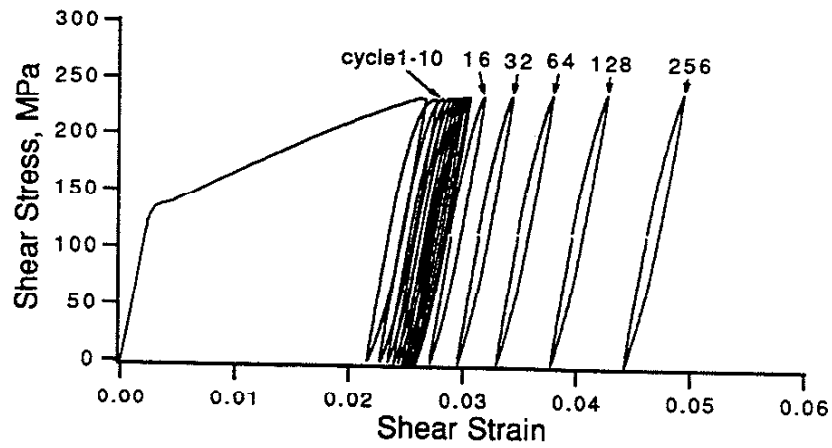
(b) Shear Stress-Strain Response
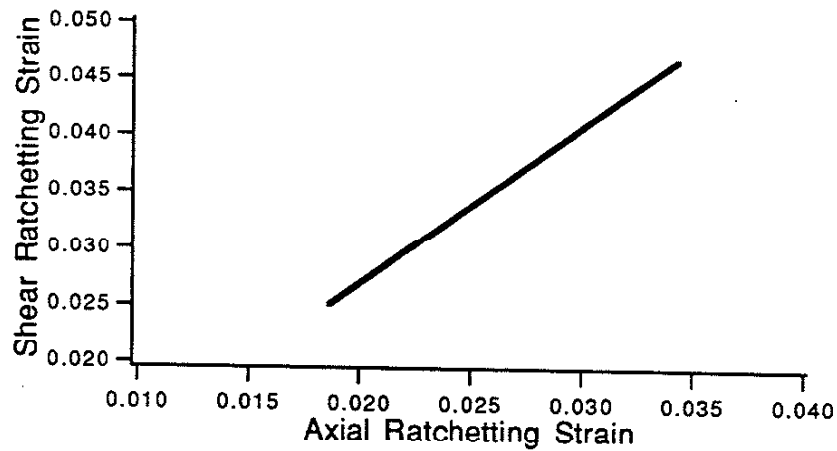
(c) Shear Ratchetting *vs.* Axial Ratchetting

Figure 3.5 Experimental Ratchetting for Proportional Axial-Torsion Loading
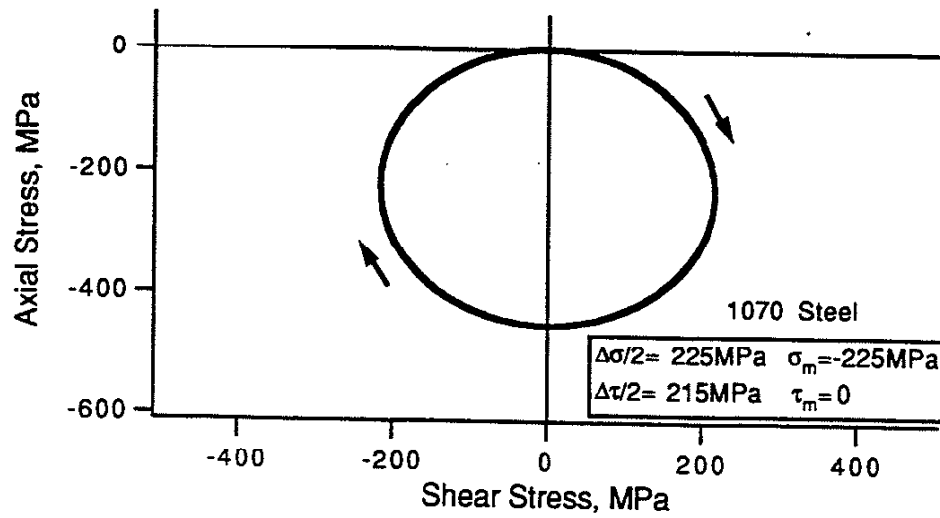
(a) Stress-Controlled Loading Path
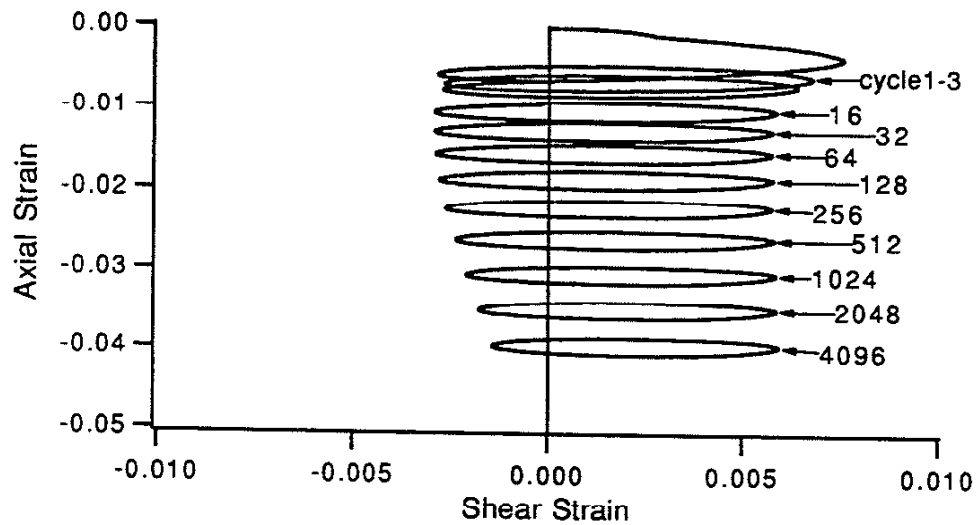
(b) Biaxial Strain Response

Figure 3.6 Experimental Ratchetting for an "Ellipse" Shaped Axial-Torsion Loading Path
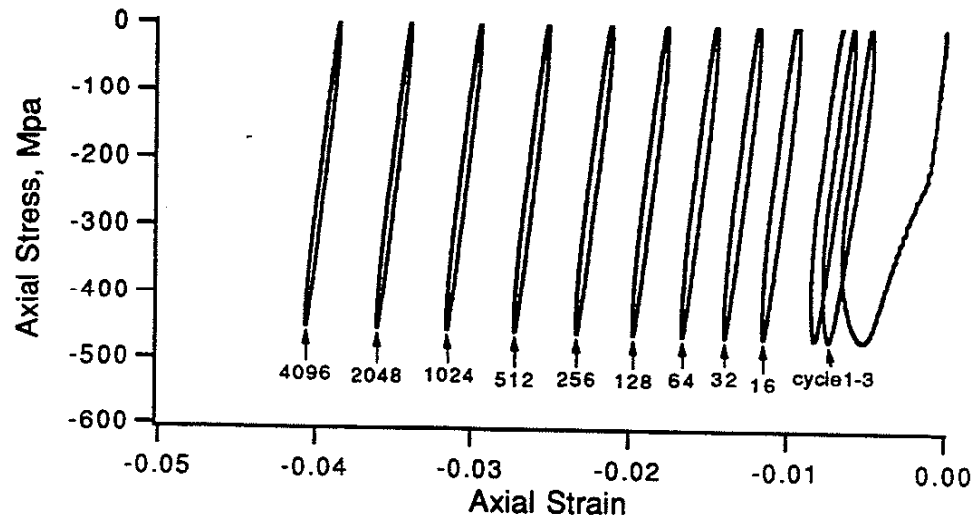
(c) Axial Stress-Strain Response
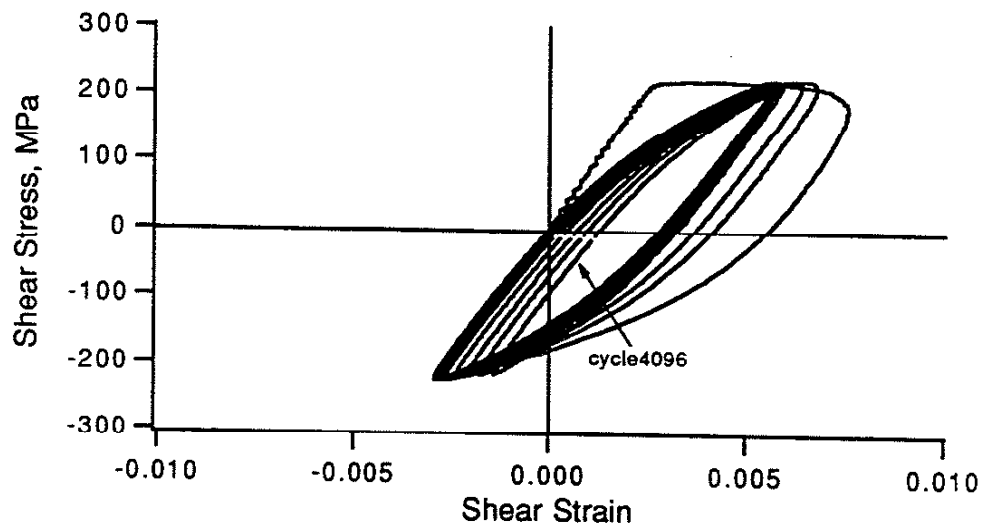
(d) Shear Stress-Strain Response

Figure 3.6 (cont.) Experimental Ratchetting for an "Ellipse" Shaped
Axial-Torsion Loading Path
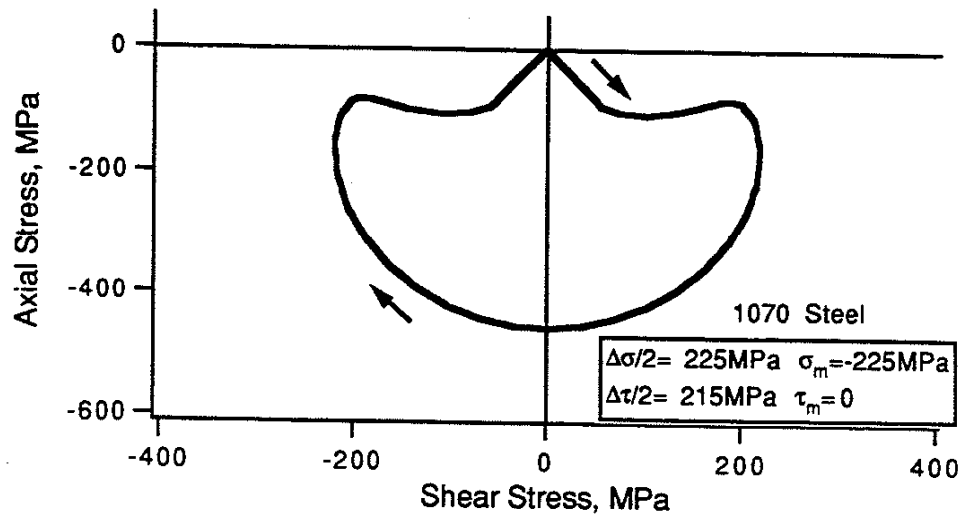
(a) Stress-Controlled Loading Path
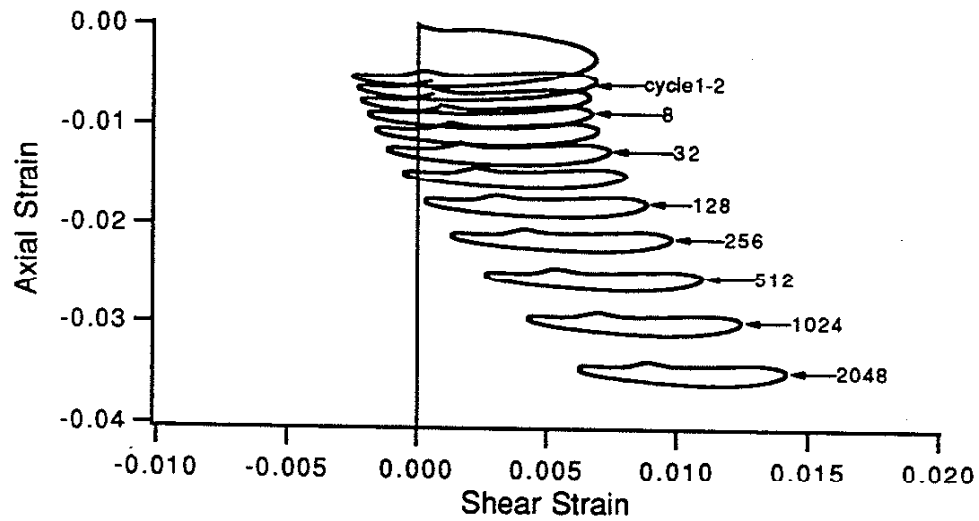
(b) Biaxial Strain Response

Figure 3.7 Experimental Ratchetting for an "Apple" Shaped Axial-Torsion Loading Path
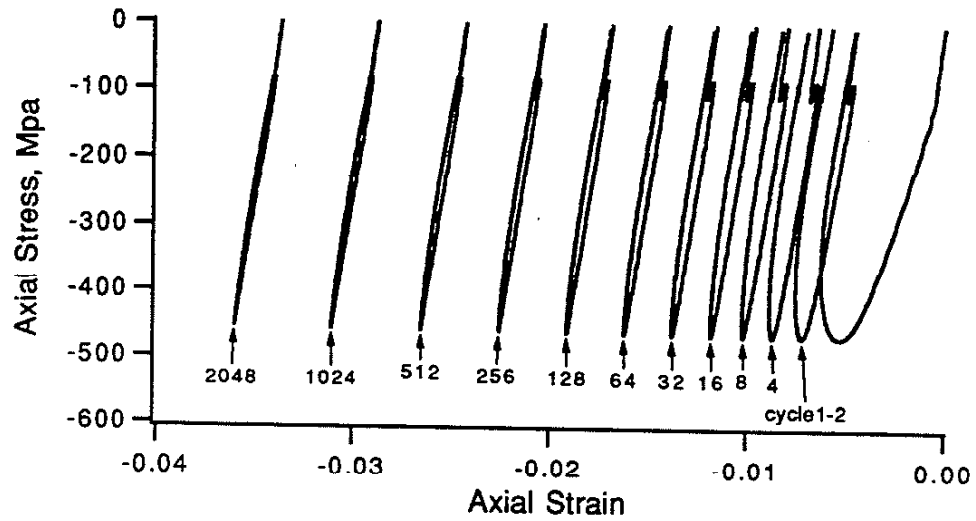
(c) Axial Stress-Strain Response
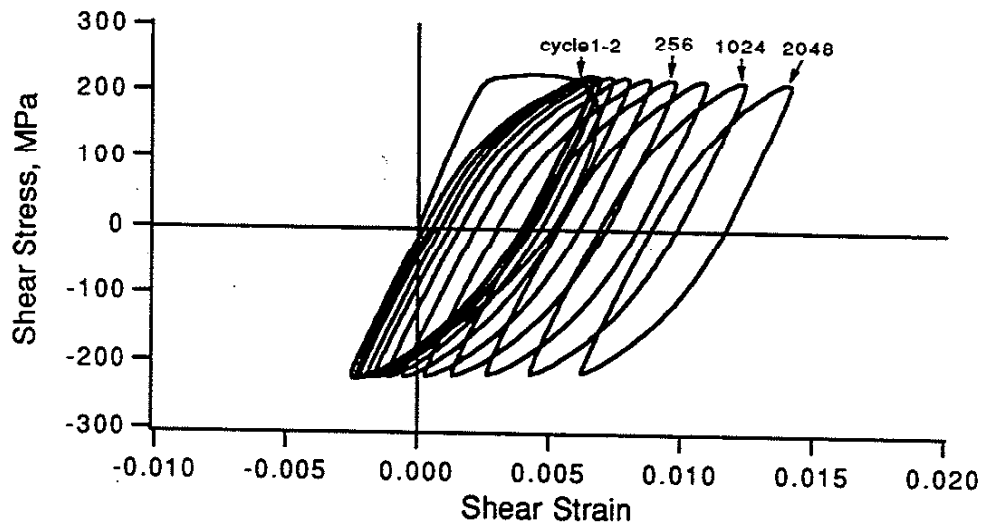
(d) Shear Stress-Strain Response

Figure 3.7(cont.) Experimental Ratchetting for an "Apple" Shaped Axial-Torsion Loading Path

1070 Steel
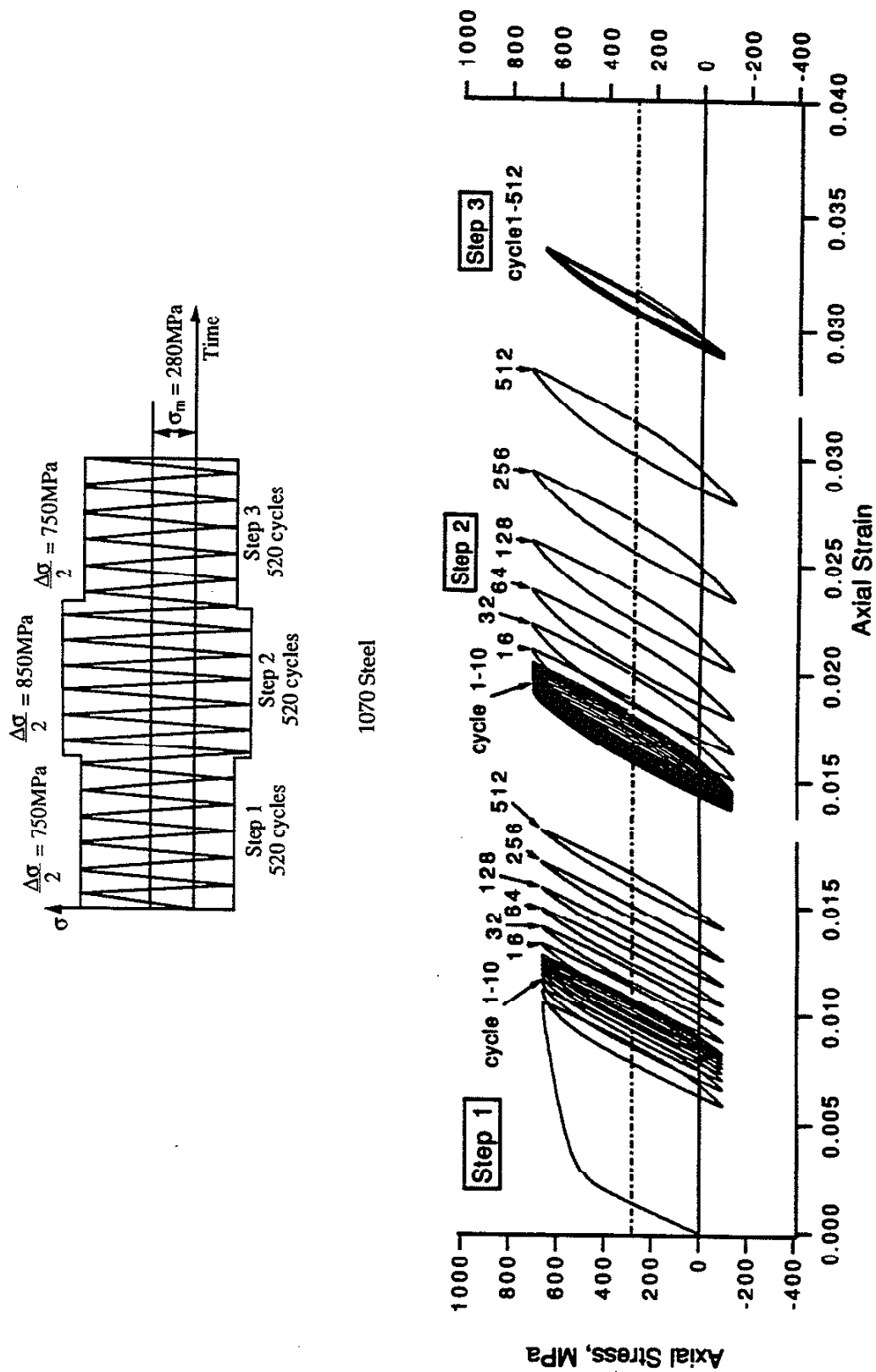
Figure 3.8 Experimental Ratchetting for a Uniaxial Step Loading with a Constant Mean Stress
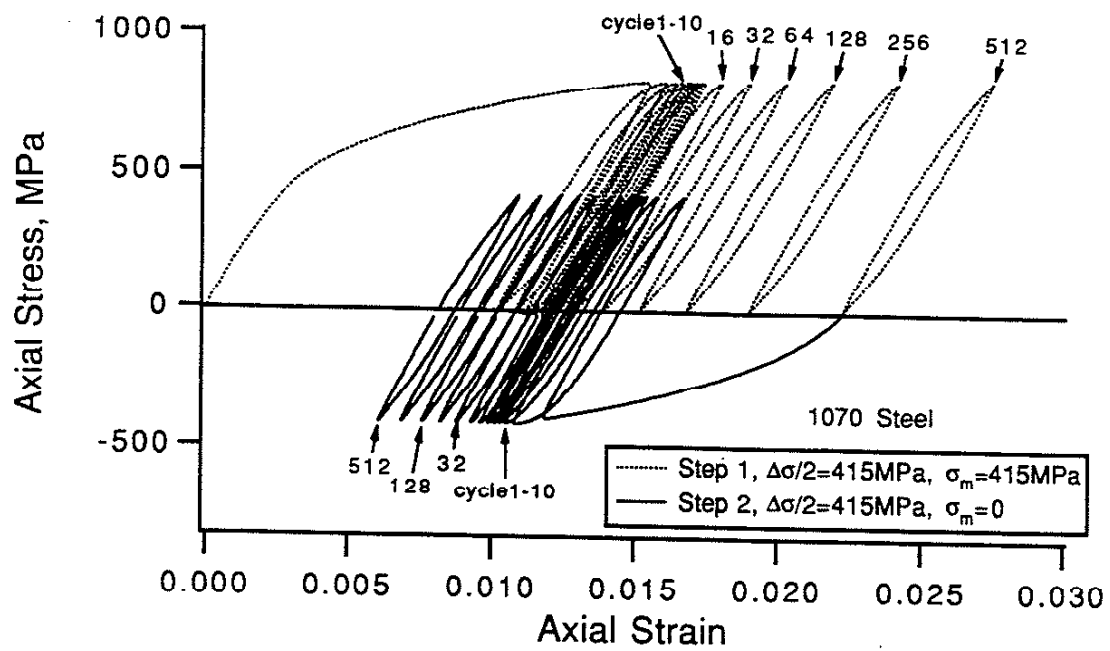
Figure 3.9 Experimental Two-Step Uniaxial Test: Positive Mean Stress
Followed by Zero Mean Stress
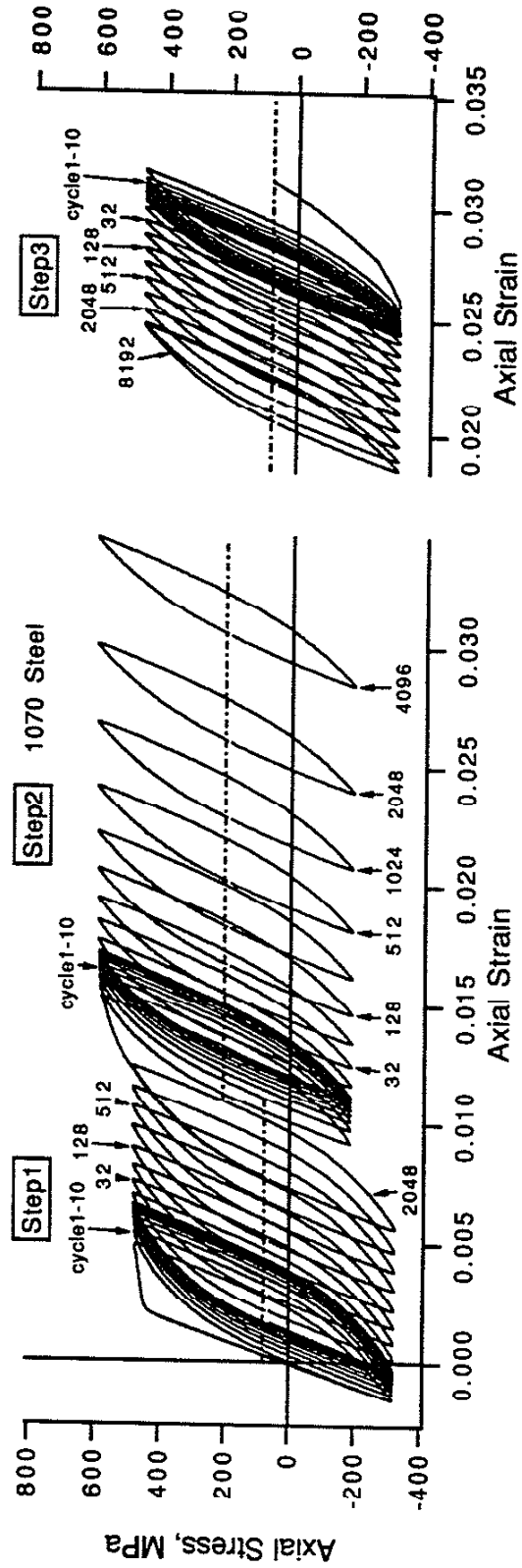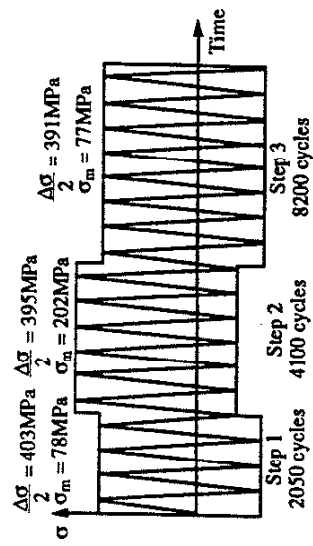
Figure 3.10 Experimental Ratchetting for a Three-Step Uniaxial Loading
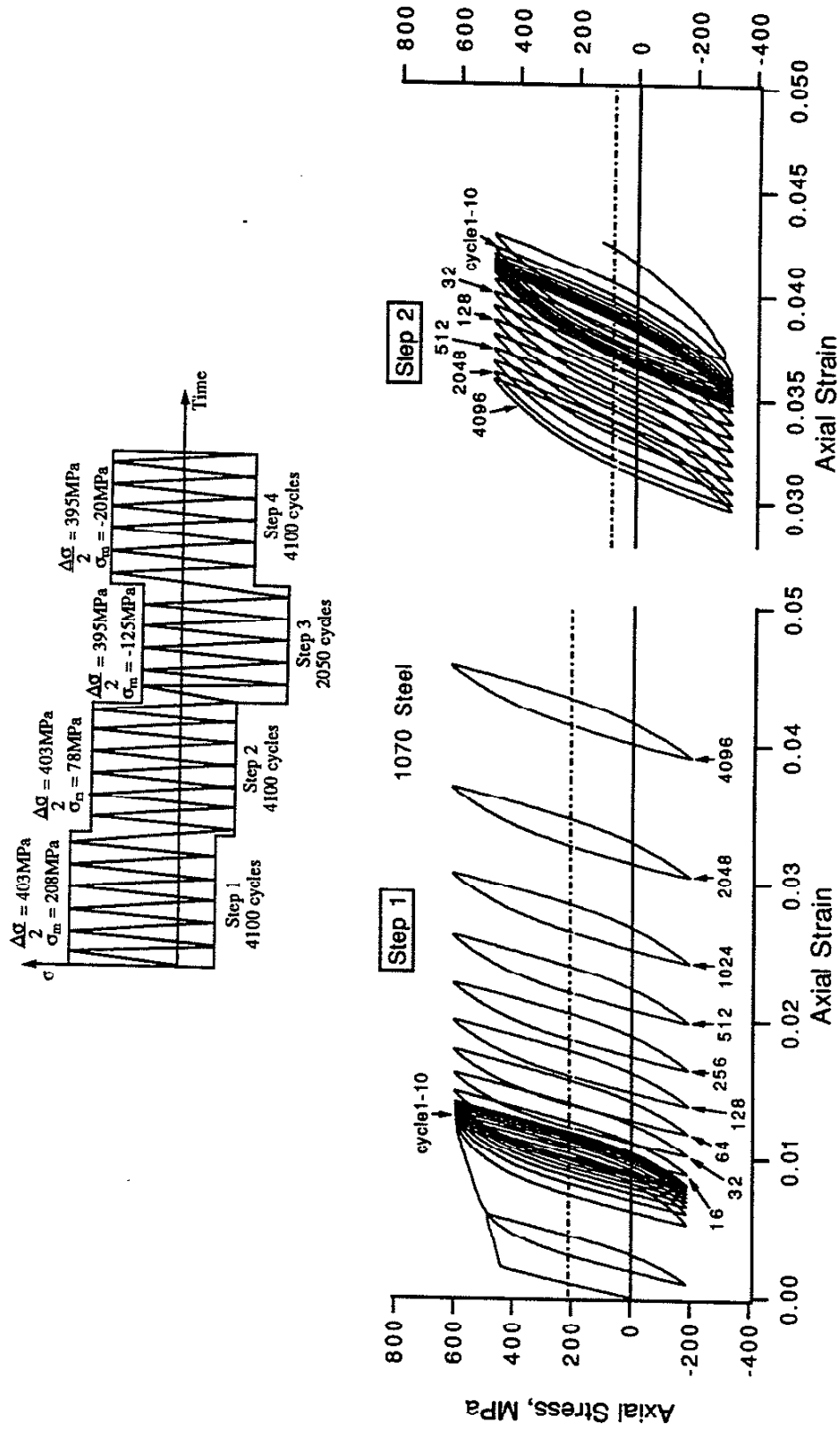
(a) Stress-Strain Response: Step 1 and Step 2

Figure 3.11 Experimental Ratchetting for a Multiple-Step Uniaxial Loading
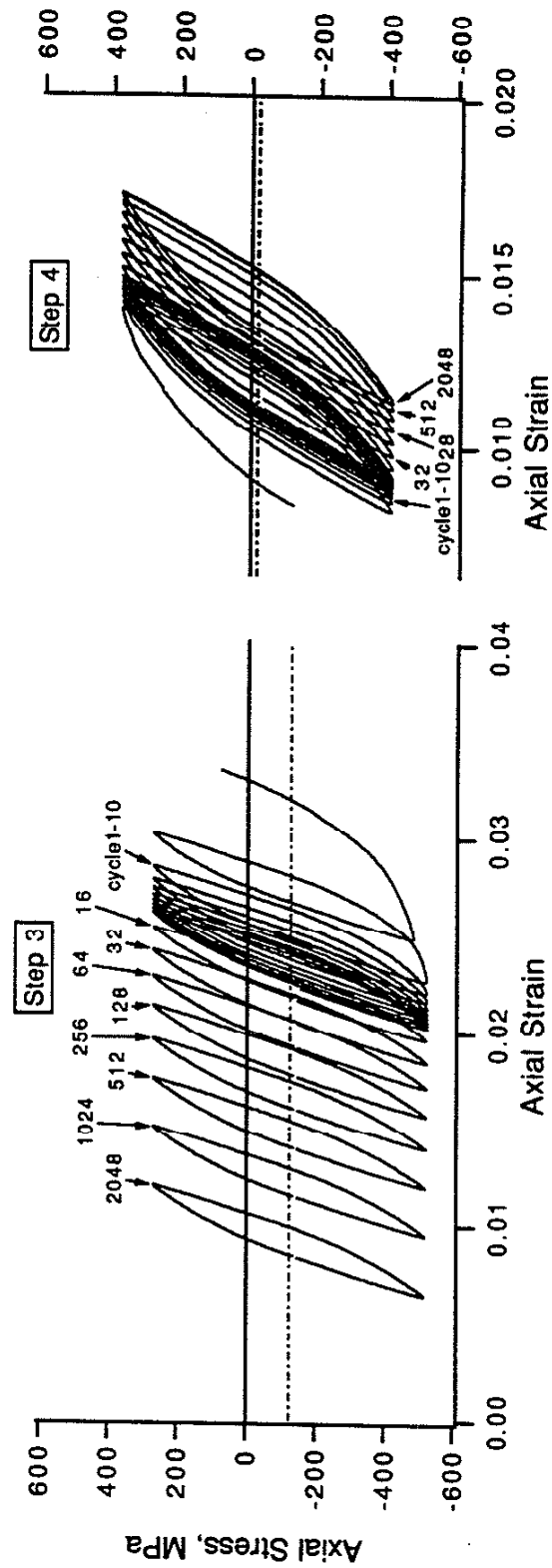
(b) Stress-Strain Response: Step 3 and Step 4

Figure 3.11(cont.) Experimental Ratchetting for a Multiple-Step Uniaxial Loading
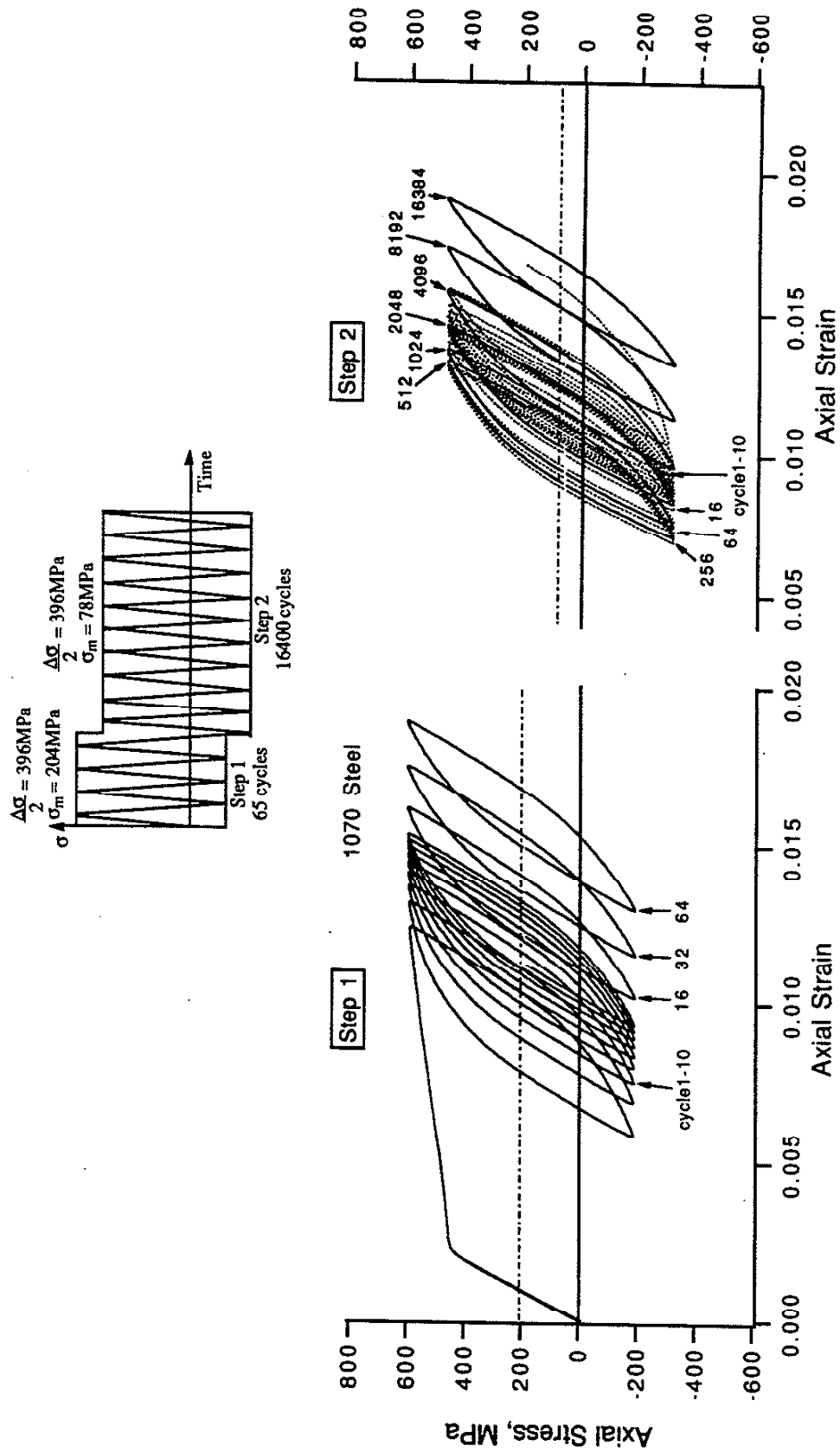
Figure 3.12 Experimental Ratchetting for a Two-Step Uniaxial Loading

114
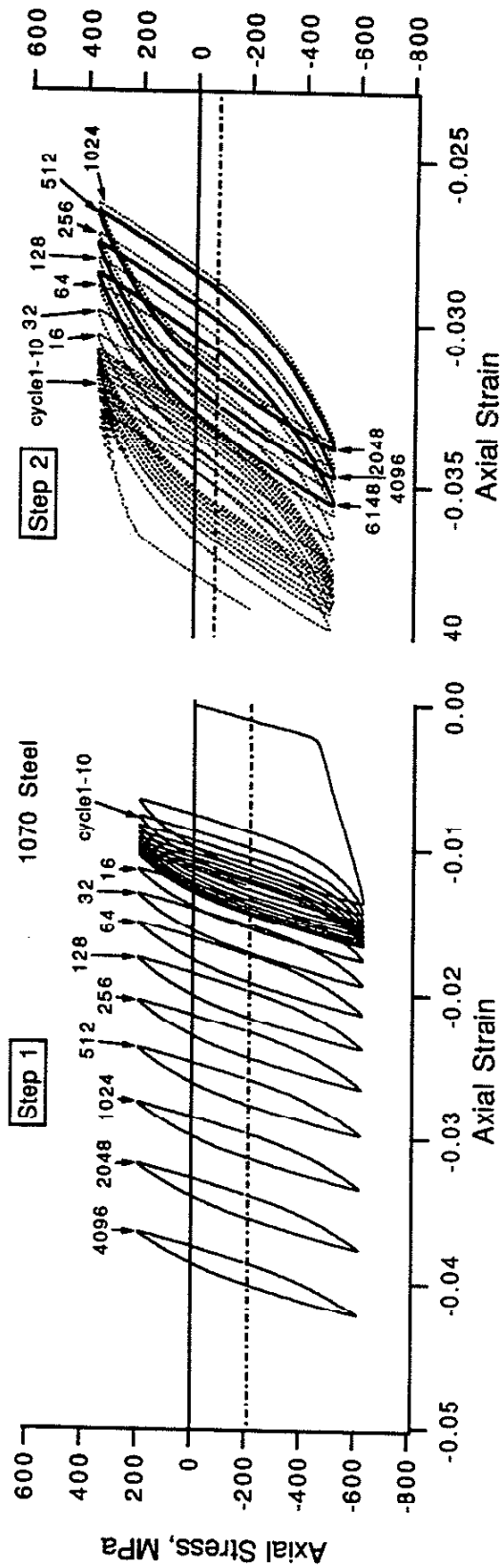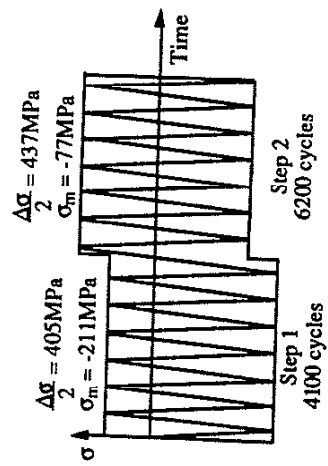
Figure 3.13 Experimental Ratchetting for a Two-Step Uniaxial Loading
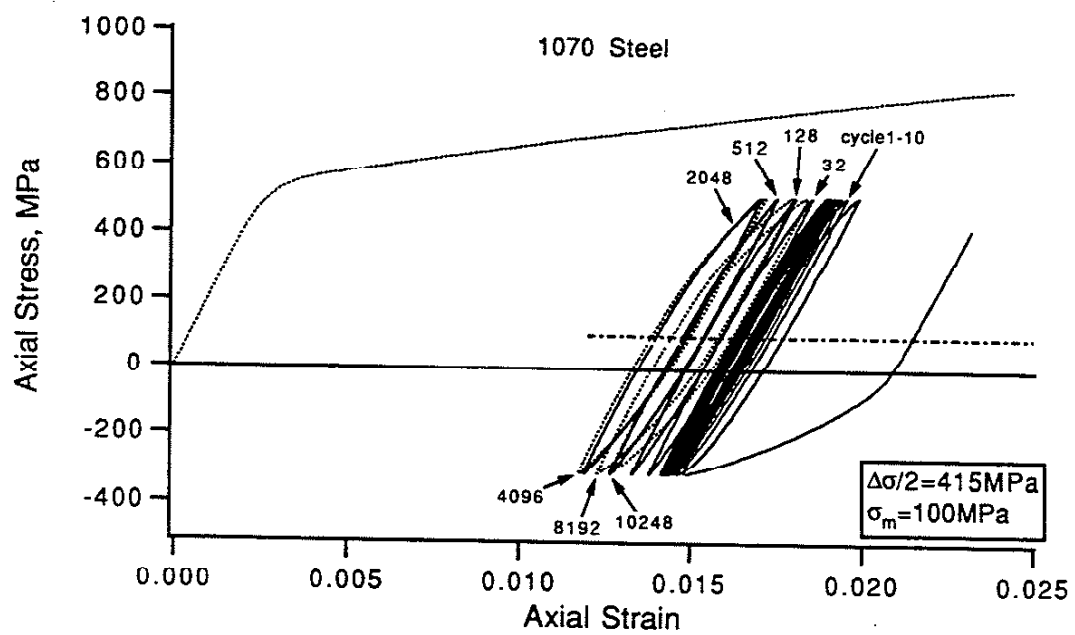
Figure 3.14 Experimental Ratchetting after a Single Tensile Overload
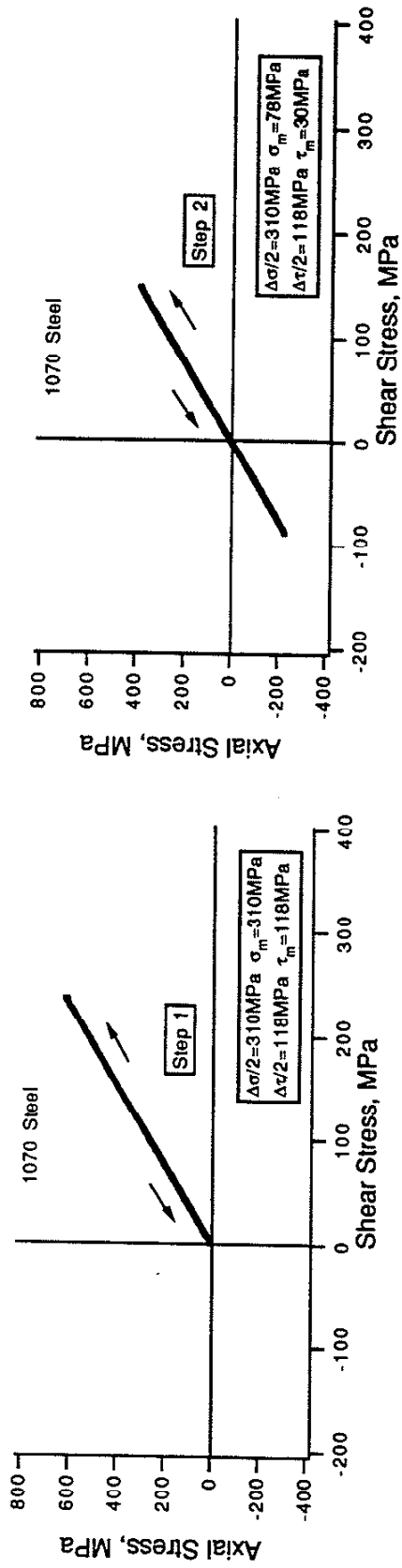
(a) Stress-Controlled Loading Paths
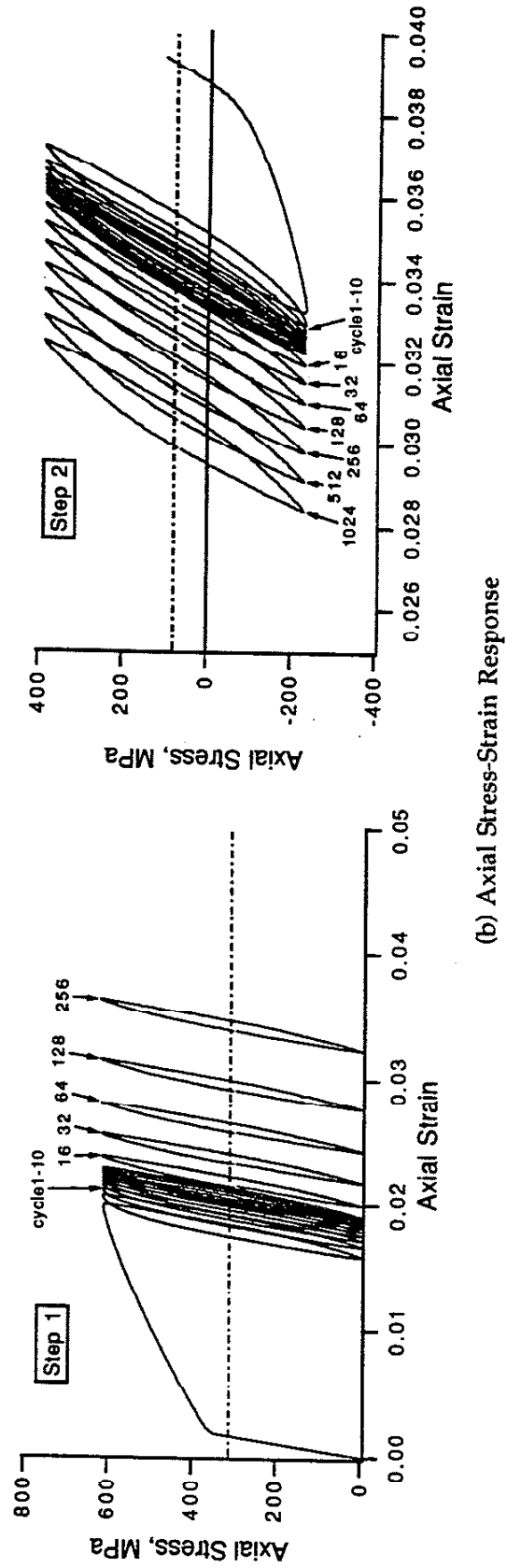
(b) Axial Stress-Strain Response

Figure 3.15 Experimental Ratchetting for a Two-Step Proportional Axial-Torsion Loading
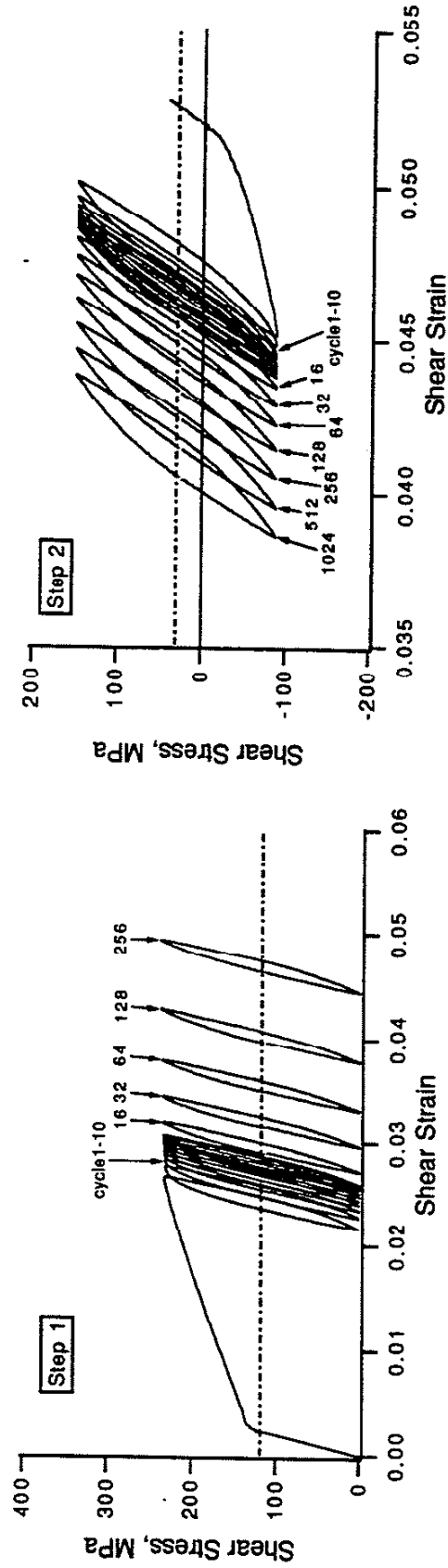
(c) Shear Stress-Strain Response

Figure 3.15(cont.) Experimental Ratchetting for a Two-Step Proportional Axial-Torsion Loading

(a) Stress-Controlled Loading Paths

(b) Axial Stress-Strain Response
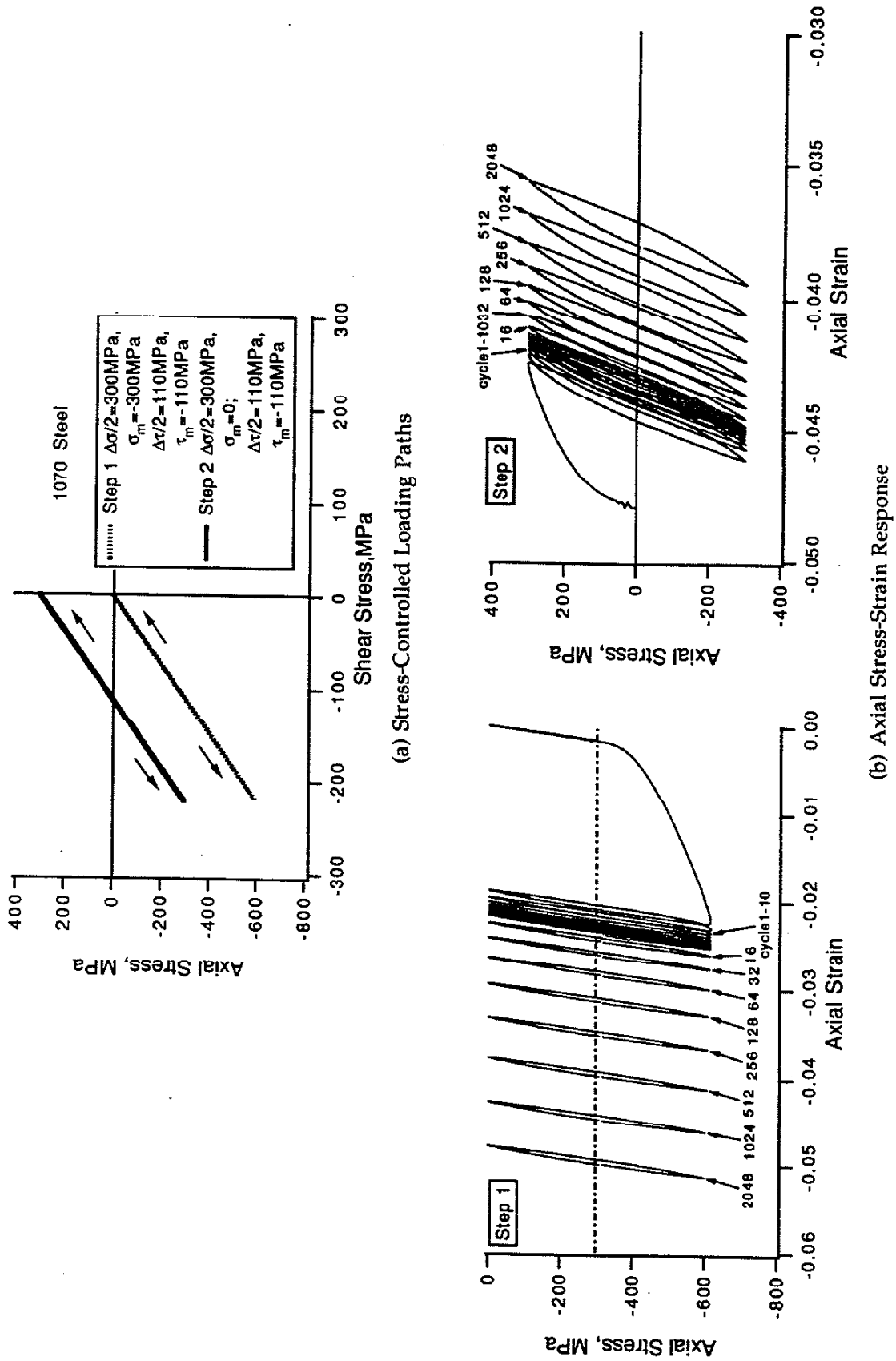
Figure 3.16 Experimental Ratchetting for a Two-Step Nonproportional Axial-Torsion Loading History
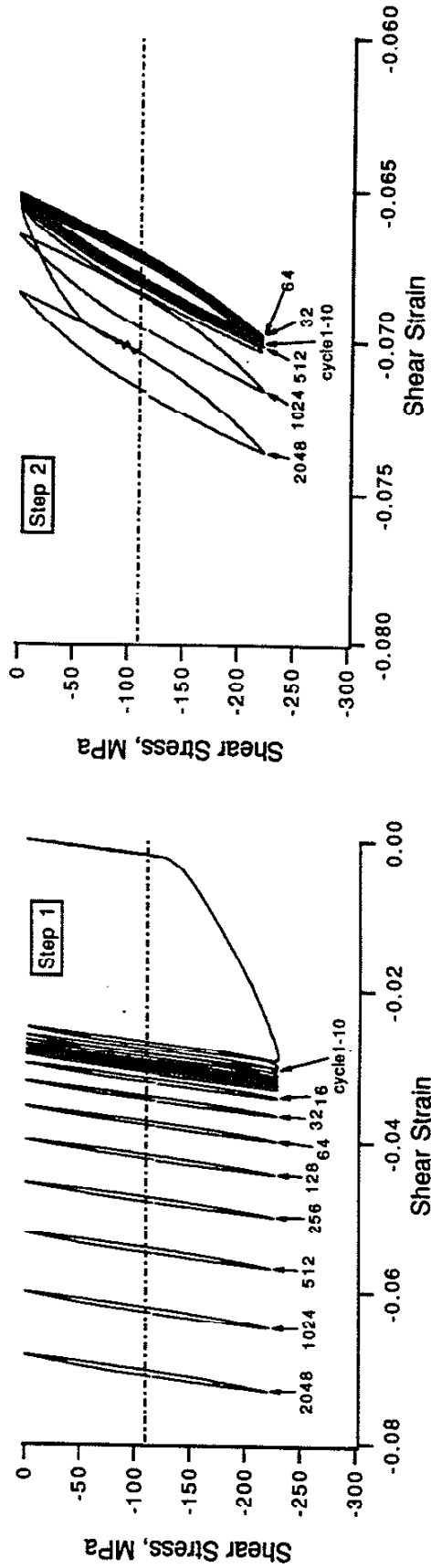
(c) Shear Stress-Strain Response

Figure 3.16(cont.) Experimental Ratchetting for a Two-Step Nonproportional Axial-Torsion Loading History

(a) Stress-Controlled Loading Paths

(b) Biaxial Strain Response: Step 1

(c) Biaxial Strain Response: Step 2
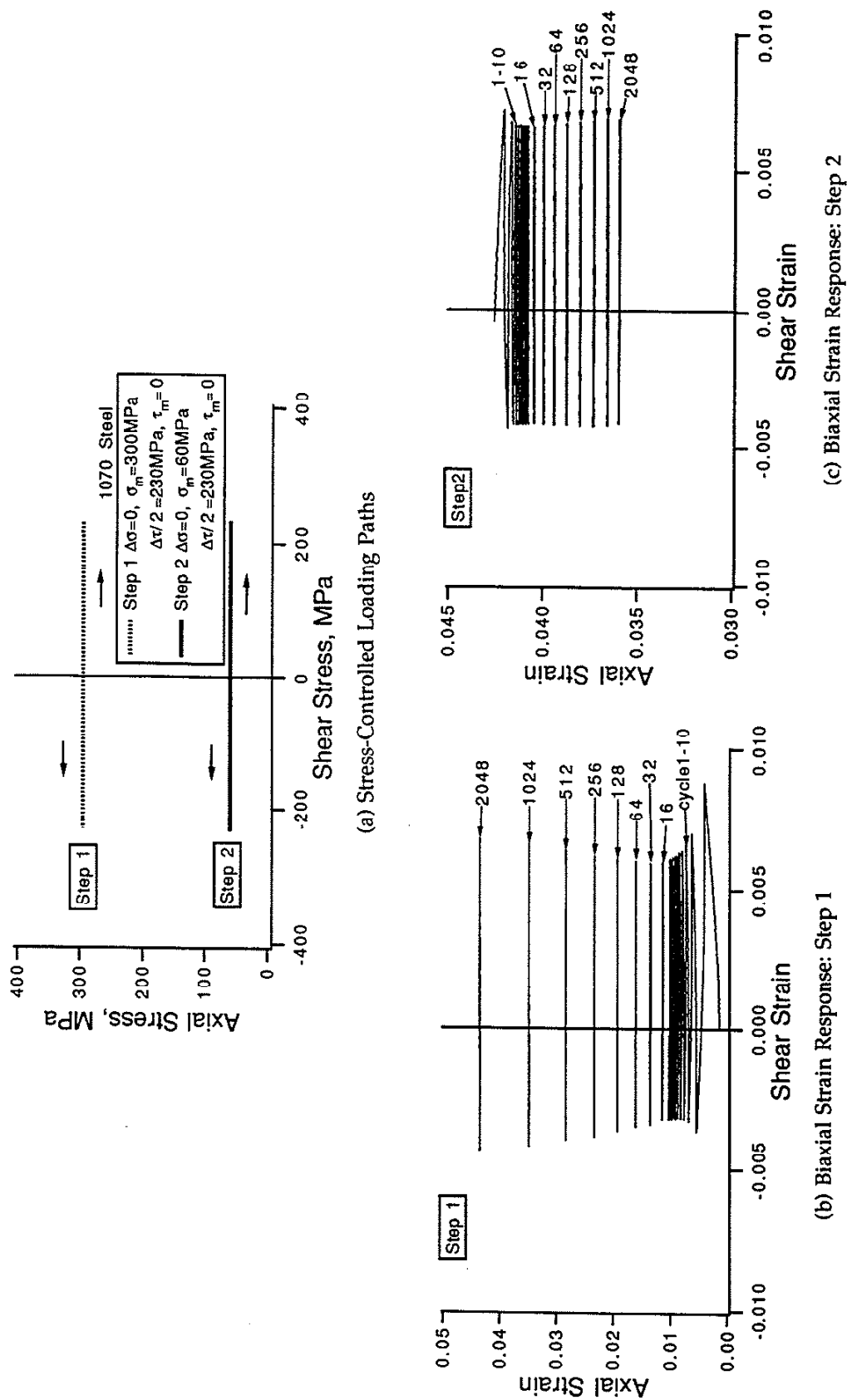
Figure 3.17 Experimental Ratchetting for a Two-Step Nonproportional Axial-Torsion Loading History

(a) Stress-Controlled Loading Paths

(b) Biaxial Strain Response: Step 1

(c) Biaxial Strain Response: Step 2
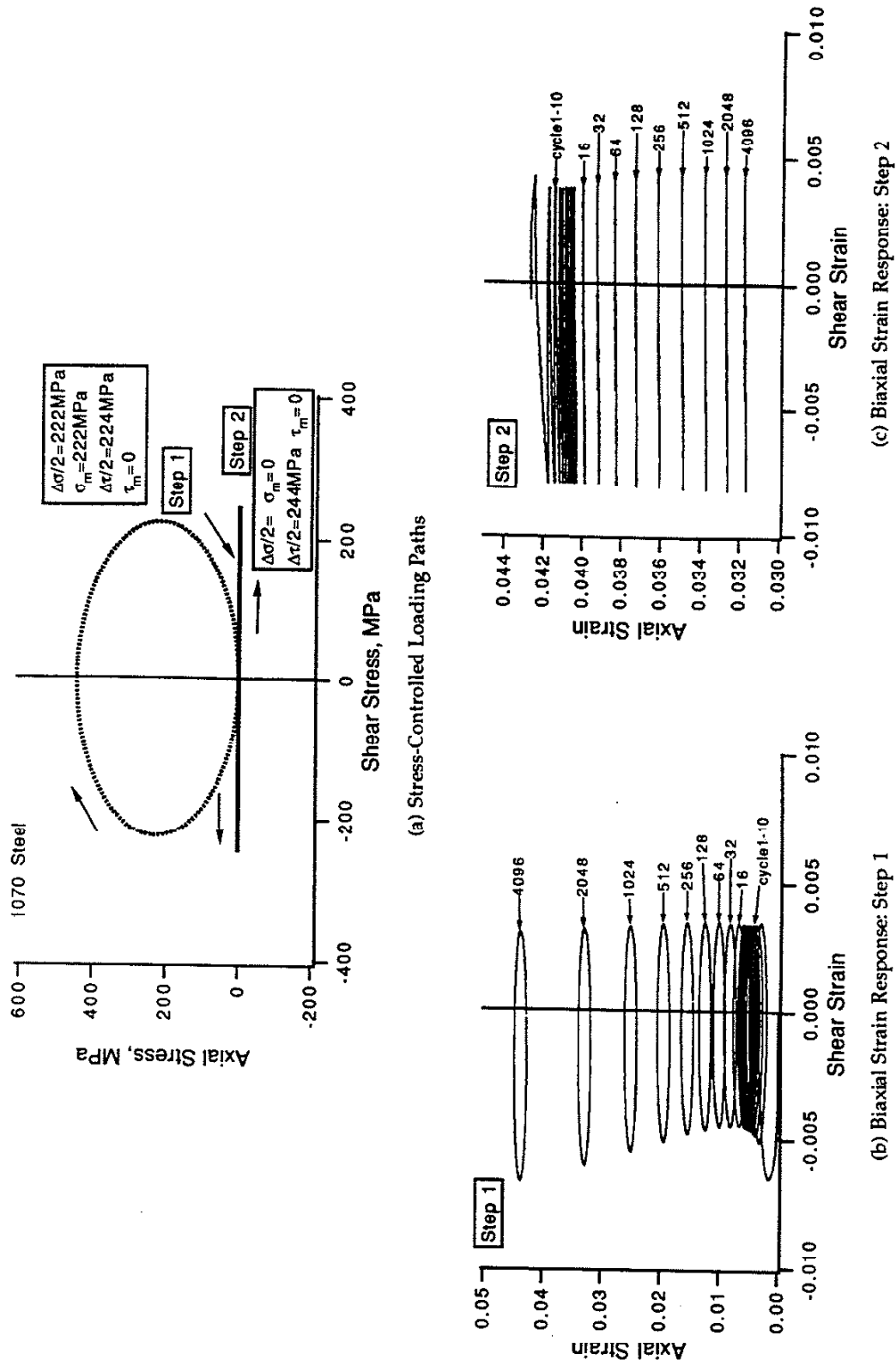
Figure 3.18 Experimental Ratchetting for a Two-Step Loading: Nonproportional Axial-Torsion Followed by Pure Torsion
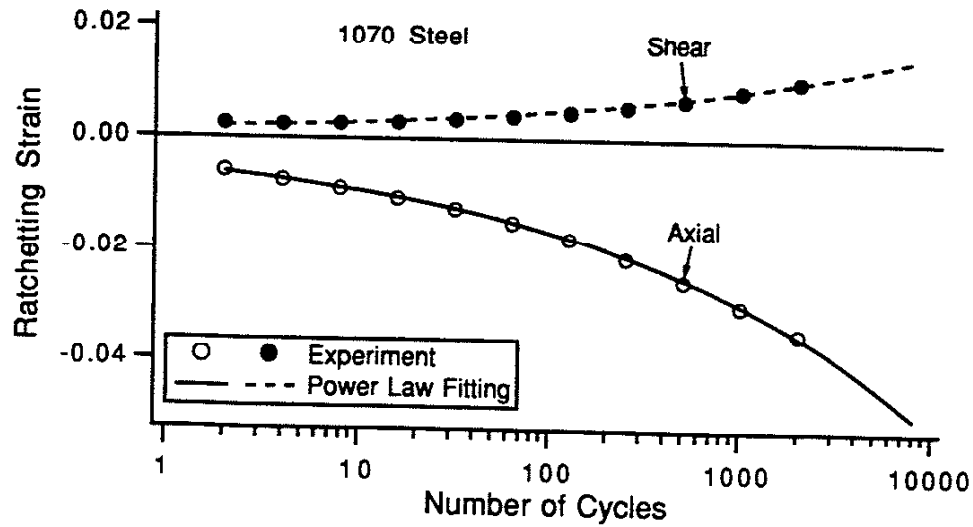
Figure 3.19 Ratchetting Strains for an "Apple" Shaped Axial-Torsion Loading Path (Figure 3.7)
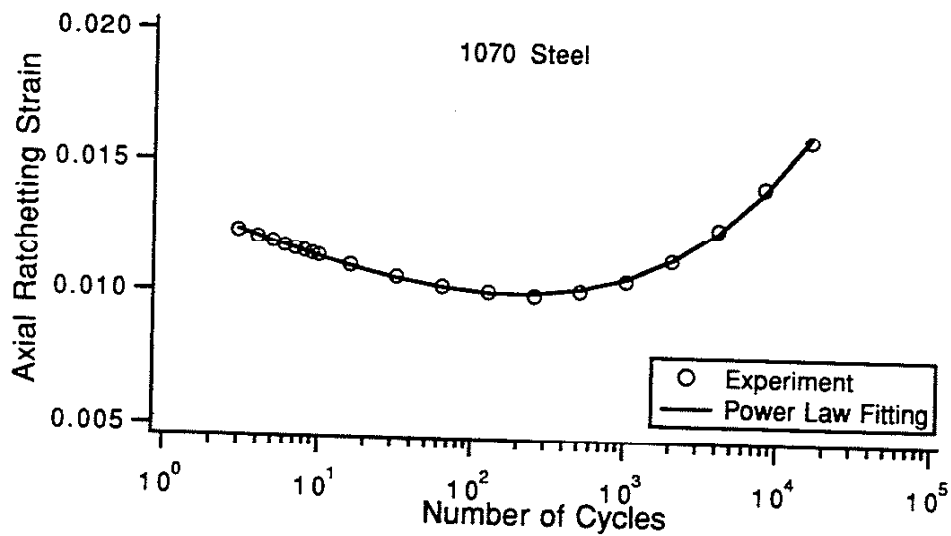
Figure 3.20 Ratchetting Strain for Step 2 of a Two-Step Uniaxial Loading (Figure 3.11)
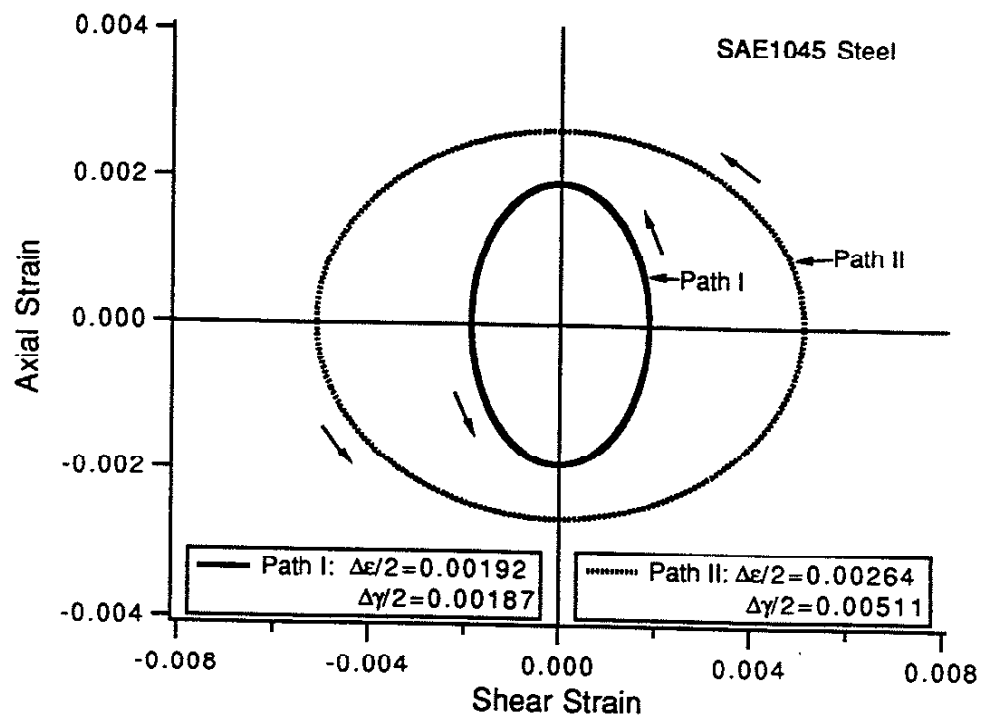
Figure 4.1 Nonproportional Strain-Controlled Axial-Torsion Loading Paths for 1045 Steel
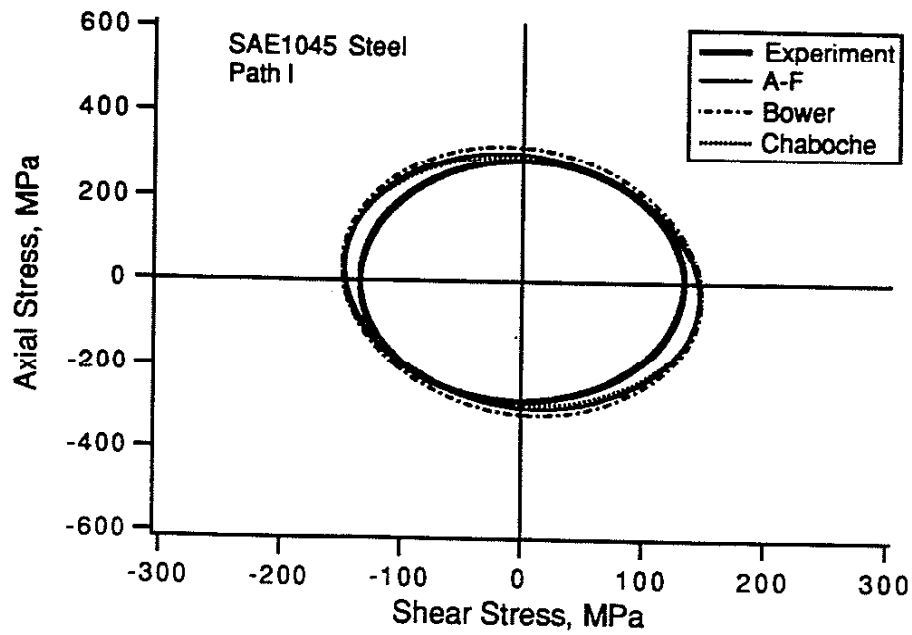
(a) Stresss Response: Path I
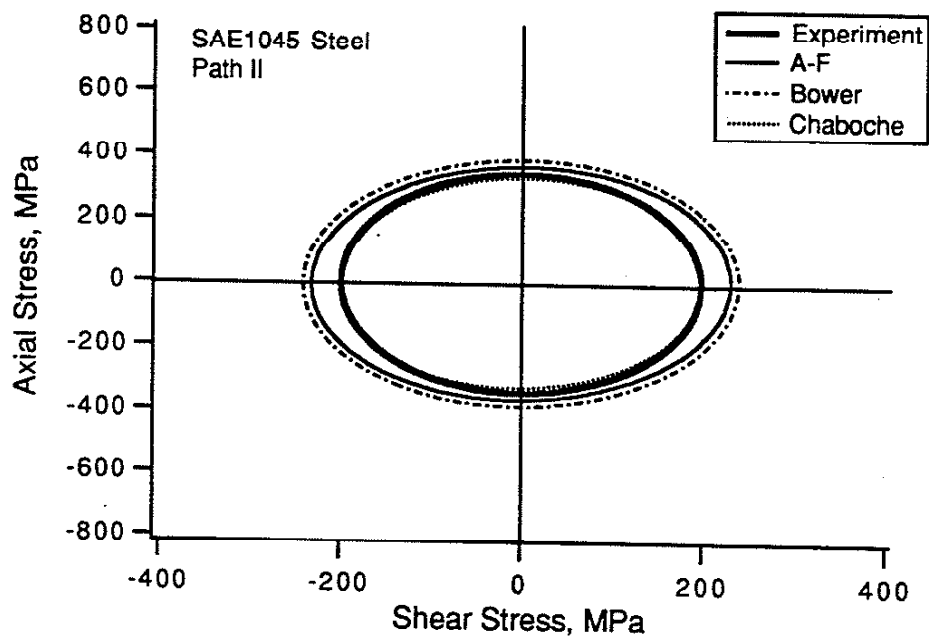
(b) Stress Response: Path II

Figure 4.2 Comparisons of Experimental Results and Predictions
Obtained with Different Plasticity Models
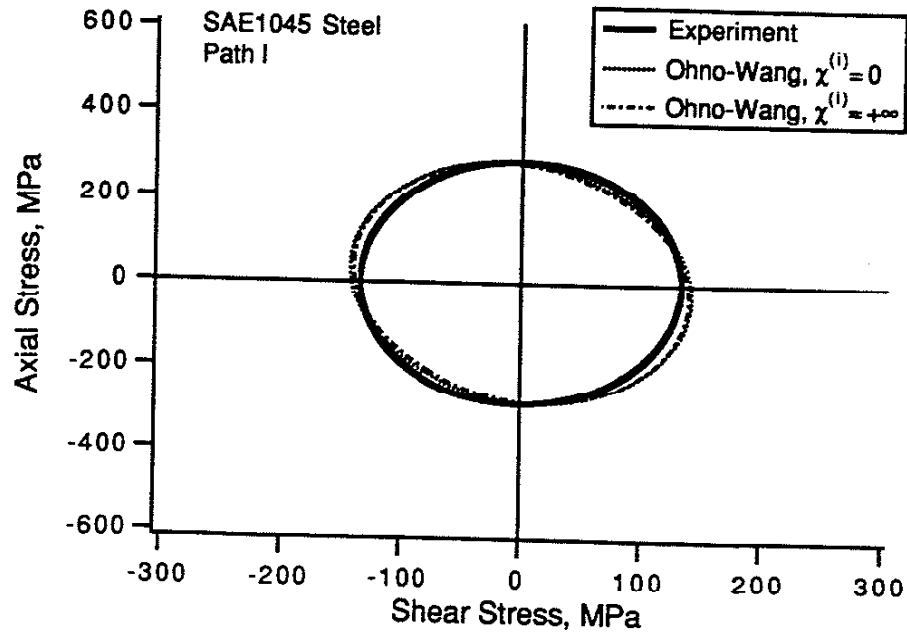
(a) Stress Response: Path I
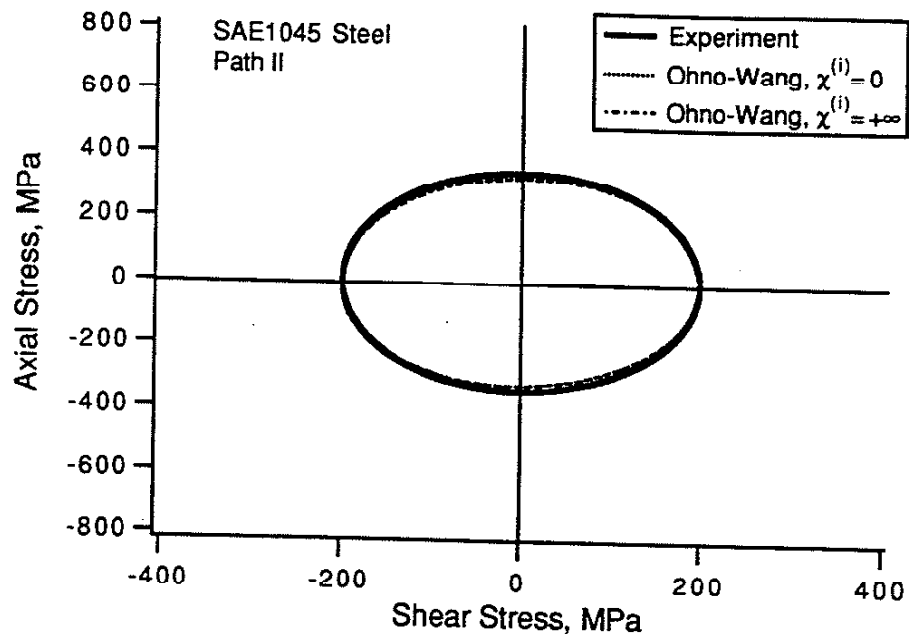
(b) Stress Response: Path II

Figure 4.3 Comparison of Experimental Data and the Ohno-Wang Predictions
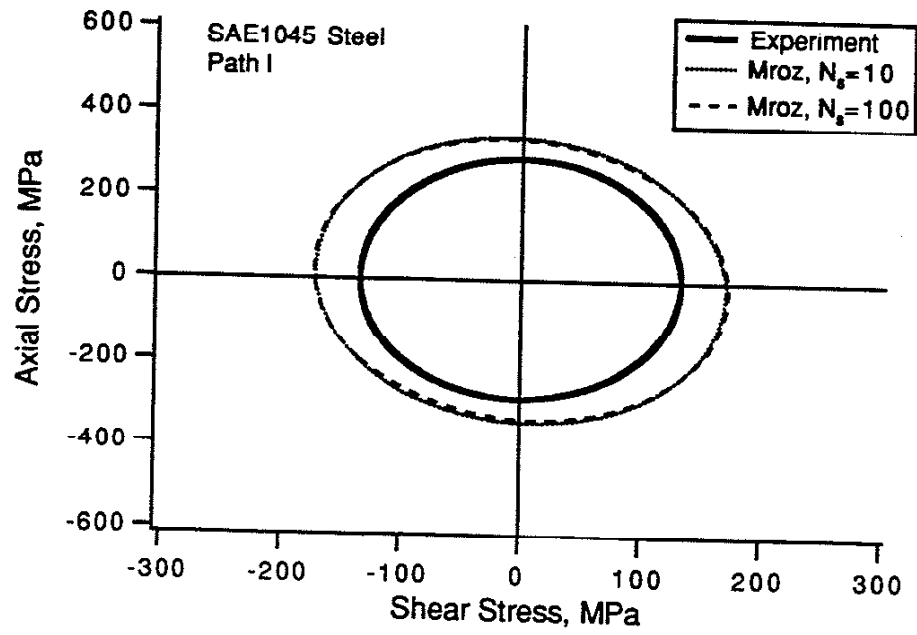
(a) Stress Response: Path I
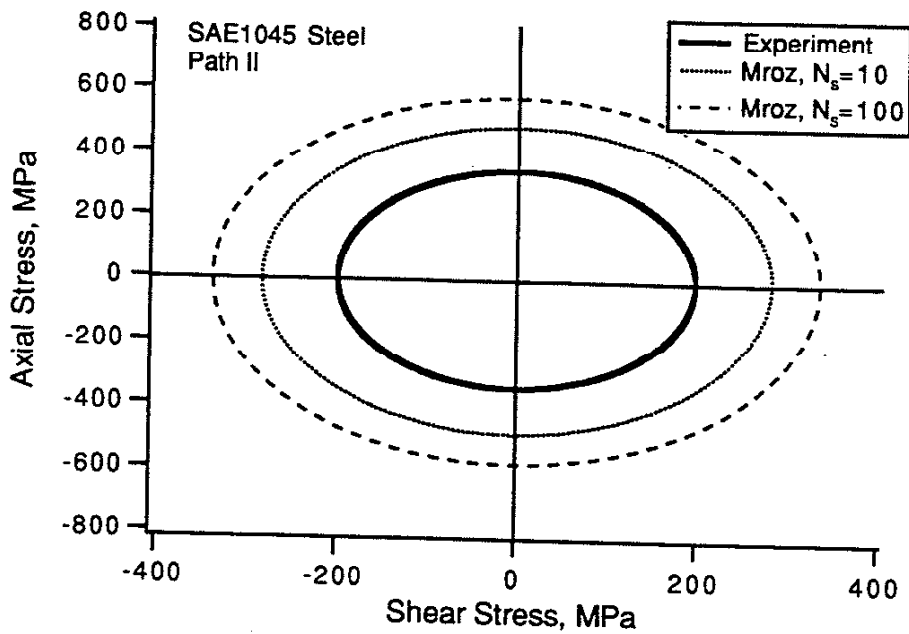
(b) Stress Response: Path II

Figure 4.4 Comparison of Experimental Data and the Mroz Predictions
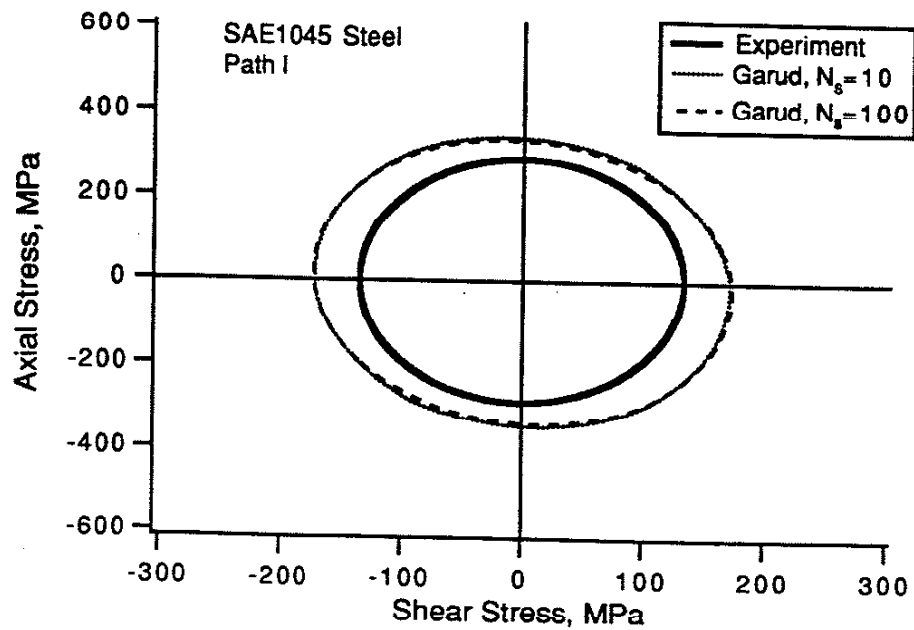
(a) Stress Response: Path I
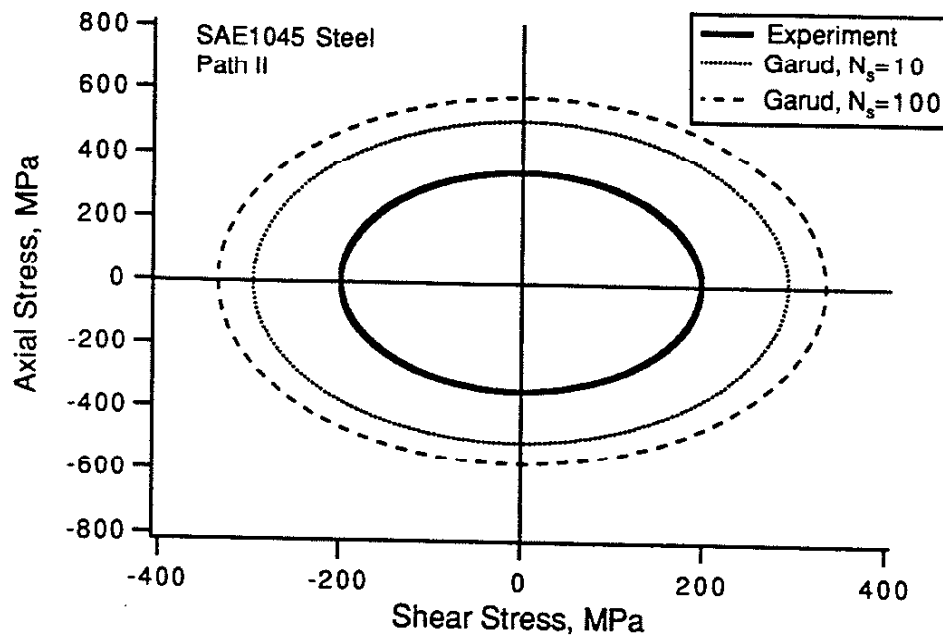
(b) Stress Response: Path II

Figure 4.5 Comparison of Experimental Data and the Garud Predictions
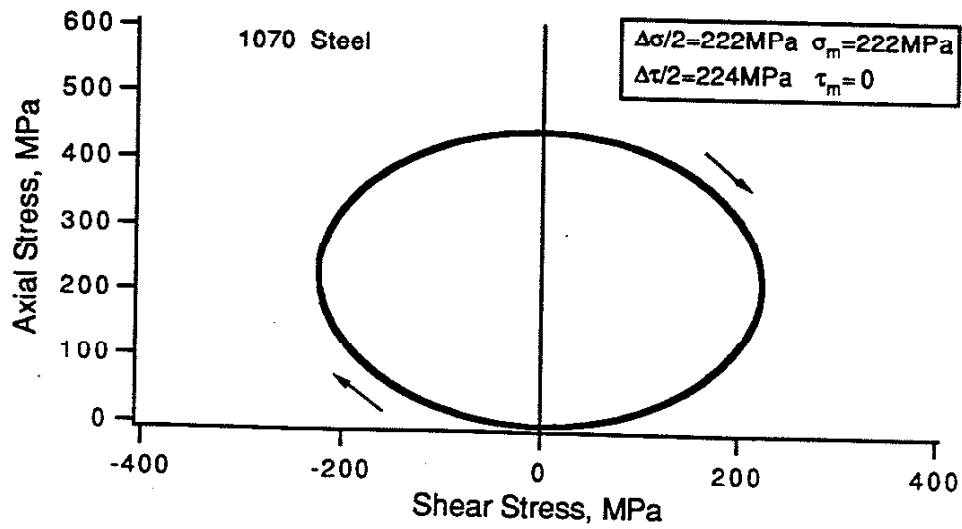
(a) Stress-Controlled Loading Path
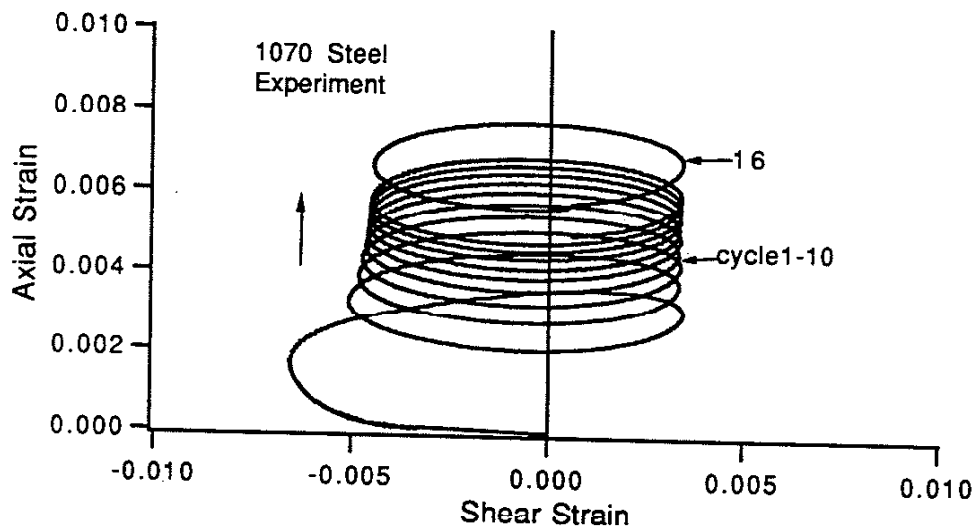
(b) Experimental Strain Response

Figure 4.6 Experimental Ratchetting of 1070 Steel for an "Ellipse" Shaped Axial-Torsion Loading Path
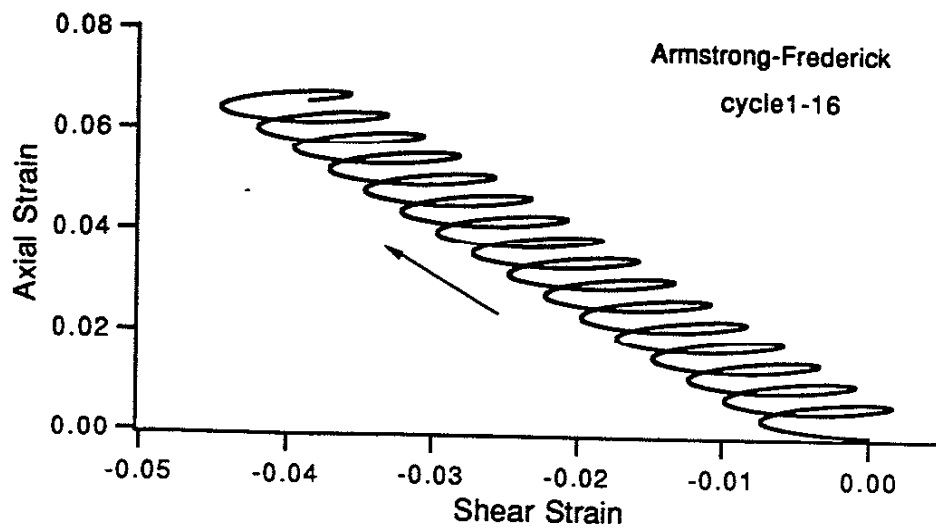
(a) Armstrong-Frederick Model
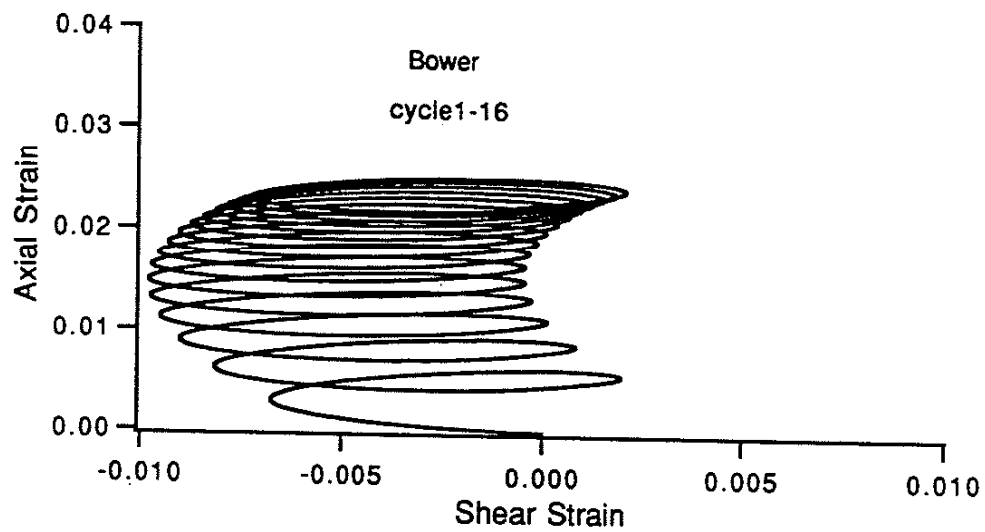
(b) Bower Model

Figure 4.7 Stress-Strain Response Predicted by Different Plasticity Models for an "Ellipse" Shaped Axial-Torsion Loading Path (Figure 4.6(a))
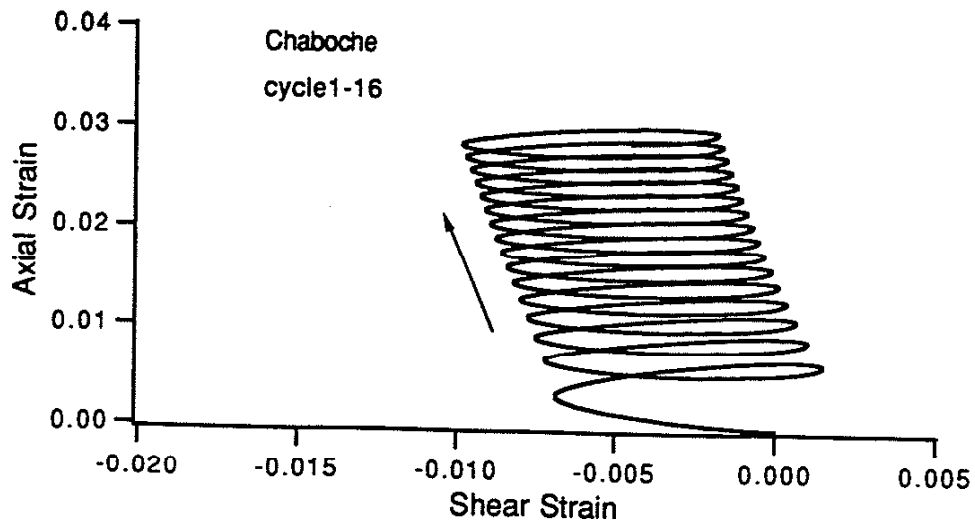
(c) Chaboche Model
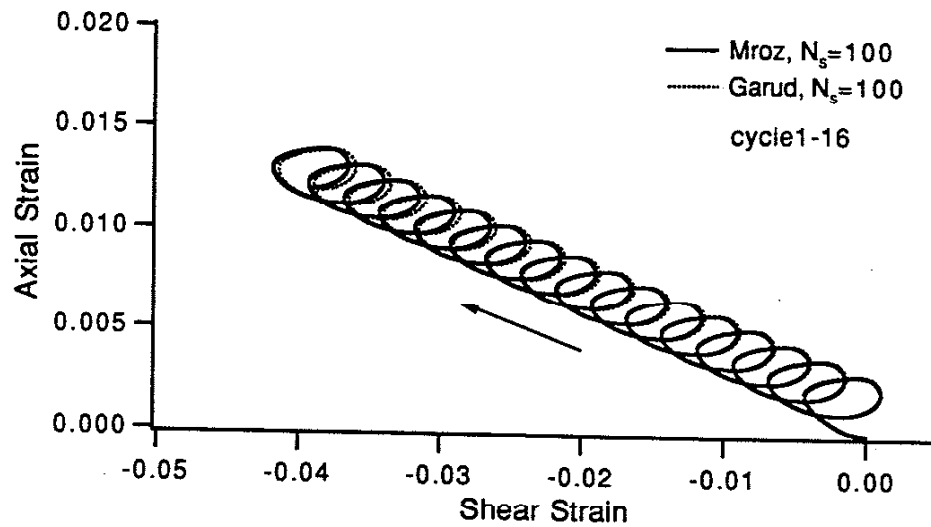
(d) Mroz and Garud Models

Figure 4.7(cont.) Stress-Strain Response Predicted by Different Plasticity Models for an "Ellipse" Shaped Axial-Torsion Loading Path (Figure 4.6(a))
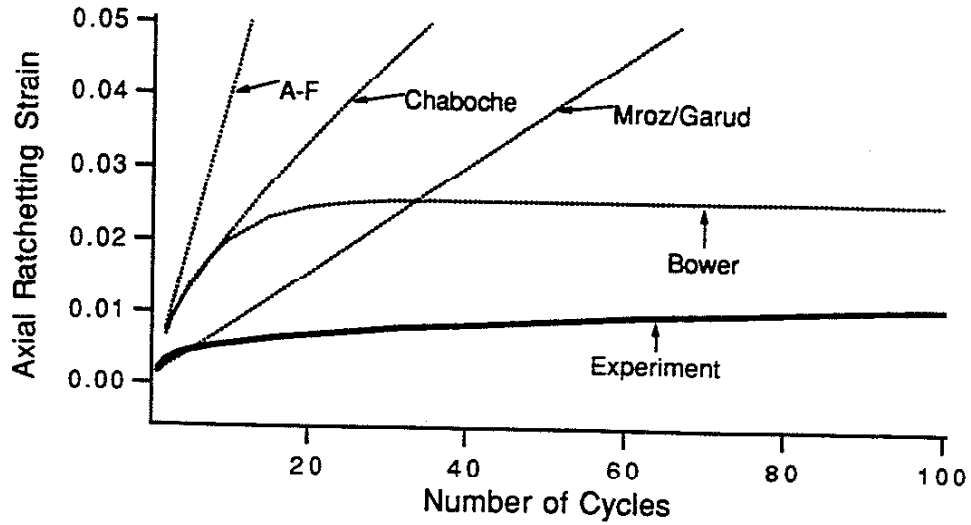
(a) Axial Ratchetting Strain *vs.* Number of Cycles
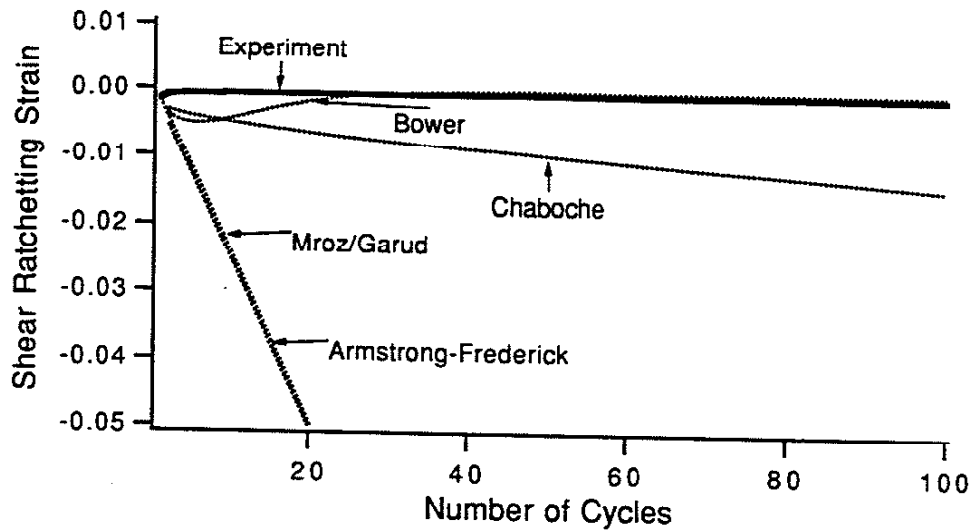
(b) Shear Ratchetting Strain *vs.* Number of Cycles

Figure 4.8 Comparison of Experimental Data and Ratchetting Results Predicted by Different Models for an "Ellipse" Shaped Axial-Torsion Loading Path (Figure 4.6(a))
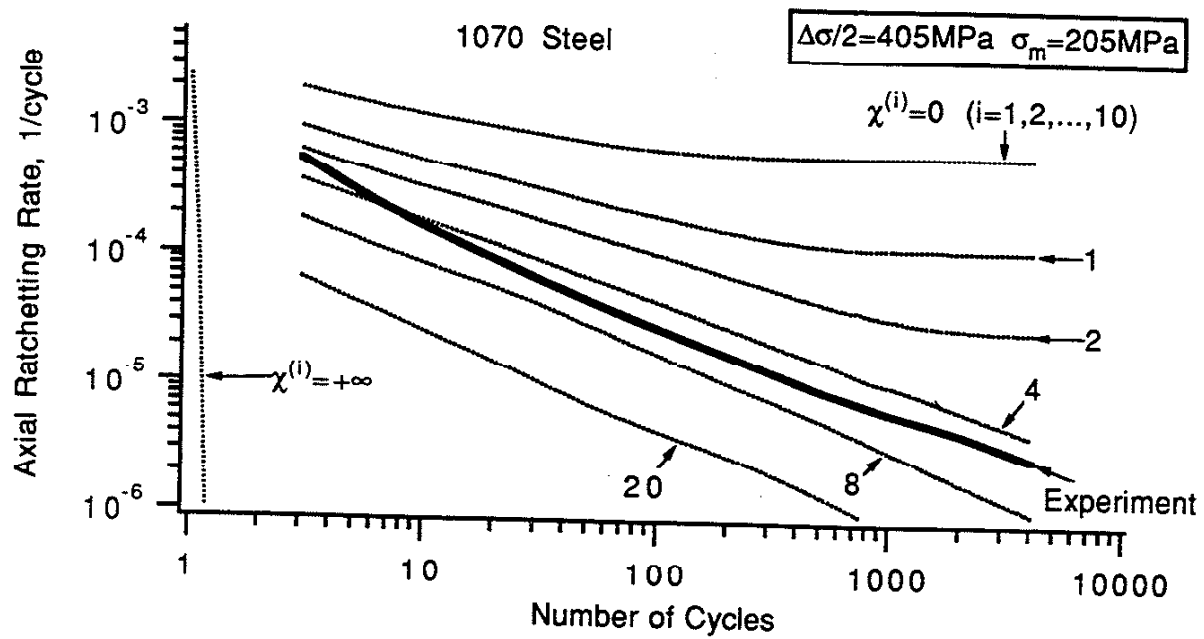
Figure 4.9 Relationship between $\chi^{(i)}$ and the Ratchetting Rates Predicted by the Ohno-Wang Model for Uniaxial Loading
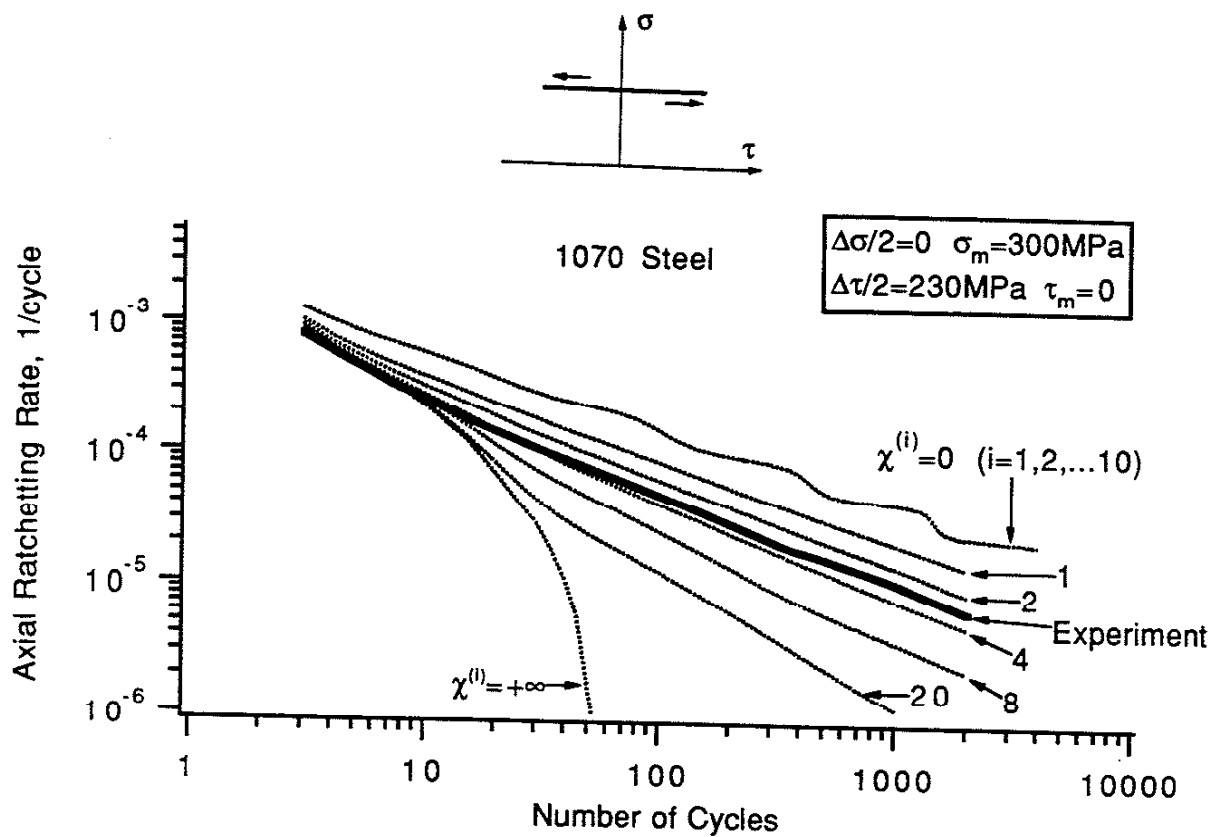
Figure 4.10 Relationship between $\chi^{(i)}$ and the Ratchetting Rates Predicted by the Ohno-Wang Model for a Nonproportional Axial-Torsion Loading Consisting of Alternating Shear with Constant Axial Stress
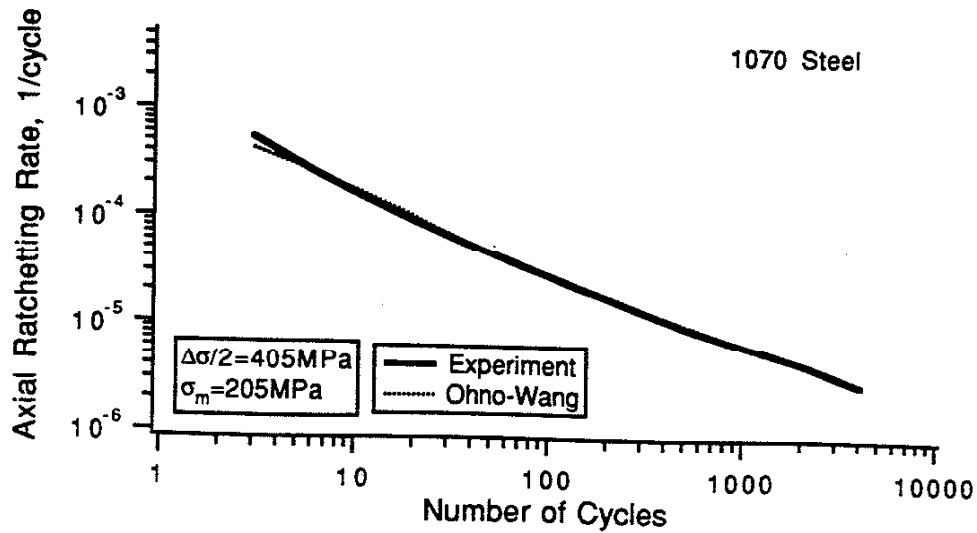
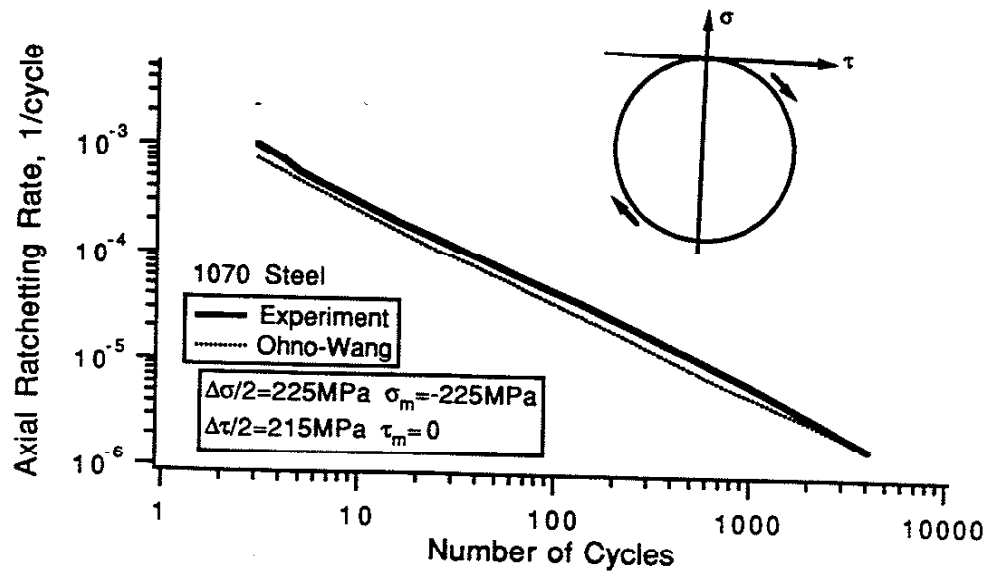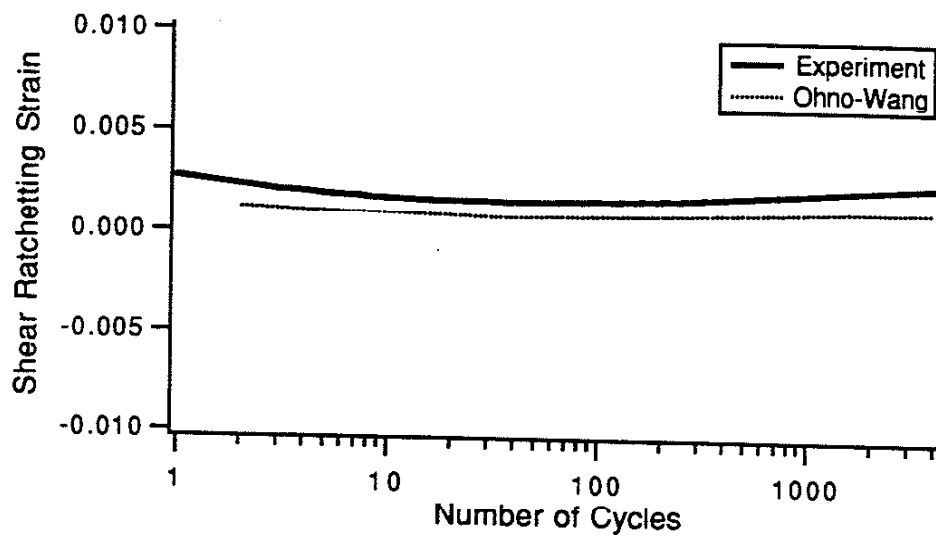Figure 4.11 Determination of $\chi^{(i)}$ for the Ohno-Wang Model Using Uniaxial Ratchetting Data
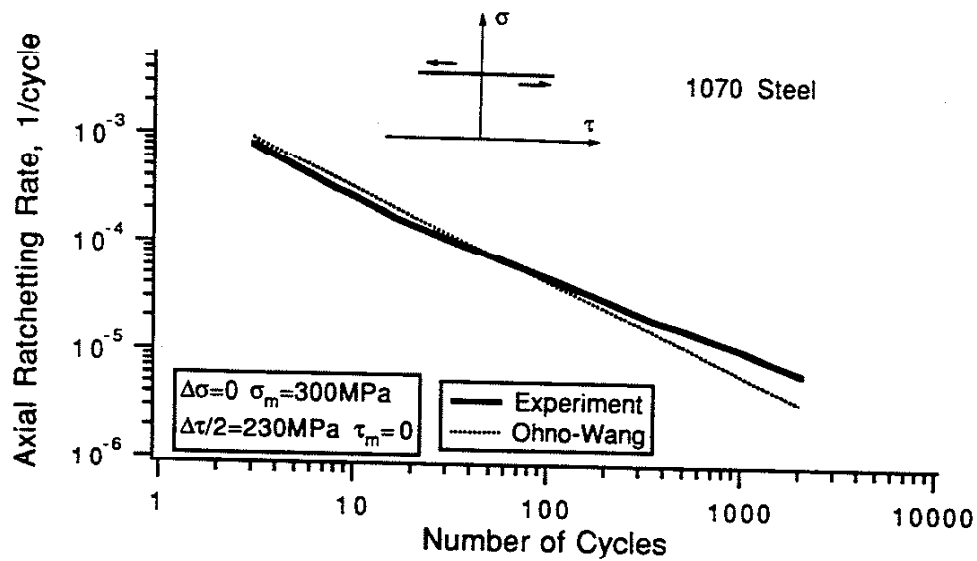
Figure 4.12 Comparison of Experimental Data and Ratchetting Rates Predicted by the Ohno-Wang Model for a Nonproportional Axial-Torsion Loading Path Consisting of Alternating Shear with Constant Axial Stress (Figure 3.17(b))
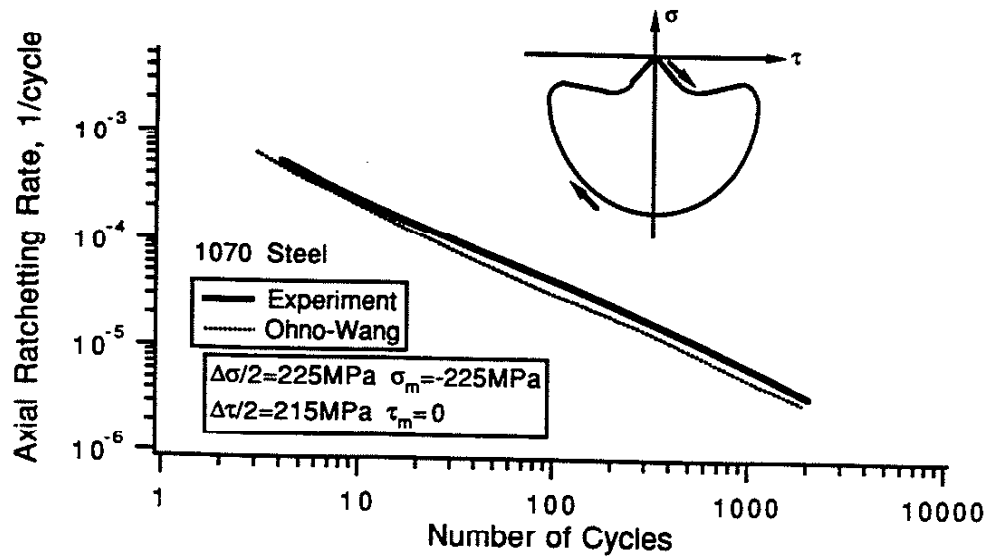
(a) Absolute Value of Axial Ratchetting Rate vs. Number of Cycles
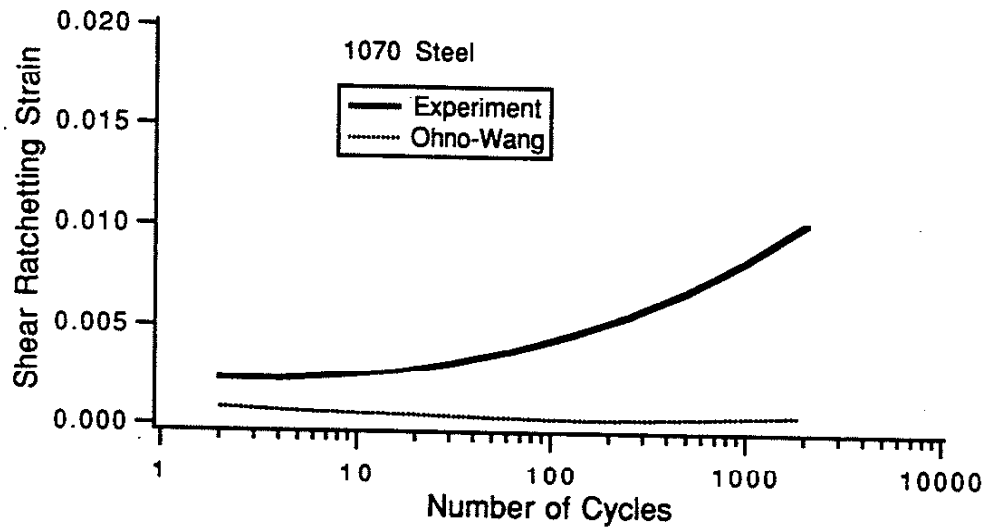(Actual ratchetting rate is negative)

(b) Shear Ratchetting Strain vs. Number of Cycles

Figure 4.13   Comparison of Experimental Data and Ratchetting Results Predicted by the Ohno-Wang Model for an "Ellipse" Shaped Axial-Torsion Loading Path
(Figure 3.6)

(a) Absolute Value of the Axial Ratchetting Rate *vs.* Number of Cycles
(Actual ratchetting rate is negative)

(b) Shear Ratchetting Strain *vs.* Number of Cycles

Figure 4.14 Comparision of Experimental Data and Ratchetting Results Predicted by the Ohno-Wang Model for an "Apple" Shaped Axial-Torsion Loading Path
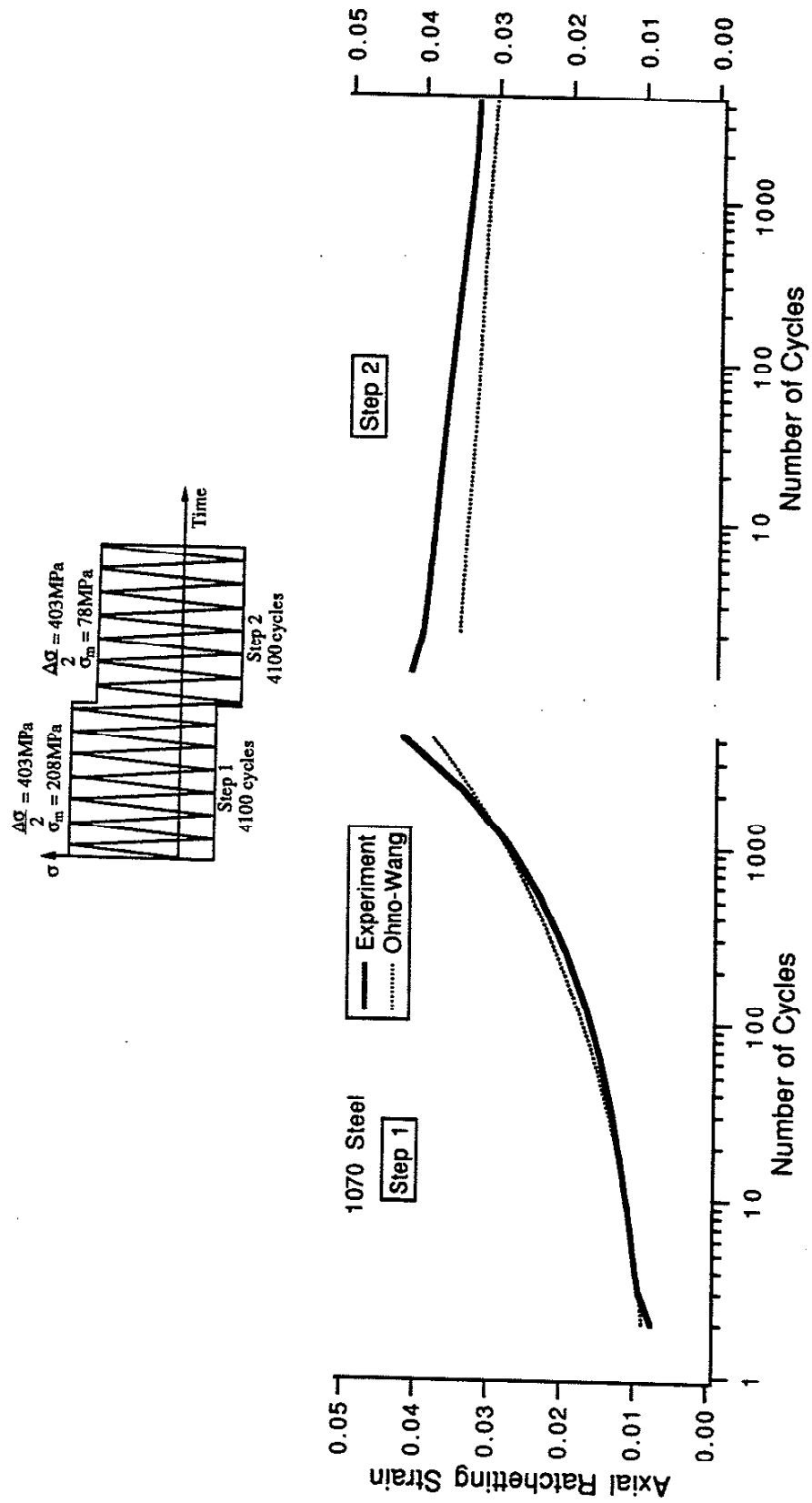(Figure 3.7)

Figure 4.15 Comparison of Experimental Data and Ratchetting Strain Predicted by the Ohno-Wang Model for a Uniaxial Two-Step Loading (Figure 3.11(a))
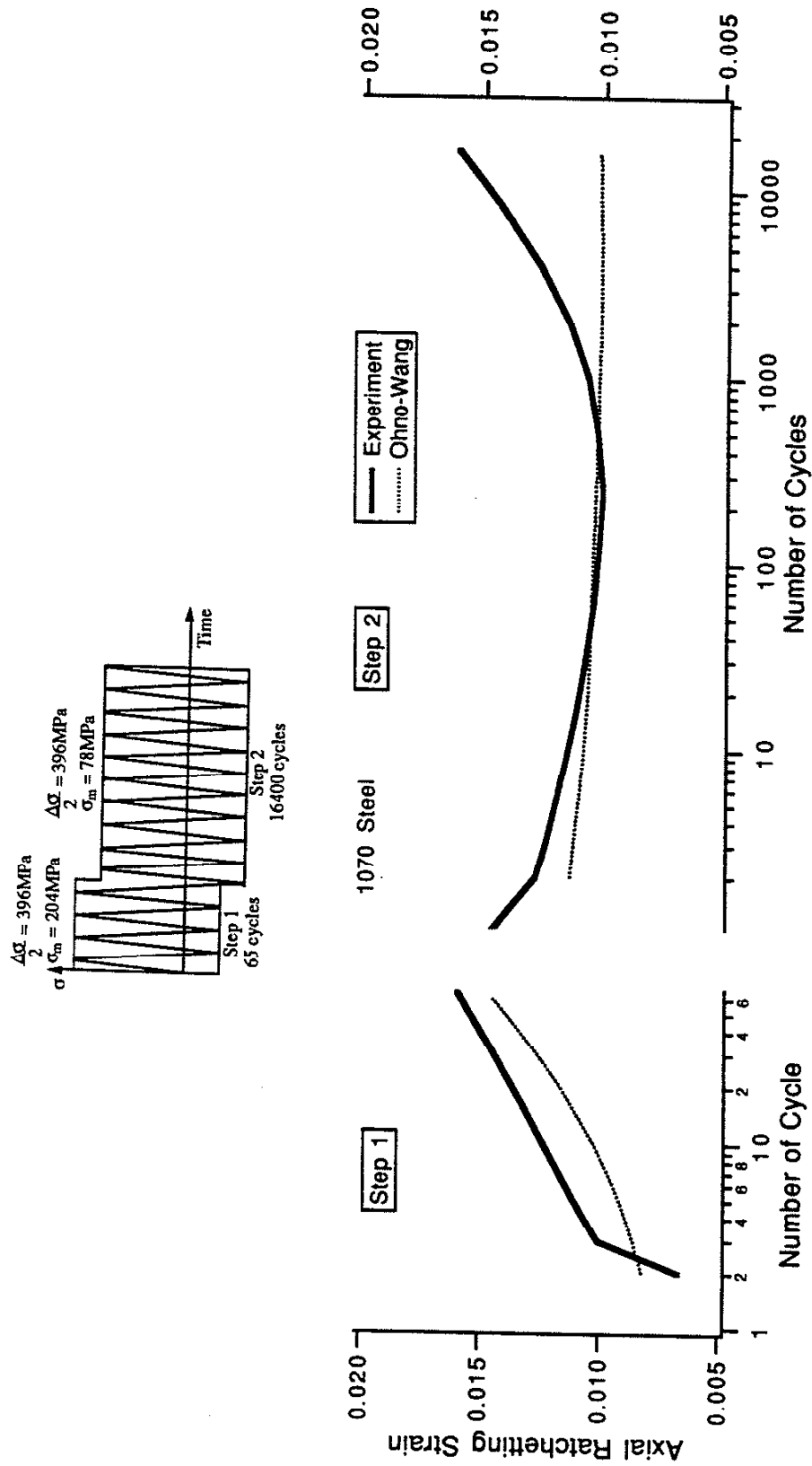
Figure 4.16 Comparison of Experimental Data and Ratchetting Strain Predicted by the Ohno-Wang Model for a Uniaxial Two-Step Loading (Figure 3.12)
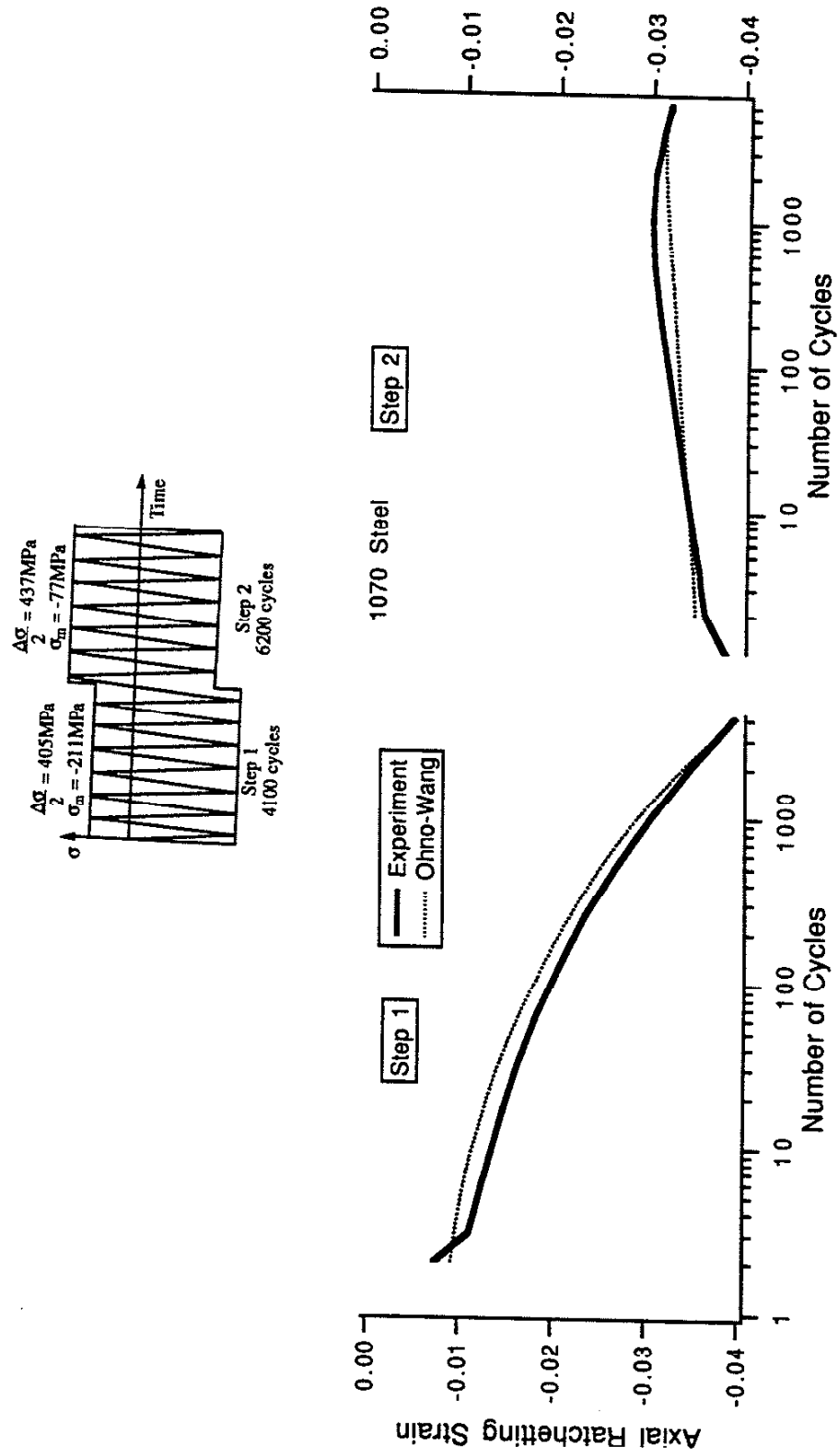
Figure 4.17 Comparison of Experimental Data and Ratchetting Strain Predicted by the
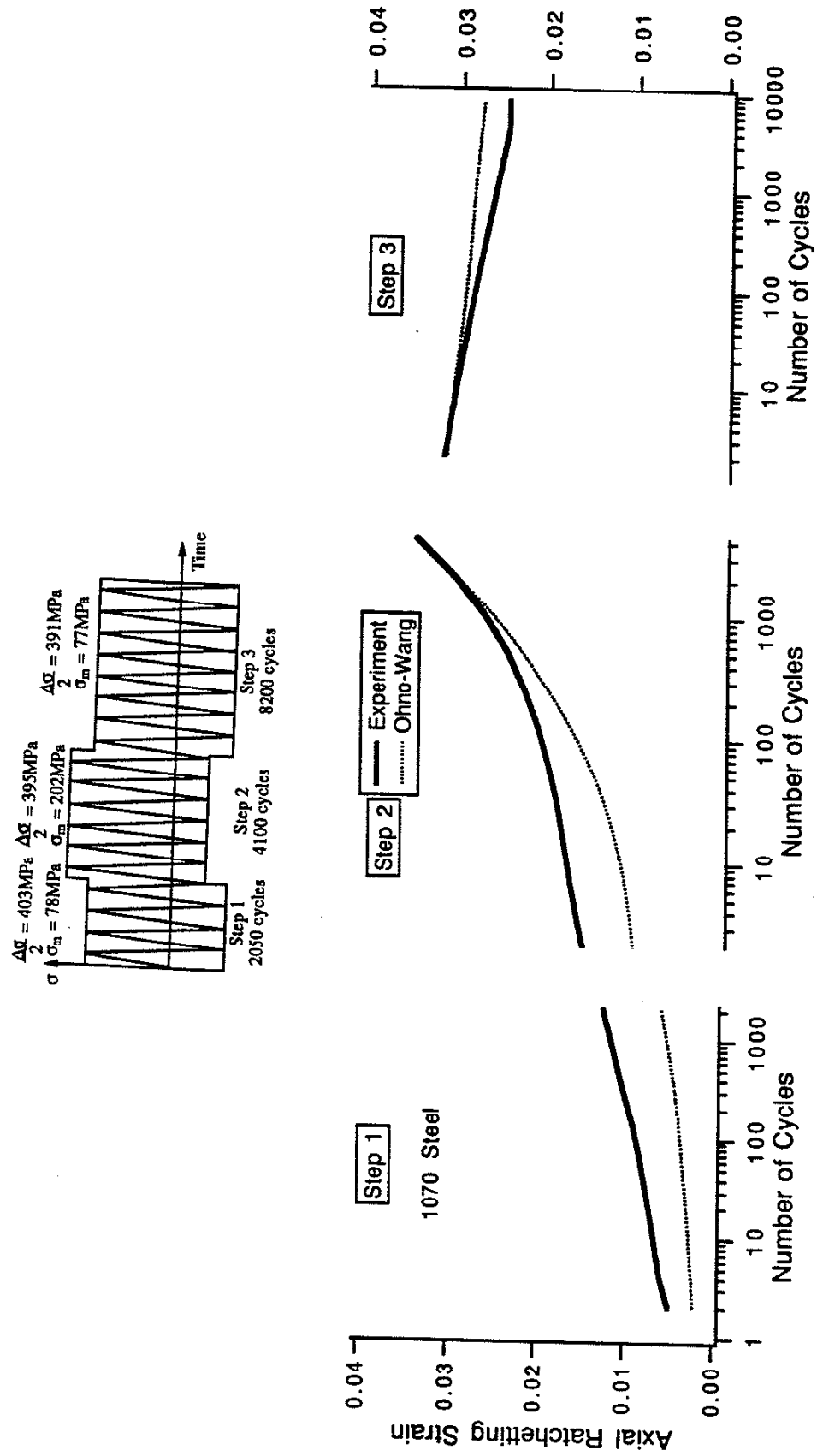Ohno-Wang Model for a Uniaxial Two-Step Loading (Figure 3.13)

Figure 4.18 Comparison of Experimental Data and Ratchetting Strain Predicted by the
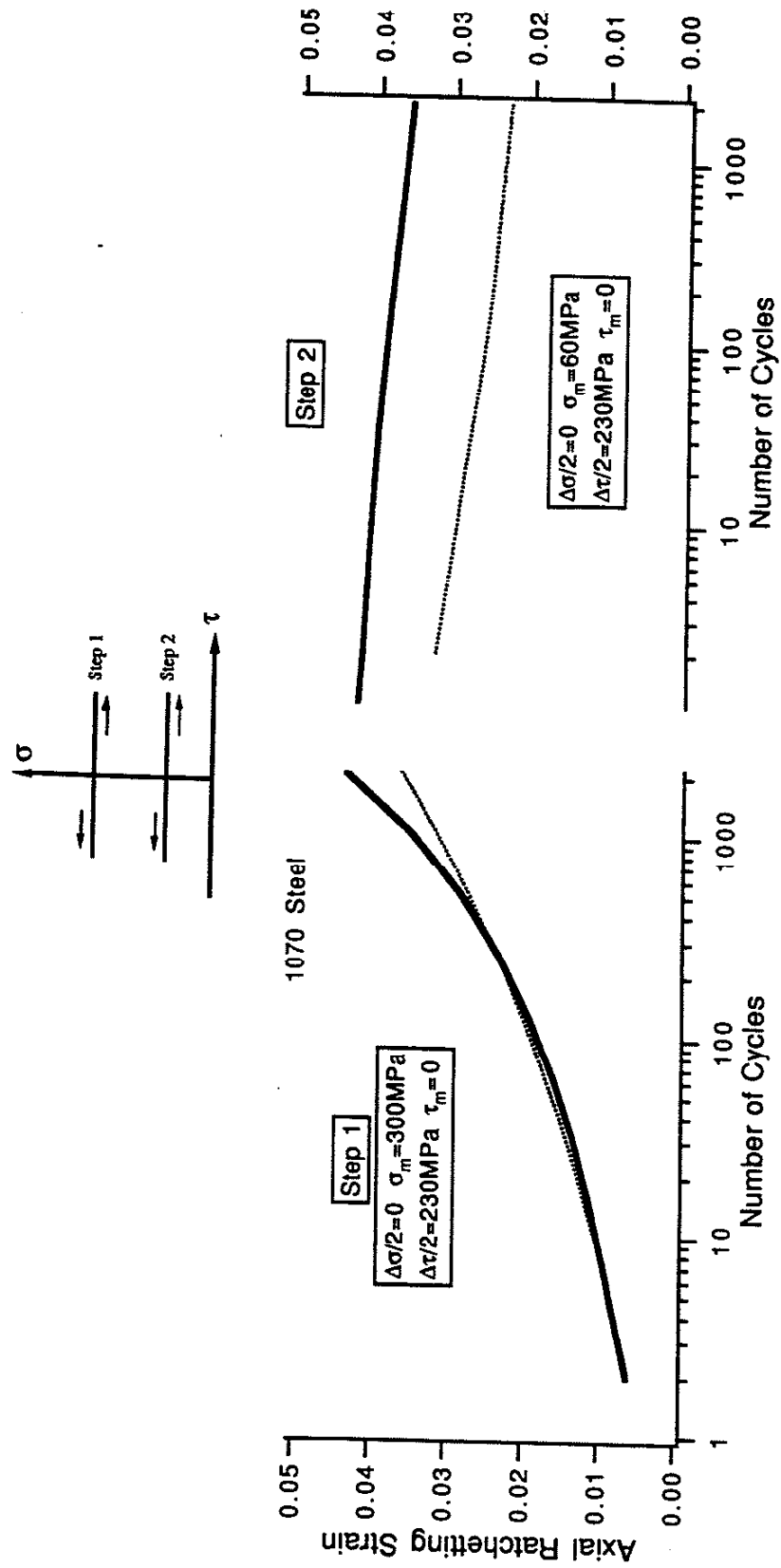Ohno-Wang Model for a Uniaxial Three-Step Loading (Figure 3.10)

Figure 4.19 Comparison of Experimental Data and Ratchetting Strain Predicted by the Ohno-Wang
Model for a Two-Step Nonproportional Axial-Torsion Loading (Figure 3.17)
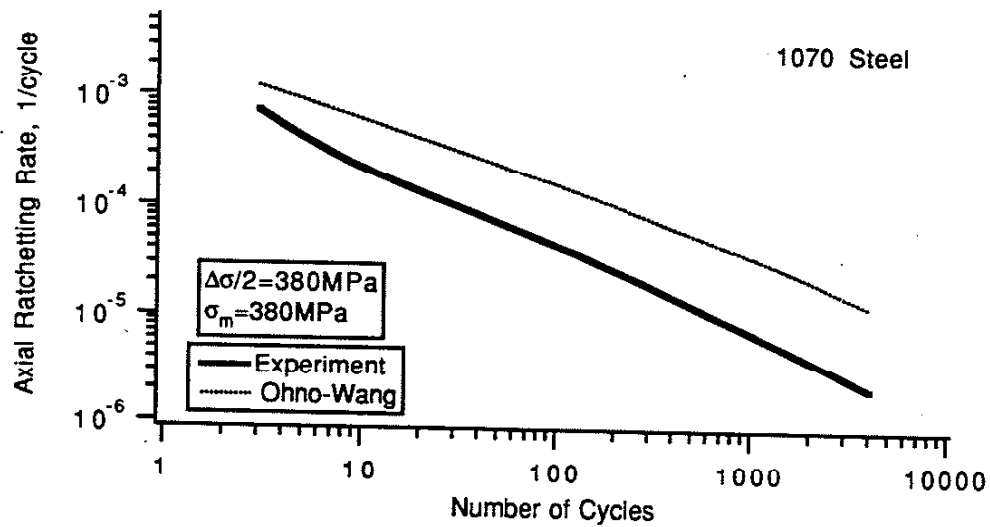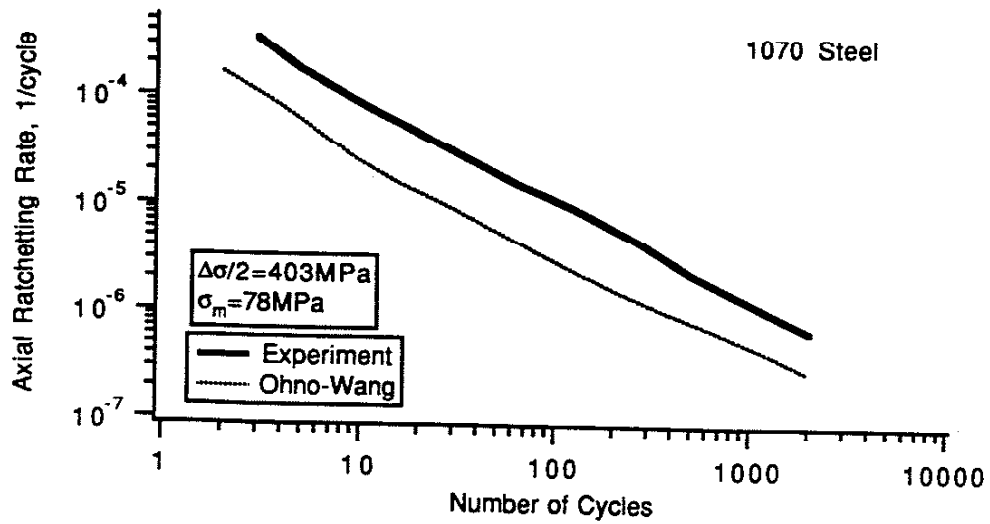
Figure 4.20 Comparison of Experimental Data and Ratchetting Rates Predicted by the Ohno-Wang Model for Uniaxial Tests with Different Mean Stresses

$dg^{(i)} = c^{(i)}r^{(i)} dp \, \underline{n}$

(a) Within Limiting Surface

$dg^{(i)} = c^{(i)}r^{(i)} dp (\underline{n} - \underline{L}^{(i)})$

(b) On Limiting Surface
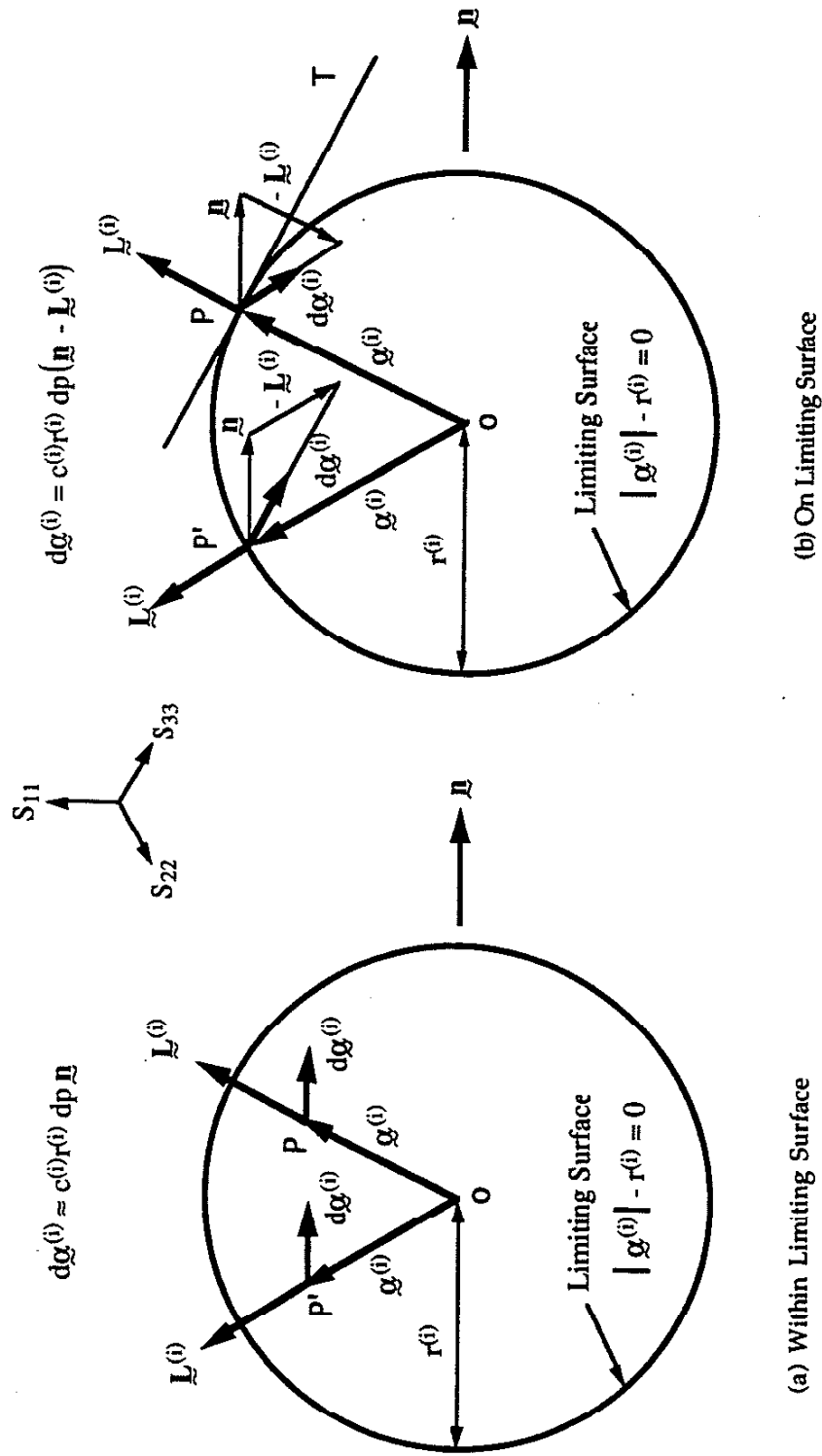
Figure 5.1 Geometric Interpretation of the New Hardening Rule

$$R_M = Max|\underline{g}|$$

$$dR_M = -c_M\left(1-\frac{|\underline{g}|}{R_M}\right)dp$$

$$\underline{L} = \frac{\underline{g}}{|\underline{g}|}$$

$$dR_M = \underline{L}:d\underline{g}$$

(a) Expansion of Memory Surface   (b) Contraction of Memory Surface   (c) Stabilized Memory Surface
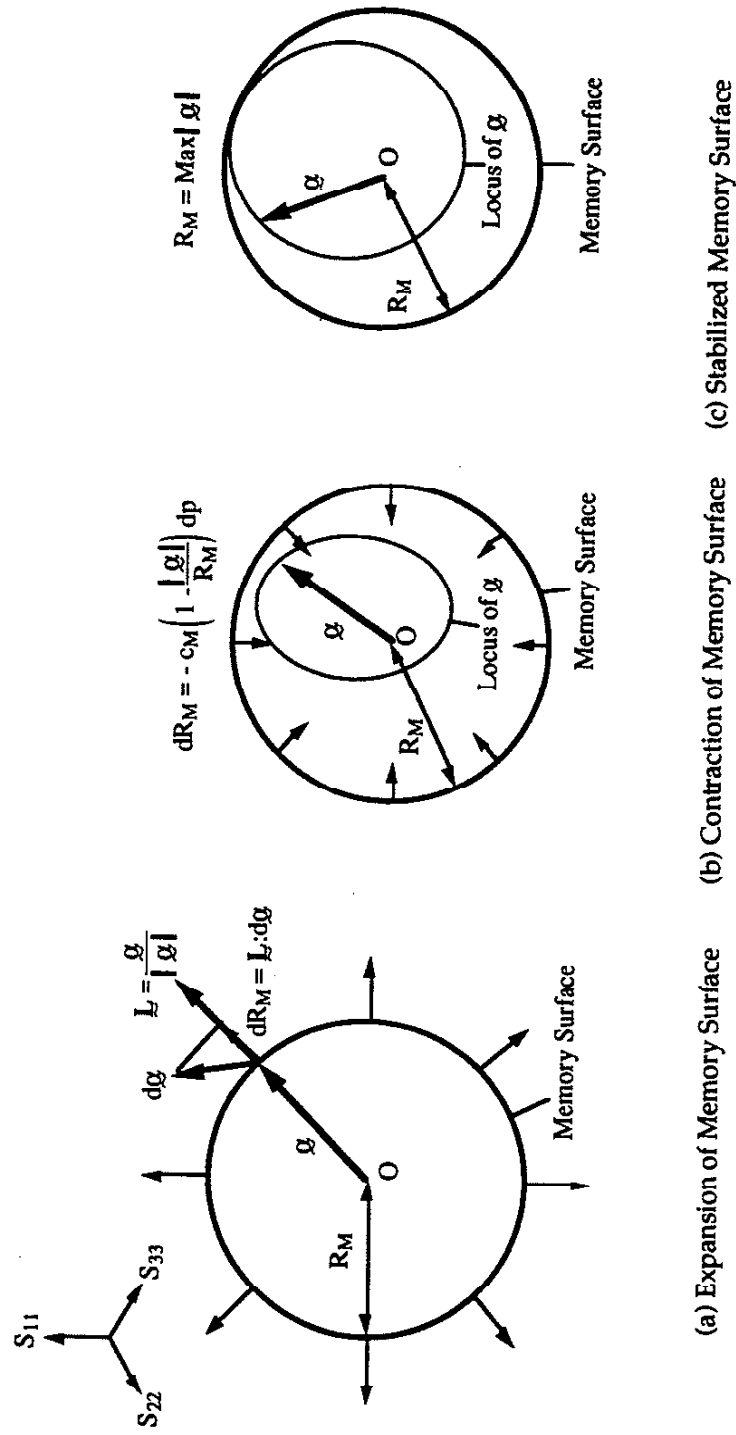
Figure 5.2 Schematic Illustration of the Memory Surface Concept
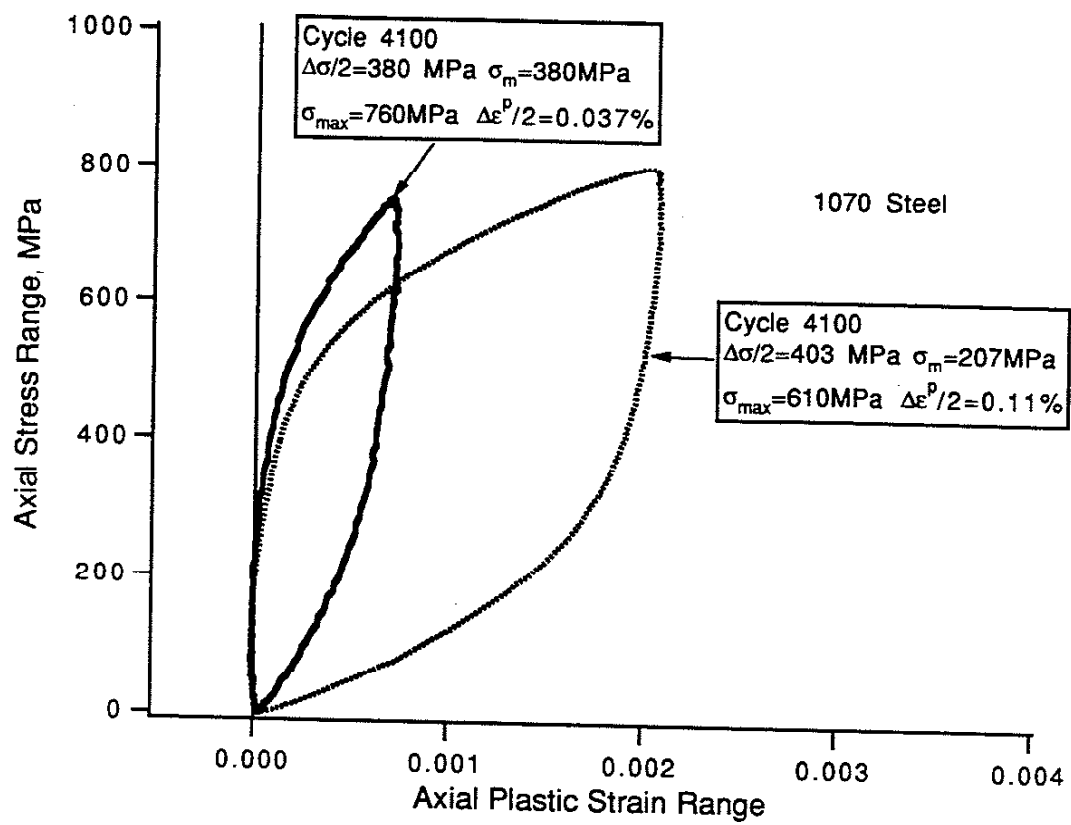
Figure 5.3 Experimental Non-Masing Behavior Observed for Unbalanced
Uniaxial Loading

(a) Experimental Results

(b) Theoretical Simulations
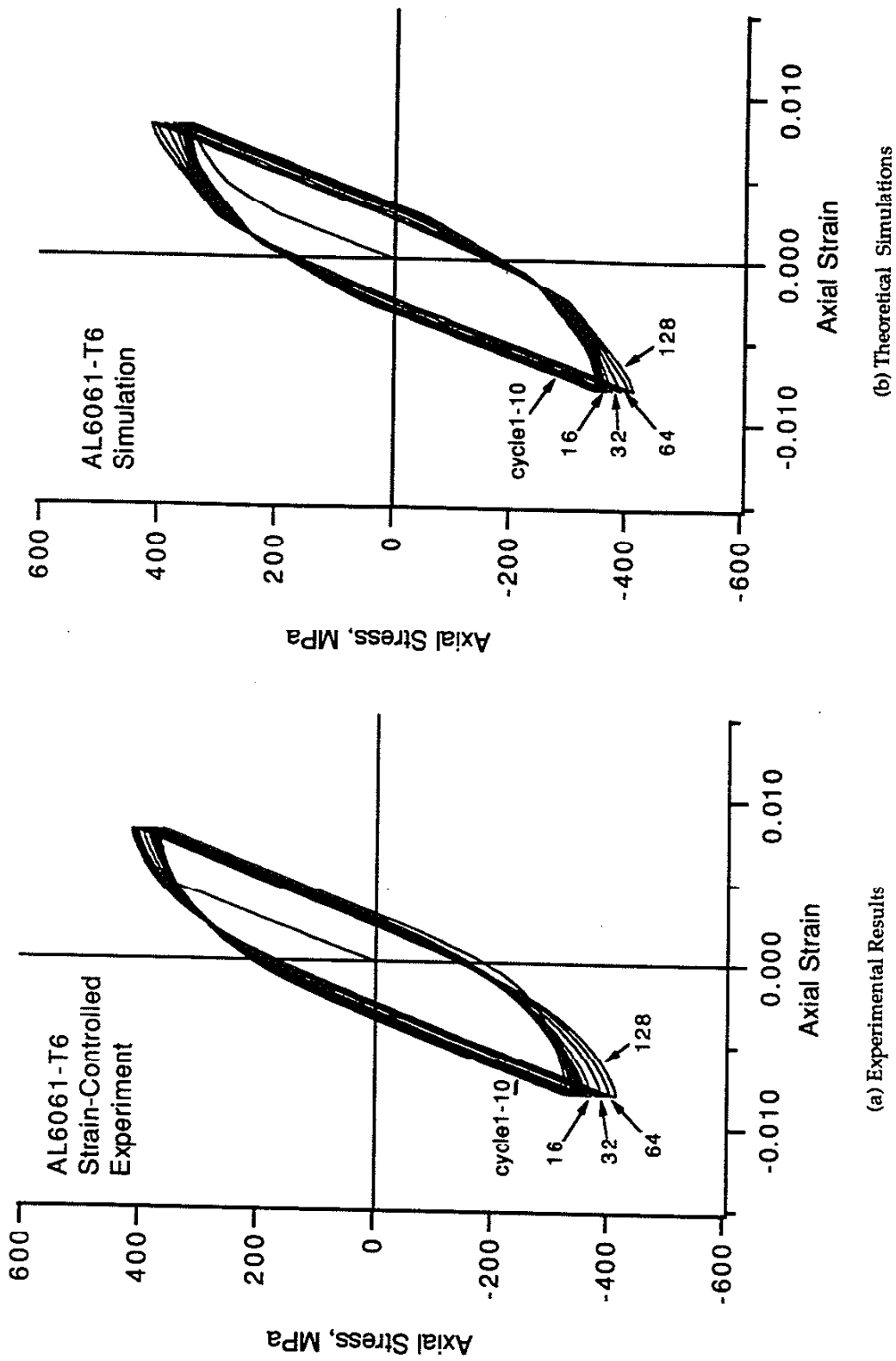
Figure 5.4 Demonstration of the Ability of the New Model to Reproduce
the Experimentally Observed Cyclic Hardening

1070 Steel
Simulation

$\Delta\varepsilon/2 = 1.00\%$

0.81%

0.56%

0.24%

(b) Theoretical Simulations

1070 Steel
Strain-Controlled
Experiment

$\Delta\varepsilon/2 = 1.0\%$

0.81%

0.56%

0.24%

(a) Experimental Results
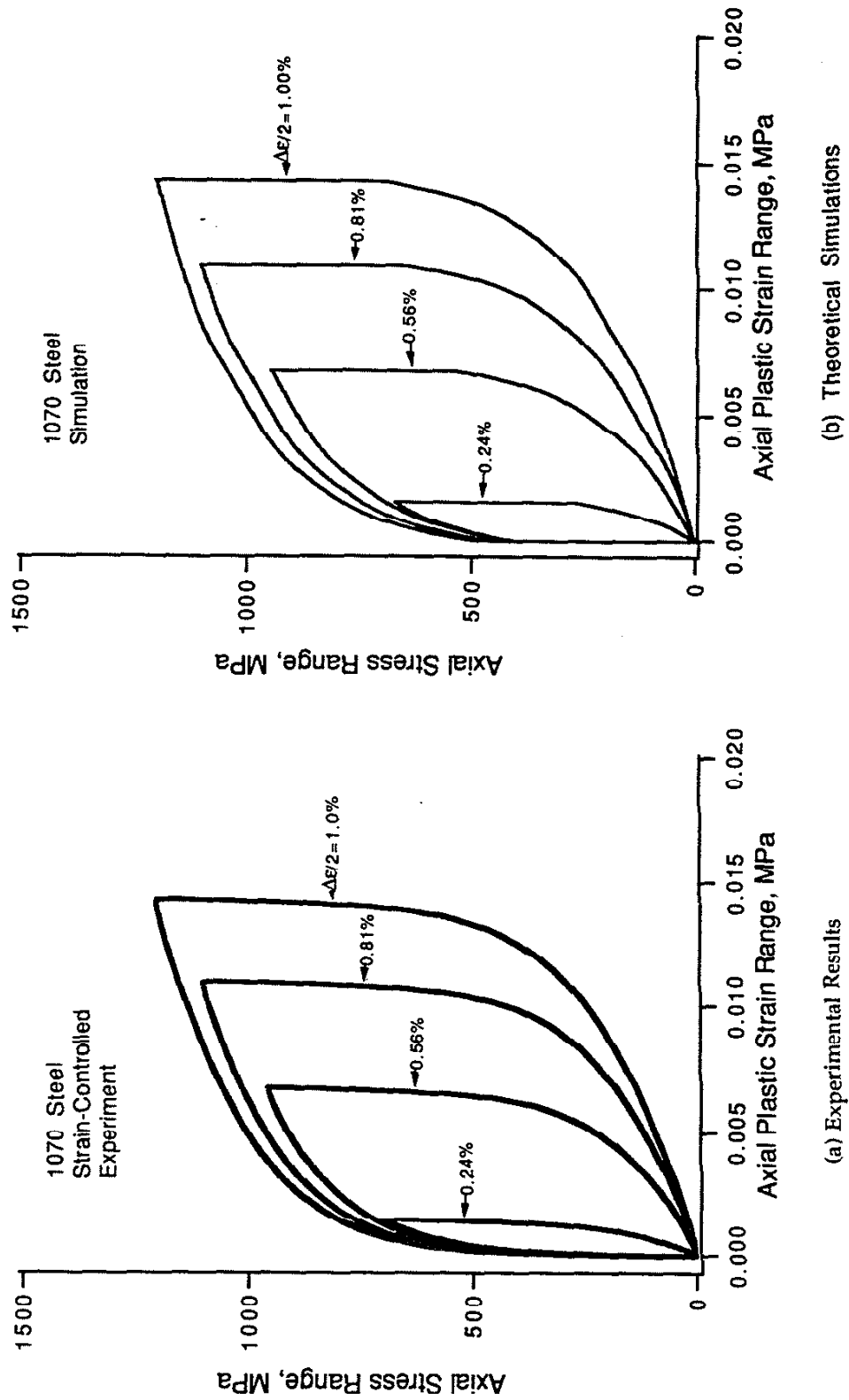
Figure 5.5   Demonstration of the Ability of the New Model to Reproduce the
Experimentally Observed Non-Masing Behavior (Figure 3.3)
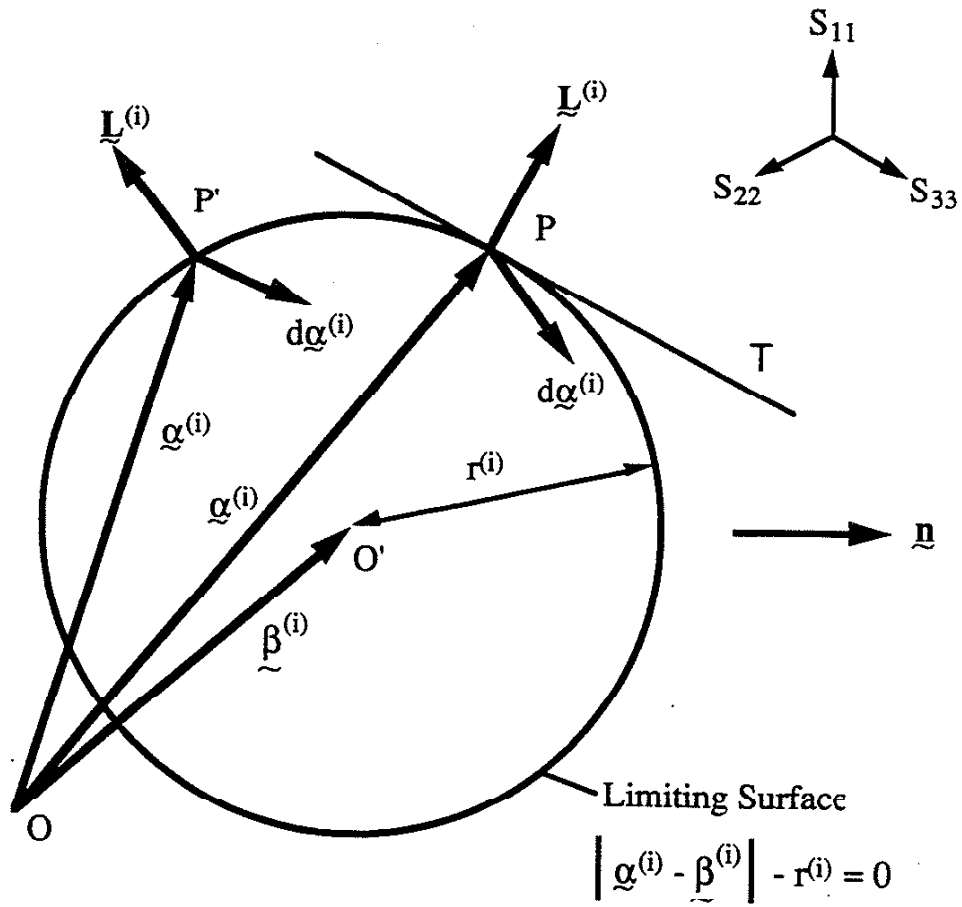
Figure 5.6 A Generilzed Shematic of the Limiting Surface Concept

$$\frac{dy}{dx} = 1 - |y|^m \, y \; ; \;\; y\,|_{x=0} = -1$$

m = 2

m = 0

m = +∞
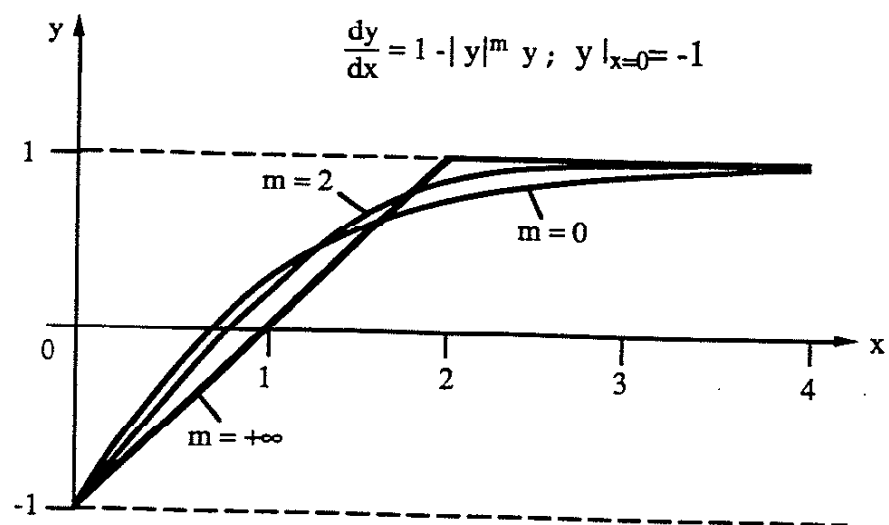
Figure 6.1 Numerical Solutions to the Differential Equation
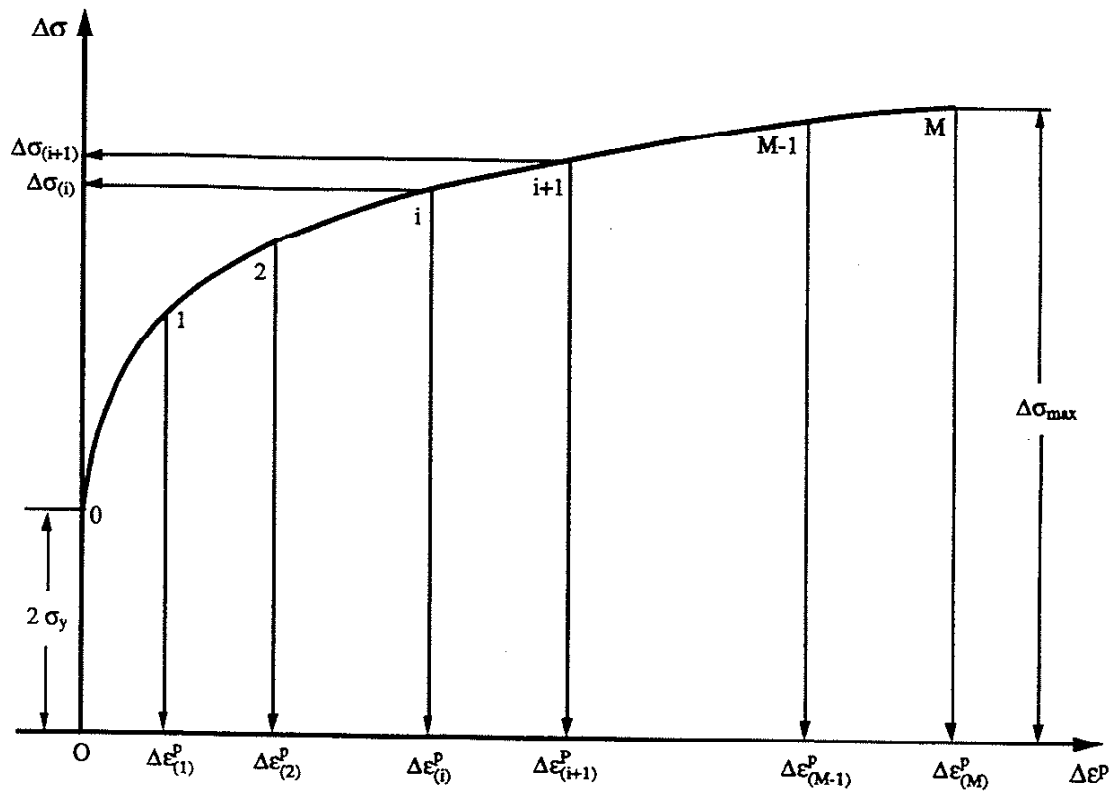
Figure 6.2 Illustration of the Procedure to Determine $c^{(i)}$ and $r^{(i)}$ from a Uniaxial Stress-Plastic Strain Reversal
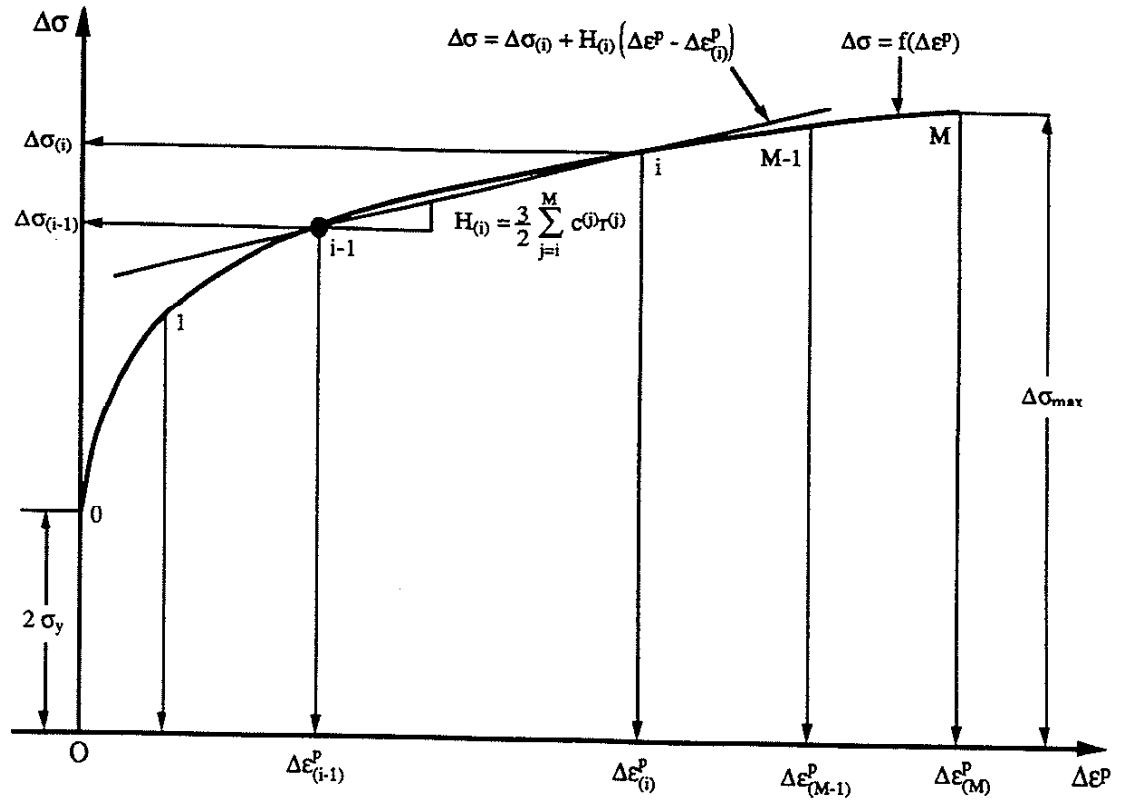
Figure 6.3 Procedure Used to Determine $c^{(i)}$ from a Uniaxial Stress-Plastic Strain Reversal with Presumed $r^{(i)}$
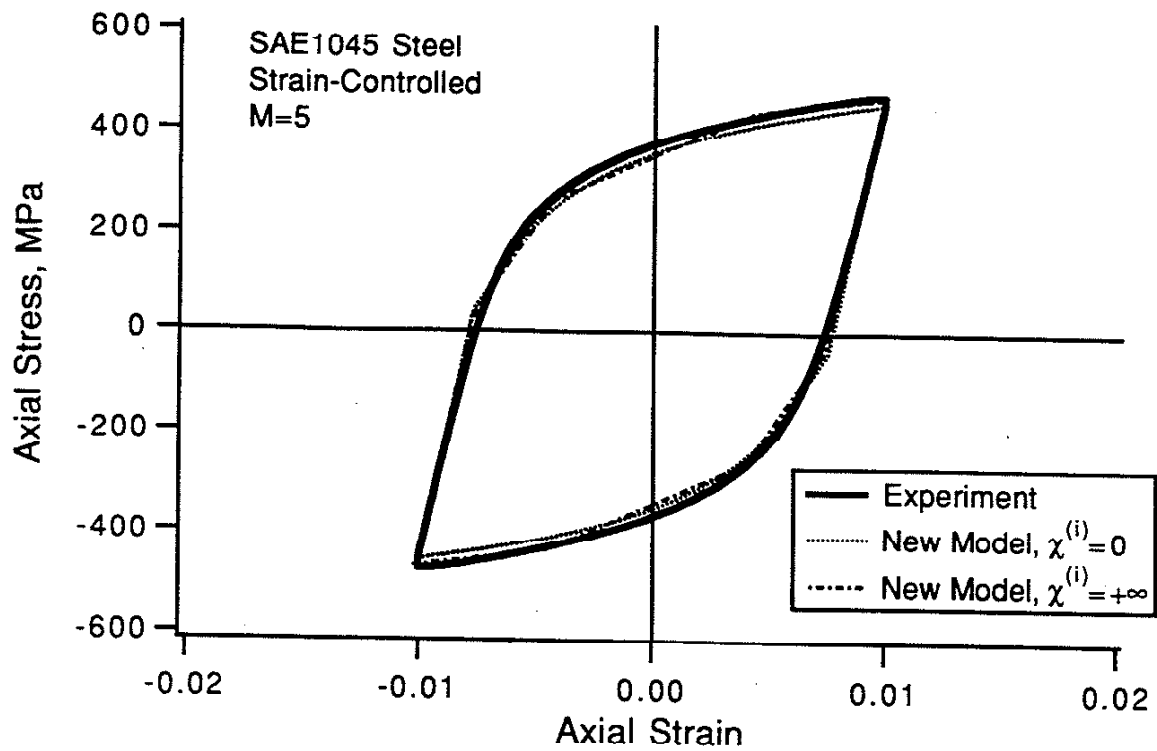
Figure 6.4 Influence of $\chi^{(i)}$ on Predicted Stress-Strain Loop for Uniaxial Balanced Loading
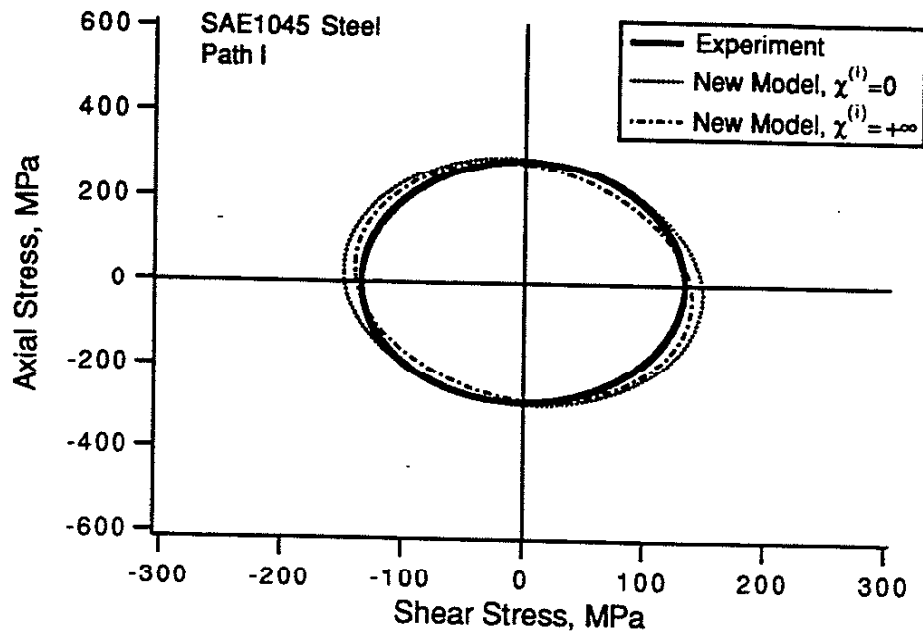
(a) Stress Response: Path I
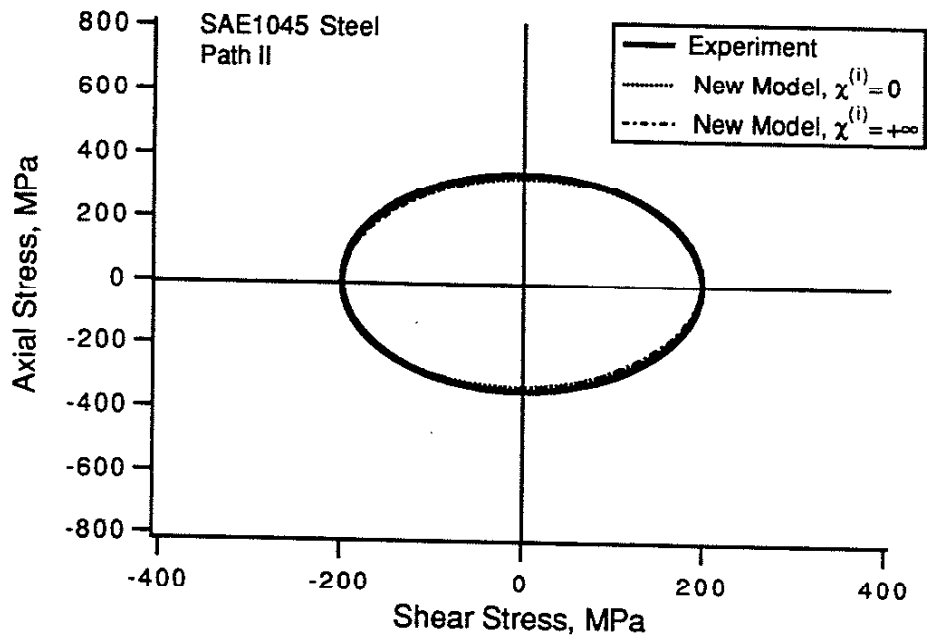
(b) Stress Response: Path II

Figure 7.1 Comparisons of Experiemental Results and the New Model Predictions for Balanced Nonproportional Axial-Torsional Loading (Figure 4.1) Showing Influence of $\chi^{(i)}$
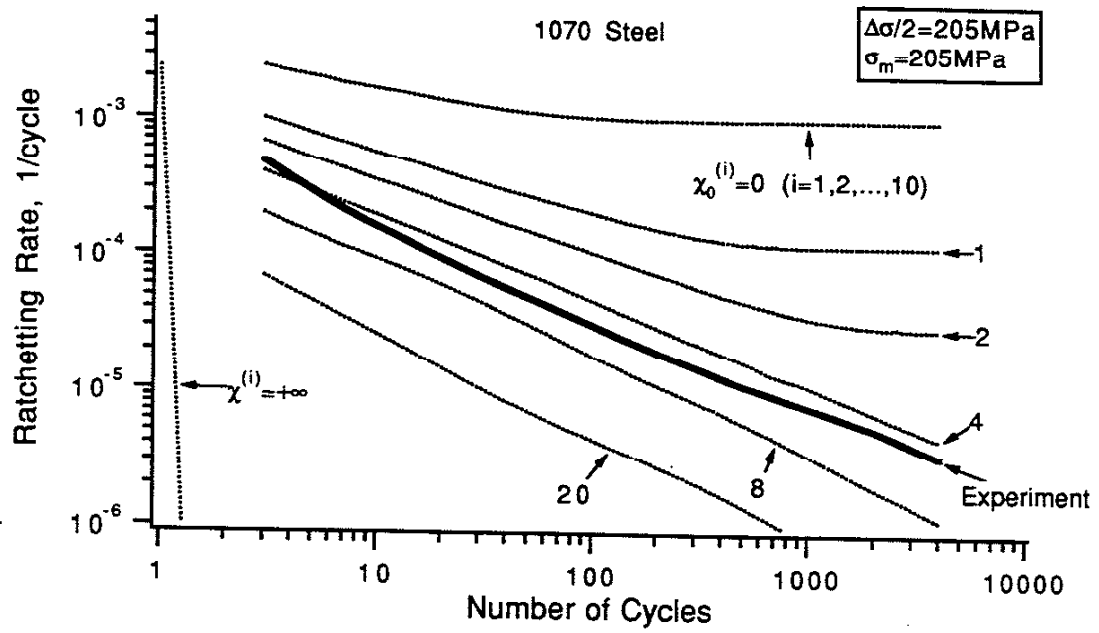
Figure 7.2 Relationship between $\chi^{(i)}$ and Ratchetting Rate Predicted by the New Model for Uniaxial Loading
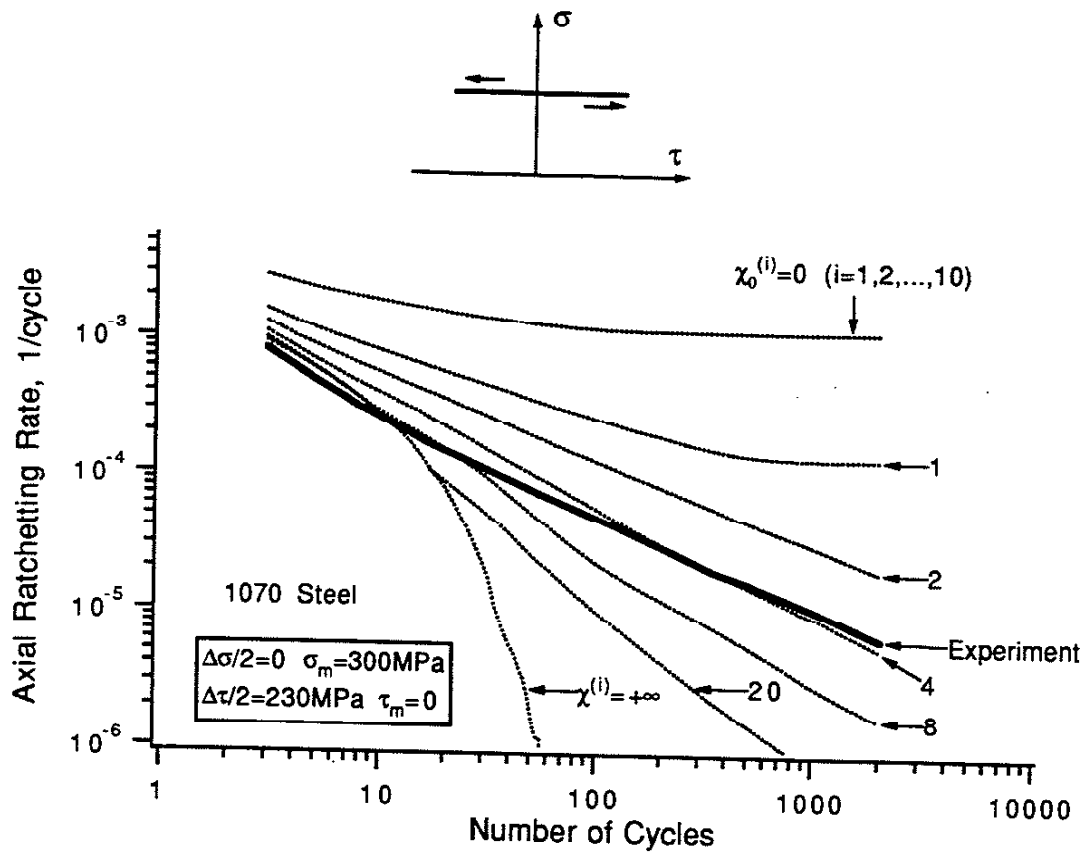
Figure 7.3 . Relationship between $\chi^{(i)}$ and Ratchetting Rate Predicted by the New Model for Nonproportional Axial-Torsion Consisting of Alternating Shear with Constant Axial Stress (Figure 3.17(b))
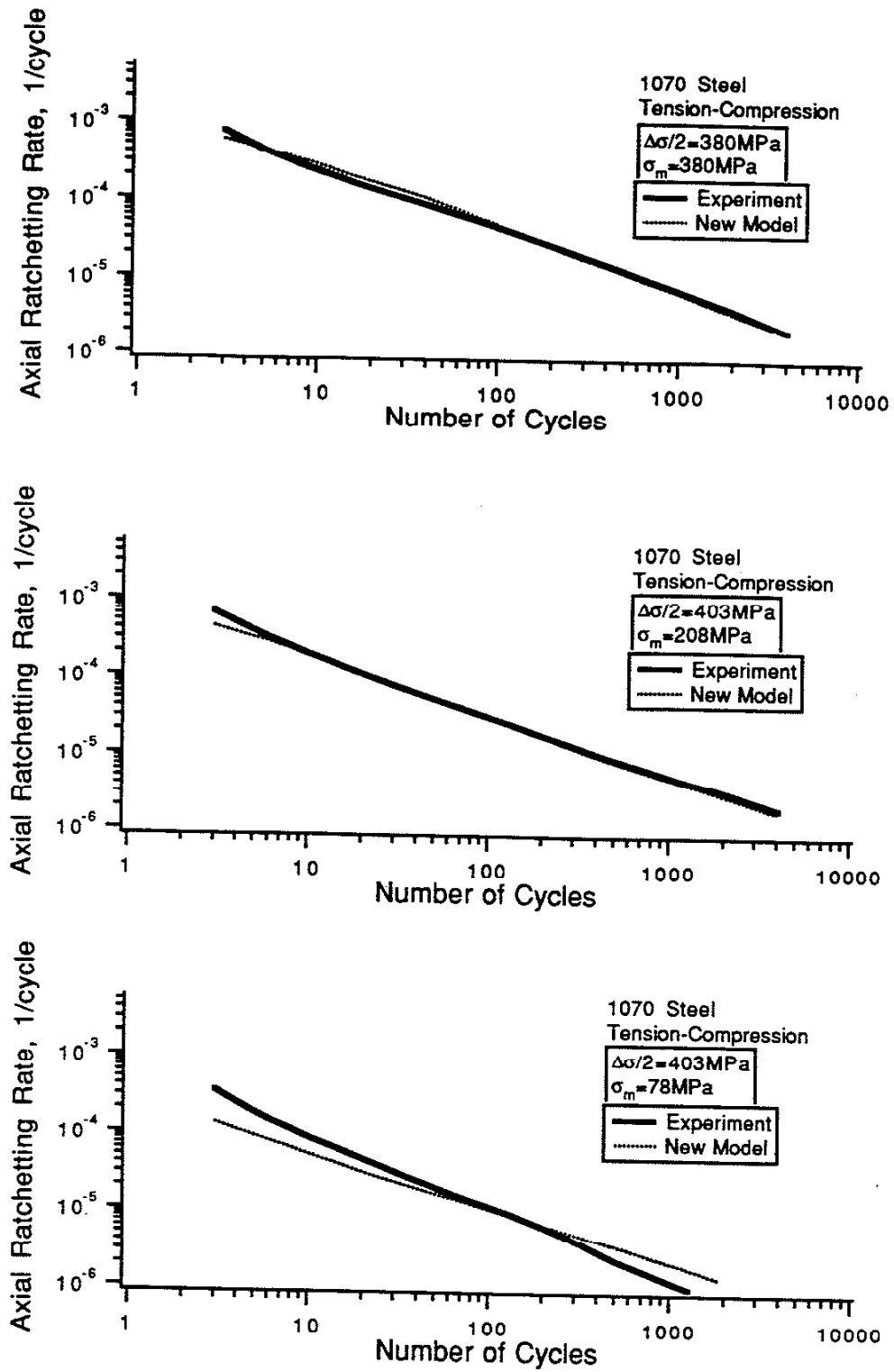
Figure 7.4 Correlation of Predicted and Experimental Ratchetting Rates for Uniaxial Tests with Different Stress Levels
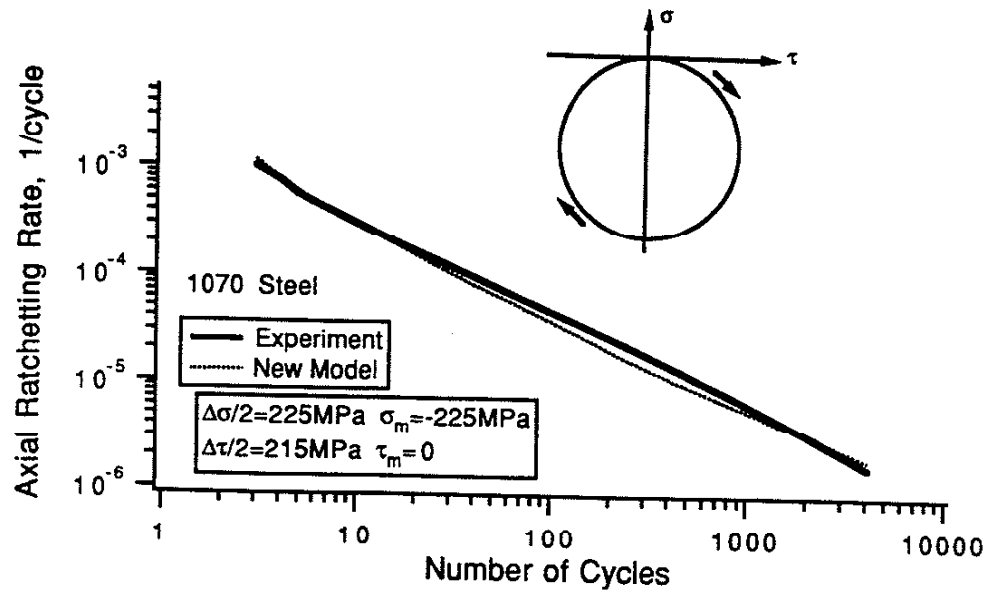
(a) Axial Ratchetting Rate *vs.* Number of Cycles
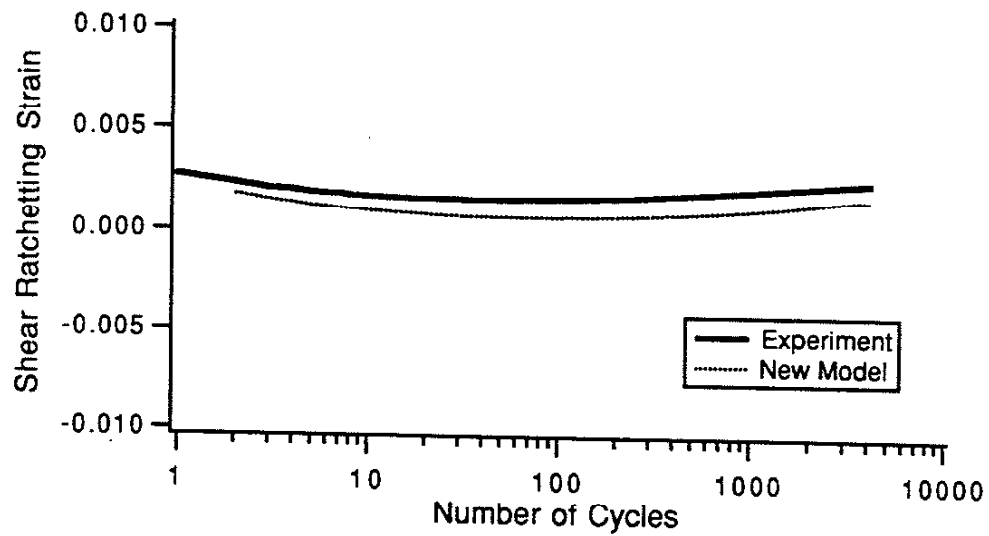
(b) Shear Ratchetting Strain *vs.* Number of Cycles

Figure 7.5   Comparison of Experimental Data and Ratchetting Results Predicted by the New Model for an "Ellipse" Shaped Axial-Torsion Loading Path (Figure 3.6)
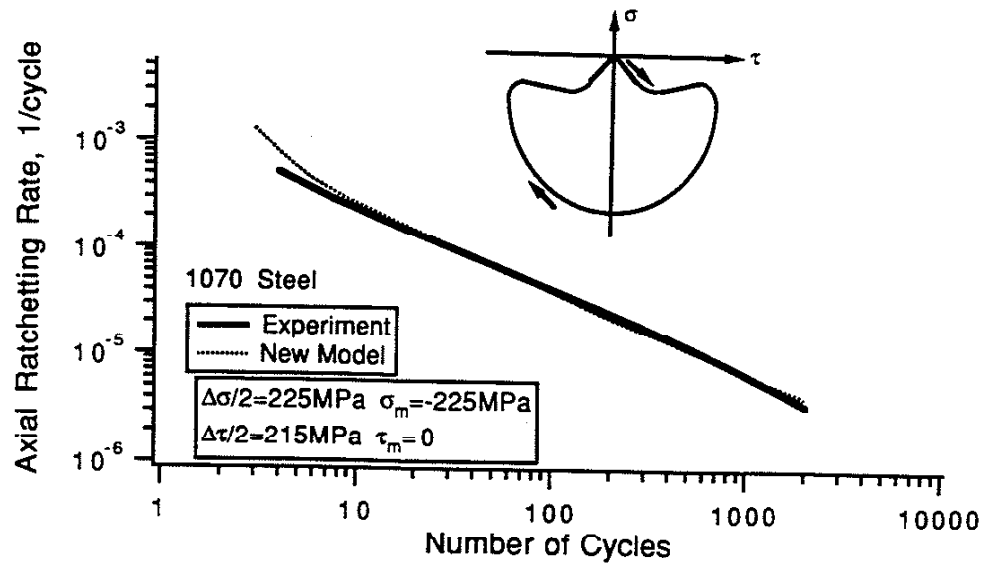
(a) Axial Ratchetting Rate *vs.* Number of Cycles
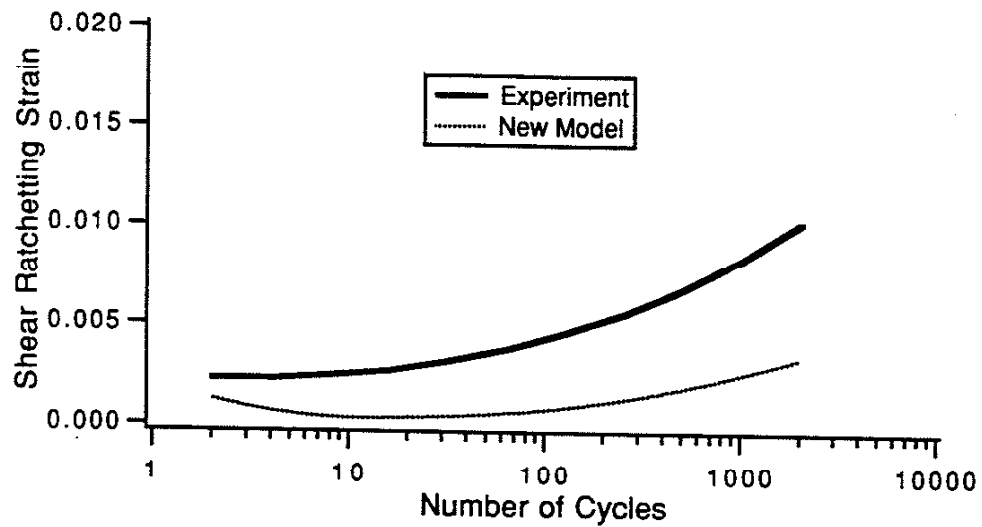
(b) Shear Ratchetting Strain *vs.* Number of Cycles

Figure 7.6 Comparison of Experimental Data and Ratchetting Results Predicted by the New Model for an "Apple" Shaped Axial-Torsion Loading Path (Figure 3.7).
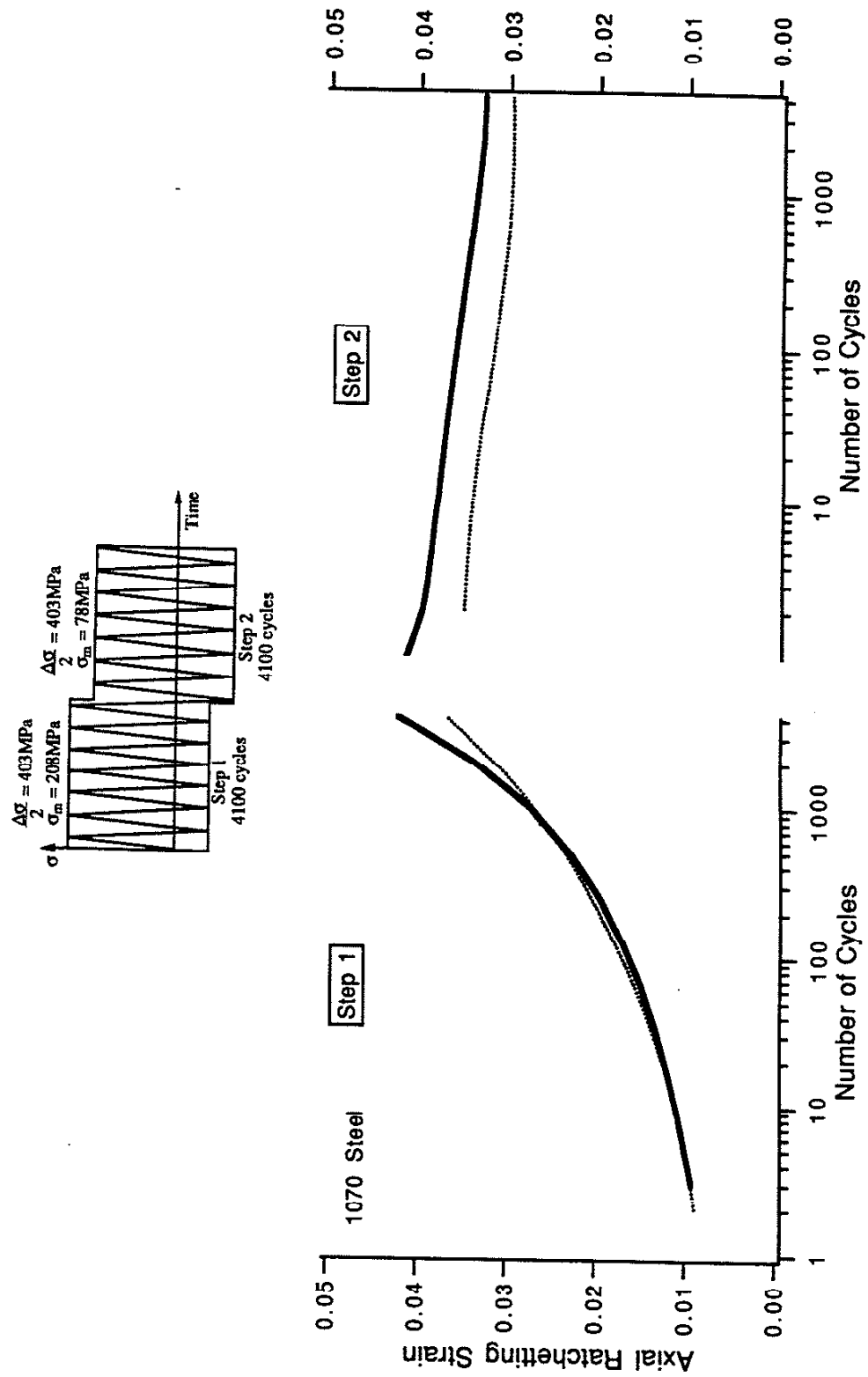
Figure 7.7 Comparison of Experimental Data and Ratchetting Strain Predicted by
the New Model for a Two-Step Uniaxial Loading (Figure 3.11(a))
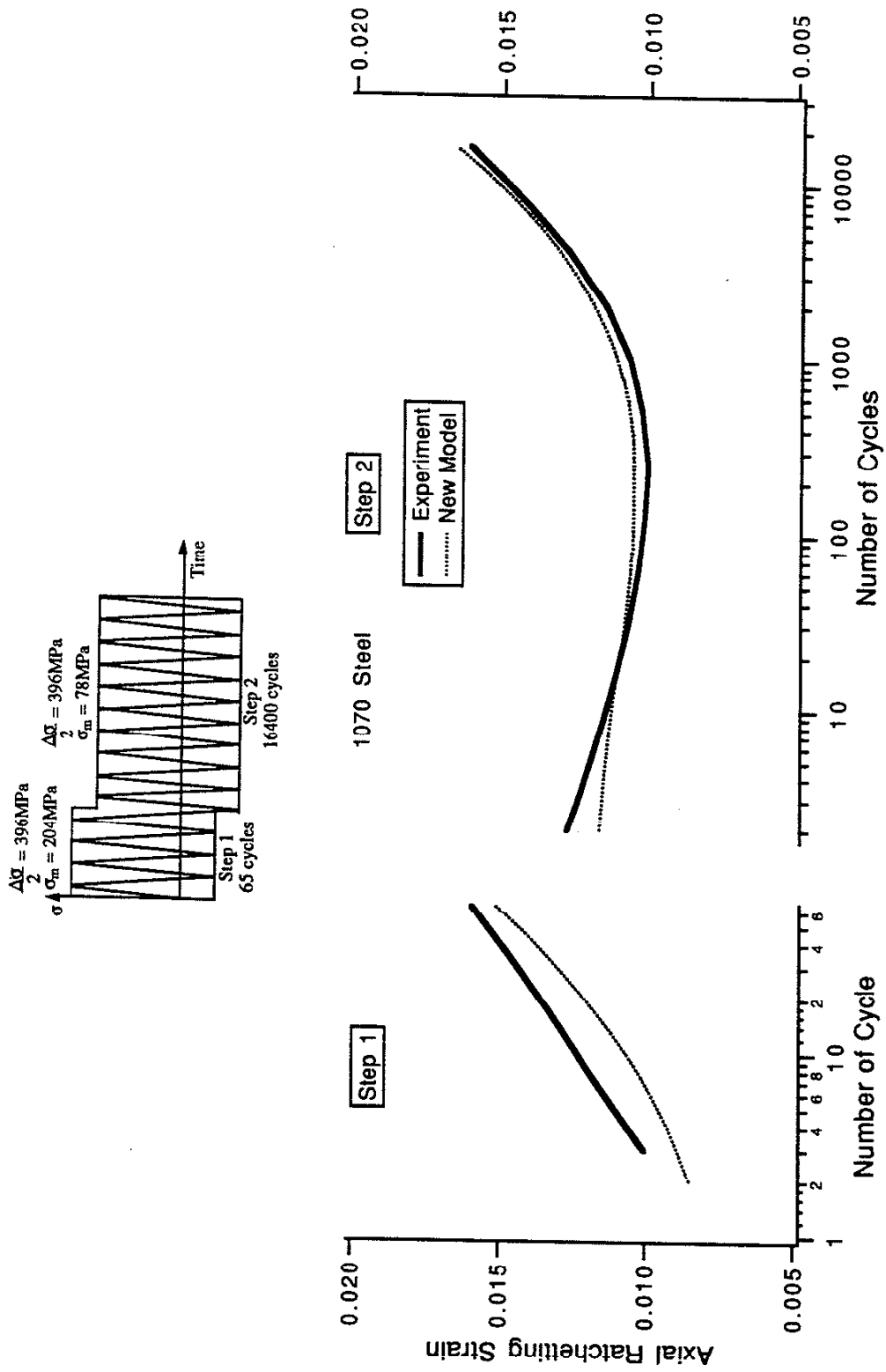
Figure 7.8 Comparison of Experimental Data and Ratchetting Strain Predicted by the
the New Model for a Two-Step Uniaxial Loading (Figure 3.12)
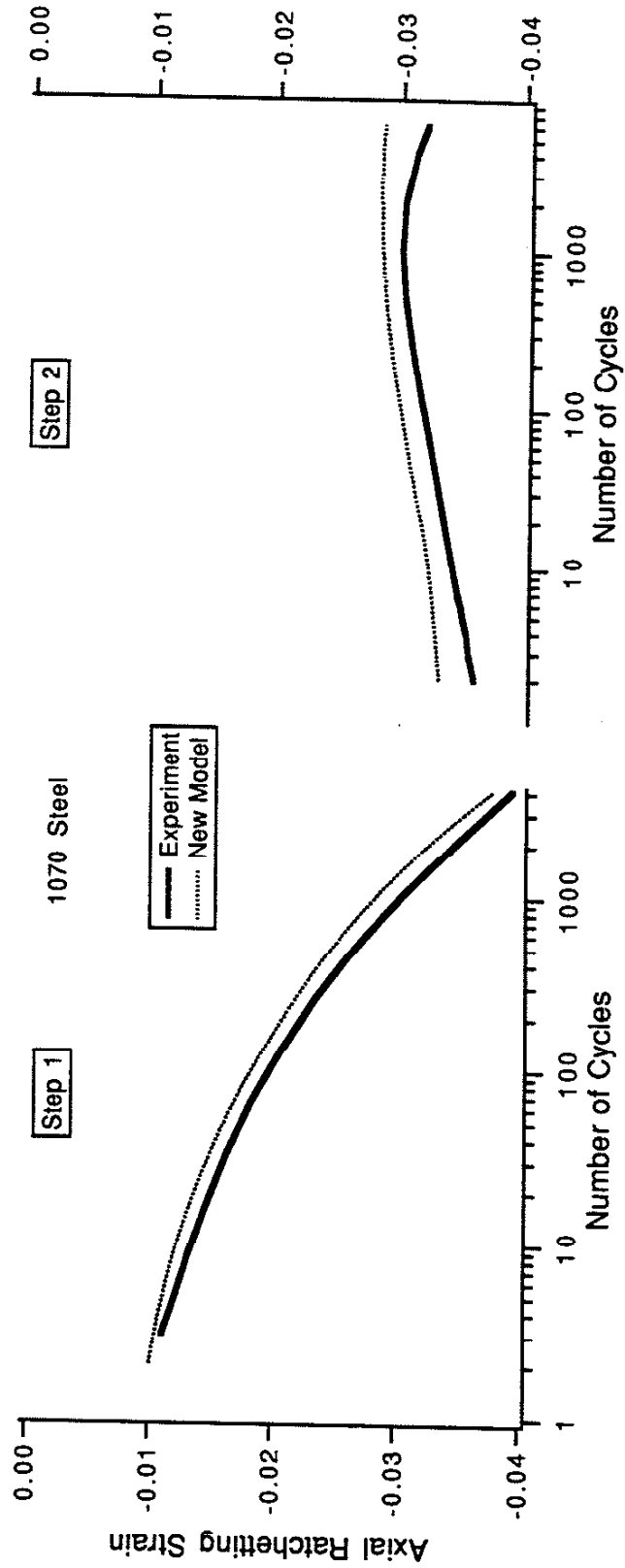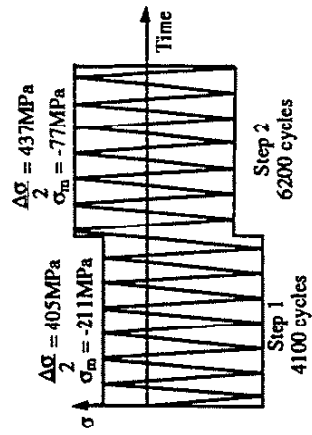
Figure 7.9 Comparison of Experimental Data and Ratchetting Strain Predicted by the
the New Model for a Two-Step Uniaxial Loading (Figure 3.13)
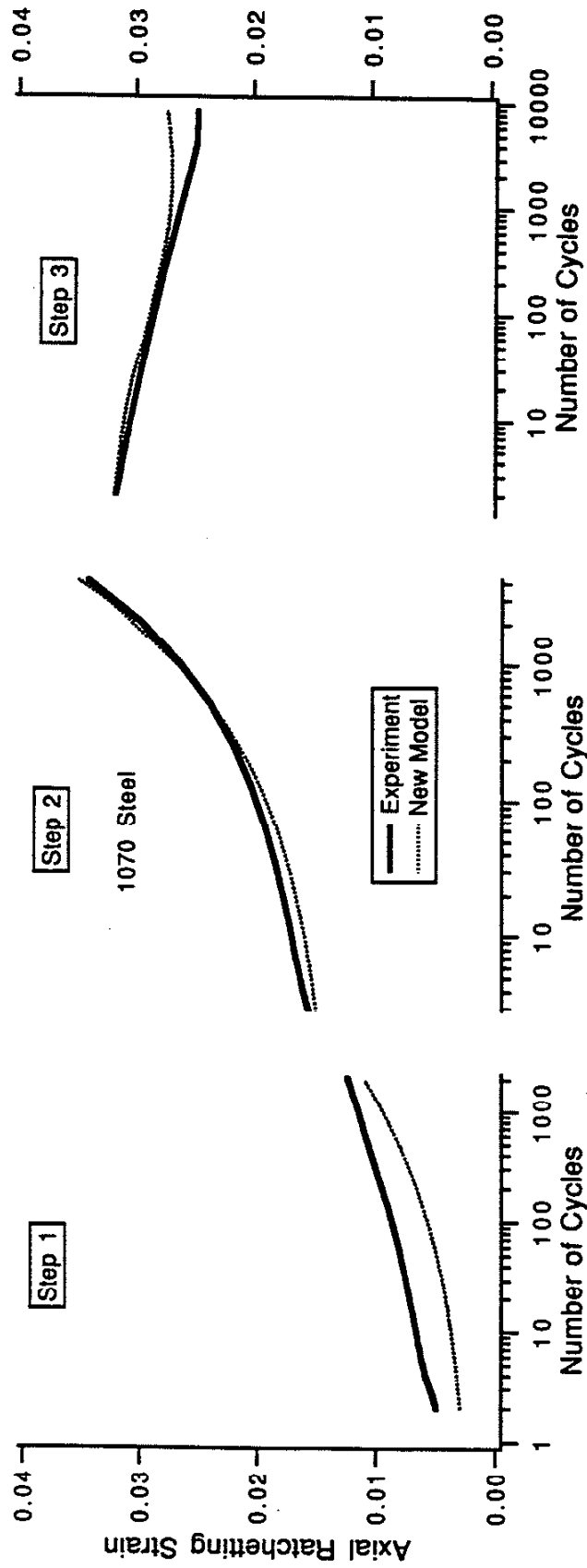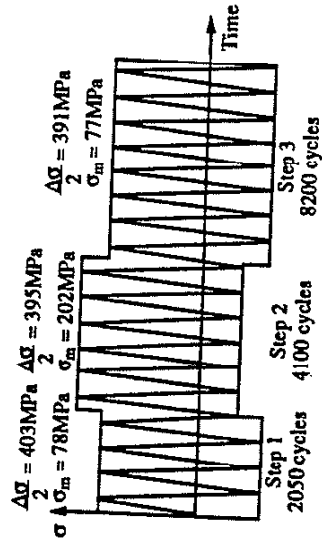
Figure 7.10 Comparison of Experimental Data and Ratchetting Strain Predicted by the New Model for a Three-Step Uniaxial Loading (Figure 3.10)
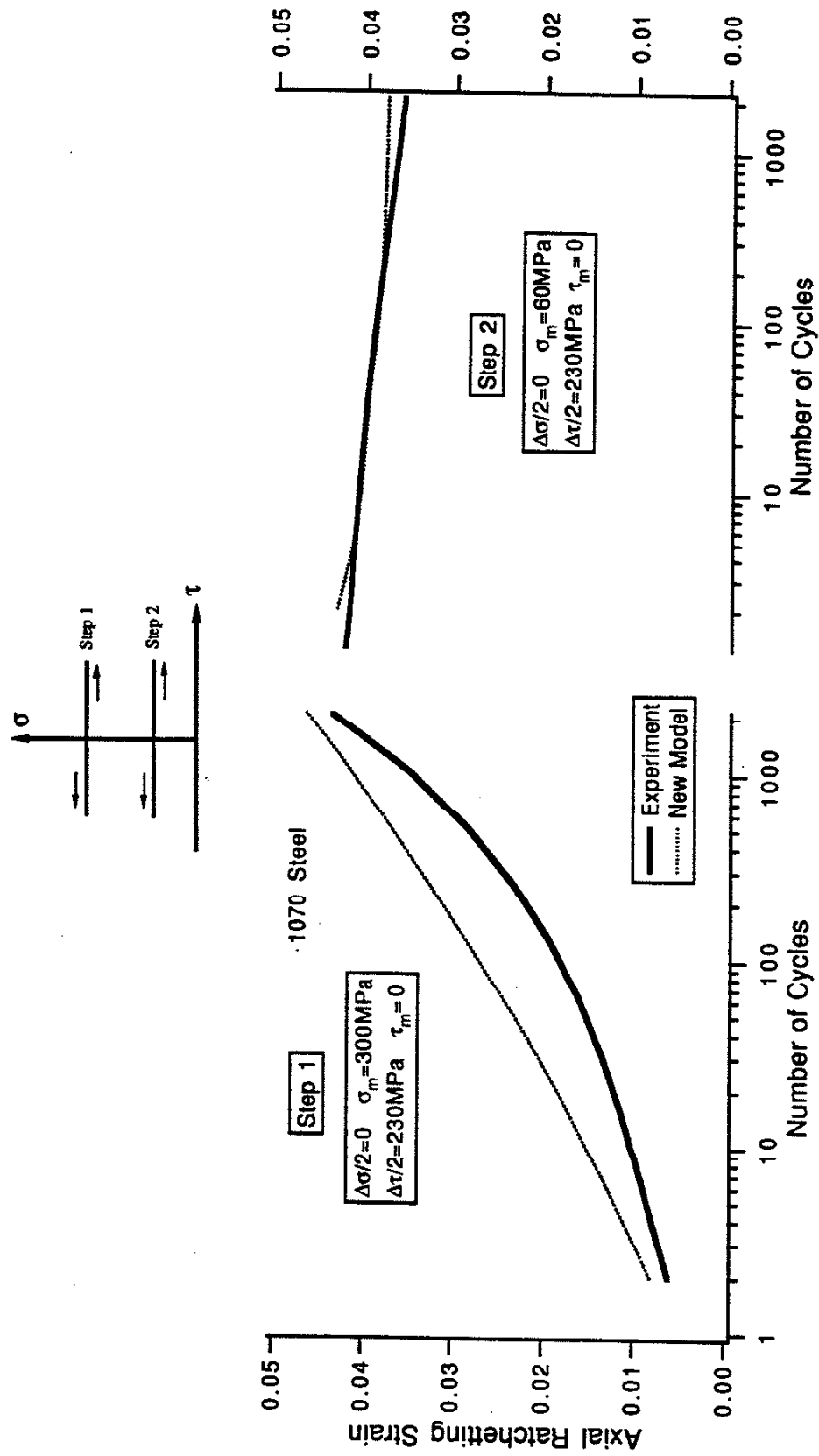
Figure 7.11 Comparison of Experimental Data and Ratchetting Strain Predicted by the New Model for a Two-Step Nonproportional Axial-Torsion Loading Consisitiong of Alternating Shear with Constant Axial Stress (Figure 3.17)
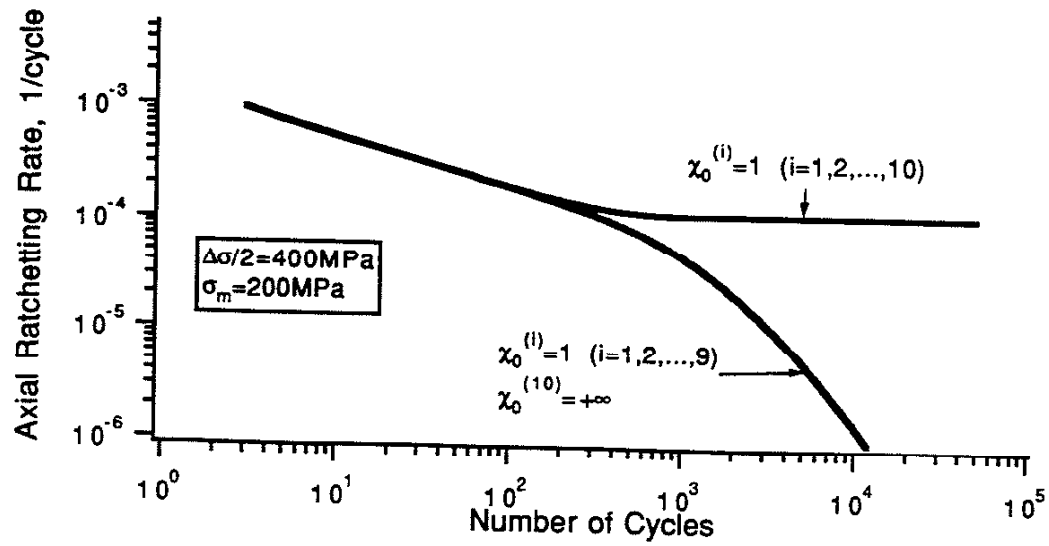
(a) Uniaxial Loading
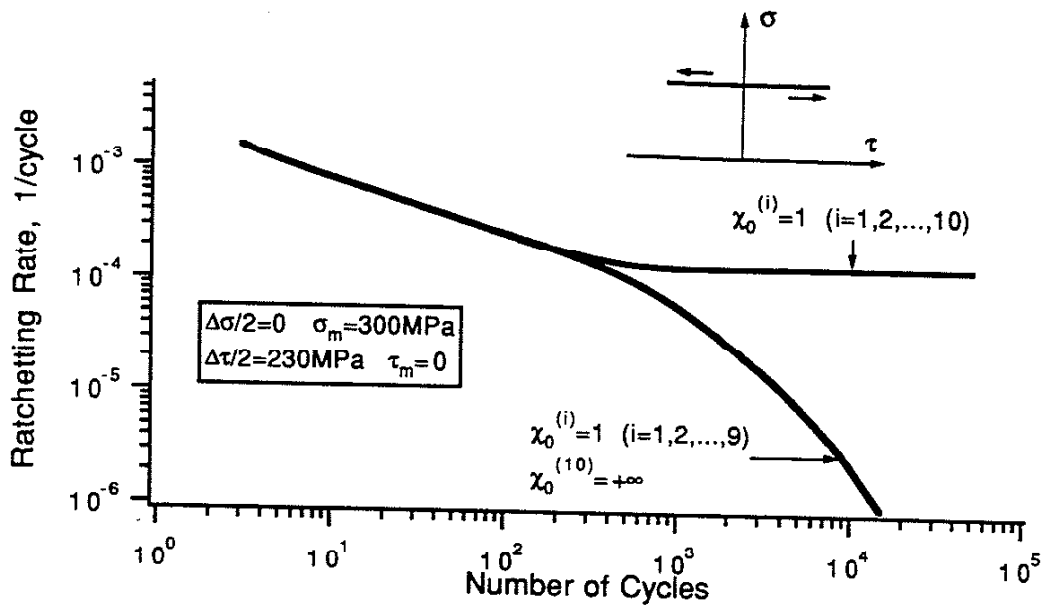
(b) Nonproportional Axial-Torsion

Figure 7.12   Relationship between Qualitative Ratchetting Behavior Predicted by the New Model and the Selection of the Exponent $\chi^{(i)}$.

Region I: Decayed Ratchetting
Region II: Constant Ratchetting

Region I | Region II

$$\log \frac{d\varepsilon_r}{dN}$$

log N

Region III: Ratchetting Arrest

Region I | Region III

$$\log \frac{d\varepsilon_r}{dN}$$

log N

Region IV: Increasing Ratchetting

Region IV | Region II

$$\log \frac{d\varepsilon_r}{dN}$$

log N
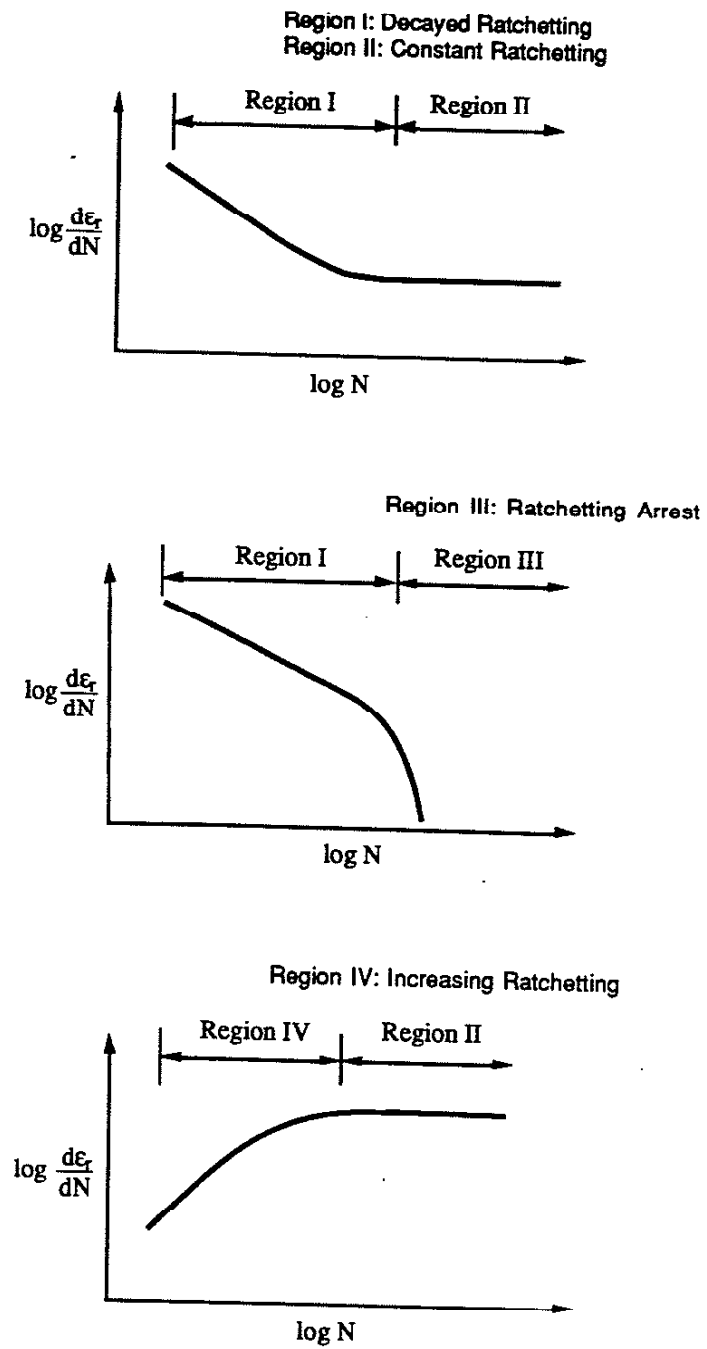
Figure 7.13 Schematic Illustration of Different Ratchetting Tendencies

$$h = \frac{2}{3} H$$

$$H = \frac{d\sigma}{d\varepsilon^p}$$
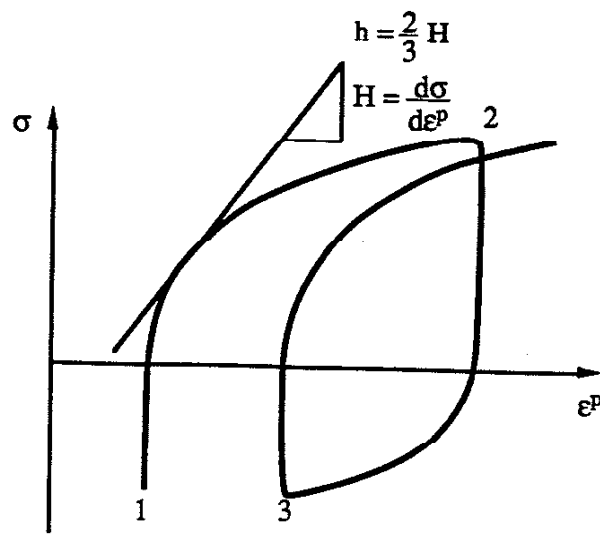
Figure 7.14 Schematic Representation of Strain Ratchetting for a
Uniaxial Simulation
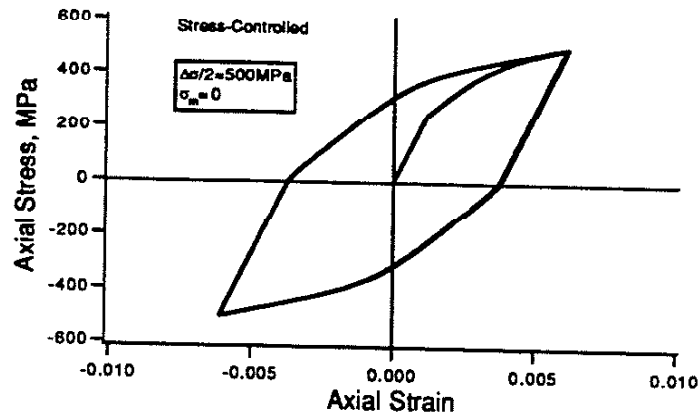
(a) Stress-Strain Response
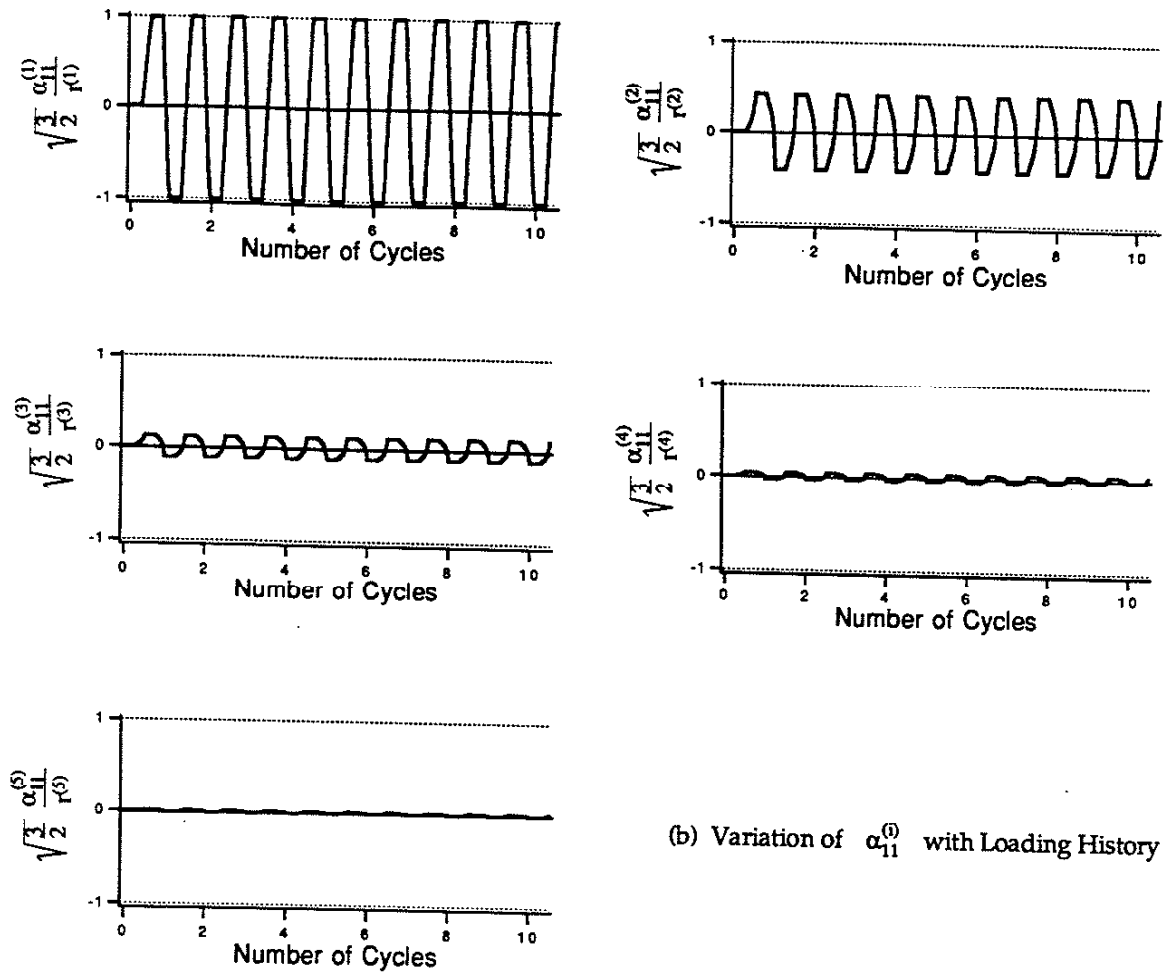
(b) Variation of $\alpha_{11}^{(i)}$ with Loading History

Figure 7.15 Stress-Strain Response and Variations of $\alpha_{11}^{(i)}$ Predicted by the New Model for Fully Reversed Uniaxial Loading
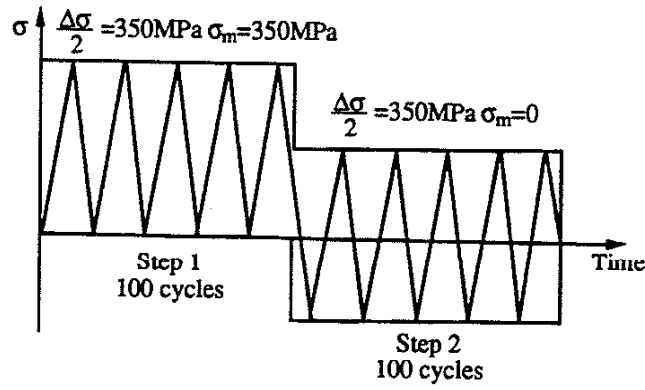
(a) Two-Step Uniaxial Loading
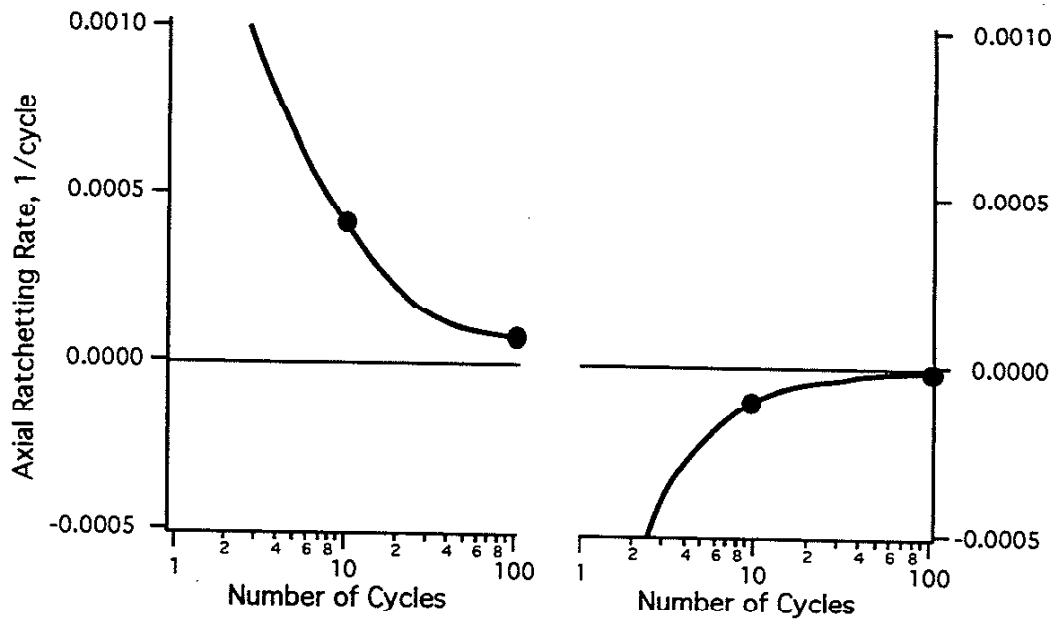
(b) Ratchetting Rate

Figure 7.16 Demonstration of Ratchetting Rate Decay Predicted by the New Model for a Two-Step Uniaxial Loading
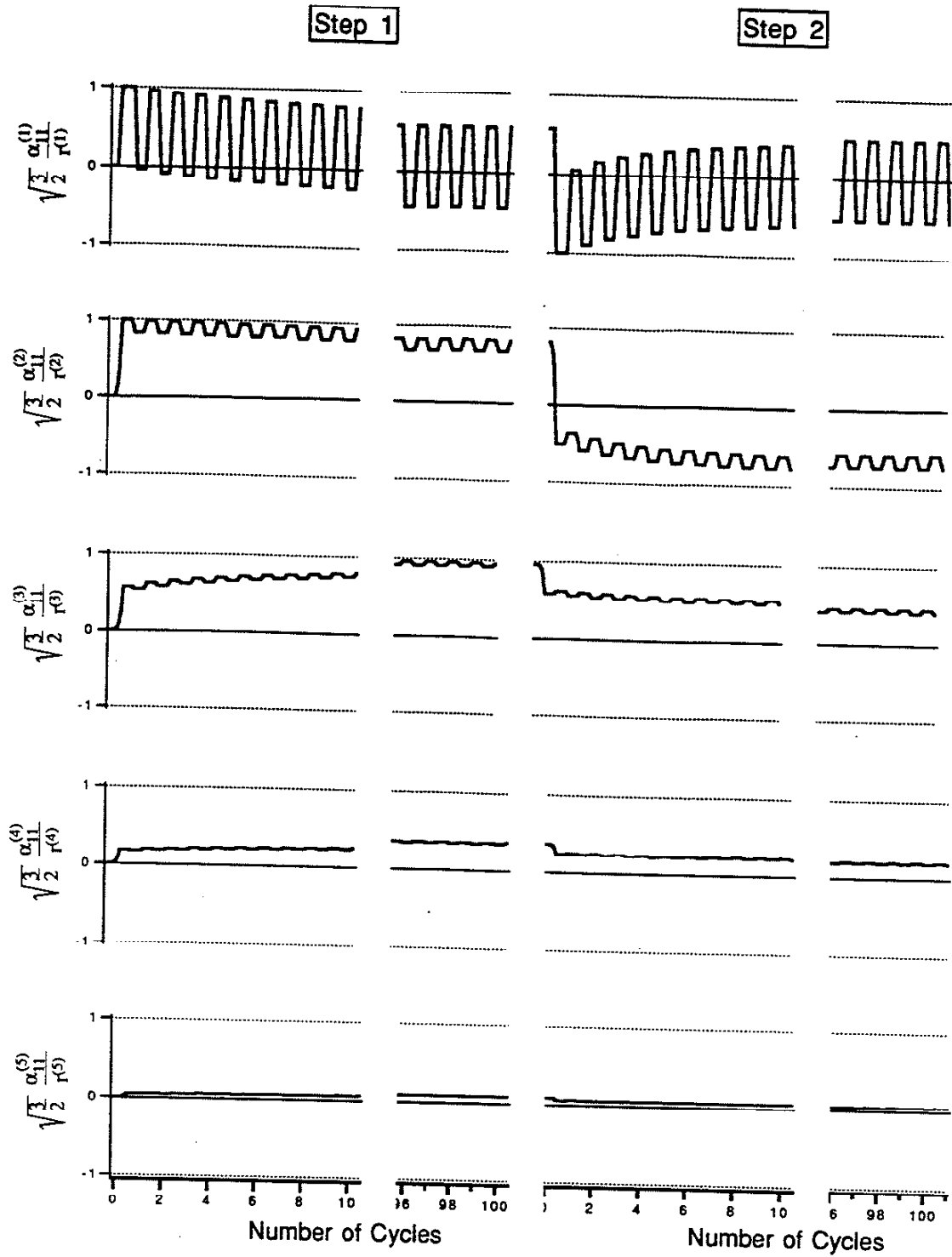
(c) $\alpha_{11}^{(i)}$ Variations with Loading Cycles

Figure 7.16(cont.) Demonstration of Ratchetting Rate Decay Predicted the New Model for a Two-Step Uniaxial Loading

BIBLIOGRAPHY

Abdel-Raouf, H., Topper, T.H., and Plumtree, A., 1977, "Cyclic Plasticity and Masing Behaviour in Metals and Alloys," *Fracture 1977*, ICF4, Vol.2, Waterloo, Canada, pp.1207-1215

Armstrong, P.J. and Frederick, C.O., 1966, "A Mathematical Representation of the Multiaxial Bauschinger Effect," *Report RD/B/N 731*, Central Electricity Generating Board

Asaro, R.J., 1983, "Crystal Plasticity," ASME *Journal of Applied Mechanics*, Vol.50, pp.921-934

ASTM, 1993, "Standard Test Methods for Tension Testing of Metallic Materials," E-8-93, *1993 Annual Book of ASTM Standards*, Vol.03.01, Metals Test Methods and Analytical Procedures

Bairstow, L., 1911, "The Elastic Limits of Iron and Steel under Cyclical Variations of Stress," *Philosophical Transactions of Royal Society*, Ser.A, Vol.210, pp.35-55

Bayerlein, M., Christ, H.-J., and Mughrabi, H., 1987, "A Critical Evaluation of the Incremental Step Test," *Low Cycle Fatigue and Elasto-Plastic Behaviour of Materials*, Rie, Ed., Elsevier Applied Science, pp.149-154

Benallal, A., Cailletaud, G., Chaboche, J.L., Marquis, D., Nouailhas, D., and Rousset, M., 1989, "Description and Modeling of Non-proportional Effects in Cyclic Plasticity," *Biaxial and Multiaxial Fatigue*, EGF3, Brown and Miller, Eds., Mechanical Engineering Publications, London, pp.107-129

Benallal, A. and Marquis, D., 1987a, "Constitutive Equations for Nonproportional Elastio-Viscoplasticity," ASME *Journal of Engineering Materials and Technology*, Vol.109, pp.326-336

Benallal, A. and Marquis, D., 1987b, "Constitutive Equations Describing Nonproportional Effect in Cyclic Plasticity," *Proceedings of the Second International Conference on Constitutive Laws for Engineering Materials: Theory and Applications*, Sedai *et al.*, Eds., Tuscson, Arizona, pp.505-512

Benallal, A., LeGallo, P., and Marquis, D., 1988, "Cyclic Hardening of Metals under Complex Loadings," *Proceedings of MECAMAT, Internal Seminar on the Inelastic Behavior of Solids: Models and Utilization*, Besancon, France, pp.361-371

Benallal, A., LeGallo, P., and Marquis, D., 1989a, "The Role of Mean Strain on the Stress Response in Nonproportional Cyclic Plasticity," *Advances in Plasticity*, Proceedings of Plasticity'89, Second International Symposium on Plasticity and Its Current Applications, MIE University, Tsukuba, Japan, Khan and Tokuda, Eds., Pergamon Press, Oxford, pp.203-206

Benallal, A., LeGallo, P., and Marquis, D., 1989b, "An Experimental Investigation of Cyclic Hardening of 316 Stainless Steel and of 2024 Aluminum Alloy under Multiaxial Loadings," *Nuclear Engineering and Design*, Vol.114, pp.345-353

Benham, P.P., 1961, "Axial-Load and Strain-Cycling Fatigue of Copper at Low Endurance," *The Journal of the Institute of Metals*, Vol.89, pp.328-338

Benham, P.P. and Ford, Hugh, 1961, "Low Endurance Fatigue of a Mild Steel and an Aluminum Alloy," *Journal of Mechanical Engineering Science*, Vol.3, No.2, pp.119-132

Besseling, J.F., 1958, "A Theory of Elastic, Plastic, and Creep Deformations of an Initially Isotropic Material Showing Anisotropic Strain-Hardening, Creep Recovery, and Secondary Creep," ASME *Journal of Applied Mechanics*, pp.529-536

Bower, Allan Francis, 1987, "Some Aspects of Plastic Flow, Residual Stress and Fatigue due to Rolling and Sliding Contact," *Ph.D. Dissertation*, Emmanuel College, Department of Engineering, University of Cambridge

Bower, A.F., 1989, "Cyclic Hardening Properties of Hard-Drawn Copper and Rail Steel," *Journal of Mechanics and Physics of Solids*, Vol.37, No.4, pp.455-470

Bower, A.F. and Johnson, K.L., 1989, "The Influence of Strain Hardening on Cumulative Plastic Deformation in Rolling and Sliding Line Contact," *Journal of Mechanics and Physics of Solids*, Vol.37, No.4, pp.471-493

Bruhns, O.T. and Pape, A., 1989, "A Three Surface Model in Nonproportional Cyclic Plasticity," *Proceedings of International Conference on Constitutive Laws for Engineering Materials*, Chonqing, China, Fan and Murakami, Eds., Pergamon Press, Vol.2, pp.703-708

Bruhns, O.T., Lehmann, T., and Pape, A., 1992, "On the Description of Transient Cyclic Hardening Behavior of Mild Steel CK 15," *International Journal of Plasticity*, Vol.8, pp.331-359

Budiansky, Bernard, 1959, "A Reassessment of Deformation Theories of Plasticity," ASME *Journal of Applied Mechanics*, pp.259-264

Burlet, H. and Cailletaud, G., 1987, "Modeling of Cyclic Plasticity in Finite Element Codes," *Proceedings of the Second International Conference on Constitutive Laws for Engineering Materials: Theory and Application*, Desai et al., Eds., Tucson, Arizona, pp.1157-1164

Cailletaud, G., Kaczmarek, H., and Policella, H., 1984, "Some Elements on the Multiaxial Behaviour of 316 L Stainless Steel at Room Temperature," *Mechanics of Materials*, Vol.3, No.4, pp.333-347

Chaboche, J.L, 1986, "Time-Independent Constitutive Theories for Cyclic Plasticity," *International Journal of Plasticity*, Vol.2, No.2, pp.149-188

Chaboche, J.-L., 1987, "Cyclic Plasticity Modeling and Ratchetting Effects," *Proceedings of the Second International Conference on Constitutive Laws for Engineering Materials: Theory and Applications*, Tucson, Arizona, Desal et al., Eds., Elsevier, pp.47-58

Chaboche, J.L., 1989a, "Constitutive Equations for Cyclic Plasticity and Cyclic Viscoplasticity," *International Journal of Plasticity*, Vol.5, pp.247-302

Chaboche, J.-L., 1989b, "A New Kinematic Hardening Rule with Discrete Memory Surfaces," *Rech. Aérosp.*, n° 4, pp.49-69

Chaboche, J.-L., 1989c, "A New Constitutive Framework to Describe Limited Ratchetting Effects," *Advances in Plasticity*, Proceedings of Plasticity'89, Second International Symposium on Plasticity and Its Current Applications, MIE University, Tsukuba, Japan, Khan and Tokuda, Eds., Pergamon Press, Oxford, pp.211-214

Chaboche, J.L., 1991, "On Some Modifications of Kinematic Hardening to Improve the Description of Ratchetting Effects," *International Journal of Plasticity*, Vol.7, pp.661-687

Chaboche, J.-L., Dang Van, K., and Cordier, G., 1979, "Modelization of the Strain Memory Effect on the Cyclic Hardening of 316 Stainless Steel," *Structural Mechanics in Reactor Technology*, Transactions of the Fifth International Conference on Structural Mechanics in Reactor Technology, Div. L, Berlin, L11/3

Chaboche, J.L. and Nouailhas, D, 1989a, "Constitutive Modeling of Ratchetting Effects-Part I: experimental Facts and Properties of the Classical Models," ASME *Journal of Engineering Materials and Technology*, Vol.111, pp.384-392

Chaboche, J.L. and Nouailhas, D, 1989b, "Constitutive Modeling of Ratchetting Effects-Part II: Possibilities of Some Additional Kinematic Rules," ASME *Journal of Engineering Materials and Technology*, Vol.111, pp.409-416

Chaboche, J.L., Nouailhas, D., Pacou, D., and Paulmier, P., 1989, "Problems of Describing Ratchetting Effects in Cyclic Plasticity and Viscoplasticity," *Rech. Aérosp.*, n° 1989-1, pp.63-79

Chaboche, J.L., Nouailhas, D., Pacou, D., and Paulmier, P., 1991, " Modeling of the Cyclic Response and Ratchetting Effects on Inconel-718 Alloy," *European Journal of Mechanics, A/Solids*, Vol.10, N°1, pp.101-121

Chang, K.C. and Lee, G.C., 1986a, "Biaxial Properties of Structure Steel under Nonproportional Loading," ASCE *Journal of Engineering Mechanics*, Vol.112, No.8, pp.792-805

Chang, K.C. and Lee, G.C., 1986b, "Constitutive Relations of Structure Steel under Nonproportional Loading," ASCE *Journal of Engineering Mechanics*, Vol.112, No.8, pp.806-820

Coffin, L.F., Jr., 1960, "The Stability of Metals under Cyclic Plastic Strain," ASME *Journal of Basic Engineering*, Vol.82, Ser.D, No.3, p.671

Cuddy, J. and Bassim, M. Nabil, 1989, "Study of Dislocation Cell Structures from Uniaxial Deformation of AISI 4340 Steel," *Material Science and Engineering*, A113, pp.421-429

Dafalias, Y.F., 1981, "A Novel Bounding Surface Constitutive Law for the Monotonic and Cyclic Hardening Response of Metals," *Transactions of the 6th International Conference on Structural Mechanics in Reactor Technology*, L3/4

Dafalias, Y.F and Popov, E.P., 1975, "A Model of Nonlinearly Hardening Materials for Complex Loading," *Acta Mechanica*, Vol.21, pp.173-192

Dafalias, Y.F and Popov, E.P., 1976, "Plastic Internal Variables Formalism of Cyclic Plasticity," ASME *Journal of Applied Mechanics*, Vol.43, pp.645-651

Dolan, J.T., 1965, "Nonlinear Response under Cyclic Loading Conditions," *Proceedings," Ninth Midwestern Mechanics Conference*, University of Wisconsin, Madison, Wisconsin, pp.2-21

Dollar, M., Bernstein, I.M., and Thompson, A.W., 1988, "Influence of Deformation Substructure on Flow and Fracture of Fully Pearlitic Steel," *Acta Metallurgy*, Vol.36, No.2, pp.311-320

Doong, Shiing-Hwa, 1989, "A Plasticity Theory of Metals Based on the Dislocation Substructures," *Ph.D Dissertation*, Department of Mechanical and Industrial Engineering, University of Illinois at Urbana-Champaign

Doong, S.H. and Socie, D.F., 1991, "Constitutive Modeling of Metals under Nonproportional Cyclic Loading," ASME *Journal of Engineering Materials and Technology*, Vol.113, pp.23-30

Drucker, D.C., 1951, "A More Fundamental Approach to Plastic Stress-Strain Relations," *Proceedings of the First U.S. National Congress of Applied Mechanics*, ASME, pp.487-491

Drucker, D.C., 1960, "Plasticity in Structural Mechanics", *Proceedings of the First (1958) symposium on Naval Structural Mechanics*, Goodier and Hoff, Eds., Pergamon, Macmillan, New York, pp.331-350

Drucker, D. C., 1984, "Material Response and Continuum Relations; or From Microscales to Macroscales," ASME *Journal of Engineering Materials and Technology*, Vol.106, pp.286-289

Drucker, Daniel C., 1987, "Some General Preliminary Comments on Anisotropic/Cyclic Plasticity," *Proceedings of the Second International Conference on Constitutive Laws for Engineering Materials: Theory and Applications*, Tucson, Arizona, Elsevier, Desai *et al.*, Eds., Vol.I, pp.95-97

Drucker, Daniel C., 1988, "Conventional and Unconventional Plastic Response and Representation," *Applied Mechanics Review*, Vol.41, No.4, pp.151-167

Drucker, D.C. and Palgen, L., 1981, "On Stress-Strain Relations Suitable for Cyclic and Other Loading," ASME *Journal of Applied Mechanics*, Vol.48, pp.479-485

Ellyin, F., 1985, "Effect of Tensile-Mean-Strain on Plastic Strain Energy and Cyclic Response," ASME *Journal of Engineering Materials and Technology*, Vol.107, pp.119-125

Fatemi, Ali, 1985, "Fatigue and Deformation under Proportional and Nonproportional Biaxial Loading," *Ph.D Dissertation*, Mechanical Engineering, The University of Iowa

Fatemi, A. and Kurath, P., 1988, "Multiaxial Fatigue Life Prediction under the Influence of Mean-Stresses", ASME *Journal of Engineering materials and Technology*, Vol.110, pp.380-388

Fatemi, Ali, Socie, D.F., 1988, " A Critical Plane Approach to Multiaxial Fatigue Damage Including Out-of-Phase Loading", *Fatigue and Fracture of Materials and Structures*, Vol.11, No.3, pp.149-165

Fatemi, Ali and Stephens, R.I., 1989, "Cyclic Deformation of 1045 Steel under In-Phase and 90 Deg Out-of-Phase Axial-Torsional Loading Conditions,"

Multiaxial Fatigue; Analysis and Experiments, AE-14, Leese and Socie, Eds., Society of Automotive Engineers, pp.139-147

Garud, Y.S., 1981a, "Multiaxial Fatigue of Metals", *Ph.D Dissertation*, Mechanical Engineering, Stanford University

Garud, Y.S., 1981b, "A New Approach to the Evaluation of Fatigue under Multiaxial Loadings", ASME *Journal of Engineering Materials and Technology*, Vol.103, pp.118-125

Garud, Y.S., 1982, "Prediction of Stress-Strain Response under General Multiaxial Loading," *Mechanical Testing for Deformation Model Development, ASTM STP 765*, Rohde and Swearengen, Eds., American Society for Testing and Materials, pp.223-238

Garud, Y.S., 1991, "Notes on Cyclic Dependent Ratchetting under Multiaxial Loads Including Bauschinger Effect and Non-Linear Strain Hardening," *Transactions of the 11th International Conference on Structural Mechanics in Reactor Technology*, Tokyo, Japan, Shibata, Ed., Vol.L, L23/1, pp.511-518

Gerald, Curtis F. and Wheatley, Patrick O., 1984, *Applied Numerical Analysis*, Chapter 4, Third Ed., Addison-Wesley Publishing Company

Golos, K. and Ellyin, F., 1988, "A Total Strain Energy Density Theory for Cumulative Fatigue Damage," ASME *Journal of Pressure Vessel Technology*, Vol.110, pp.36-41

Guionnet, C., 1992, "Modeling of Ratchetting in Biaxial Experiments," ASME *Journal of Engineering Materials and Technology*, Vol.114, pp.56-62

Hasegawa, T. and Takou, T., 1986, "Forwar and Reverse Rearrangements of Dislocations in Tangled Walls," *Materials Science and Engineering*, Vol.81, pp.267-276

Hashiguchi, K., 1988, "A Mathematical Modification of Two Surface Model Formulation in Plasticity," *International Journal of Solids and Structures*, Vol.24, pp.987-

Hashiguchi, K., 1993a, "Fundamental Requirements and Formulation of Elastoplastic Constitutive Equations with Tangential Plasticity," *International Journal of Plasticity*, Vol.9, pp.525-549

Hashiguchi, K., 1993b, "Mechanical Requirements and Structures of Cyclic Plasticity Models," *International Journal of Plasticity*, Vol.9, pp.721-748

Hassan, T., Corona, E., and Kyriakides, S., 1991, "Ratchetting in Cyclic Plasticity: Experiments and Predictions," *Transactions of the 11th International Conference on Structural Mechanics in Reactor Technology*, Tokyo, Japan, Shibata, Ed., Vol.L, L23/2, pp.519-525

Hassan, Tasntin and Kyriakides, Stelios, 1992, "Ratchetting in Cyclic Plasticity, Part I: Uniaxial Behavior," *International Journal of Plasticity*, Vol.8, pp.91-116

Hassan, T., Corona, E., and Kyriakides, S., 1992, "Ratchetting in Cyclic Plasticity, Part II: Multiaxial Behavior" *International Journal of Plasticity*, Vol.8, pp.117-146

Hill, R., 1965, "Continuum Micro-Mechanics of Elastoplastic Polycrystals," *Journal of Mechanics and Physics of Solids*, Vol.13, pp.89-101

Hunsaker, B., Jr., Vaughan, D.K., and Stricklin, J.A., 1976, "A Comparison of the Capability of Four Hardening Rules to Predict a Material's Plastic Behavior," ASME *Journal of Pressure Vessel and Technology*, pp.66-74

Inoue, T, Igari, T., Yoshida, F., Suzuki, A, and Murakami, S., 1985, "Inelastic Behaviour of $2\frac{1}{4}$ Cr-Mo Steel under Plasticity-Creep Interaction Conditions," *Nuclear Engineering and Design*, Vol.90, pp.287-297

Inoue, T., Ohno, N., Suzuki, A., and Igari, T., 1989, "Evaluation of Inelastic Constitutive Models under Plastic-Creep Interaction for $2\frac{1}{4}$ Cr-1Mo Steel at 600 ∞ C," *Nuclear Engineering and Design*, Vol.114, pp.295-309

Inoue, T., Yoshida, F., Niitsu, Y., Ohno, Kawai, M., Niitsu, Y., and Imatani, S., 1991, "Evaluation of Inelastic Constitutive Models under Plasticity-Creep Interaction in Multiaxial Stress State," *Nuclear Engineering and Design*, Vol.126, pp.1-11

Inoue, T., Yoshida, F., Niitsu, Y., Ohno, N., Uno, T., and Suzuki, A, 1991, "Inelastic Stress/Strain Response of $2\frac{1}{4}$ Cr-1Mo Steel under Combined Tension-Torsion at 600 ∞ C," *Transactions of the 11th International Conference on Structural Mechanics in Reactor Technology*, Tokyo, Japan, Shibata, Ed., Vol.L, L01/1, pp.1-12

Ishikawa, H. and Sasaki, K., 1989, "Numerical Simulation of Nonproportional Cyclic Plasticity," *Advances in Plasticity*, Proceedings of Plasticity'89, Second International Symposium on Plasticity and Its Current Applications, MIE University, Tsukuba, Japan, Khan and Tokuda, Eds., Pergamon Press, Oxford, pp.231-234

Iwan, W.D., 1967, "On a Class of Models for the Yielding Behaviour of Continuous and Composite Systems," ASME *Journal of Applied Mechanics*, Vol.34, pp.612-617

Iwata, K., 1991, "A New Constitutive Model for Cyclic Plasticity," *Transactions of the 11th International Conference on Structural Mechanics in Reactor Technology*, Tokyo, Japan, Shibata, Ed., Vol.L, L22/4, pp.499-504

Jhansale, H.R., 1975, "A New Parameter for the Hysteric Stress-Strain Behavior of Metals," ASME *Journal of Engineering Materials and Technology*, pp.33-38

Jiang, Yanyao and Sehitoglu, Huseyin, 1993a, "Cyclic Ratchetting of 1070 Steel under Multiaxial Stress State," Submitted to *International Journal of Plasticity*

Jiang, Yanyao and Sehitoglu, Huseyin, 1993b, "Multiaxial Cyclic Ratchetting under Multiple Step Loading," Submitted to *International Journal of Plasticity*

Jiang, Yanyao and Sehitoglu, Huseyin, 1993c, "An Analytical Approach to Elastic-Plastic Stress Analysis of Rolling Contact," to appear in ASME *Journal of Tribology*

Jiang, Yanyao and Sehitoglu, Huseyin, 1993d, Unpublished Data

Kanazawa, K., Miller, K.J., and Brown, M.W., 1979, "Cyclic Deformation of 1 percent Cr-Mo-V Steel under Out-of-Phase Loads," *Fatigue of Engineering Materials and Structures*, Vol.2, pp.217-228

Kapoor, A. and Johnson, K.L., 1992, "Ratchetting Failure and Low Cycle Fatigue in Metals in Relation to Rolling/Sliding Contact," Private Communication

Kennedy, A.J., 1956, "Effect of Fatigue Stresses on Creep and Recovery," *International Conference on Fatigue of Metals*, The Institution of Mechanical Engineers and ASME, London/New York, 1956, pp.401-407

Klisinski, M., Mroz, Z., and Runesson, K., 1992, "Structure of Constitutive Equations in Plasticity for Different Choices of State and Control Variables," *International Journal of Plasticity*, Vol.8, pp.221-243

Krempl, E., 1969, "Cyclic Plasticity: Some Properties of Hysteresis Curve of Structural Metals at Room Temperature," ASME *Winter Annual Meeting*, Los Angeles, 69-WA/Met-4

Krempl, E., 1975, "On the Interaction of Rate and History Dependence in Structural Metals," *Acta Mechanica*, Vol.22, pp.53-90

Krempl, E and Lu, H., 1983, "Comparison of the Stress Responses of an Aluminum Alloy Tube to Proportional and Alternate Axial and Shear Strain Paths at Room Temperature," *Mechanics of Materials*, Vol.2, pp.183-192

Krempl, E and Lu, H., 1984, "The Hardening and Rate Dependence Behaviour of Fully Annealed AISI Type 304 Stainless Steel under Biaxial in-Phase and Out-of-Phase Strain Cycling at Room Temperature," ASME *Journal of Engineering Material and Technology*, Vol.106, pp.376

Krempl, E and Lu, H., 1989, "The Path and Amplitude Dependence of Cyclic Hardening of Type 304 Stainless Steel at Room Temperature," *Biaxial and Multiaxial Fatigue*, EGF3, Brown and Miller, Eds., Mechanical Engineering Publications, London, pp.89-106

Krempl, E. and Yao, D., 1987, "The Viscoplasticity Theory Based on Overstress Applied to Ratchetting and Cyclic Hardening," *Low-Cycle Fatigue and Elasto-Plastic Behavior of Materials*, Rie, Ed., Elsevier Applied Science Publishers, pp.137-148

Krieg, R.D., 1975, "A Practical Two Surface Plasticity Theory," ASME *Journal of Applied Mechanics*, Vol.42, pp.641-646

Kuhlmann-Wilsdorf, D., 1982, "Theory of Dislocation Cell Sizes in Deformed Metals," *Materials Science and Engineering*, Vol.55, pp.79-83

Kuhlmann-Wilsdorf, D., 1989, "Theory of Plastic Deformation:-Properties of Low Energy Dislocation Structures," *Materials Science and Engineering*, A113, pp.1-41

Kuhlmann-Wilsdorf, D. and Laird, Campbell, 1979, "Dislocation Behavior in Fatigue; II. Friction Stress and Back Stress as Inferred from an Analysis of Hysteresis Loops," *Materials Science and Engineering*, Vol.37, pp.111-120

Kurath, P., 1992, "Cyclic Ratchetting and Fatigue of AL6061-T6 Alloy," Unpublished Experimental Results, Private Communication

Kurath, P., 1993, "Comparison of Life Predictions Based on Three Plasticity Models," *SAE Fatigue Design and Evaluation Committee Meeting*, Cincinnati

Lamba, H.S., 1976, "Nonproportional Cyclic Plasticity," *T & AM Report*, No.413, Department of Theoretical and Applied Mechanics, University of Illinois of Urbana-Champaign

Lamba, H.S. and Sidebottom, O.M., 1976, "Biaxial Cyclic Hardening of Annealed OFHC Copper," *Proceedings of the Second International Conference on*

Mechanical Behavior of Materials, The American Society of Metals, Boston, Aug.16-20, pp.48-52

Lamba, H.S. and Sidebottom, O.M., 1978a, "Cyclic Plasticity for Nonproportional Paths: Part I--Cyclic Hardening, Erasure of Memory, and Subsequent Strain Hardening Experiments", ASME *Journal of Engineering Materials and Technology*, Vol.100, pp.96-104

Lamba, H.S. and Sidebottom, O.M., 1978b, "Cyclic Plasticity for Nonproportional Paths. Part II: Comparison with Predictions of Three Incremental Plasticity Models," ASME *Journal of Engineering Materials and Technology*, Vol.100, pp.104-111

Landgraf, R.W., 1970, "The Resistance of Metals to Cyclic Deformation," *Achievement of High Fatigue Resistance in Metals and Alloys, ASTM STP467*, American Society for Testing and Materials, pp.3-36

Landgraf, R.W., Morrow, J.D., and Endo, T., 1969, "Determination of Cyclic Stress-Strain Curve," *Journal of Materials*, Vol.4, pp.176-183

Lazan, B.J., 1949, "Dynamic Creep and Rupture Properties of Temperature-Resistant Materials under Tensile Stress," *Proceedings*, American Society for Testing and Materials, Vol.49, pp.757-787

Lebey, J. and Roche, R., 1979, "Tests on Mechanical Behaviour of 304 L Stainless Steel under Constant Stress Associated with Cyclic Strain," *Fatigue of Engineering Materials and Structures*, Vol.1, pp.307-318

Lefebvre, D. and Ellyin, F., 1984, "Cyclic Response and Inelastic Strain Energy in Low Cycle Fatigue," *International Journal of Fatigue*, pp.9-15

Li, Yuanfeng and Laird, Campbell, 1993, "Masing Behavior Observed in Monocrystalline Copper During Cyclic Deformation," *Materials Science and Engineering*, A161, pp.23-29

Lindholm, U.S., Chan, K.S., Bonder, S.R., Weber, R.M., Walker, K.P., and Cassenti, B.M., 1984, "Constitutive Modeling for Isotropic Materials," *Report SWRI-7576/30*, NASA CR-174980

Lu, W.Y. and Mohamed, Z.M., 1987, "A Two-Surface Plasticity Theory and Its Application to Multiaxial Loading," *Acta Mechanica*, Vol.69, pp.43-57

Manjoine, M.J., 1949, "Effect of Pulsating Loads on the Creep Characteristics of Aluminum Alloy 14S-T," *Proceedings*, American Society for Testing and Materials, Vol.49, pp.788-798

Marquis, D., 1979, "Etude Théorique et Vérification Expérimentale d'un Modéle de plasticité cyclique," *Thése,* Paris VI

Masing, G., 1926, "Eigenspannungen und Verfestigung beim Messing," *Proceedings of the 2nd International Congress for Applied Mechanics,* Zurich, Swissland, pp.332-335

McDowell, D.L., 1981, "Multiaxial Nonproportional Cyclic Deformation", *Report No.102,* Design and Materials Division, Department of Mechanical and Industrial Engineering, University of Illinois at Urbana-Champaign

McDowell, D.L., 1983a, "Transient Nonproportional Cyclic Plasticity," *Ph.D Dissertation,* Department of Mechanical and Industrial Engineering, University of Illinois at Urbana-Champaign

McDowell, D.L., 1983b, "On the Path Dependence of Transient Hardening and Softening to Stable States under Complex Biaxial Cyclic Hardening," *Proceedings of International Conference on Constitutive Laws for Engineering Materials,* Desai and Gallagher, Eds., Tucson, Arizona, pp.125-132

McDowell, D.L., 1985a, "A Two Surface Model for Transient Nonproportional Cyclic Plasticity, Part I: Development of Appropriate Equations," ASME *Journal of Applied Mechanics,* Vol.52, pp.298-302

McDowell, D.L., 1985b, "A Two Surface Model for Transient Nonproportional Cyclic Plasticity, Part II: Comparison of Theory with Experiments," ASME *Journal of Applied Mechanics,* Vol.52, pp.303-308

McDowell, D.L., 1985c, " An Experimental Study on the Structure of Constitutive Equations for Nonproportional Cyclic Plasticity," ASME *Journal of Engineering Materials and Technology,* Vol.107, pp.307-315

McDowell, D.L., 1987, "An Evaluation of Recent Developments in Hardening and Flow Rules for Rate-Independent, Nonproportional Cyclic Plasticity," ASME *Journal of Applied Mechanics,* Vol.54, pp.323-334

McDowell, David L., 1989, "Evaluation of Intersection Conditions for Two-Surface Plasticity Theory," *International Journal of Plasticity,* Vol.5, pp.29-50

McDowell, D.L., 1991, "Nonproportional Cyclic Plasticity of Rail Steels," *Final Report for AAR,* Contract META-91-290

McDowell, D.L., 1992, "Description of Nonproportional Cyclic Ratchetting Behavior," *Progress Report on AAR,* Contract No. META-92-195

McDowell, D.L. and Lamar, A.B., 1989, "Modeling Ratchetting and Anisotropic Deformation with Hardening Dynamic Recovery Format Models," *Advances in Plasticity*, Proceedings of Plasticity'89, Second International Symposium on Plasticity and Its Current Applications, MIE University, Tsukuba, Japan, Khan and Tokuda, Eds., Pergamon Press, Oxford, pp.247-251

McDowell, D.L. and Moyar, G.J., 1991, "Parametric Study of Cyclic Plastic Deformation in Rolling and Sliding Line Contact with Realistic Nonlinear Material Behavior," *Wear*, Vol.144, pp.19-37

McDowell, D.L. and Socie, D.F., 1985, "Transient and Stable Deformation Behavior under Cyclic Nonproportional Loading," *ASTM STP 853*, American Society for Testing and Materials, pp.64-87

McMeeking, Robert M., 1982, "The Finite Strain Tension Torsion Test of a Thin-Walled Tube of Elastic-Plastic Material," *International Journal of Solids and Structures*, Vol.18, No.3, pp.199-204

Meleka, A.H. and Evershed, A.V., 1960, "The Dependence of Creep Behavior on the Duration of a Superimposed Fatigue Stress," *Journal of the Institute of Metals*, Vol.88, pp.411-414

Moosbrugger, J.C. and McDowell, D.L., 1989, "On a Class of Kinematic Hardening Rules for Nonproportional Cyclic Plasticity," ASME *Journal of Engineering Materials and Technology*, Vol.111, pp.87-98

Moosbrugger, J.C. and McDowell, D.L., 1990, "A Rate-Dependent Boundary Surface Model with a Generalized Image Point for Cyclic Nonproportional Viscoplasticity," *Journal of the Mechanics and Physics of Solids*, Vol.38, No.5, pp.627-656

Morrow, JoDean, 1964, "Cyclic Plastic Strain Energy and Fatigue of Metals," *Internal Friction, Damping, and Cyclic Plasticity, ASTM STP 378*, American Society for Testing and Materials, pp.45-84

Morrow, JoDean and Sinclair, G.M., 1958, "Cycle-Dependent Stress Relaxation," *Symposium on Basic Mechanisms of Fatigue, ASTM STP 237*, American Society for Testing and Materials, pp.83-103

Moyar, G.J., 1960, "A Mechanics Analysis of Rolling Element Failure," *T.& A.M. Report No.182*, University of Illinois at Urbana-Champaign

Moyar, G.J. and Sinclair, G.M., 1962, "Cyclic Strain Accumulation under Complex Multiaxial Loading," *T.& A.M. Report No.231*, University of Illinois at Urbana-Champaign

Moyar, G.J. and Sinclair, G.M., 1963, "Cyclic Strain Accumulation under Complex Multiaxial Loading," *Proceedings of Joint International Conference on Creep,* London

Mroz, Z., 1967, "On the Description of Anisotropic Workhardening," *Journal of Mechanics and Physics of Solids,* Vol.15, No.3, pp.163-175

Mroz, Z., 1969, "An Attempt to Describe the Behavior of Metals under Cyclic Loads Using a More General Workhardening Model," *Acta Mechanica,* Vol.7, No.2-3, pp.199-212

Mroz, Zenon, 1981, "On Generalized Kinematic Hardening Rule with Memory of Maximum Prestress," *Journal De Mechnique Appliqué,* Vol.5, N°3, pp.241-260

Mroz, Z, 1983, "Hardening and Degradation Rules for Metals under Monotonic and Cyclic Loading," ASME *Journal of Engineering Materials and Technology,* Vol.105, pp.113-118

Mroz, Z. and Trampczynski, W.A., 1984, "On the Creep-Hardening Rule for Metals with a Memory of Maximum Prestress," *International Journal of Solids and Structures,* Vol.20, No.5, pp.467-486

Mshana, J.S. and Krausz, A.S., 1985, "Constitutive Equation of Cyclic Softening," ASME *Journal of Engineering Materials and Technology,* Vol.107, pp.7-12

Mughrabi, H., 1978, "The Cyclic Hardening and Saturation Behaviour of Copper Single Crystals," *Materials Science and Engineering,* Vol.33, pp.207-223

Mughrabi, H., 1983, "Dislocation Wall and Cell Structures and Long-Rang Internal Stress in Deformed Metal Crystals," *Acta Metall,* Vol.31, pp.1367-1379

Murakami, H. and Chopra, A., 1987, "On Simulating Cyclic Hardening of Metals," *Proceedings of the Second International Conference on Constitutive Laws for Engineering Materials: Theory and Applications,* Desai, *et al.,* Eds., Tucson, Arizona, Vol. I, pp.615-622

Ning, Jie and Chen, Xu, 1991, "On the Properties of Plastic Flow of Material under Nonproportional Cyclic Loading," *International Journal of Solids and Structures,* Vol.28, No.4, pp.403-412

Nouailhas, D., Policella, H., and Kaczmarek, H. 1983, "On the Description or Cyclic Hardening under Complex Loading Histories," *Proceedings of International Conference on Constitutive Laws for Engineering Materials,* Desai and Gallagher, Eds., Tucson, Arizona

Ohashi, Y., Kawai, M., and Kaito, T., 1985a, "Inelastic Behaviour of Type 316 Stainless Steel under Multiaxial Non-Proportional Cyclic Stressings at Elevated Temperature," ASME *Journal of Engineering Materials and Technology*, Vol.107, pp.101-109

Ohashi, Y., Tanaka, E., and Ooka, M., 1985b, "Plastic Deformation Behavior of Type 316 Stainless Steel Subjected to Out-of-Phase Strain Cycles," ASME *Journal of Engineering Materials and Technology*, Vol.107, pp.286-292

Ohno, N., 1982, "A Constitutive Model of Cyclic Plasticity with a Nonhardening Strain Region," ASME *Journal of Applied Mechanics*, Vol.49, pp.721-727

Ohno, N, 1990, "Recent Topics in Constitutive Modeling of Cyclic Plasticity and Viscoplasticity," *Applied Mechanics Reviews*, Vol.43, No.11, pp.283-295

Ohno, N. and Kachi, Y., 1986, "A Constitutive Model of Cyclic Plasticity for Nonlinear Hardening Materials," ASME *Journal of Applied Mechanics*, Vol.53, pp.395-403

Ohno, N and Wang J.-D., 1991a, "Nonlinear Kinematic Hardening Rule: Proposition and Application to Ratchetting Problems," *Structural Mechanics in Reactor Technology, Transactions of the 11th International Conference on Structural Mechanics in Reactor Technology*, Shibata, Ed., Vol.L, Tokyo, Japan, L22/1, pp.481-486

Ohno, N and Wang J.-D., 1991b, "Transformation of a Nonlinear Kinematic Hardening Rule to a Multisurface Form under Isothermal and Nonisothermal Conditions," *International Journal of Plasticity*, Vol.7, pp.879-891

Ohno, N and Wang J.-D., 1991c, "Nonlinear Kinematic Hardening Rule with Critical State for Activation of Dynamic Recovery," *Anisotropy and Localization of Plastic Deformation*, Proceedings of PLASTICITY'91: The Third International Symposium on Plasticity and Its Current Applications, Boehler and Khan, Eds., Grenoble, France, pp.455-458

Ohno, N. and Wang J.-D., 1993a, "Kinematic Hardening Rules with Critical State of Dynamic Recovery: Part I--Formulation and Basic Features for Ratchetting Behavior," *International Journal of Plasticity*, Vol.9, pp.375-390

Ohno, N. and Wang J.-D., 1993b, "Kinematic Hardening Rules with Critical State of Dynamic Recovery: Part II: Application to Experiments of Ratchetting Behavior," *International Journal of Plasticity*, Vol.9, pp.391-403

Pedersen, O.B., 1987, "The Flow Stress in Copper," *Acta Metall*, Vol.35, pp.2567-2581

Peirce, D., Asaro, R.J., and Needleman, A., 1982, "An Analysis of Nonuniform and Localized Deformation in Ductile Single Crystals," *Acta Metall*, Vol.30, pp.1087-1119

Pellissier-Tanon, A., Bernard, J.L., Amzallag, C., and Rabbe, P., 1982, "Evaluation of the Resistance of Type 316 Stainless Steel Against Progressive Deformation," *Low-Cycle Fatigue and Life Prediction, ASTM STP 770*, Amzallag, Leis, and Rabbe, Eds., American Society for Testing and Materials, pp.69-80

Prager, W., 1945, "Strain Hardening under Combined Stress," *Journal of Applied Physics*, Vol.16, pp.837-840

Prager, W., 1955, "The Theory of Plasticity: A Survey of Recent Achievements," *Proceedings*, Institution of Mechanical Engineers, London, Vol.169, No.21, pp.41-57

Ruggles, M.B. and Krempl, E., 1989, "The Influence of Test Temperature on the Ratchetting Behavior of Type 304 Stainless Steel," ASME *Journal Engineering Materials and Technology*, Vol.111, pp.378-383

Sehitoglu, H. and Jiang, Yanyao R., 1992, "Residual Stress Analysis in Rolling Contact," *FRA/ERRI International Conference on Rail Quality and Maintenance for Modern Railway Operation*, Delft, The Netherlands, June 24-26

Shaw, P.K. and Kyriakides, S., 1985, "Inelastic Analysis of Thin-Walled Tubes under Cyclic Bending," *International Journal of Solids and Structures*, Vol.21, pp.1073-1100

Shield, Rich. Thorpe and Ziegler, Hans, 1958, " On Prager's Hardening Rule," *Journal of Applied Mathematics and Physics (ZAMP)*, Vol. IXa, Fasc.3, pp.260-276

Takahashi, Yukio and Ogata, Takashi, 1991, "Description of Nonproportional Cyclic Plasticity of Stainless Steel by a Two-Surface Model," ASME *Journal of Applied Mechanics*, Vol.58, pp.623-630

Tanaka, E., Murakami, S., and Ooka, M., 1985a, "Effects of Plastic Strain Amplitudes on Non-proportional Cyclic Plasticity," *Acta Mechanica*, Vol.57, pp.167-182

Tanaka, E., Murakami, S., and Ooka, M., 1985b, "Effects of Strain Path Shapes on Non-proportional Cyclic Plasticity," *Journal of Mechanics and Physics of Solids*, Vol.33, pp.559-575

Tanaka, E., Murakami, S., and Ooka, M., 1987, "Constitutive Modeling of Cyclic Plasticity in Non-Proportional loading Conditions," *Proceedings of the*

Second International Conference on Constitutive Laws for Engineering Materials: Theory and Applications, Sedai et al., Eds., Tuscson, Arizona, pp.639-646

Trampczynski, Wieslaw, 1988, "The Experimental Verification of the Evolution of Kinematic and Isotropic Hardening in Cyclic Plasticity," *Journal of Mechanics and Physics of Solids*, Vol.36, No.4, pp.417-441

Trampczynski, W. and Mroz, Z., 1991, "Anisotropic Hardening Model and Its Application to Cyclic Loading," *Anisotropy and Localization of Plastic Deformation*, Proceedings of Plasticity'91: The Third International Symposium on Plasticity and Its Current Applications, Boehler and Khan, Eds., pp.467-472

Tseng, N.T and Lee, G.C., 1983, "Simple Plasticity Model of the Two-Surface Type," ASCE *Journal of Engineering Mechanics*, Vol.109, pp.795-810

Tsuji, B., 1989, "Cyclic Plasticity Model of Two Surface Type," *Advances in Plasticity*, Proceedings of Plasticity'89, Second International Symposium on Plasticity and Its Current Applications, MIE University, Tsukuba, Japan, Khan and Tokuda, Eds., Pergamon Press, Oxford, pp.273-276

Umakoshi, Y., Pope, D.P., and Vitek, V., 1984, "The Asymmetry of the Flow Stress in Ni_3 (Al, Ta) Single Crystals," *Acta Metall*, Vol.32, pp.449-456

Valanis, K.C., 1971a, "A Theory of Viscoplasticity without a Yield Surface, Part I. Application to Mechanical Behavior of Metals," *Archives of Mechanics* (Archiwum Mechaniki Stosowanej), Vol.23, No.4, pp.535-551

Valanis, K.C., 1971b, "A Theory of Viscoplasticity without a Yield Surface, Part II. General Theory," *Archives of Mechanics*, Archiwum Mechaniki Stosowanej, Vol.23, No.4, pp.517-533

Valanis, K.C., 1980, "Fundamental Consequences of a New Intrinsic Time Measure Plasticity as a Limit of the Endochronic Theory," *Archives of Mechanics*, Archiwum Mechaniki Stosowanej, Vol.32, pp.171-191

Valanis, K.C., 1984, "Continuum Foundations of Endochronic Plasticity," ASME *Journal of Engineering Materials and Technology*, Vol.106, pp.367-375

Voyiadjis, George Z. and Sivakumar, Srinivasan M, 1991, "Constitutive Model for Cyclic Plasticity with Ratchetting Effects," *Anisotropy and Localization of Plastic Deformation*, Proceedings of PLASTICITY'91: The Third International Symposium on Plasticity and Its Current Applications, Boehler and Khan, Eds., Grenoble, France, pp.473-476

Wang, J.-D. and Ohno, N., 1991, "Two Equivalent Forms of Nonlinear Kinematic Hardening: Application to Nonisothermal Plasticity," *International Journal of Plasticity*, Vol.7, pp.637-650

Weng, G.J., 1979, "Kinematic Hardening Rule in Single Crystals," *International Journal of Solids and Structures*, Vol.15, pp.861-870

Winter, A.T., 1974, "A Model for the Fatigue of Copper at Low Plastic Strain Amplitudes," *Philosophy Magazine*, Vol.30, pp.719-738

Wood, W.A. and Bendler, H.M., 1962, "Effect of Superimposed Static Tension on the Fatigue Process on Copper Subjected to Alternating Torsion," *Transaction of the Metallurgical Society of AIME*, Vol.224, p.18-26

Wu, Han C. and Yao, Jen-Che, 1984, "Analysis of Stress Response to Various Strain-Paths in Axial-Torsional Deformation of Metals," ASME *Journal of Engineering Materials and Technology*, Vol.106, pp.361-366

Yamanouchi, H., Kino, H., and Nakano, S, 1976, "Ratchetting in Thin Tube under Cyclic Axial Strain and Internal Pressure," *Proceedings of the Second International Conference on Mechanical Behavior of Materials*, The American Society of Metals, Boston, Aug.16-20, pp.53-57

Ziegler, H., 1959, "A Modification of Prager's Hardening Rule," *Quarterly of Applied Mechanics*, Vol.17, No.1, pp.55-65

VITA

Yanyao Jiang was born on December 2, 1963 in Zhejiang Province, China. He finished high school in 1979 and was enrolled in the Northeastern University of Technology in Shengyang, China. In 1983, he graduated with a Bachelor of Science degree in Mechanical Engineering. After a competitive graduate enrollment examination, he was admitted to the Graduate School of Zhejiang University in Hangzhou, China. He studied Solid Mechanics for the required three years, and earned the degree of Master of Science in June of 1986. After his graduation, he worked in the Department of Mechanical Engineering at Zhejiang Institute of Technology located in Hangzhou, China. Part of his responsibilities during three and half years at the university included teaching undergraduate classes such as Theoretical Mechanics, Mechanics of Materials, Engineering Mechanics, and Experimental Mechanics. He also served as a supervisor for senior undergraduate projects. Major research interest areas are Fracture and Fatigue of Metals, Experimental Stress Analysis, and Machine Design. In the Spring of 1990, he began his graduate study at the University of Illinois at Urbana-Champaign pursuing a Doctor of Philosophy degree in Mechanical Engineering. He has held Research Assistantships during his studies at the University of Illinois. Primary areas of research include Rolling Contact, Multiaxial Fatigue, and Cyclic Plasticity. Yanyao was married to Wei Wu on December 14, 1991 in Champaign.